Novel Phosphate Glasses for Bone Regeneration Applications

By Luke Donald Burling, BSc (Hons)

Thesis submitted to the University of Nottingham for the degree of Doctor of Philosophy, September 2005

Abstract

Phosphate glass with additions of sodium, magnesium and/or calcium were investigated for their potential to be used as the reinforcing phase in a completely degradable long fibre composite. Glasses were prepared from phosphate salts as opposed to oxides and melted under air in platinum/gold crucibles. The effect of cation addition on the material properties and biocompatibility was investigated. Glasses were characterised using a number of complimentary techniques, including: XRD, XPS, DSC, IR and EDX. The findings from these techniques were used to explain the observed thermal and dissolution properties.

The thermal and dissolution properties were found to be dependant on both the thermal history and composition of the phosphate glass. For a phosphate glass with low cation content, the temperature and length of time held at that temperature increased the T_g by 10 °C for sodium phosphate glass and slightly improved the durability of sodium phosphate glass containing 10 mol.% $MgHPO_4$, as phosphate chain growth was greater under those conditions. Addition of divalent cations increased the T_g of phosphate glasses from 295 °C for sodium phosphate glass by up to 150 °C with the addition of 50 mol.% $MgHPO_4$. The dissolution rate was decreased exponentially with the addition of calcium phosphate or magnesium phosphate to sodium phosphate glass. Rates as low as $1x10^{-7}$ g cm^{-2} h^{-1} were achieved with the addition of 50 mol.% divalent cation phosphates. The divalent cations inhibited phosphate chain growth but formed a new network based upon divalent cation/non bridging oxygen cross-links. These cross-links were found to exert greater influence over the material properties then the phosphate chain length.

Cell culture assays were used to establish the biocompatibility of phosphate glasses with different compositions. Preliminary tests were conducted with craniofacial derived osteoblast like cells cultured on glass surfaces. Initial assays performed showed that the most durable glasses sustained the greatest amount of proliferation and differentiation over a seven day period. The most promising glass compositions, 40 Ca, 40 Mg, 30 Mg/20 Ca and 20 Mg/30 Ca, and were selected for longer term osteoblast culture and short term macrophage culture. Long term osteoblast culture showed that cells were able to attach, spread and proliferate throughout the 28 day duration of the study. Assays performed on the culture showed that cells were differentiating, producing specific osteoblast markers for each of the three differentiation phases of proliferation, matrix maturation and mineralisation. ECM production and mineralisation was confirmed on all surfaces tested via type I collagen staining and alizarin red staining respectively. Over the 28 day period, it was found that the composition did not have a significant effect on the production of the osteoblast markers, namely alkaline phosphatase, collagen, osteocalcin and mineral deposition. Immunological studies show that macrophages are not activated by the presence of phosphate glass. This demonstrated that phosphate glass has shown potential for use a biomaterial.

Acknowledgments

I would like to take this opportunity to thank both Dr Gavin Walker and Dr Colin Scotchford, under whose supervision this work has been carried out. Their continued support, guidance and encouragement throughout this project has been much appreciated.

Particular thanks are given to Graham Aitchison and Dr Andy Parsons who aided my research throughout the project.

I would also like to thank the members of the research and technical staff who have give invaluable assistance. Special thanks are given to Martin Roe for his help with XPS and electron microscopy, Keith Dinsdale for his help and expertise with many different instruments and Bushra Sim for teaching me all manner of cell culture techniques and assays. Thanks are also given to Rory Screaton and Graham Malkinson of the workshop for their help constructing all manner of devices.

Special thanks go to my parents, without whom this work would not be possible.

Finally I would like to thank all the countless people who have ensured that my postgraduate days in Nottingham will not be forgotten. Special thanks to the Charlbury lads: Neil, Matt and Mia, as well as all from Taekwondo, especially Richard, Helen and Yutaro.

Contents List

List of Abbreviations

ANOVA	Analysis of Variance
ALP	Alkaline Phosphatase
BMP	Bone Morphogenic Protein
BSA	Bovine Serum Albumen
CFC	Human Craniofacial Derived Osteoblast like Cells
CLSM	Confocal Laser Scanning Microscope/scopy
DABCO	1,4-Diazabicyclo-(2,2,2) Octane
DMEM	Dulbecco's Modified Eagle Medium
DMSO	Dimethyl Sulphoxide
DNA	Deoxyribonucleic Acid
DSC	Differential Scanning Calorimetry
EBSS	Earl's Balanced Salt Solution
ECM	Extracellular Matrix
EDX	Energy Dispersive X-Ray Analysis
ESEM	Environmental Scanning Electron Microscope
FBS	Foetal Bovine Serum
FEG	Field Emission Gun
FITC	Fluoroscein-isothyocynate
GAG	Glycosaminoglycan
LPS	Lipopolysaccharide
HBSS	Hank's Buffered Salt Solution
IL-1β	Inter Leukin-1β
IR	Infra Red Spectroscopy
Mϕ	Macrophage
MIDAS	Metal Ion-Dependant Adhesion Site

OC	Osteocalcin
ON	Osteonectin
OP	Osteopontin
PBS	Phosphate Buffered Saline
PCL	Polycaprolactone
PGA	Polyglycolic acid
PI	Propidium Iodide
PLA	Poly lactic acid
SD	Standard Deviation
sem	Standard Error of the Mean
SEM	Scanning Electron Microscope
TBS	Tris Buffered Saline
T_c	Crystallisation Temperature
T_g	Glass Transition Temperature
T_m	Melting Temperature
TCP	Tissue Culture Plastic
XPS	X-Ray Photoelectron Spectroscopy (a.k.a. ESCA)
XRD	X-Ray Diffraction

1 Introduction

Research into novel materials for biomedical applications is ever increasing as the medical community look to improve the way in which disorders and trauma are treated. Issues with current materials and the additional trauma associated with the use of bone grafts has pushed research towards new materials to aid the required repair and/or the regeneration of bone after fracture or the removal of bony defects or cancerous bone. Many new materials have been developed in an attempt to address these concerns but there are still issues surrounding the appropriateness of their mechanical properties, the ability of degradable materials to retain their properties once implanted and the ability to form the material in situ to the requirements of the surgeon.

A possible solution to this is a completely degradable long fibre composite comprised of a fully degradable matrix reinforced with degradable phosphate glass fibres, which will possess the potential to be used within the upper facial regions and cranium, including the maxilla, zygomatic and frontal bones. Phosphate glass with additions of calcium, magnesium and sodium are being considered for use as a biomaterial as they are all constituents of bone, with the exception of sodium, and as such, regulatory mechanisms exist to control the plasma levels of these. The ideal biodegradable composite will retain 80 % of its initial properties for a minimum of 6 weeks (Pietrzak *et al.*, 2000; Fisher, 2001) after which the material will be resorbed, leaving the site of repair in its original state without the need for follow up surgery.

The work detailed here is concerned with the assessment of phosphate glass made from salts as a potential reinforcement phase for a composite biomaterial.

1.1 Craniofacial Bone Repair

Craniofacial bone repair may be required to compensate for a bony deficit, which may be due to congenital malformation, removal of tumour or trauma. This type of bone damage or deformity can be particularly distressing for the patient as it can be debilitating and depressing as facial features are closely linked to self confidence. The quality of life is greatly affected by craniofacial defects, for example, an intact maxilla and mandible are essential for breathing and speech, while the structure of the orbital bone, especially the orbital floor is essential for the correct positioning of the eyes and hence binocular vision and focusing. Also, disorders of the skull may result from or cause problems with the brain, especially for children when growing. Successful craniofacial repair is essential for an aesthetically acceptable face and fundamental aspects of good quality of life.

The size of the craniofacial bony deficit to undergo repair determines the manner of treatment. Very small gaps may be capable of healing unaided. However, if the deficit is too great, then repair may require support from an implanted material to establish bony continuity across the defect. With larger defects, such as removal of a cyst or tumour, implantation of an osteoconductive material is necessary, to fill the gap, prevent fibrous in-growth and finally to guide bone regeneration.

1.2 Biomaterials

There are a number of definitions describing biomaterials, but the most widely accepted definition is as follows: "a biomaterial is a nonviable material used in a medical device, intended to interact with biological systems" (Williams, 1987).

1.2.1 Concepts and Current Applications

The ideal goal of surgery is to restore the structure and function of the body to its natural state (Pietrzak *et al.*, 2000). For bone fractures this is usually accomplished using a metal plate attached via screws to stabilise the fracture site and decrease the chance of non or mal-union during healing.

Bone is a unique tissue in that it can heal itself without scarring, a process referred to as regeneration (Clokie *et al.*, 2000). Developers of new materials for bone regeneration applications are faced with the challenge of utilising this feature.

Applications for bone regeneration materials can be broadly classified into three classes: inlays, used to fill bony defects; onlays, used for augmentation of bony contours or fusions and finally for the stabilisation of two bony units. Within maxillofacial surgery, the majority of applications are inlay and onlay, with only a relatively small amount of fusion (Clokie *et al.*, 2000).

1.2.2 Classes of Biomaterials

Materials used for bone applications are categorised into four groups: autografts, allografts, xenografts and alloplastics.

Autograft refers to a graft of tissue taken from one site and transferred to another within an individual. The most common sites for autograft bone donation are the iliac crest, tibia and ribs. These grafts are osteogenic, osteoinductive and osteoconductive and do not instigate a host response. The drawbacks from using this type of graft are: a second surgical procedure to procure the graft with related donor site morbidity, and more practically, only limited amounts may be harvested.

Allograft (a.k.a. homografts) bioimplants are tissues taken from an individual of one species and transferred to another of the same species. Allografts are available in much larger quantities than autografts but they vary in osteoinductive capability from graft to graft, may be potentially immunogenic and can transfer disease.

Xenografts refer to the transfer of tissues between two individuals of different species. There is a virtually limitless supply of bone from animals, typically bovine, however, the chance of potential immunogenicity and disease transfer, especially since possible links between BSE and CJD, have led to the discontinuation of Xenografts (Clokie *et al.*, 2000).

Alloplastic grafts are materials which are synthetically fabricated that can be used for bone reconstruction and form the basis for the vast majority of research within this area and are termed biomaterials.

The development of a successful biomaterial requires careful consideration of the requirements placed upon it after implantation. The internal

environment of the body is extremely corrosive, similar to that of the sea, including large variations in pH depending on the final application. Immunological response and inadequate mechanical properties will lead to the failure of the implant. Overall, biomaterials need to fulfil a large number of criteria to be a success.

1.2.3 Current Craniofacial Biomaterials

The wide diversity of materials currently used in medicine is testimony to the number of advances that have occurred over the past fifty years. Biomaterials currently used fit into 4 classes, namely metals, ceramics, polymers and natural materials (of both plant and animal origin). Further to this, two classes of materials may be combined to form a composite, which is a fifth class of biomaterial.

1.2.3.1 Metals

Currently there are three metals used for fixation devices: stainless steel (316L), cobalt chromium alloy and titanium, which is either commercially pure or alloyed with vanadium, aluminium and/or niobium. Of these, titanium and its alloys are the most popular for craniofacial use because of its high strength and reduced artefacts on CT and MR imaging (Saxe *et al.*, 1982; Fiala *et al.*, 1994).

Permanent metal fixation implants leave a residual implant within the body, which may cause secondary problems. Metal implants may cause stress shielding and subsequent bone weakening in load bearing applications;

implants may be palpable and cause tissue irritation and pain, necessitating their removal. There are also concerns of implant migration and interference with diagnostic and therapeutic applications of radiation, for a review see (Pietrzak *et al.*, 2000). Metallic implants are often darker than the surrounding tissue and may cause discolouration, also, due to the rigidity of metals, it is often difficult to match the implant to the contours of the underlying bone. This may result in implant edges that are visible through the skin (Ahn *et al.*, 1997). The application of metallic implants close to the skin may result in temperature effects. During cold weather the implant may be cooled sufficiently to cause pain or discomfort (Daniels *et al.*, 1990).

Observations of malignancy in association with metal fixation devices are rare, with only 20 reported in the literature (Rubin *et al.*, 1997), with latencies between 1-30 years. Only one was reported to occur above the neck. This implies that the local risk of cancer is low with metallic implants. However, it has been found that there is a significant increase in the risk of systematic tumours, e.g. lymphatic, in patients who have undergone total hip replacement (Gillespie *et al.*, 1988). It should be noted that there are other factors associated with arthritic disease which may have contributed.

The release of metal ions from implants via corrosion has raised concerns over system toxicity. The accumulation of ions can result in local fibroblastic tissue reaction which has been implicated in implant failure of maxillofacial plates (Byrne *et al.*, 1973; Thomas *et al.*, 1988).

1.2.3.2 Polymers

There are many different polymers that have been used in maxillofacial surgery, however, only the most popular will be considered here. Cancer associated with a polymer implant is very rare, with none reported in association with a polymer craniofacial implant (Rubin *et al.*, 1997).

Polyethylene

This is normally used in its ultra high molecular weight form as the low friction acetabulum cup part of total hip replacement.

It is also made as a porous implant, Medpor, which allows the in growth of both soft tissue and bone, which makes the implant very difficult to remove. It has been used in orbital fracture repair and in the management of cosmetic and post traumatic facial deformities (Rubin *et al.*, 1997).

Polytetrafluoroethylene (PTFE)

Proplast is a porous composite of PTFE and carbon fibres, Proplast I, or aluminium oxide, Proplast II. It has been used since 1960 as a filler in non load bearing applications because of its porous surface and consequential in-growth of fibrous tissue.

Proplast has been used for malar, chin, nasal and orbital floor implants with acceptable complication rates. When it was used as an interpositional disc implant within the temporomandibular joint, complication rates rose to well above acceptable limits. Nearly all implants fractured under the load of the joint. Additionally, the Proplast particulates caused a vigorous foreign body reaction and subsequent erosion of the joint (Rubin *et al.*, 1997).

Polymethylmethacrylate (PMMA)

This is commonly used as cement, formed by mixing powdered polymer with liquid monomer. The resultant chemical reaction is exothermic, and toxicity has been associated with the unreacted monomer (Rubin *et al.*, 1997). The hardened methylmethacrylate is brittle and prone to fracture. HTR (Biomet Inc), derives its name from hard tissue replacement, it is a porous composite of PMMA and polyhydroxylmethacrylate. It has a calcium hydroxide coating which is thought to impart a negative surface charge to encourage bony in-growth (Eppley *et al.*, 1990).

Methylmethacrylate has been shown experimentally to cause vasodilatation, (Peebles *et al.*, 1972). After insertion of hip prostheses with freshly mixed MMA cement into the femur, patients have suffered acute hypotension that can progress to cardiovascular collapse and death (Kepes *et al.*, 1972; Milne, 1973; Monteny *et al.*, 1978).

Polysiloxane (silicone)

This material can be manufactured with viscosities ranging from a mobile liquid to a solid. It can be used in a room temperature vulcanised, (RTV) form. RTV polysiloxane is mixed with a hardening agent and custom moulded by the surgeon either before implantation or *in-situ*. The normal host response to this material is fibrous encapsulation. The manufacturing process plays an important role in the purity and integrity of this material.

There have been suggested links between silicone breast implants and connective tissue damage, however, two controlled studies have dismissed these claims (Gabriel *et al.*, 1994; Sanchezguerrero *et al.*, 1995).

Systematic toxicity of silicone has been documented after injection of large volumes of liquid silicone for breast augmentation. Two cases of hepatitis and

one lethal oedema, albeit after inadvertent intravascular injection of liquid silicone, were reported (Ellenbogen *et al.*, 1975).

1.2.3.3 Ceramics and Glasses

Alumina

This hard ceramic was used as a coating for the articulating surfaces in total hip replacement as it has very favourable wear and corrosion properties as well as good biocompatibility. However, its use was discontinued after complaints of post-operative pain.

Hydroxyapatite

This is the mineral phase of bone, which can be formed synthetically in either dense or porous forms. Porous hydroxyapatite is too brittle to bear a load but will allow bony in-growth when used as an onlay.

Bioglass

Bioglass is a bioactive material which can develop a bond with bone (Hench, 1996). It is a silica based glass that contains phosphate, calcium and sodium: the Ca/P ratio is at least 5 as bioglasses with lower ratios do not bond to bone. After implantation, alkali ion/hydrogen ion exchange occurs producing an alkali deficient surface. Si-O-Si bonds are hydrolysed to give silanols, resulting in a silica gel layer. Calcium, phosphate and carbonate ions adsorb onto the glass surface and crystallise to form hydroxyl carbonate apatite, it is this layer which bonds to bone.

Bioglass has been used extensively in non load bearing applications such as alveolar ridge augmentation and maxillofacial reconstruction. However, its use is limited by its brittleness, which produces difficulties in shaping the implant and limits its applications.

Particulate bioglass was added to high density polyethylene in an attempt to produce superior properties without losing any bone bonding capabilities

(Wang *et al.*, 1998). Material hardness increased with bioglass content while tensile strength and fracture strain decreased. Apatite layer formation was still observed when the composite was placed in simulated body fluid.

Recently bioglass has been drawn into fibres and mechanically tested for inclusion into composites (De Diego *et al.*, 2000), but research into this area is limited at this time.

1.2.3.4 Composite Materials

Composite materials allow the use of two materials which individually, would be unsuitable for the desired application. This allows the combination of polymers with insufficient mechanical properties with ceramics and glasses of low fracture toughness to produce a material which possesses the best of both worlds that is both tough and strong/stiff.

Composite used within medicine can be broadly cast into two classes: particulate reinforced or fibre reinforced. Particulate reinforcement is easier to produce as the composites are isotropic; hence may be prepared in-situ, however, this leads to lower mechanical properties. Fibre reinforced composites are anisotropic, as is bone, and possess superior mechanical properties to their particulate analogues.

1.2.4 Bioresorbable Materials

Due to their nature, resorbable materials are usually utilised in short term non load bearing applications such as sutures and drug delivery devices,

however, applications for medium term such as fracture fixation are being considered as new, novel materials are researched.

As discussed previously, metallic implants are the material of choice to stabilise fractures, but they may exhibit complications such as stress shielding, migration, tissue irritation and pain. These complications may require secondary surgery to remove the implant. This presents the patient with prolonged trauma and recovery time, whilst adding to the cost of surgery and requiring more theatre time.

Resorbable materials offer a potential solution to these problems, by eliminating the need for follow up surgery to remove the implant. Stress shielding is eliminated as a gradual loss of material, and hence material properties, exposes the immature bone to gradually increasing levels of stress, aiding remodelling. This will clearly be beneficial to medicine as patient trauma, surgical time and related costs are all reduced.

Ideally, a resorbable polymer should serve its temporary need, be metabolically eliminated completely by the body within an acceptable time period, without eliciting an adverse physiological response (Pietrzak *et al.*, 2000).

The current market for resorbable biomaterials is dominated by poly-lactic acid, PLA, and poly-glycolic acid, PGA, or co-polymers of the two. PGA is not used on its own due to its fast resorbtion rates. The low mechanical properties of PLA and PLA/PGA copolymers have limited their use to non or low load bearing applications. The relatively fast degradation of these polymers may lead to the build up of degradation products, which leads to a decrease in pH and possible aseptic foreign body reactions (Rubin *et al.*, 1997).

Applications within craniomaxillofacial surgery include: plates, screws and mesh panels.

1.3 Project Objectives

The aims of this project were:

- To produce phosphate glasses using phosphate salts.
- To determine the effects of processing conditions and composition on physical properties.
- To determine the effects of processing conditions and composition on the phosphate chain length.
- To determine the dissolution rates of phosphate glasses.
- To use short term cytotoxic assays to determine the most promising glasses for further long term testing.
- To determine the effect of phosphate glass on the osteoblast cell cycle.
- To determine whether phosphate glasses initiate a macrophage immune response.

2 Literature Review

2.1 Introduction

This chapter presents a review of the literature, beginning with the anatomy, function and histology of bone, which is the material to be fixated or replaced. The use of *in vitro* studies to assess the materials potential for use as a biomaterial and their limitations are discussed, accompanied by descriptions of bone cells and the extracellular matrix which they produce. This precedes a commentary on the *in vitro* work which has been performed by other groups.

A brief insight to glass science and glass manufacture is included as a general background. A detailed review of the short and medium range order in phosphate glass and how it is affected by composition follows, while the affect of glass structure on the T_g and dissolution in aqueous media is also discussed.

2.2 Bone

Bone is a complex and dynamic living tissue which is continuously remodelled. It performs several basic functions such as protection, storage of minerals and the production of red blood cells, but its primary function is support, providing a framework for the body by supporting the soft tissues and providing points of attachment for most skeletal muscles.

2.2.1 Anatomy of Bone

Individual bones are classified according to their shape as long, short, flat or irregular. Long bones are longer than they are wide, and consist of most of the bones from the limbs. Short bones are about as broad as they are wide. They are nearly cube-shaped or round and are exemplified by the carpals and the tarsals of the hands and feet respectively. Flat bones have a relatively thin, flattened shape and are usually curved, such as some skull bones, ribs, the sternum and the scapulae. Irregular bones, such as vertebrae and facial bones, have shapes that do not fit into the other three categories.

2.2.1.1 Long Bone Structure

Each growing long bone has three major components: the diaphysis, epiphysis and the epiphyseal, figure 2.1. The diaphysis comprises mostly of cortical bone, or compact bone, which is virtually all bone matrix surrounding a few small spaces. The epiphysis consists of cancellous, or spongy, bone which has many small spaces surrounded by bone matrix. The outer layer of the epiphysis consists of cortical bone, and within joints the epiphyses are covered in articular cartilage. The epiphyseal, or growth plate, is hyaline cartilage located between the diaphysis and the epiphysis, which ossifies when bone growth stops. This is the site of bone length growth, when growth stops the epiphyseal and is called the epiphyseal line. The diaphysis also contains a large space called the medullary cavity, which are filled with marrow.

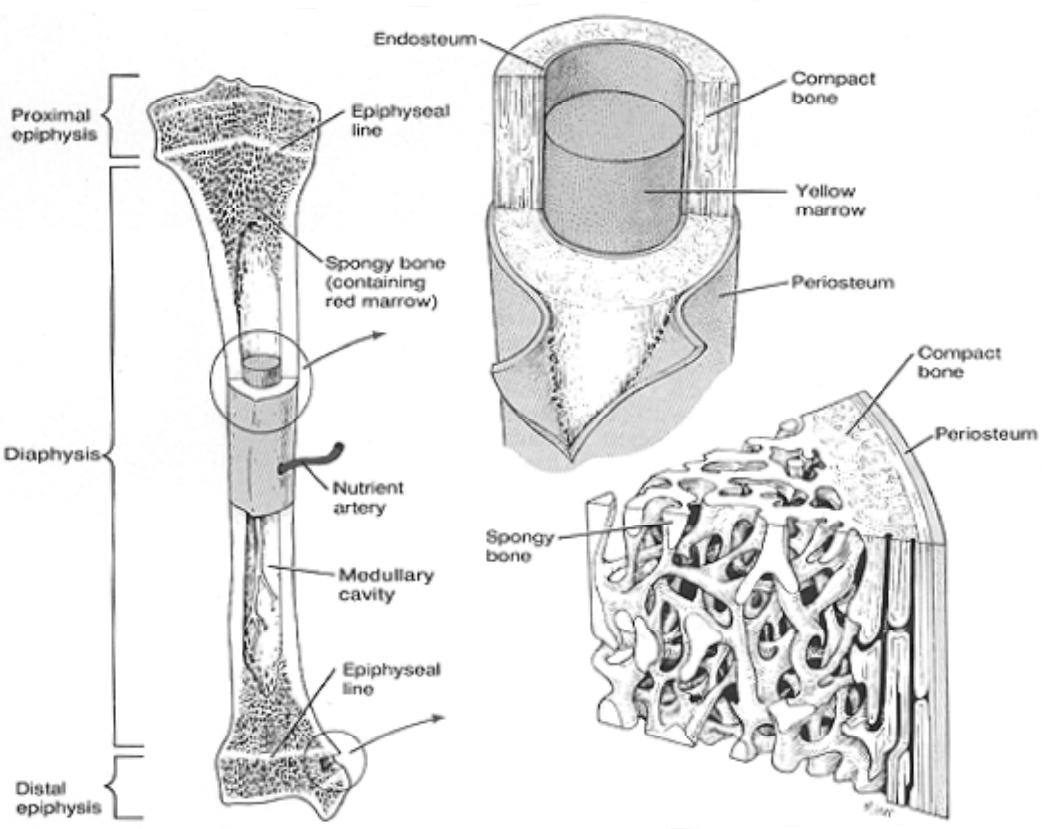

Figure 2.1 The structure of long bones within the adult human body, taken from (pharyngula, 2003)

2.2.1.2 The Anatomy of Flat, Short and Irregular Bones

Flat bones possess no diaphysis or epiphysis; they comprise an internal framework of cancellous bone which is sandwiched between two layers of cortical bone, figure 2.2. Short and irregular bones have a structure similar to that of the epiphysis of long bones, with cortical bone surfaces surrounding a cancellous bone centre with small spaces that are usually filled with marrow.

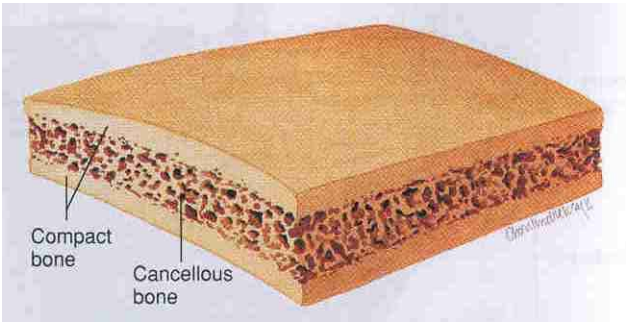

Figure 2.2 The structure of flat bones in the human body, cancellous bone sandwiched in-between sheets of cortical bone. In some cases the layers are of cortical bone are thin and only contain circumferential cortical bone. Taken from (Seeley, 2000).

2.2.2 Histology of Bone

Bone consists of extracellular bone matrix and bone cells. The composition of the bone matrix is responsible for the characteristics associated with bone. The bone cells are responsible for the production, maintenance, removal and remodelling of the bone itself.

By weight, mature bone consists of approximately 35 % organic material and 65 % inorganic material. The organic material consists mainly of collagen and proteoglycans while the inorganic material consists of a calcium phosphate mineral called hydroxyapatite, $Ca_{10}(PO_4)_6(OH)_2$.

Collagen fibres and hydroxyapatite are the components responsible for the major functional characteristics of bone. The bone matrix resembles a long fibre composite with a hydroxyapatite matrix reinforced with collagen fibres. Hydroxyapatite gives bone its weight bearing capacity, compressive strength, while the collagen fibres improve the toughness of bones (Seeley, 2000). Cortical bone has an elastic modulus of 15-30 GPa, a yield strength of 30-70 MPa and a fracture toughness of 2-12 MPa $m^{0.5}$ (Cooke *et al.*, 1996).

Bone tissue is classified as either woven or lamellar bone, according to the organisation of the collagen fibres within the extracellular matrix.

Woven bone is formed within foetal bone or in wound healing after a fracture. It consists of randomly orientated collagen fibres. After its formation, woven bone is broken down by osteoclasts and new matrix is deposited by osteoblasts in the form of highly organised lamellar bone. This process is known as remodelling.

Most of the hydroxyapatite within bone is in the form of rod like crystals 40 nm in length and 1.5-3 nm in thickness, but there is a very small

amorphous component. The crystals are regularly spaced at intervals of 60-70 nm along the length of collagen fibres (Seeley, 2000).

Non-collagenous proteins comprise of 10-15 % of the total bone protein content. Many non-collagenous proteins have been identified including: osteopontin, bone sialoprotein (Fisher *et al.*, 1987), osteocalcin (Hauschka *et al.*, 1975), osteonectin (Termine *et al.*, 1981; Young *et al.*, 1990a) and the proteoglycans biglycan and decorin (Fisher *et al.*, 1987; Fisher *et al.*, 1989)

A more detailed description of the organic components of bone is discussed later.

2.2.2.1 Cancellous and Cortical Bone

Cancellous bone is comprised of a network of connected rods and plates of bone called trabeculae, figure 2.3. The spaces between trabeculae are filled with bone marrow and blood vessels.

Trabeculae are orientated along the lines of stress within a bone, if the direction of the stress is changed slightly, e.g. mal aligned healing after

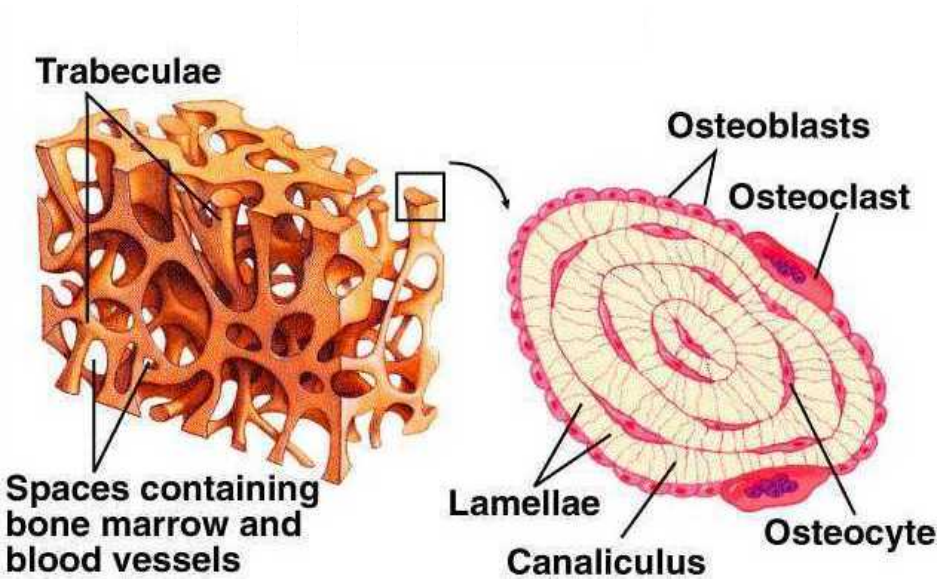

Figure 2.3 Structure of cancellous bone and the trabeculae within. Taken from (Seeley, 2000)

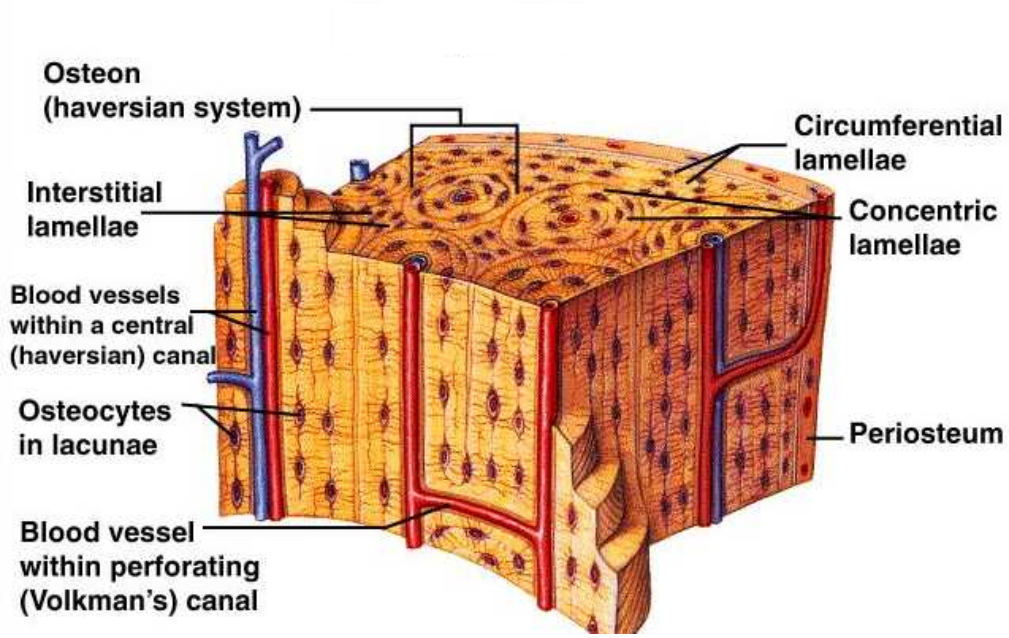

Figure 2.4 The structure of cortical bone. Taken from (Seeley, 2000).

trauma, then the trabeculae realign with the new direction of stress (Seeley, 2000).

Cortical bone is far denser with fewer spaces than cancellous bone, figure 2.4. Blood vessels enter the bone itself, with the lamella of cortical bone arranged around these. Vessels that run parallel to the long axis of the bone are contained within central, or haversian, canals that are lined with endosteum. Concentric lamellae surround the central canal in circular layers. The central canal, its contents, the concentric lamella and the osteocytes are collectively known as an osteon or haversian system.

The outer surface of cortical bone is covered with circumferential lamellae, which are flat plates that extend around the bone. In some cases, such as certain bones of the face, the layer of cortical bone is so thin that no osteons exist and it is composed only of circumferential lamellae

2.2.3 Bone cells

There are three types of bone cells: osteoblasts, osteocytes and osteoclasts. Osteoblasts are derived from multi-potential stem cells, which have the capability to differentiate into many different cell types. Exposure to specific markers, e.g. dexamethasone in-vitro, causes the stem cells to give rise to mono-potential progenitor cells called osteoprogenitors, which have an extensive proliferation capability (Aubin, 2000). The now default differentiation pathway leads to preosteoblasts, with limited matrix production, and then mature osteoblasts that are responsible for the deposition of extracellular matrix (Aubin, 2000). Once engulfed by the bony matrix, osteoblasts become osteocytes.

Osteoclasts precursors are derived from stem cells within the bone marrow, but unlike osteoblast differentiation, they arise via the monocytic lineage.

Osteoblasts are primarily responsible for the formation and mineralisation of the extracellular matrix of the bone, called osteogenesis, and the regulation of access to its surfaces (Stevens *et al.*, 1997). Osteoblasts are highly active cells, producing large amounts of proteins from their extensive endoplasmic reticulum, numerous ribosomes and well developed Golgi apparatus. Calcium and phosphate ions are accumulated within vesicles, which are used to deposit the mineral phase of bone, hydroxyapatite (Seeley, 2000).

Once an osteoblast becomes surrounded by bone matrix, it is a mature bone cell called an osteocyte. Osteocytes are relatively inactive compared to osteoblasts, but they retain the ability to produce matrix components and maintain the bone which surrounds them (Bloom *et al.*, 2002).

The spaces which osteocytes occupy are known as lacunae, while the spaces which are occupied by the osteocyte cell processes with which the cells communicate and receive nutrients are called canaliculi (Marks *et al.*, 1988).

Osteoclasts are large cells containing 4 to 40 nuclei, which are responsible for the resorption of bone, acting as the bone macrophage. The area of osteoclasts that is in contact with the bone is sealed and the membrane within this possesses many projections and is called the ruffled border. The cavity under the osteoclast is known as Howship's lacuna. Hydrogen ions are pumped across the ruffled border to reduce the pH and create an environment that causes decalcification. Proteases are also released to breakdown the organic phase of the matrix (Parfitt, 1994).

Bone is normally covered with an un-mineralised organic layer which is broken down by enzymes produced by osteoblasts, enabling the osteoclasts to come into direct contact with the mineralised tissue.

2.2.4 Organic Matrix Components

The extracellular matrix of bone is synthesised by osteoblasts. It comprises of many proteins that are split into collagenous and non-collagenous proteins. Collagen is the most prominent protein in bone, with other non-collagenous proteins such as osteocalcin, osteonectin, bone sialoproteins, proteoglycans and osteopontin making up the balance.

2.2.4.1 Collagen

At 90 %, collagen is by far the most abundant organic component of the bone matrix. Of this, 97 % is type I collagen and the remainder consists of type II, III, V and X collagen, but these are generally considered to be contamination from blood vessels or cartilage (Marks *et al.*, 1988).

Type I collagen is a class 1, banded, fibre forming collagen. Type I collagen consists of a triple helix where each of the chains are comprised mainly of glycine, with every third amino acid being of this type. Each molecule of type I collagen is comprised of two α1 chains and one α2 chain. Due to this peptide sequence, each chain is coiled in a left handed helix, and the three chains assemble in a right handed triple helix with glycine residues at the centre of the triple helix. Proline and hydroxyproline are present in equal amounts and make up roughly one third of the remaining amino acid residues. Hydroxyproline is an essential constituent as it stabilises the triple helix (Rossert *et al.*, 1996).

Type I collagen is secreted as a propeptide with an N terminal and C terminal telopeptide, which are rapidly cleaved by specific proteases. Mature collagen molecules are assembled into fibrils, in which the molecules run parallel to each other and overlap by multiples of 67 nm, where each collagen molecule is 300 nm. Within tissues, fibrils can be parallel to each other to form bundles, or fibres, or they can be randomly orientated to form networks. In bone, hydroxyapatite crystals seem to lie in the gaps between collagen molecules (Rossert *et al.*, 1996).

Collagen in bone is essential for strength and cell attachment.

2.2.4.2 Osteonectin

Osteonectin is the most abundant non-collagenous protein, and despite its name, it is not produced exclusively by osteoblasts but also by fibroblasts. It possesses numerous disulphide bonds and can interact with Ca^{2+}, collagen (Young *et al.*, 1990b) and hydroxyapatite (Wasi *et al.*, 1984), and nucleate hydroxyapatite deposition (Termine *et al.*, 1981).

The osteonectin molecule contains several different structural features, most notably, the presence of two high affinity calcium binding sites, which are usually found in intracellular proteins, such as calmodulin, that function in calcium metabolism (Robey, 1996).

2.2.4.3 Osteocalcin

Osteocalcin, a.k.a. bone Gla protein – BGP, is an abundant non-collagenous protein which contains three γ-carboxyglutamic acid, Gla, residues (Hauschka *et al.*, 1975; Price *et al.*, 1976) whose synthesis is vitamin K dependant. Osteocalcin exhibits a calcium dependant α-helical conformation in which the three Gla residues are aligned to facilitate the absorption to hydroxyapatite (Price, 1985; Hauschka *et al.*, 1989b). Osteocalcin also possessed a COOH terminal beta sheet domain that may be the locus for interaction with cellular receptors, (Hauschka *et al.*, 1989b).

The precise function of osteocalcin is still not fully understood (Hauschka *et al.*, 1989a; Ducy *et al.*, 1996). It has been suggested that osteocalcin may have a role in the regulation of bone resorption and the recruitment of cells of osteoclast linage. Bone particles which were completely deficient in

osteocalcin, were implanted subcutaneously into rats. These particles were resistant to resorption and had a decreased ability to recruit and differentiate osteoclast progenitors compared to control particles (Ducy *et al.*, 1996).

Further suggesting that osteocalcin has a role in the remodelling of bone via the recruitment of osteoclasts and their precursors. Synthesised hydroxyapatite/collagen implants were press-fit into the tibial head of adult wistar rats. To one implant group, osteocalcin was added. It was found that the addition of osteocalcin lead to the accelerated onset and increased rate of bone remodelling. Transformation from woven bone to lamellae bone was also accelerated (Rammelt *et al.*, 2005).

2.2.4.4 Osteopontin

Osteopontin is phosphorylated glycoprotein known to occur in many tissues (Butler *et al.*, 1996), and binds to hydroxyapatite. Immunolocalisation studies have shown that osteopontin is synthesised by preosteoblasts, osteoblasts and osteocytes and was secreted into the osteoid (Mark *et al.*, 1987), where the most intense signal was found at the mineralisation front.

Osteopontin was shown to promote the attachment and spreading of osteoblasts (Oldberg *et al.*, 1987), and fibroblasts (Somerman *et al.*, 1987), in a concentration dependant fashion. These observations lead to the hypothesis that osteopontin is secreted by osteoblasts early in bone development and facilitates the attachment of these cells to the extracellular matrix (Butler, 1989; Butler *et al.*, 1996). Subsequently it has been found that osteopontin is important in the attachment of osteoclasts and their action in resorbing bone (Ross *et al.*, 1993).

2.2.4.5 Proteoglycans

Proteoglycans consist of core protein molecules, to which long chain polysaccharides, glycosaminoglycans GAGs, are attached. GAGs are comprised of repeating carbohydrate units that are sulphated to varying degrees and include keratan sulphate, chondroitin sulphate and heparin sulphate.

Two examples of proteoglycans are decorin and biglycan. Decorin is comprised of a leucine rich 130 kDa protein core and a single chondroitin side chain, which is associated with fibrillar collagen. It is thought to have a fibril diameter limiting function. Biglycan is comprised of a 270 kDa core protein with two chondroitin side chains. Both decorin and biglycan have been found to bind to TGF-β but it is not yet proven as to how the activity of TGF-β is affected (Robey, 1996). Decorin and biglycan are known to inhibit bone cell attachment to the extracellular matrix by binding to fibronectin and preventing bonding with cells. The presence of these proteoglycans in the osteoid makes them potential candidates as nucleators for hydroxyapatite precipitation. However, it is thought that they mask the sites that will ultimately act as nucleators, and must be removed prior to matrix mineralisation (Robey *et al.*, 1995).

2.2.4.6 Glycoproteins

Glycoproteins, are carbohydrates attached to a protein core and have many functionally distinct, active domains. They may react with cell surface receptors, other matrix molecules or the mineral phase of bone. Examples of

glycoproteins are the adhesive glycoproteins: fibronectin, vitronectin, bone sialoprotein and the previously discussed osteocalcin, osteopontin and osteonectin (Robey, 1996).

Fibronectin is a multi domain, multi functional adhesive glycoprotein, which may assemble into fibrous networks in the extracellular matrix through interaction between cell surface receptors and the amino region of fibronectin molecule. Fibronectin can also bind to collagen, ensuring interaction between collagen and the fibronectin network. The most important activity of fibronectin is its interaction with cells, acting as the substrate for adhesion, spreading and cell migration.

Vitronectin is another molecule heavily involved in the attachment of cells, especially in-vitro, via integrins. However, vitronectin is also involved in the regulation of extracellular proteolysis, coagulation and complement factors.

Bone sialoprotein is involved in the attachment of osteoblast to the mineralised matrix via integrins.

2.2.4.7 Alkaline Phosphatase

Although this enzyme is not a structural matrix component, it is reviewed here as it is a glycoprotein.

This high molecular weight membrane bound enzyme attacks phosphate groups and possesses pyrophosphatase (a mineralisation inhibitor) and ATPase activity (Doty *et al.*, 1976). Magnesium is a known activator, although it is not an absolute requirement for enzyme activity. Magnesium and zinc ions are present as functional ions within the active site (Sowadski *et al.*, 1981).

Alkaline phosphatase is an enzyme long associated with mineralisation within bone and cartilage, however, the enzyme has been found in tissues which do not undergo mineralisation (Wuthier *et al.*, 1984) leading to doubts about its role in mineralisation. On the other hand, evidence that patients suffering from hypophosphatasia, a genetic deficiency in alkaline phosphatase activity, often suffer from severe rickets and/or osteomalacia (Wuthier *et al.*, 1984), again pointed to a connection between the enzyme and mineralisation. However, the specific role of alkaline phosphatase in the context of bone mineralisation is not known (Henthorn, 1996).

2.2.5 Bone Development

During foetal development, bone development occurs by one of two possible mechanisms: Intramembranous or endochondral ossification. The terms describe the tissues in which ossification, bone formation, occurs. Intramembranous ossification occurs within fibrous connective tissue while endochondral ossification occurs within hyaline cartilage

2.2.5.1 Intramembranous Ossification

The flat bones of the skull and mandible are examples of bones which form by Intramembranous ossification.

Embryonic mesenchyme condenses to form a membrane of randomly orientated collagen fibres. At the site of initial bone development, mesenchymal cells cluster together and differentiate, first into osteogenic cells then osteoblasts. The site of such a cluster is called a centre of ossification. Osteoblasts secrete the organic matrix of bone until they are completely surrounded by it.

The secretion of matrix ceases, then the cells, now called osteocytes, lie in lacunae and extend their narrow cytoplasmic processes into canaliculi. Calcium and other mineral salts are deposited and the matrix calcifies.

As the bone matrix forms, it develops into trabeculae that fuse with one another to form cancellous bone. Blood vessels grow into the spaces between trabeculae and the mesenchyme along the surface of the newly formed bone. Red bone marrow develops from the connective tissue associated with the blood vessels.

At the periphery of the bone, the mesenchyme condenses and develops into the periosteum. Eventually the surface layers of the cancellous bone are replaced with cortical bone. The majority of the bone is then remodelled as the bone matures into adult size and shape.

2.2.5.2 Endochondral Ossification

At the site of where bone formation is going to occur, mesenchymal cells group together in the shape of the future bone and then develop into chondroblasts. The chondroblasts secrete cartilage matrix, producing a cartilage model consisting of hyaline cartilage. The perichondrium, a membrane covering the cartilage model, develops.

As the cartilage model grows in length and diameter, chondroblasts in the mid-region bring about chemical changes which trigger calcification. This change causes the localised chondroblasts to die through malnourishment as the diffusion is slower through calcified tissue. The thin walls between adjacent lacunae break down forming small cavities. Concurrently, arteries penetrate the perichondrium and the newly formed bone, through a hole called nutrient foramen, in the mid-region of the cartilage model. As a result, osteogenic cells within the perichondrium are stimulated to develop into osteoblast which then lay down a thin shell of compact bone under the perichondrium, which is then called the periosteum.

Near the centre of the cartilage model, periosteal arteries grow into the disintegrating calcified cartilage. Capillaries stimulate the growth of a primary ossification centre, an area where bone tissue will replace most of the cartilage. Osteoblasts then deposit bone matrix over the remnants of the

cartilage, forming cancellous bone trabeculae. As the ossification centre moves to the ends of the bone, osteoclasts break down some of the newly formed trabecular bone, producing a cavity, the medullary cavity, which fills with red bone marrow. This is how the diaphysis, once a solid mass of hyaline cartilage, is replaced with cortical bone and red bone marrow.

When branches of the epiphyseal artery enter an epiphysis, a secondary ossification centre develops, in much the same way as a primary ossification centre develops.

One difference between the formation of bone in the primary and secondary ossification centres is that cancellous bone remains in the epiphysis, no medullary cavities are formed in the epiphysis. Also, hyaline cartilage is not fully replaced in the epiphysis; it covers it as articular cartilage and separates it from the diaphysis as the epiphyseal plate. Eventually, in early adulthood, the epiphyseal plate is replaced with bone. The new structure is known as the epiphyseal line.

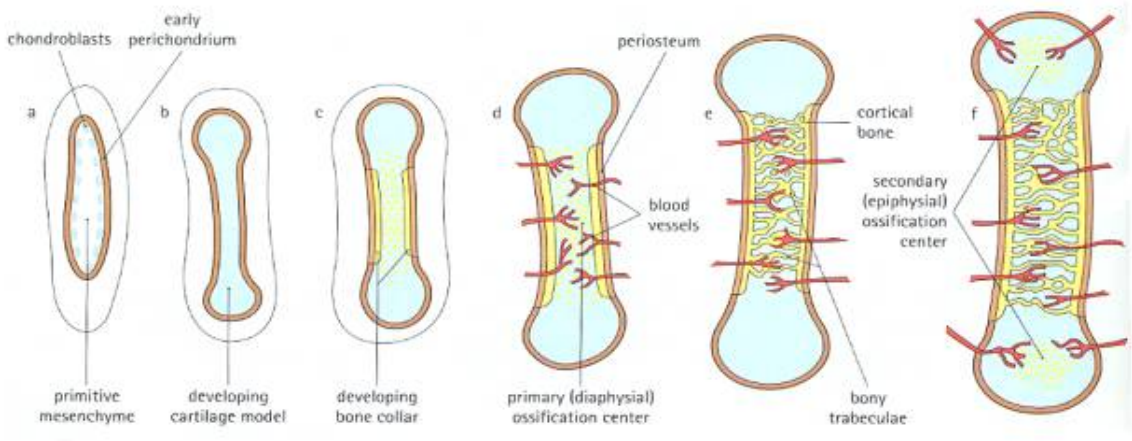

Figure 2.5 Endochondral ossification. Taken from (Seeley, 2000).

The site of osteoblast origin is known to have an effect on the proliferation and the levels and temporal expression of the phenotype. Osteoblasts were taken from two sites, the iliac crest and the mandible, per patient, to eliminate

the factor of age. Studies showed that alkaline phosphatase and osteocalcin expression were greater for the cells from the iliac crest, but proliferation was fastest for the osteoblasts of the mandible (Kasperk *et al.*, 1995). This was in direct contrast with studies performed elsewhere (McDougall, 2001). Here, comparisons between osteoblasts from the femoral head and the skull agreed with the results concerning alkaline phosphatase, but stated that the proliferation of the femoral head derived osteoblasts was greater than those from the skull. The most likely cause for the differences is the route of ossification of the bones of origin, with bones of the skull and mandible developing from intramembranous ossification, while the hip and femur develop via endochondral ossification.

In contrast to Kasperk, McDougall obtained skull and femoral head osteoblasts from different patients, which may explain why the two sets of results differed over proliferation.

2.2.6 Osteoblast Differentiation

The temporal expression of osteoblast phenotypic markers, such as type I collagen, alkaline phosphatase and osteocalcin, and proliferation has been studied by a number of groups (Aronow *et al.*, 1990; Owen *et al.*, 1990; Stein *et al.*, 1990; Stein *et al.*, 1996). It has been shown that osteoblasts exhibit three distinct stages of differentiation, proliferation, matrix maturation and mineralisation, figure 2.6 and that the up-regulation of the genes from one stage are accompanied by the down regulation of genes from the previous stage (Stein *et al.*, 1990; Stein *et al.*, 1996).

Proliferation involves cell growth and the deposition of type I collagen which forms the base of bone extracellular matrix. Collagen production continues throughout the differentiation sequence of osteoblasts, but at a decreasing rate. Other molecules produced in the proliferation stage are fibronectin, and TGF-β, which is involved in the regulation of extracellular matrix biosynthesis (Ramoshebi *et al.*, 2002).

Proliferation is followed by matrix maturation, during which the matrix is prepared for the deposition of the mineral phase of bone by alkaline phosphatase.

Markers for mineralisation are osteopontin and osteocalcin, which have been discussed previously.

There is some difference in opinion over which stage has which phenotypic markers. Osteopontin was initially allocated to the matrix maturation stage (Stein *et al.*, 1990), probably as it is down-regulated late in the osteoblast cell cycle. Later work by the same author has placed in within the mineralisation stage (Stein *et al.*, 1996), probably due to its synonymous rise with

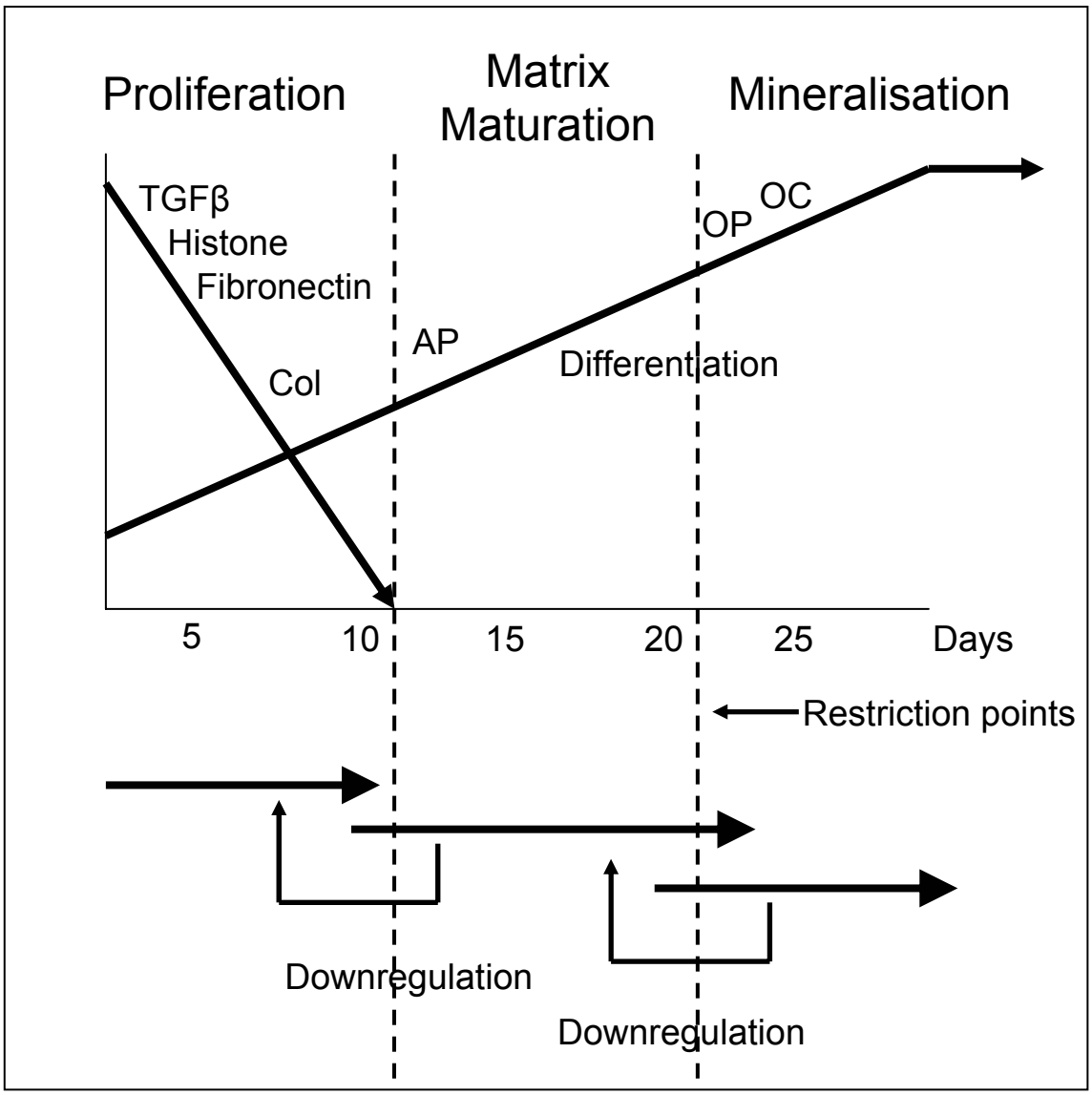

Figure 2.6 A model of the relationship between proliferation and differentiation during the osteoblast developmental sequence. Taken from (Woodruff, 2005), adapted from (Stein *et al.*, 1996).

osteocalcin. Owen et al, confusingly, have placed osteopontin in both the matrix maturation and mineralisation stage.

Proliferation of osteoblasts was shown to decrease as the cells terminally differentiate into matrix production. Levels of histone, which is a packaging protein associated with DNA to form chromatin (Matthews *et al.*, 2000), mRNA were seen to diminish upon the onset of differentiation (Stein *et al.*, 1989a; Stein *et al.*, 1989b).

The temporal expression of osteoblast phenotypic markers was shown to follow the sequence: alkaline phosphatase, osteocalcin then mineral deposits

(Aronow *et al.*, 1990). Further work linked the up-regulation of alkaline phosphatase and osteopontin with the down-regulation of proliferation, defining a distinct change in stage within the developmental sequence of the osteoblast (Stein *et al.*, 1990), as osteoblasts were thought to leave the proliferation stage and enter the matrix development/maturation stage. The inhibition of DNA synthesis in actively proliferating, sub confluent, osteoblasts by treatment with hydroxyurea, resulted in the four fold increase of alkaline phosphatase mRNA levels an hour later (Owen *et al.*, 1990). However, the forced down-regulation of proliferation does not induce the production of osteocalcin, implying the existence of a further stage within osteoblast differentiation.

2.3 *In Vitro* Osteoblast Adhesion to Biomaterials

Within the biomaterial domain, the term adhesion covers two distinct phenomena: the attachment phase which occurs rapidly, involving short term effects such as physicochemical linkages between cells and materials and the adhesion phase that occurs over a longer period and involves extracellular proteins, cell membrane proteins and cytoskeleton proteins (Anselme, 2000).

The extracellular matrix of bone is comprised of many organic molecules, including collagen, osteocalcin, proteoglycans and osteopontin. All of these molecules are synthesised by osteoblasts and most are involved in cell adhesion. *In vitro*, other proteins such as fibronectin and vitronectin have been shown to be involved in *in vitro* osteoblast cell adhesion (El-Amin *et al.*, 2003).

However, cells do not adhere to a naked material either *in vitro* or *in vivo*. Upon implantation or *in vitro* testing, the material is conditioned by biological fluid components from either tissue fluid or serum respectively (Boyan *et al.*, 1996).

Experiments using patterned surfaces obtained by photolithography have shown differentiated adsorption of serum proteins on charged or uncharged surfaces, where cell adhesion only occurred on the charged surfaces. The importance of vitronectin absorption for *in vitro* cell adhesion has been established, sera depleted of this protein greatly reduced cell attachment and spreading on surfaces which were charged. The presence or absence of fibronectin was reported to have no effect on cell adhesion (Thomas *et al.*, 1997).

In order to determine which proteins are involved in cell adhesion, primary human osteoblasts have been cultured on dishes coated with extracellular matrix proteins. In one such experiment, osteoblasts were reported to adhere preferentially to fibronectin as compared to type I, type IV collagen and vitronectin but weakly to laminin and type V collagen (Gronthos *et al.*, 1997).

Some of the proteins involved in osteoblast adhesion, for e.g. fibronectin, vitronectin and type I collagen, possess an Arg-Gly-Asp (RGD) peptide sequence which is specific to the fixation of cell membrane receptors such as integrins. RGD peptide coated surfaces were demonstrated to induce significantly higher calvarial cell adhesion, as deduced by radial flow, compared to a RGE (Arg-Gly-glu) peptide coated surface (Rezania *et al.*, 1997). Elsewhere, synthesised RGDS (Arg-Gly-Asp-Ser) and GRGDS peptides in culture medium were demonstrated to partially inhibit attachment of osteoblasts to vitronectin in a competitive manner (Puleo *et al.*, 1991; Grzesik *et al.*, 1994). Demonstrating that osteoblasts bind to vitronectin via the RGD peptide sequence.

The sites of adhesion between cultured cells and the adsorbed protein substrate surfaces are called focal contacts or adhesion plaques. The extracellular face of focal adhesions present specific receptor proteins, such as integrins, while the cytoplasmic face involves proteins such as talin, paxillin, vinculin and tensin which are involved in mediating interactions between actin filaments and integrins (Anselme, 2000). Many proteins such as protein kinases, phosphatases and signalling molecules are colocalised with vinculin and talin, and are involved in signal transduction.

The primary adhesive proteins in osteoblasts are integrins which are involved in cell-substrate adhesion. Cadherins are also produced by osteoblasts but they are involved in cell-cell adhesion.

Integrins are heterodimers composed of two transmembrane glycoproteins, an α sub unit and a β subunit. There are 16 known α subunits and 8 known β subunits (Anselme, 2000), all of which contain disulfide bridges to protect them from proteolysis (Siebers *et al.*, 2005). The extracellular regions of the two subunits interact with each other to form a specific ligand binding region. Different combinations of subunits have different binding affinities for different molecules, for a review see (Anselme, 2000), e.g. the $\alpha_v\beta_1$ heterodimer is produced by cultured osteoblastic cells and known to bind to fibronectin and vitronectin.

All integrins contain divalent cation binding domains which are required for cell-matrix adhesion through regulated interactions with ligands (Xiong *et al.*, 2001). Magnesium (Michishita *et al.*, 1992; Lee *et al.*, 1995) and calcium (Ajroud *et al.*, 2004) are known to form part of the structural integrity of integrins and are important in metal ion dependant adhesion sites (MIDAS) which binds protein ligands. This may be due to the effect of Ca^{2+} on the regulation of integrin interactions with their ligands. Ajroud *et al* stated that magnesium was found to facilitate the interaction of integrins with their protein ligands while mM levels of calcium inhibit this interaction, although low levels of calcium (μM) were stated to support ligand binding (Calderwood *et al.*, 1997).

Groups have previously attempted to take advantage of the calcium or magnesium requirement of integrins by ion implanting these cations into titanium (Nayab *et al.*, 2005) and alumina (Howlett *et al.*, 1994) respectively.

Ion implantation of magnesium into alumina was reported to significantly enhance the attachment and spreading of human bone derived cells compared to alumina alone. Calcium ion implantation into titanium was reported to enhance MG63 osteosarcoma spreading while inhibiting cell attachment, after prolonged culture cell adhesion was significantly greater than the control titanium surface.

If the interaction between integrins and the extracellular matrix is disrupted, e.g. by the addition of specific antibodies, osteoblast differentiation and mineralisation will not occur. This is especially true for integrins which involve the binding of the ligands collagen and fibronectin. The interaction between extracellular ligands and integrins is necessary for the expression of osteoblastic genes, however, this signal transduction pathway is not yet fully understood (Franceschi, 1999).

2.4 *In vitro* Biocompatibility Testing

In vitro testing of biomaterials is used to provide rapid and relatively inexpensive data on the biological interaction of materials with cells, compared to *in vivo* testing. However, the question of how the *in vitro* data correlates with the much more complex *in vivo* system must be addressed. For example, TCP, surface modified polystyrene, will readily allow attachment and the growth of most mammalian cells *in vitro* while untreated polystyrene will not. Yet when implanted, these two materials elicit an almost identical response with only a thin foreign body capsule (Ratner, 2004). Hence the results of *in vitro* testing do not provide information relevant to the implant situation.

So why perform *in vitro* testing? Primarily, *in vitro* testing minimises the use of animals, a worthy goal, but is also required by most regulatory agencies in the device approval process for clinical application. *In vitro* testing also provides useful insights as to whether a device needs further evaluation in expensive *in vivo* experimental models (Ratner, 2004).

Generally speaking, there are two types of cells which may be used for *in vitro* testing. They are either primary cells that have been recently isolated from tissue or cell lines which have been developed especially for cell culture. Cell lines are the most popular as they possess greater reproducibility within assays, reducing variation. Cell lines are the *in vitro* equivalent of inbred animal lines used for *in vivo* testing, which maintain their genetic and morphological characteristics over a long time span (Northup, 2004). However, these cells have undergone some dedifferentiation and have lost receptors and metabolic pathways. For example, MG63 osteosarcoma cells are a commonly used cell line, which do not produce the mineral phase of

bone, unlike primary osteoblasts (Richards, 2004). Primary cells are used as no dedifferentiation has taken place, but much greater biological variation is present. For example, osteoblasts taken from different sites around the body, namely the femoral head, skull and clavicle, have been shown to possess significantly different rates of proliferation and phenotypic expression (McDougall, 2001). Primary osteoblasts only have a finite useful life span, approximately 10-100 days after the 'birth' of the cell, osteoblasts will lose their functionality (Parfitt, 1995).

2.4.1 *In vitro* Cytotoxicity Assays

Three types of cell culture assays are used to evaluate the cytotoxic potential of materials: direct contact, where test materials are placed on top of a confluent cell layer; agar diffusion, where a confluent cell layer is coated with agar and test materials are placed on top of the layer to assess possible diffusion of toxins; and elution, where an extract of the material is dissolved and exposed to a confluent cell layer (Northup, 2004). These tests all rely on morphological analysis of cells post testing to evaluate their biocompatibility, their disadvantages are listed in table 2-1:

Direct Contact	Agar Diffusion	Elution
Cellular trauma if material moves	Requires flat surface	Additional time and steps
Cellular trauma with high density materials	Solubility of toxicant in agar	
Decreased cell population with highly soluble toxicants	Risk of thermal shock when preparing agar overlay	

Table 2-1 The disadvantage of the direct contact, agar diffusion and elution methods of cytotoxic analysis (Northup, 2004).

These tests must be standardised to allow valid comparison of the results. Variables include the number of cells seeded, growth phase of cells, cell type, duration of exposure, test sample size and surface area of the samples to be tested (Northup, 2004). This is especially true when the amount of toxic extract is close to the threshold value and a small change in sample size could change the result from non toxic to moderate or severe toxicity (Northup, 2004).

In addition to these methods, new biochemical assays have been developed which are faster, easier and more accurate as they do not rely on microscopy. MTT and Alamar blue are the most popular biochemical assays which assess not only the cytotoxicity of materials but also the proliferation of cells seeded upon them by quantifying the metabolic activity of the cells, for a detailed comparison see (Hamid *et al.*, 2004). MTT is the older of the two and has been modified since its initial development (Mosmann, 1983). This assay is based upon the transformation of tetrazolium salt by mitochondrial succinic dehydrogenases in viable cells to purple formazan crystals that are not soluble in aqueous solution (Bernas *et al.*, 2002; Hamid *et al.*, 2004). Alamar blue, which has been available for over a decade (Fields *et al.*, 1993), is a sensitive oxidation-reduction indicator that fluoresces and changes colour upon reduction by living cells. Its reduction is thought to be mediated by mitochondrial enzymes (O'Brien *et al.*, 2000), but more recent data has suggested cytosolic enzymes also contribute to the reduction of the dye (Gonzalez *et al.*, 2001). Of the two assays, Alamar blue is gaining more popularity as it is a simpler and quicker test which, unlike the MTT test, is non toxic to cells and does not necessitate killing them to obtain measurements (O'Brien *et al.*, 2000).

With all of the previously described assays, it is only possible to deduce whether the cells are metabolically active and/or proliferating. Further assays need to be performed analysing the production of proteins present in each of the three phases of osteoblast differentiation (Stein *et al.*, 1996) to understand how the material affects the cell cycle.

2.4.2 Previous Cell Culture studies on Phosphate Glass

The ternary phosphate system containing calcium and sodium is the most common phosphate glass series investigated with *in vitro* analysis (Uo *et al.*, 1998; Salih *et al.*, 2000; Gough *et al.*, 2003; Bitar *et al.*, 2004). Uo *et al*, 1998, used human pulp cells in a direct contact cytotoxic assay, which was quantified with Alamar blue, to assess glass powders. It was found that increasing the calcium content decreased the cytotoxicity. These studies were accompanied by light microscopy but no attempt was made to investigate the long term effect of glass particles on cells.

Salih *et al* studied calcium/sodium phosphate glass using elution tests involving MG63 and human osteosarcoma (HOS) cells. As well as MTT cytotoxic testing, the affect of the glass upon the expression of BSP, ON and fibronectin (FN) was studied using ELISA. The highly soluble glasses with lower calcium concentrations caused some inhibition of growth and bone antigen expression, while extracts from the more durable glasses with higher levels of calcium upregulated proliferation and expression of BSP, ON and FN. No testing post 5 days was performed, and no markers of the matrix maturation or mineralisation phases were studied.

Elsewhere, osteosarcoma cells were cultured on the surface of phosphate glass that contained calcium and sodium (Bitar *et al.*, 2004). Morphology and cell number were studied using SEM and the CyQuant cell proliferation assay kit, respectively. Fluorescence immunocytochemistry was employed to identify BSP, ON and OP. The most durable compositions supported greater proliferation and BSP, ON and OP were detected. No tests were conducted for longer than seven days and quantification of the proteins studied was not performed.

Franks *et al* studied the effect of exchanging calcium for magnesium in sodium phosphate glass. Elution tests were performed using MG63 osteosarcoma cells and quantified with the MTT cytotoxic assay. No real difference was observed over a five day period. No attempt was made to assess any morphological changes or the production of osteoblastic markers.

All of the previous cell culture studies were short term despite the fact that the final material applications were medium to long term. Some studies looked at the production of particular osteoblast phenotypic markers but with the exception of OP these are all produced early in the osteoblast cell cycle. No products of the matrix maturation or mineralisation phase were investigated.

Conversely work performed by Gough *et al.*, 2003 looked at the long term culture (28 days) of CFCs seeded on to calcium/sodium phosphate glass surfaces. As well as investigations of cell morphology and proliferation, collagen, ALP and calcium deposits were studied. This demonstrated how osteoblasts cultured on these glasses progress through all the temporal stages of the osteoblast differentiation cell cycle.

2.4.3 The Need for Immunological Testing

Unlike transplants, implanted biomaterials are generally not 'rejected'. Organ rejection denotes a specific immune response which causes tissue death while synthetic biomaterials comprise non specific inflammation. While injury (i.e. the surgical procedure) initiates the inflammation, it is mediated by plasma, cells or the injured tissue. There are many chemical mediators, including, but not limited to histamines, cytokines (such as IL-1β), growth factors and oxygen derived free radicals (such as H_2O_2) (Schoen, 2004).

As well as inflammation, a foreign body reaction may occur (Anderson, 2004). Central to this foreign body response are macrophages, which attempt to phagocytose the implant, with varying success. However, the macrophages become activated during this frustrated phagocytosis with the biomaterial, and may secrete various cytokines (e.g. prostaglandin, TNF-α and IL-1β) which stimulate inflammation or fibrosis as well as the release of enzymes (exocytosis) (Schoen, 2004). These enzymes, while critical in the destruction of micro organisms, damage the extracellular environment and surrounding tissue.

As such, it is important to have some understanding of the possible immune reaction the implanted material may cause. To try and answer this, macrophages, as the initiators of the non specific immune response, were cultured on the biomaterial and studied for any sign of activation such as specific cytokine release and oxygen derived free radicals.

To the knowledge of the author, only two studies involving macrophages cultured on phosphate glass have been published (Gough *et al.*, 2002; Parsons *et al.*, 2004b). These studied involved iron/sodium and calcium/sodium

phosphate glasses respectively. Both groups investigated the morphology of macrophages cultured on the glass surface as well as the possible production of IL-1β and H_2O_2. Both groups reported that macrophages cultured on phosphate glass did not produce IL-1β and cells did not adopt spread morphology, but slightly elevated levels of H_2O_2 compared to the negative control were observed

2.5 Phosphate Glass

2.5.1 Historical Overview

Man has been producing glass for thousands of years, and making use of it for even longer. Obsidian, glass made from sand melted by the intense heat of a volcanic eruption, was used by man as spear tips.

Glass was first created by the Egyptians in the form of beads from about 4000 BC. It was not until 1500 BC that the first hollow glass container was made by covering a sand mould with a layer of molten glass.

Glass manufacture spread over Europe and the Middle East with the expansion of the Roman Empire from about 200 BC. However, it was not until the collapse of the Roman Empire from 350 AD when glass making skills that were closely guarded were able to spread to the local populations. During the fourth crusades, glass manufacture was advanced by the Venetians with the production of intricate and complex glass artefacts after the influx of Islamic glass art in 1204.

Towards the end of the seventeenth century, lead was introduced into the glass by George Ravencroft, in an attempt to reduce the clouding effect which

sometimes occurred in blown glass. This glass was softer and easier to decorate and had a higher refractive index, this proved invaluable to the optical industry, allowing the development of astronomical telescopes, microscopes and good quality mirrors.

During the late nineteenth century there was an acceleration in technological developments in glass by Faraday, Zeiss, Abbe and Scott to name a few. Their primary interest lay in glasses for optical use.

Arguably the greatest technological advancement in the glass industry occurred in the 1950's when Sir Alistair Pilkington introduced the float glass manufacturing process. This allowed the large scale production of perfectly flat glass for such applications as windows. Today 90 % of all flat glass is made using Pilkington's float glass technique.

Phosphate glass has been researched for over one hundred and fifty years (Graham, 1833), however, despite P_2O_5 being one of the four classic Zacarhiason glass forming oxides (along with SiO_2, GeO_2 and B_2O_3), the nature of the glass, its applications, research and development have been limited due to its hygroscopic nature. It was not until the addition of at least 30 mol.% of metal oxides was found to significantly improve the durability of the glass that possible applications of the glass were actively pursued (Van Wazer *et al.*, 1950).

2.5.2 Applications of Phosphate Glass

As research into phosphate glasses improves the understanding of these materials and the ways to control their properties, more and more applications

are being considered. A small selection of these non-medical applications are discussed below.

Different compositions of phosphate glasses have been researched with the goal of vitrifying nuclear waste. Recently, iron phosphate glass has come to the forefront of this application as a possible solution. Currently, only borosilicate glass has been approved by the U.S. Department of Energy to vitrify high level nuclear waste. A group led by Delbert Day has developed an iron phosphate glass with good chemical durability, which is able to accept both more types of nuclear waste and up to six times more nuclear waste per unit volume than borosilicate glasses (Mesko *et al.*, 2000; Huang *et al.*, 2004a; Huang *et al.*, 2004b; Kim *et al.*, 2004; Huang *et al.*, 2005).

Phosphate glasses containing fluoride, which have been doped with rare earth ions, have shown great promise for optical and laser applications due to their low absorption at particular frequencies, see for e.g. (Ebendorff-Heidepriem *et al.*, 2000; Philipps *et al.*, 2001; Ebendorff-Heidepriem *et al.*, 2002a; Ebendorff-Heidepriem *et al.*, 2002b; Philipps *et al.*, 2002).

Phosphate glasses are also attractive as glass-metal seals due to their low melting temperature, low viscosity and high thermal expansion coefficients (Wei *et al.*, 2001).

The lack of durability of some phosphate glasses was utilised to find a cure for trace element deficiencies in cattle and sheep (Allen *et al.*, 1978; Allen *et al.*, 1984; Allen *et al.*, 1985)

2.5.3 Glass in General

This section was composed to give an overview of glass science, including what a glass is and the popular parameters used to characterise it.

Glasses have been defined a number of ways by many authors, its definition changing as research progresses and pushes back the boundaries of glass science. A definition by Shelby seems to be the most appropriate: "an amorphous solid completely lacking in long range, periodic atomic structure and exhibiting a region of glass transformation behaviour".

2.5.3.1 Glass Structure Theory

A simple theory on glass structure proposed by Goldschmidt, stated that glasses of the formula R_nO_m form most easily when the ionic radius ratio of the cation to the oxygen atom were between 0.2-0.4, reference taken from (Shelby, 1997). Since these ratios tend to produce tetrahedrally coordinated cations, it was proposed that only these structures can form glasses.

Later work by Zachariasen, proposed that glass formation may occur if an open network of oxygen tetrahedra or triangles with sufficient bonding to produce a continuous network structure exists (Zarhariasen, 1932). Additions of alkaline or earth alkaline cations were placed in the hollow spaces within the structure without forming any chemical phase. According to this theory, any metal or non metal oxide should form a glass. However, the non existence of TiO_2 or Al_2O_3 could not be explained with this theory.

A refinement of the theory was proposed, focusing on the cooling process (Hagg, 1935). It was stated that glasses consist of chains or two dimensional

nets. The symmetry and bulkiness of the glass forming units above the melting temperature were thought to be responsible for the glass forming capacity. This theory explained why species like SiO_2 formed a glass while TiO_2 and Al_2O_3 did not.

Bond strength has also been used in an attempt to predict the ease of glass formation. It was argued that strong bonds prevent the reorganisation of the melt structure into a crystalline structure during cooling, promoting glass formation (Sun, 1947).

2.5.3.2 Glass Formation

Glass formation usually takes place by rapidly cooling a molten mass past the glass crystallisation point with solidification at the glass transformation range, a.k.a. the glass transition point. The glass transition temperature is the temperature above which the glass solid starts behaving like a viscoelastic solid. It is normally described on the basis of either enthalpy or volume versus temperature diagrams, figure 2.7. The cooling of a melt to any temperature below the melting temperature (T_m) would normally result in conversion to the crystalline state, with an abrupt decrease in enthalpy. Further cooling would result in a continued decrease in enthalpy due to the heat capacity of the crystal. If a melt cools without crystallisation, then a supercooled liquid is obtained. Enthalpy continues to decrease due to the decreasing amplitude of atomic vibrations and structural rearrangement. As the melt continues to cool, the viscosity becomes high, so that atoms cannot completely rearrange to the equilibrium structure during the time allowed by the experiment, and the enthalpy begins to deviate from the equilibrium line,

following a curve of gradually decreasing slope until it becomes determined by the heat capacity of the frozen liquid. The temperature lying between the limits where enthalpy is that of a super-cooled liquid and that of a frozen solid is the glass transformation temperature. Since the temperature at which the enthalpy departs from the equilibrium is controlled by the viscosity of the supercooled liquid, use of a slower cooling rate will allow the enthalpy to follow an equilibrium curve to a lower temperature. The T_g will shift to a lower temperature accordingly.

If a fast cooled glass is held at a temperature a little below the T_g, then the enthalpy will decrease until it hits the extrapolation of the supercooled liquid line, as the glass continues to compact, then continue to decrease at the same rate as previously. The structure of the glass reaches an equilibrium configuration, albeit a meta-stable configuration.

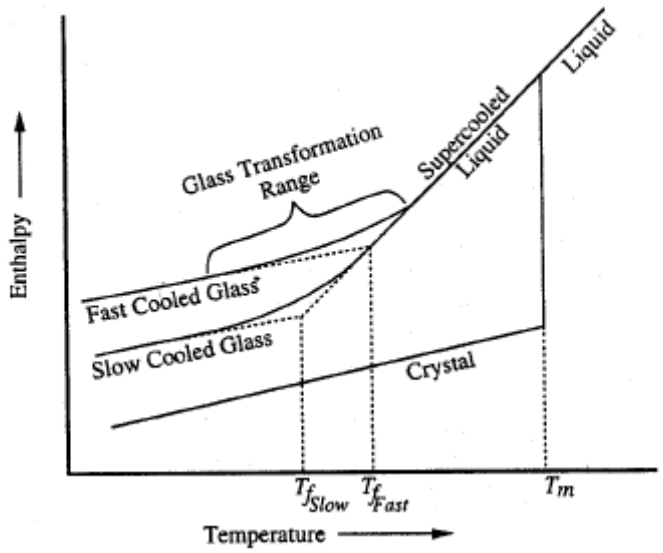

Figure 2.7 The effect of temperature on the enthalpy (or volume) of a glass forming melt. Taken from Shelby 1997.

2.5.3.3 Devitrification (crystallisation)

The term crystallisation actually refers to a combination of two processes, namely nucleation and crystal growth. Nucleation can be either homogeneous, spontaneous nuclei formation within the melt, or heterogeneous, forming at a pre-existing surface such as an impurity or the crucible surface. If no nuclei are present then crystal growth cannot occur and the material will form a glass. Even if some nuclei are present, but no growth has occurred, their extremely small size and low volume fraction prevents detection, so for all practical purposes the material is a glass.

Crystal growth and nucleation occur at temperature ranges below the melting point of the glass. There exists an overlap between the two, with crystal growth occurring at a higher temperature range than nucleation. The temperature range where the overlap occurs must be passed through quickly upon cooling of the glass to prevent the formation of large crystals.

2.5.4 Phosphate Glass Structure

Phosphate glasses are inorganic polymers based upon the tetrahedral phosphate anion, figure 2.8, which results from the formation of sp^3 hybrid orbitals by the phosphorus outer electrons ($3s^2 3p^3$). The fifth electron is promoted to the 3d orbital where strong π-bonding molecular orbitals are formed with oxygen 2p electrons, see, e.g. (Cruickshank, 1961; Mitchell, 1969), with charges balanced by polymerisation or the presence of metallic ions.

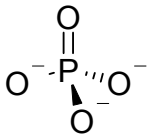

Figure 2.8 The tetrahedral phosphate anion, charges are balanced by either polymerisation or metal cations.

In the absence of cations, these tetrahedra link via covalent bridging oxygens to form various phosphate anions, figure 2.9.

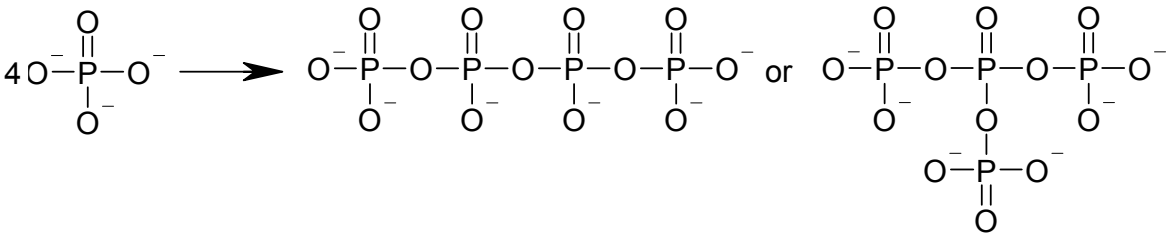

Figure 2.9 Polymerisation of the phosphate anion gives rise to various polyphosphate anions linked via oxygen bridges which may be branched or linear or a combination of the two.

The tetrahedra are classified using the Q^i terminology originally devised for silicon glasses, e.g. (Lippmaa *et al.*, 1980) but has been applied to phosphates (Van Wazer, 1958), where i represents the number of bridging oxygens per tetrahedron, figure 2.10.

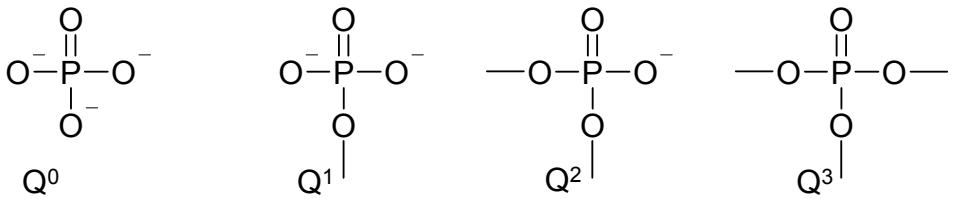

Figure 2.10 The four type of Q^i species found in condensed phosphates, where i is the number of bridging oxygens present within a particular phosphate tetrahedron.

The prevalence of any particular Q species is dependant on the cation content of the glass composition. If a charge on an oxygen atom is balanced by a cation then it will not be possible for an oxygen bridge to form (Martin, 1991). If phosphorus pentoxide, without any cation additions, is heated, then the Q^3 species will be the only phosphate group present forming a highly cross-linked phosphate network. The addition of metal cations, so that $[M_2O] = [P_2O_5]$ (where M is any mono-valent cation, e.g. Na^+, K^+ or Li^+), will make Q^2 the only species present, hence produce non-branched phosphate chains, theoretically of infinite length (Van Wazer, 1958). When there is one positive charge for every phosphate anion, hence when theoretically infinite phosphate chain lengths are possible, then these phosphates are named meta-phosphates. The addition of any more M_2O will introduce terminating Q^1 species, decreasing the theoretically possible chain length (Van Wazer, 1950a). When the concentration of M_2O is twice that of P_2O_5, the terminating Q^1 species is dominant. As this anion can only form one oxygen bridge it is termed a chain terminator, producing only phosphate dimers, or pyrophosphates, when it is the only species present (Van Wazer, 1958). When the concentration of M_2O is at least three times higher than that of P_2O_5 then the non-bridging Q^0 species, a.k.a. orthophosphate, is dominant. Of course, concentrations of metallic cations between these limits would create a distribution of Q species. This information is expressed diagrammatically in

figure 2.11. Generally, all non-branched phosphate glasses with the exception of meta-phosphates are known as polyphosphates.

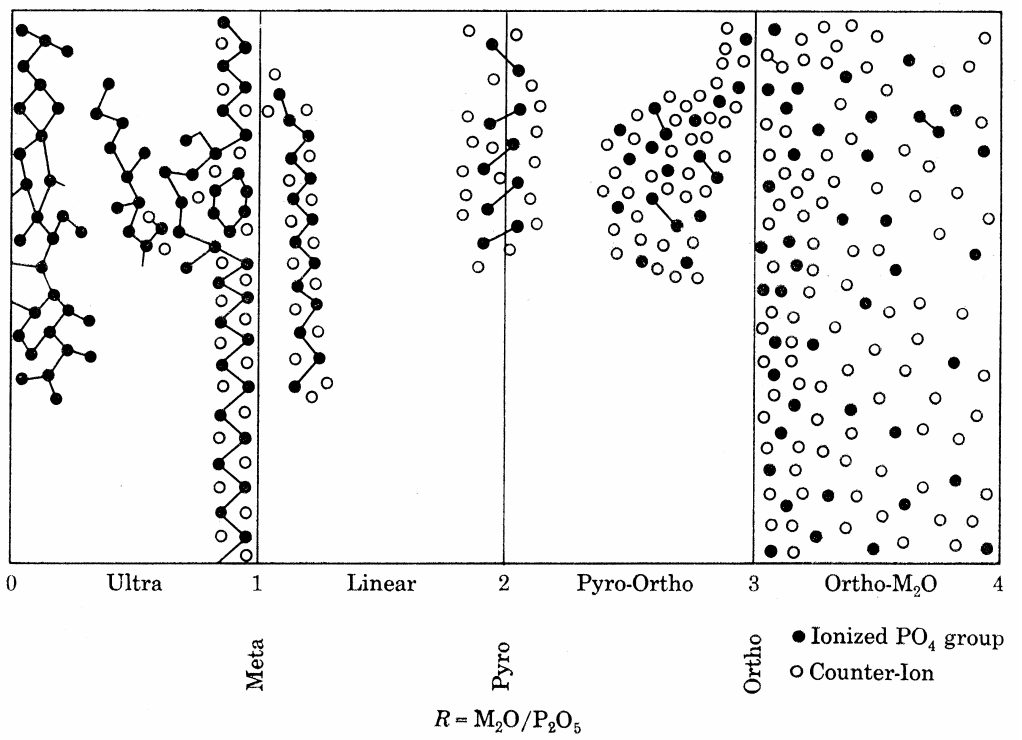

Figure 2.11 Schematic phosphate structures as a function of composition, note that linear phosphates are also known as polyphosphates. Taken from (Van Wazer, 1958).

Polymerisation of phosphates occurs in the absence of or low concentration of metallic cations, however, the addition of higher numbers of metal cations results in the inhibition of phosphate polymerisation. This occurs as the number of bridging oxygens available per phosphate anion decrease. It should be noted that contamination with water is a problem when making phosphate glasses. Water is considered in a similar manner to alkali oxide as it reduces the polymerisation by the formation of hydroxyl groups (Brow *et al.*, 1990b).

2.5.4.1 Ultra-Phosphate Glasses

Ultra-phosphate glasses possess compositions in the range 0<x<0.5 where x is the mol.% of metal oxide, and are defined by the presence of Q^3 tetrahedra but may also contain Q^2 species.

Because of their volatility and preparation difficulty, very little information is known about the structure of ultra-phosphates. However, Raman spectroscopy was performed upon vitreous phosphate glass (P_2O_5 only) and the spectra compared to that of POF_3 and PF_5 (Galeener *et al.*, 1978; Galeener *et al.*, 1979). The presence of a PO double bond was confirmed as POF_3 is known to possess this bond while PF_5 does not. A second conclusion from this study was the assignment of a second peak to the symmetrical stretching of POP bridging oxygens. Hence it was concluded that vitreous phosphates consisted of a three dimensional network of corner sharing PO_4 tetrahedron that contain three bridging and one non-bridging oxygen atoms, Q^3 species. Neutron diffraction studies identified two bonds that were 14.32 nm and 15.81 nm in length, these were assigned to double and single bonded oxygen atoms respectively (Hoppe *et al.*, 2000), supporting the results of Galeener *et al*. The peak area for the single bonded oxygen is three times larger than that of the double bonded oxygen, supporting Galeener's conclusions.

The fractions of Q2 and Q3 species are given by the following equations, (Van Wazer, 1958):

$$f(Q^2) = \frac{x}{(1-x)} \qquad \textit{Equation 2.1}$$

$$f(Q^3) = \frac{(1-2x)}{(1-x)} \qquad \textit{Equation 2.2}$$

Where x is the mol.% of metal oxide within the system.

The evolution of a cross-linked Q^3 network to the chain-like Q^2 network of a meta-phosphate, figure 2.12, is confirmed by ^{31}P NMR spectroscopy of sodium phosphate glasses (Kirkpatrick *et al.*, 1995). Identification of Q species was achieved and an increase in the Q^2 peak at the expense of the Q^3 peak was observed as the Na_2O concentration increased from 5 mol.% to meta-phosphate composition.

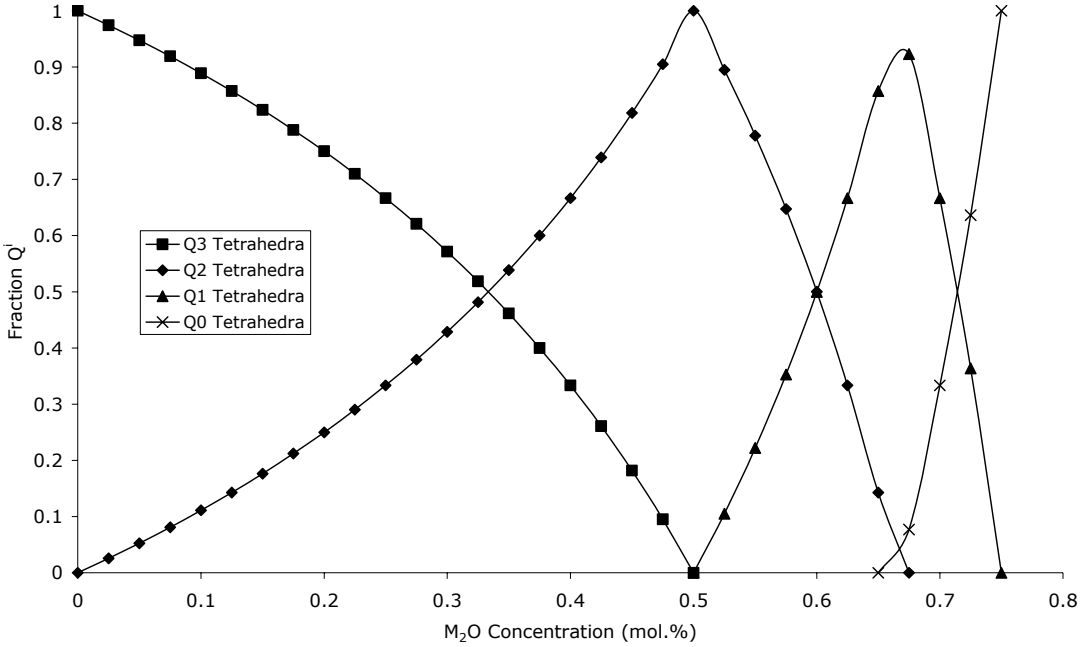

Figure 2.12 Graphical representation of the relationship between the proportion of Q^0, Q^1, Q^2, Q^3 species in phosphate glass and the metal oxide concentration. Beyond 0.75 mol.% M_2O, orthophosphates only exist and the excess metal cations exist as unreacted metal oxide Adapted from (Van Wazer, 1958).

2.5.4.2 Meta and Poly-Phosphate Glasses

When the concentrations of M_2O or MO and P_2O_5 are equimolar, phosphate glass is composed only by Q^2 species and is termed meta-phosphate. Any other glass which possesses only linear phosphate chains but is not of this exact concentration is known as a polyphosphate. The relationship between the average linear chain length and the mol.% M_2O has been expressed mathematically by Van Wazer and Bunker *et al* in equation 2.3 and equation 2.4:

$$n_{av} = \frac{2(1-x)}{(2x-1)} \quad \textit{Equation 2.3}$$

$$n = \frac{2}{\left(\frac{M+2M'}{P}-1\right)} \quad \textit{Equation 2.4}$$

Where *n* is the number average chain length, *x* is the mol.% of metal oxide, *M* is the mol.% of monovalent cations, *M'* is the mol.% of divalent cations and *P* is the mol.% of phosphorus.

From the above equations, it can be seen that as the metal cation concentration increases the phosphate chain length decreases. When x or M+2M' is equal to 0.5 (the meta-phosphate stoichiometry) then the equations break down as n equals infinity.

Such chain lengths are not possible in practice due to contamination with water, inhomogeneity at the molecular level within the melt and the requirement of the starting materials to possess an R ratio between 1.000002 and 1.000000 for theoretical chain lengths of one million or more, which is extremely difficult considering the purity of most commercially available chemicals. Typical phosphate chain lengths are in the order of 40-100 phosphates (Griffith, 1995). Chain lengths of up to 400 can be achieved by crystallising the melt and re-melting to drive off the water impurities (Griffith, 1995). Chain lengths of 1000 or more achieved by driving off the water in alkaline earth meta-phosphates were reported elsewhere (Abe, 1983). In contrast, crystalline phosphates made from Kurroll's salt ($K_2O.P_2O_5$) reach chain lengths of 10,000 (Griffith, 1995).

The possibility of infinitely long chains at the meta-phosphate composition also assumes that there are no cyclic anions, which would reduce the average chain length. In general the fraction of cyclic anions is greatest at the meta-

phosphate composition and decreases with increasing metal cation concentration (Westman *et al.*, 1957).

As the phosphate network and chain length is limited by the inclusion of network modifying cations (Walter *et al.*, 2001), a network formed from the appearance of cross-links between terminal oxygen atoms bridged by cations is built up (Rouse *et al.*, 1978; Nelson *et al.*, 1979; Matic *et al.*, 1998). Mono-valent cations such as sodium have only a small effect on this network, however the addition of multi-valent cations such as Al^{+3}, Fe^{+3}, Mg^{+2} and Ca^{+2}, see for e.g. (Rinehart *et al.*, 1999; Mogus-Milankovic *et al.*, 2001; Franks *et al.*, 2002; Parsons *et al.*, 2004a; Parsons *et al.*, 2004b), provide iono-covalent cross-links which form the bulk of the cationic network. The strength of these cationic cross-links are controlled by the ionic field strength of the modifier cations, as the ionic field strength of the cation increases the bond between the cation and the non-bridging oxygen gains a more covalent character (Rouse *et al.*, 1978; Nelson *et al.*, 1979; Matic *et al.*, 1998). The directional nature of the covalent bond increases the rigidity of the network, which in turn affects the glass transition temperature (Eisenberg *et al.*, 1966). Thus the properties of the poly-phosphate glass are less dependant on the P-O-P bridges that form the phosphate chains compared to the P-O-M inter-chain cross-links (Brow, 2000).

The number of Q^2 and Q^1 species for a given metal oxide concentration (mol.%) may be predicted, figure 2.12, using the following equations:

$$f(Q^1) = \frac{(2x-1)}{(1-x)} \qquad \textit{Equation 2.5}$$

$$f(Q^2) = \frac{(2-3x)}{(1-x)} \qquad \textit{Equation 2.6}$$

Where x is the mol.% of metal oxide.

Early X-ray photoelectron studies suggested that a Q^2 tetrahedron is composed of one P=O and one $P\text{-}O^-M^+$ terminal oxygen bond, including the two bridging oxygen atoms, to give three oxygen species (Bruckner *et al.*, 1980). This was supported by deconvolution of the O 1s peak into three components representing the three oxygen species previously mentioned. However, *ab initio* studies of sodium phosphate glass have shown that, unlike Q^3, no distinction can be made between the double bonded oxygen atom and the non-bridging oxygen atom within the Q^2 tetrahedra and that the bond length of these identical oxygen atoms was significantly longer than that of the double bonded oxygen in the Q^3 tetrahedra (Uchino *et al.*, 1995b; Uchino *et al.*, 1995a). This is in agreement with previous Raman work on sodium phosphate glass (Brow *et al.*, 1994). Raman spectroscopy of phosphorus pentoxide and phosphate glass containing up to 50 mol.% Na_2O revealed two distinct peaks at 1380 and 1163 cm^{-1} which were assigned to P=O and 'terminating' oxygen respectively. As the sodium concentration is increased the P=O peak decreases and the terminating oxygen peak increases, the extremes of this range only show one of these peaks. This evidence suggest that the P=O bond is only present in ultra-phosphate, Q^3, tetrahedra and that the associated π bond is delocalised over both non-bridging oxygen atoms present in Q^2 phosphate tetrahedra. Given these results, the correct way to deconvolute the O 1s spectra from simple phosphate glasses would be to fit two peaks, one for bridging oxygen and the other for non bridging oxygen, as has been previously suggested (Gresch *et al.*, 1979).

Further work by Gresch *et al* detailed a simple method to quantify the ratio of Q_1 species to Q_2 species using the O 1s spectra obtained from XPS. Deconvolution of this spectrum reveals two peaks at 531 and 533 eV which

are assigned to the non-bridging and bridging oxygen atoms respectively. However, no attempt was made to deduce the phosphate chain length from this data. Since the theoretical number of bridging oxygen and non-bridging atoms can be deduced from the chain length using simple maths, then the ratio of BO to NBO can be calculated. By comparing this with the measured ratio, which was calculated using the areas under the BO and NBO peaks, an equation may be derived to calculate the phosphate chain length from XPS spectra. Since this technique is based upon the number of terminating oxygen tetrahedra, Q^1, per Q^2 tetrahedra, there will be greater error when the chains are longer, i.e. when the ratio approaches 0.5 which corresponds to meta-phosphates.

Other methods used to quantify the phosphate chain length include end group titration (Van Wazer, 1950b) and high performance liquid chromatography (Sales *et al.*, 1998).

The distribution of P-O bond lengths has been analysed with ^{31}P NMR spectroscopy and shown to vary more as the field strength of the modifying cation increases via peak broadening (Brow *et al.*, 1991; Kirkpatrick *et al.*, 1995). This trend was also observed in neutron diffraction studies (Hoppe *et al.*, 1995) and luminescence studies of Eu-doped meta-phosphate glasses, (Zhmyreva *et al.*, 1988). These neutron diffraction studies have also shown a decrease in the average P-O bond length (Hoppe *et al.*, 1995).

However, no comparison of chain lengths measured with different techniques for validation has been reported.

2.5.4.3 Nitrogen Containing Phosphate Glasses

So far the discussion on the modification of the phosphate network has focussed on the addition of metal cations which change the fraction of terminal oxygen atoms. However, there has been research into the possibility of substituting oxygen anions for nitrogen anions (N^{-3}). As a nitride anion is expected to be quite basic, it should readily attack the phosphate chain structure, but instead of downgrading the structure, it acts to create a three dimensional structure from the two dimensional chains (Martin, 1991).

Nitrided phosphate glasses are made by either melting phosphate salt under flowing dry ammonium (Marchand, 1983; Marchand *et al.*, 1988), or by re-melting pre-made phosphate glass under a flowing dry ammonium atmosphere (Brow *et al.*, 1988; Le Sauze *et al.*, 2000a; Le Sauze *et al.*, 2000b; Le Sauze *et al.*, 2001).

The incorporation of nitrogen into the phosphate chains of sodium meta-phosphate was confirmed via XPS, where it was found that the addition of nitrogen caused a decrease of 1 eV to 133.9 eV in the average binding energy of the P 2p peak, which is a result of the reduction in the average ionic charge on the phosphorus ions (Brow *et al.*, 1988). The presence of nitrates within the glass was disregarded as the N 1s binding energy would have been in excess of 402 eV, which was not observed. Nitrate formation had been suggested as a possible mechanism for nitrogen incorporation (Reidmeyer *et al.*, 1986).

The tri-valent nitrogen ions can replace either the bridging or non-bridging oxygen atoms; both give rise to cross-links between chains in poly-phosphates, figure 2.14 (Navarro, 1998). Within the XPS spectra of sodium

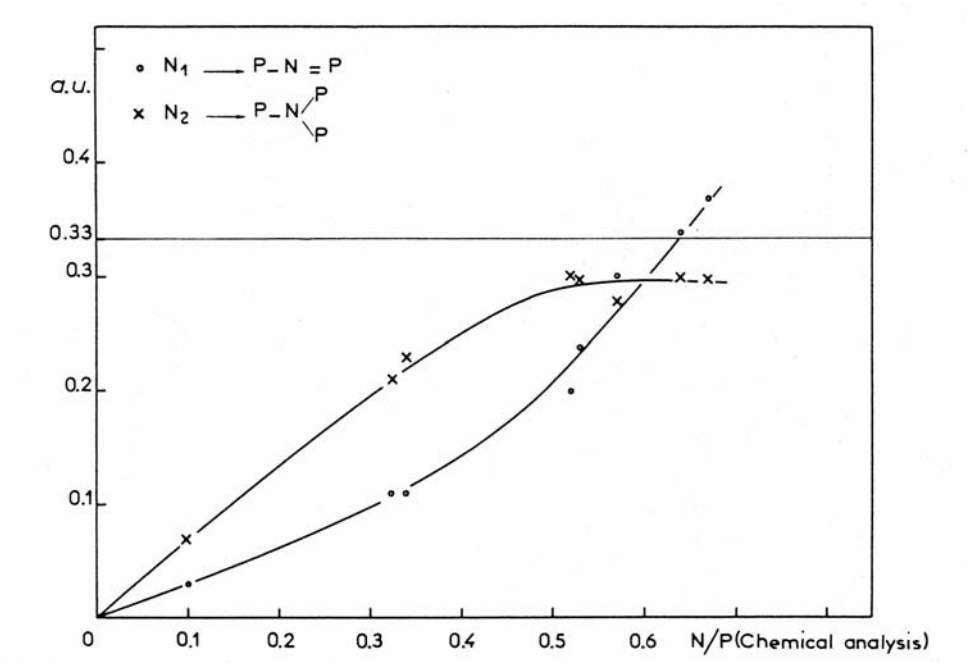

Figure 2.13 Respective areas of N_1 and N_2 parts within the N 1s spectra, as a function of total nitrogen, reproduced from (Marchand *et al.*, 1988).

phosphate glasses, the N 1s peak was deconvoluted into two peaks with binding energies of 397.9 and 399.4 eV (Brow *et al.*, 1988; Marchand *et al.*, 1988), which where assigned to NP_2 and NP_3 respectively, as shown in figure 2.14 (Marchand *et al.*, 1988). NMR studies have confirmed that nitrogen can be bonded to two or three phosphorus atoms (Bunker *et al.*, 1987). XPS was further utilised to show that the fraction of NP_3/P levelled out at 0.3 as the concentration of N is increased, while the fraction of NP_2/P initially lags before overtaking that of NP_3 (figure 2.13, Marchand *et al.*, 1988). Brow *et al*, 1988, used XPS to find that the number of bridging oxygen atoms decreased as the nitrogen concentration was increased, which was confirmed by others (Le Sauze *et al.*, 2000b), and that the NP_3 nitrogen species was formed in preference to NP_2, although the actual concentrations of nitrogen were not stated so that a comparison with Marchand *et al* was not possible.

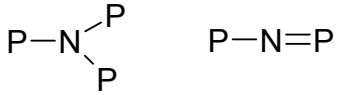

Figure 2.14 The two possible chemical states for nitrogen within the phosphate glass network.

The possibility of interactions between nitrogen and metal cations was previously disregarded due to the weak stability of the stability of the N^- M^+ bond, while the continued presence of oxygen anions serves to balance the positive charge of the cations (Marchand *et al.*, 1988), forcing the assumption that there is a maximum concentration of nitrogen possible. NMR studies of lithium sodium meta-phosphate glasses have indicated that the most nitrogen atoms which can be substituted into a phosphate tetrahedra are two to give PO_2N_2 (Le Sauze *et al.*, 2000b).

2.5.5 Glass Transition Temperature

Thermal analysis of glass reveals such properties as: glass transition temperature, crystallisation temperature and the melting point. Within the scope of the work performed here, only the glass transition temperature will be discussed.

2.5.5.1 Ultra-phosphate Compositions

The effect of cation addition to the vitreous phosphate network was studied via the thermal analysis of lithium ultra-phosphate glasses (Hudgens *et al.*, 1993). The addition of lithium to phosphorus pentoxide caused the T_g to decrease, then increase after 20 mol.% Li. The breakdown of the ultra-phosphate network, and hence formation of non-bridging oxygen, was deemed to be the cause of the fall in T_g. The cause of the rise in T_g was suggested to be two fold. As the cation concentration increases, the ultra-phosphate network is changed to a meta-phosphate long chain structure and the tortuosity of the chains increases the T_g. Secondly, the increase in cation mediated cross link density with cation concentrations of 33 mol.% or higher was suggested to contribute to the rise in T_g.

A similar study was performed with sodium oxide addition to phosphorus pentoxide (Suzuya *et al.*, 1998). The same decrease and increase after 20 mol.% Na_2O was observed. Again the decrease was associated with the destruction of the ultra-phosphate network and formation of non-bridging units, which is structurally studied in Brow *et al.*, 1994. However, the theory concerning chain entanglement was dismissed and it was suggested that the

increase in T_g was due to the ordering of PO_4 chain-like units around the cations and the aggregation of MeO_n polyhedra. Hence the deconstruction and reconstruction of the network is the cause of the T_g change.

Further work by Hudgens *et al* on lithium and sodium ultra-phosphate glass again confirmed the presence of a minimum T_g at 20 mol.% M_2O. However, in this report thermal analysis was accompanied by Raman spectroscopy. It was noted that the concentration of Q^2 tetrahedra increased at the expense of Q^3 tetrahedra, confirming that the decrease in T_g is due to the de-polymerisation of the ultra-phosphate network. With increasing cation content to levels above, it was shown that the delocalisation of π bonds resulted in longer P=O bonds and shorter, stiffer P-O-P bonds. The P=O delocalisation resulted in the formation of alkali oxygen bridges (Kreidl, 1983). This ionic interconnection of the network and a concomitant increase in the strength of the covalent interconnection was suggested to be the cause of the increasing T_g.

2.5.5.2 General Cation Effect on Tg

The effect of different cations added to the glass on the T_g was investigated, (Eisenberg *et al.*, 1966). Their results showed that the substitution of one cation for another of higher valence or smaller atomic radius, hence higher charge density, caused an increase in T_g. A plot of T_g versus q/a, where q is the ionic charge and a is the sum of the cation and oxygen radius exhibited a linear relationship. The order of effect was found to be: $Cs^+<Rb^+<K^+<Na^+<Li^+$ for the alkali elements and $Ba^{2+}<Sr^{2+}<Ca^{2+}<Mg^{2+}$ for the earth alkali elements (Hudgens *et al.*, 1998), as following the periodic table, with Al^{3+} possessing a higher T_g than all of the previous elements listed. These trends are supported

by work performed elsewhere, e.g. see (Shih *et al.*, 1998; Hiki *et al.*, 1999; Zhou *et al.*, 2000; Karabulut *et al.*, 2001; Metwalli *et al.*, 2001; Mogus-Milankovic *et al.*, 2001; Montagne *et al.*, 2001). An increase in T_g when the cation is changed for one with a higher valence is thought to increase the total possible number of phosphate chain cross links, giving a more cross-link dense network (Kreidl, 1983; Hudgens *et al.*, 1998). The effect of higher field strength, or charge density, was thought to impart a greater covalent character on the cation/phosphate cross links, the directional nature of the covalent bonds giving a stiffer network with a correspondingly higher T_g.

2.5.6 Dissolution of Phosphate Glasses

The first systematic study of phosphate glass dissolution was performed by Bunker *et al* where phosphate glasses containing calcium and sodium were studied. Substitution of sodium for calcium decreased the dissolution rate. It was found that glasses dissolved uniformly with two distinct stages. The initial stage was a $t^{1/2}$ stage followed by a stage where dissolution is linear with time. The first stage is said to be controlled by an ion exchange process within the hydrated layer. When chains are entirely surrounded by water, they can then disentangle from partially hydrated chains and dissolve into solution. Once the hydrated layer is constant then dissolution is linear with time. This is questioned by Delahaye *et al* who performed the same tests but concluded that the $t^{1/2}$ law was in fact due to the ionic strength of solution increasing as dissolution proceeds and not ion exchange. If the media is changed on a regular basis, hence the ionic strength of solution is not allowed to increase, then the kinetics is shown to obey a t^{1} law.

The dissolution and mechanics of dissolution for a variety of glass compositions, including calcium/sodium/phosphate and sodium/phosphate, have recently been reported (Gao *et al.*, 2004b; Gao *et al.*, 2004a). Calcium was found to improve the durability of glasses when added at the expense of sodium. It was stated that dissolution occurred via the formation of a hydrated layer which then dissolved the phosphate chains by hydrolysis rather than simple hydration as hypothesised earlier by Bunker *et al*. Increasing the concentration of cations within the glass was stated to reduce the dissolution rate by decreasing the velocity of water molecules inside the hydration layer.

However, the dissolution mechanism of sodium calcium meta-phosphate glasses was studied in detail by Delahaye *et al*. Here, pristine and dissolved surfaces were studied by XPS to determine the phosphate chain length, as detailed previously. It was found that the two surfaces were identical, demonstrating that no hydrolysis had taken place and that phosphate chains dissolve intact.

The decrease in dissolution rate at the start of the test, as stated by Bunker *et al* was reported elsewhere (Delahaye *et al.*, 1998; Gao *et al.*, 2004b; Gao *et al.*, 2004a). Gao *et al* suggested that water moisture from the air initially cleaved some phosphate chains reducing their length, these molecules then dissolved almost immediately upon immersion in water producing an initially high dissolution rate. This is disproved by Delahaye *et al*, as stated previously. It was thought that saturation (Roshchina *et al.*, 1995), limitation of reactant transports away from the dissolving glass or ion exchange (as discussed previously) was the cause of the decrease in dissolution rate. Delahaye *et al* dissolved phosphate glass in excess water and agitated water and found that this had no significant effect. It was then hypothesised that the ionic strength of solution caused this effect. This was supported by tests in which the dissolving media was changed regularly, here the decrease in dissolution rate is not observed.

The corrosion behaviour of phosphate glasses containing copper and sodium were studied by Shih *et al*. It was reported that the substitution of sodium with copper or decreasing the phosphate concentration increased the durability of the glass. This was stated to be due to the formation of P-O-Cu bonds which replaced $P\text{-}O^{-}\ Na^{+}$ bonds, increasing the cross link density of the glass.

This view explaining the changes in dissolution rate is also stated by Montagne *et al*, who investigated the effect of zinc on the durability of sodium phosphate glasses. It was found that the dissolution rate decreased from 2 g cm^{-2} $h^{-1}$for sodium phosphate glass with 10 mol.% ZnO to 0.5 g cm^{-2} h^{-1} for glass containing 33 mol.% ZnO.

The phosphate/sodium/calcium ternary system has also been studied by Uo *et al*, who also found that additions of calcium decreased the dissolution rate. However, here dissolution was performed in distilled water and simulated body fluid (SBF). By changing the dissolving media, it was reported to decrease the dissolution rate by a factor of approximately five in all cases. This is in agreement with Franks *et al* who dissolved calcium/sodium phosphate glass in water and Hank's buffered saline solution (HBSS).

The effect of magnesium on the solubility behaviour of a calcium/sodium phosphate glass in water was investigated, where sodium and phosphate concentrations were kept constant at 23 and 45 mol.% respectively and the ratio of calcium to magnesium was altered (Franks *et al.*, 2002). Magnesium was found to cause a small decrease in dissolution rate. Compared to the calcium ternary composition, the substitution of 22 mol.% CaO with MgO showed a decrease of 0.007 g cm^{-2} h^{-1} from 0.015 to 0.008 g cm^{-2} h^{-1}.

The effect of trivalent cations, such as iron, were reported to have a greater effect on the dissolution rate than divalent cations (Ahmed *et al.*, 2004a; Parsons *et al.*, 2004b). Ahmed found that small additions of iron oxide (max 5 mol.%) to calcium/ sodium phosphate glasses reduces the dissolution up to ten fold with the addition of mol.% FeO. Parsons investigated the effect of iron phosphate on the dissolution of sodium phosphate glass. Additions of 20 mol.% $FePO_4$ demonstrated a dissolution rate of approximately $1x10^{-6}$

g cm^{-2} h^{-1} while glasses with 1 mol.% $FePO_4$ possessed dissolution rates of approximately $1x10^{-1}$ g cm^{-2} h^{-1}.

Comparison of all the dissolution rates discussed show that cations with higher valence decrease the dissolution rate to a greater extent than cations with a low valence. Also, cations with small ionic radii have a greater effect on the dissolution rate, i.e. Mg>Ca.

3 Materials and Methods

3.1 Introduction

This chapter describes the methods used to manufacture the phosphate glass samples from their salts and the experimental set up that was utilised to characterise the material on both a materials science and cell culture level. There is also a short discussion of sample handling and preparation where relevant and of data processing with respect to the techniques used.

3.2 Material Manufacture and Analysis

3.2.1 Glass Production

The required amounts of salt (NaH_2PO_4 ≥99%, CaH_2PO_4 ≥98% and $MgHPO_4.3H_2O$ ≥97%, Sigma Aldrich, UK) were weighed out and mixed, table 3-1. The salt mixture was then transferred to a 95% Pt/5% Au crucible (Birmingham Metal, UK) and dried at 350 °C for 1 hour in an air recirculation furnace (Carbolite, UK). The crucible was then transferred to rapid heating muffle furnace (Carbolite, UK) preheated to 800 – 1200 °C, as required, for 1 to 16 hours. The standard regime was 1200 °C for 4 hours. The melt was then cast into a graphite mould (materials from Le Carbone (Great Britain) Ltd, UK, and mould made in house) that had been preheated to 5 °C above the Tg of the glass. The glass moulding was then annealed at this temperature for 90 minutes and then cooled to 100 °C below this temperature

at a rate of ¼ °C min^{-1}. The glass was then allowed to cool to room temperature at its own rate.

Mg Series	NaH_2PO_4 (mol.%)	$MgHPO_4$ (mol.%)	$CaHPO_4$ (mol.%)
10 Mg	90	10	-
20 Mg	80	20	-
30 Mg	70	30	-
40 Mg	60	40	-
50 Mg	50	50	-
Ca Series			
10 Ca	90	-	10
20 Ca	80	-	20
30 Ca	70	-	30
40 Ca	60	-	40
Quaternary Series			
10 Mg/40 Ca	50	10	40
20 Mg/30 Ca	50	20	30
25 Mg/25 Ca	50	25	25
30 Mg/20 Ca	50	30	20
40 Mg/10 Ca	50	40	10

Table 3-1 Composition of all glasses studied and their shorthand names.

3.2.2 Dissolution Study

Glass rods of 10 mm diameter were cut into 10 mm lengths using a low speed saw (South Bay Technologies; California, USA) equipped with a high concentration diamond wafering blade (Buehler; Coventry, UK). A cooling fluid consisting of 50% water and 50% methanol (Fisher Chemicals, UK) was used. Experiments were undertaken in triplicate where a sample was dissolved in 25 ml of the appropriate media (deionised water or simulated body fluid), the temperature was kept at 37 °C by using a water bath (Grant, UK). Initial and subsequent weights and dimensions were recorded using a Mettler AE130 balance (Mettler Toledo, UK) and a Roebuck outside micrometer (Buck and Hickman, UK). Dissolution was plotted as dissolution rate (g cm^{-2} hr^{-1}) against time (hours).

3.3 Microstructural Analysis

3.3.1 Differential Scanning Calorimetry (DSC)

DSC analysis was carried out using a Perkin-Elmer DSC-7 instrument. Data acquisition and processing was done using Perkin-Elmer's Pyris software. Known masses (~30 mg) of crushed sample were placed into an aluminium pan then sealed with a crimped lid and heated from 25 °C to 550 °C at a rate of 10 °C/min under an argon atmosphere.

3.3.2 X-ray Photoelectron Spectroscopy (XPS)

XPS was first developed, as a modern surface analytical tool, by Kai Siegbahn and his research group in the mid-1960's under the acronym Electron Spectroscopy for Chemical Analysis (ESCA).

Surface analysis by XPS is accomplished by irradiating the sample surface with monoenergetic x-rays and analysing the energy of the detected electrons. The photons have limited penetration in a solid, normally in the region of 1-10 μm. The photons interact with an atom, causing the ejection of a photoelectron. The ejected electrons have kinetic energies, KE, given by:

$$KE = h\nu - BE - \phi$$

where $h\nu$ is the energy of the photon, BE is the binding energy of the atomic orbital from which the electron originates, and ϕ is the spectrometer work function.

In addition to photoelectrons, Auger electrons are also emitted. Auger electrons are emitted because of relaxation that occurs after photoemission.

After a photoelectron is emitted, an outer electron falls into the vacancy, and a second electron, the Auger electron, is emitted, carrying off the excess energy.

The probability of an electron interaction with an atom is far greater than a photon. So while ionisation occurs to a depth of up to 10 μm, only electrons that originate from a depth of up to 10 Å can escape from the surface without energy loss. Electrons that escape the material surface without energy loss form the characteristic peaks seen in the spectra, those that undergo inelastic loss before leaving the surface form the background.

XPS analysis of the phosphate glass samples were carried out using a Kratos AXIS ULTRA XPS system fitted with a monochromated Al Kα X-ray source and a hemispherical analyser with eight channeltrons. The source was operated at 10 mA and 15 kV.

A wide scan was run for all samples from 0 to 1100 eV using a step size of 1 eV and a pass energy of 80 eV to determine the elements present and which regions required high resolution scans. High resolution scans were run over the appropriate regions using a step size of 0.1 eV and a pass energy of 40 eV.

All data was manipulated using the CASA XPS data analysis software. The C 1s photoelectron peak at 285 eV was used for charge correction. A Shirley background type was used to correct the background. Gaussian/Lorentzian curves with a 30 % Gaussian contribution were used to fit the sample peaks. The relative surface composition of the glass samples were calculated from the relative intensities of the O 1s, P 2p, Na 1s, Mg 2p, Ca 2p peaks by taking integrated intensities of the high resolution peaks with standard library Schofield sensitivity factors applied.

Due to the hygroscopic nature of phosphate glass and the surface sensitivity of XPS, care had to be taken not to expose the surface to moisture. Samples were transferred to a glove box with a water content of less than 0.1 parts per million and fractured using a tungsten carbide blade to score the glass and a high carbon steel blade to fracture the glass. Samples were adhered to the sample stage using carbon cement (Agar Scientific, UK). The stage was then transferred to an airtight container before removal from the glove box. The airtight container was then transferred to a water free nitrogen glove bag attached to the XPS sample entry chamber before the samples were moved into the chamber and kept under vacuum.

3.3.3 Energy Dispersive X-ray Analysis (EDX)

EDX analysis was performed using an Oxford Instruments ISIS 300 series machine fitted with a Si (Li) crystal spectrometer that was controlled by the reference spaced ZAF correction program supplied with the machine. The EDX was attached to a Phillips XL30 scanning electron microscope, which was operated in secondary electron imaging mode. An ultra thin entrance window to the EDX spectrometer allowed X-rays from elements as light as boron to pass through. Samples were embedded in cold setting resin before grinding and polishing to a 1 μm finish.

Samples were analysed over 120 seconds using an accelerating voltage of 20 kV and a working distance of 10 mm. Quantitative analysis was performed using stoichiometry normalised results and jadeite, GaP, wollastonite and MgO as standards for sodium, phosphorus, calcium and magnesium respectively. Averages of three different areas were used for the final material composition.

3.3.4 Infrared Spectroscopy (IR)

Infrared spectroscopy was performed on a Brüker Tensor 27 spectrometer, operated in reflectance mode. Spectra were recorded in the region of 600 to 2000 wavenumbers in DRIFTS mode using an Easi Diff^{TM} workhorse diffuse reflectance unit (Pike Technology, UK).

Samples were crushed and ground into a fine powder using a mineral mortar and pestle. Crushed sample powder was added to dry KBr powder in the ratio 1:4 and reground before analysis.

3.3.5 X-ray Diffraction (XRD)

XRD diffraction patterns were recorded using a Siemans Kristalloflex 810 diffractometer, operated at 40 kV and 20 mA, utilising a CuK α radiation source. The scans were controlled by the Diffrac-AC software program. Data was taken in step mode, using intervals of 0.02°, over a 2θ range of 15-80° using a dwell time of 2 seconds.

Samples cut using a low speed diamond saw were used for XRD analysis. They were mounted onto an in-house made stage and secured using plastiscine.

3.3.6 Profilometry

Surface roughness was measured using a Surfcom profilometer (Advanced Metrology Systems Ltd; Leicester, England). Multiple R_a values were obtained using a traversing length of 2 mm and a cut-off of 0.08 mm.

R_a is the universally recognised parameter of roughness; it is the arithmetic mean of the departure y of the profile from the mean line.

3.4 General Cell Culture Techniques

3.4.1 Osteoblast Culture

Human cranial facial osteoblast like cells (CFCs) were obtained from paediatric skull fragments using a method described elsewhere (McDougall, 2001). Osteoblasts were cultured in Complete Dulbecco's Modified Eagle Media (CDMEM) consisting of Dulbecco's Modified Eagle Media supplemented with 10 % foetal calf serum (FCS), 2 % hepes buffer, 2 % penicillin/streptomycin, 1 % glutamine, 1 % non-essential amino acids (all Gibco Invitrogen, UK) and 0.85 mM of ascorbic acid (Sigma Aldrich, UK). CFC's were cultured in flasks (Falcon, Becton, Dickinson and Company; UK) at 37 °C in a humidified atmosphere with 5 % CO_2.

Cells were sub-cultured at 80-90 % confluency. CDMEM was removed and the CFC's were washed with phosphate buffered saline (PBS, Oxoid; UK). A trypsin solution (20 mg trypsin and 1 ml of hepes buffer in 100 ml of PBS) was added, to aid CFC detachment from the surface of the flask, and left in an incubator for 10 minutes. The flask surface was scraped firmly and thoroughly and the cells were rinsed off using 5 ml of CDMEM and removed to a universal (centrifuge tube) and centrifuged at 1200 rpm for 5 minutes. The supernatant was removed and the cells were resuspended in fresh CDMEM using a Pasteur pipette then transferred to flasks.

CFC's that were not required were harvested as previously described. The supernatant was removed and the cell pellet was resuspended in freezing mix (90% FBS, 10% dimethylsulfoxide, Gibco Invitrogen and Sigma Aldrich respectively) and transferred to 1 ml cryo-vials. The suspension was placed in a -80 °C freezer overnight to freeze at the optimum rate of 1 °C min^{-1} then transferred to a liquid nitrogen dewer.

Frozen cells were revived by rapid heating in a 37 °C water bath. CDMEM was added drop wise to the cell suspension, which was then transferred to a universal and centrifuged at 1200 rpm for 5 minutes. The supernatant was removed and the cell pellet resuspended in CDMEM and seeded in flasks.

3.4.2 Macrophage Culture

The murine BALB/c monocyte/macrophage cell line J774A.1 (mϕ) was obtained from the ECACC (No. 91051511). Cells were cultured in mϕ media consisting of Dulbecco's Modified Eagle Medium (Gibco Invitrogen, UK) supplemented with 2 mM glutamine (Gibco Invitrogen, UK) and 10% Foetal Calf Serum (Gibco Invitrogen, UK). Cells were cultured in Nunc tissue culture flasks (Nuncleon, Denmark) at 37 °C in a humidified atmosphere with 5 % CO_2.

Cells were sub-cultured before confluency by shaking to remove loosely attached cells then by gently scraping the flask surface. Cells were removed from the supernatant by centrifuging at 1500 rpm for 5 minutes. The supernatant was removed and the cell pellet resuspended in culture media before reseeding in the required number of flasks.

Cells not required were frozen down using the same method as previously described, except the trypsin solution was not used.

Frozen cells were revived by using the rapid thawing method previously described in this chapter.

3.4.3 Cell Counting

Cells were harvested using previously described methods. After the supernatant was removed, the cell pellet was resuspended in 1 cm^3 of CDMEM or mϕ media, as required, using a syringe and needle for CFC's and a transfer pipette for mϕs. 40 µl of trypan blue was added to the 40 µl of cell suspension and mixed thoroughly. Liquid was transferred to a haemocytometer and viable cells were counted under a phase contrast microscope (x100).

3.5 Osteoblast Assay Techniques

3.5.1 Alamar Blue Assay

The Alamar blue assay measures cell proliferation via detection of metabolic activity. The assay incorporates an oxidation-reduction reaction indicator that both fluoresces and changes colour, from blue to red, when reduced from its oxidised form. Cell growth results in a reduced environment while inhibition of growth maintains an oxidised environment. The reduction of Alamar blue is relative to cell growth (when Alamar blue is in contact with the cell layer), allowing quantitative analysis of cell metabolic activity (Lancaster *et al.*, 1996).

This assay is particularly useful as it is minimally toxic to living cells (alamarBlue., 2003), allowing further assays to be performed on the cells.

Cranial-facial osteoblasts were harvested and counted as previously described. The cell suspension was diluted to allow a cell concentration of 400,000 cells ml^{-1}. Cells were seeded onto the sample surfaces at a concentration of 40,000 cells cm^{-2}. Samples were incubated at 37 °C in a humidified atmosphere with 5 % CO_2 for 2, 48, 96 and 168 hours. At each time point, CDMEM was removed and the sample's surfaces were washed with PBS. 500 µl of Alamar Blue solution, 90 % Hank's buffered saline solution (HBSS, Gibco Invitrogen, UK), 10 % Alamar Blue (Serotec, UK), were added to each well and then the well plate was returned to the incubator for 90 minutes. After 90 minutes, the well plate was gently shaken to homogenise the liquid, and 100 µl was removed to a 96 well plate. The fluorescence at 530 nm excitation and 590 nm emission was measured using a Perspective Bioscience's fluorescence micro-plate reader. Excess Alamar Blue solution was removed and the samples were washed with Earl's buffered saline solution (EBSS, Gibco Invitrogen, UK). 1 ml of deionised water was added to each well and the well plate was transferred to a -80 °C freezer in preparation for further analysis, typically the DNA (Hoechst 33258) and alkaline phosphatase assay.

3.5.2 DNA (Hoechst 33258) Assay

The Hoechst 33258 assay was used to determine cell proliferation by measuring the DNA content of the cell layer.

Samples frozen in deionised water were thawed and frozen three times to lyse the cells and free membrane bound proteins into the media. One hundred micro litre aliquots of test samples were transferred to a 96 well plate. DNA standards were prepared using a bovine stock solution (Sigma, UK) and TNE buffer (10 mM TRIS, 2 M NaCl and 1 mM EDTA in deionised water, pH 7.4) as a diluent. The Hoechst 33258 stain was made by dissolving 1 mg of bisbenzimide H 33258 in deionised water, which was further diluted to 1:50 in TNE buffer. 100 µl of the Hoechst 33258 stain was added to each well. The plate was mixed and read on a fluorescence plate reader at 360 nm excitation and 460 nm emission. DNA concentrations were derived from the standard curve.

3.5.3 Alkaline Phosphatase Assay

Alkaline phosphatase activity was measured using the Granutest 25 alkaline phosphatase assay (Randox, UK). Here, the substrate p-nitrophenylphosphate was hydrolysed into phosphate and p-nitrophenol in the presence of the enzyme alkaline phosphatase. The product was yellow in colour, the intensity was proportional to the concentration of alkaline phosphatase, and was measured using an absorbance reader.

The samples that were stored in water at -80 °C were freeze-thawed three times to obtain the cell homogenates. 50 µl of cell homogenate was added to a 96 well plate with 50 µl of alkaline phosphatase reagent (p-nitrophenylphosphate in diethanolamine HCl buffer, pH 9.8). The plate was mixed and the absorbance read, at regular intervals up to 30 minutes, on an Anthos Labtec plate reader 2001 at 405 nm, reference filter 620 nm.

3.5.4 Quantification of Collagen

Collagen quantification was achieved by using the Soluble Collagen Assay (Sircol, UK). The assay works by utilising the sirius red dye, which is also known by the name Direct Red 80. Sirius red is an anionic dye with sulphonic side chains, it is these groups that react with the side chain groups of the basic amino acids present in collagen. The specific affinity of the dye for collagen, under assay conditions, is due to the elongated dye molecules aligning parallel with the long rigid structure of native collagens that have intact triple helix organisation (Sircol, 1992).

CFCs were seeded onto sample and thermanox (as a positive control) surfaces at a density of 40,000 cells/cm^2 and cultured for 7, 14, 21 and 28 days. At each time point the CDMEM was removed and the samples were washed in PBS. 1 ml of water was added to each sample before freezing at -80 °C. The samples were freeze-thawed three times and the water/lysate was removed for collagen analysis. The assay was performed as described in the instructions enclosed with the assay.

3.5.5 Osteocalcin Quantification

Osteocalcin, also known as bone γ-carboxylglutamic acid protein, is a vitamin K dependant Ca^{2+} binding protein, which is produced exclusively by osteoblasts and odontoblasts (Price *et al.*, 1976). It contains three carboxylated glutamic acid residues which bond strongly to hydroxyapatite (Poser *et al.*, 1980).

Here, osteocalcin quantification is performed using a commercially available kit (Zymed, UK). This kit is an enzyme immunoassay based on a sandwich method that utilises two mouse monoclonal anti-osteocalcin antibodies to detect osteocalcin. The first antibody is immobilised on a microplate, the samples are added and any osteocalcin present binds. The second antibody is labelled with peroxidase and binds to the osteocalcin-primary antibody complex. The reaction between peroxidase and the substrate, H_2O_2 and tetramethylbenzidine, results in colour development with intensities proportional to the amount of osteocalcin present. Hence, osteocalcin concentration can be determined using standards and an absorbance plate reader.

Samples, including thermanox as a positive control, were seeded with CFCs at a concentration of 40,000 cells/cm^2 for periods of 7, 14, 21 and 28 days. At each time point the CDMEM was removed and the samples washed in PBS. 1 ml of water was added before each sample was freeze-thawed three times. The lysate was collected and tested for the presence of osteocalcin following the kit instructions.

3.6 Macrophage Assay Techniques

3.6.1 H2O2 Production

Hydrogen peroxide production is quantified by utilising the properties of 2'-7'-dichlorofluorescin diacetate, a cell permeable non-fluorescent probe. It is de-esterified intracellularly, upon oxidation, and changes into highly

fluorescent 2'-7'-dichlorofluorescin. This allows sensitive and rapid quantification of oxygen reactive species such as H_2O_2 production by mϕs.

Macrophages were harvested and centrifuged as previously described, the cell pellet was then dispersed in Hank's balanced salt solution (HBSS) and centrifuged again. Cells were then resuspended in dichloroflourescein (DCF, 2 mM in methanol):HBSS at a working ratio of 1:100. Cells were seeded onto sample surfaces as well as tissue culture plastic and copper, as negative and positive controls respectively, at a concentration of 80,000 cells/cm^2 into Nunc well plates (Nuncleon, Denmark). Cells were incubated at 37 °C, under 5 % CO_2 for 6 h. At hourly intervals, the samples were agitated to homogenise the media and 50 µl aliquots were removed from each well and placed into a fresh 96 well plate. The fluorescence was measured at 485 nm excitation and 530 nm emission and the aliquots were returned to the original wells.

3.6.2 IL-1β Production

This assay employs the quantitative sandwich enzyme immunoassay technique. A polyclonal antibody specific for mouse IL-1β is pre-coated onto a microplate, any IL-1β in the solution added to the wells is bound by the immobilised antibodies. An enzyme linked polyclonal antibody, specific to mouse IL-1β was added. A substrate was then added to the wells, which yielded a blue coloured product that turned yellow when diluted hydrochloric acid was added. The intensity of the colour is proportional to the amount of IL-1β present and can easily be measured using an absorbance reader.

Samples were sterilised by rinsing in ethanol then washed in sterile PBS. Samples were placed into Nunc tissue culture plates (Nuncleon, Denmark).

Thermanox, treated polystyrene surfaces, were used for negative controls and lipopolysaccharide (LPS) was used as a positive control at concentrations of 10 x 10^{-6} and 100 x 10^{-6} g cm^{-3}. Macrophages were harvested and seeded onto the sample and control surfaces, in mϕ media, at a concentration of 80,000 cells cm^{-2}. The plates were incubated at 37 °C, under 5 % CO_2 for 2 and 48 h. After 2 h, the media was removed from each well and stored in individual eppendorfs at -20 °C until assayed. Each sample then receives fresh media, included fresh LPS, and the plates are incubated for a further 48 h. After 48 h the media was removed from each well and transferred to eppendorfs and stored at -20 °C until assayed. Samples were assayed according to the kit instructions and the optical density of each well was determined using a microplate reader at 450 nm measurement and 540 nm reference wavelengths. Concentrations of IL-1β were determined by using standard solutions of known IL-1β, which were supplied with the kit.

3.7 Imaging Techniques

3.7.1 Phalloidin/Propidium Iodide Staining

Cell spreading and morphology was studied by labelling F-actin filaments of the cytoskeleton with FITC-labelled phalloidin (Sigma Aldrich, UK), the cell nucleus was counter stained with propidium iodide. Samples were washed three times in 1% bovine serum albumen in PBS (BSA/PBS) and fixed in 4 % paraformaldehyde (4 % paraformaldehyde, 2 % sucrose in PBS) for ten minutes. Samples were washed three times in BSA/PBS and permeabilised in a buffered 0.5 % triton X-100 solution at -20 °C for 5 mins, but were not

allowed to freeze. Samples were washed three times in BSA/PBS and then covered with 10 μg ml^{-1} phalloidin in BSA/PBS and incubated at 4 °C for 30 mins. Samples were washed three times in BSA/PBS and covered in 0.1 % propidium iodide in PBS for approximately 3 s. Samples were mounted on to glass using PBS/glycerol mountant containing diazobicyclo 2-2-2 octane (DABCO).

The samples were then viewed using a Leica TCS 4d Confocal Laser Scanning Microscope (CLSM). Excitation of the FITC label and PI was achieved using 488 nm and 568 nm laser lines respectively. Simultaneous recording of the two channels was performed to achieve a composite image.

3.7.2 Scanning Electron Microscopy of Cells

Samples were fixed in 3 % glutaraldehyde in 0.1 M cacodylate buffer for 2 hours, washed twice in 0.1 M cacodylate buffer, and post fixed in 1 % osmium tetroxide in Millonigs buffer for 45 mins. Samples were dehydrated through a graded ethanol series (20, 30, 40, 50, 60, 70, 80, 90, 96 and 100%) with 80 % ethanol in water saturated in uranyl acetate. Samples were then dried via hexamethyldisilazine before being sputter coated in gold and viewed with a Philips XL30 scanning electron microscope operated at 10 kV.

3.7.3 Immunolocalisation of Type I Collagen

Samples were seeded with CFCs at a density of 40,000 cells/cm^2 and cultured for periods of 7, 14, 21 and 28 days. At the required time point the CDMEM was removed and the cell layer washed in PBS. The cells were fixed in

a 1:1 mixture of acetone and methanol for 10 minutes at 4 °C before permeabilising for 5 minutes at -20 °C. The cells were then washed in PBS/BSA and the monoclonal mouse-anti-human type I collagen primary antibody (Sigma Aldrich, UK) was added at a dilution of 1:2000 in PBS/BSA and incubated at 37 °C for 60 minutes. The primary antibody was removed and the cells washed, several times, in PBS/BSA. The appropriate secondary antibody (rabbit anti-mouse), with fluorescent conjugate (FITC) (DakoCytomation, UK) was added and the cells were incubated at 37 °C for 60 mins. The secondary antibody was removed and the cells were washed in PBS/BSA and counterstained with 1 % propidium iodide (PI) (Sigma Aldrich, UK) in PBS for approximately 3 s. The PI was removed and the cells were washed in PBS/BSA and mounted in DABCO/glycerol mountant under glass. The cells were viewed using a Leica TCS 4d Confocal Laser Scanning Microscope (CLSM). Excitation of the FITC label and PI was achieved using 488 nm and 568 nm laser lines respectively. Simultaneous recording of the two channels was performed to achieve a composite image.

3.7.4 Alizarin Red S Staining

The Alizarin red assay is used to positively identify any CaP mineral phase that has been deposited by the CFCs. This assay utilises a lake reaction in which a bright pigment is produced by combination of an organic colouring matter with an inorganic compound, which is usually a metallic salt, oxide or hydroxide. In the Alizarin red lake reaction, calcium salts are stained an orange/red colour.

CFC's were seeded onto surfaces at a concentration of 40,000 cells/cm^2 and cultured for 7, 14, 21 and 28 days. At the appropriate time point, the CDMEM was removed and the cells were washed in Tris Buffered Saline (TBS, 0.05 M Tris(hydroxymethyl)methylamine, 0.037 M hydrochloric acid adjusted to pH 7.4), and fixed in 1.5 % glutaraldehyde in 0.1 % sodium cacodylate buffer for 30 minutes. Cells were rinsed in TBS and stained with 1 % Alizarin Red S (Sigma Aldrich, UK) in 0.028 % ammonium hydroxide, pH 6.4, for 2 minutes. Cells were washed in TBS and mounted onto glass using PBS/glycerol mountant containing DABCO.

3.8 Statistical Analysis

Mean values and standard error of the mean were computed for 4 replicate samples. One way ANOVA with Tukey post test and two way ANOVA with Bonferelli post test was performed using GraphPad Prism version 4.00 for Windows, GraphPad Software, San Diego California USA. Significance is stated as either not significant ($P>0.05$), significant ($0.05>P>0.01$), very significant ($0.01>P>0.001$) or extremely significant ($P<0.001$).

4 Material Characterisation

4.1 Introduction

This chapter details how the thermal properties and dissolution rate are affected by the manufacturing process and composition of the glass. The XPS and IR spectra of all glasses are also presented.

4.2 Results

4.2.1 Glass Production

Glass was successfully prepared in a variety of compositions, table 3-1, from the following salts: NaH_2PO_4, $MgHPO_4$ and $CaHPO_4$. XRD was used to confirm that the glasses were amorphous to within a maximum of 5% crystal

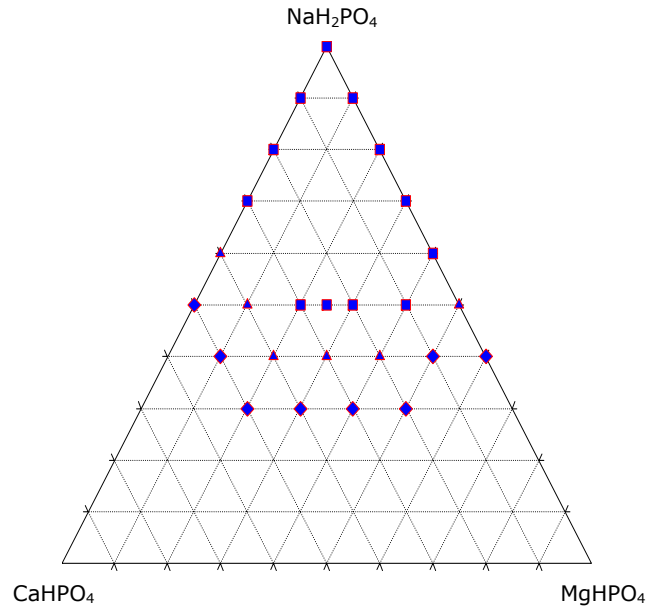

Figure 4.1 Ternary diagram showing the glass forming compositions of glasses composed of NaH_2PO_4, $MgHPO_4$ and $CaHPO_4$. Glass ■, glass with some crystals ▲, crystalline ♦.

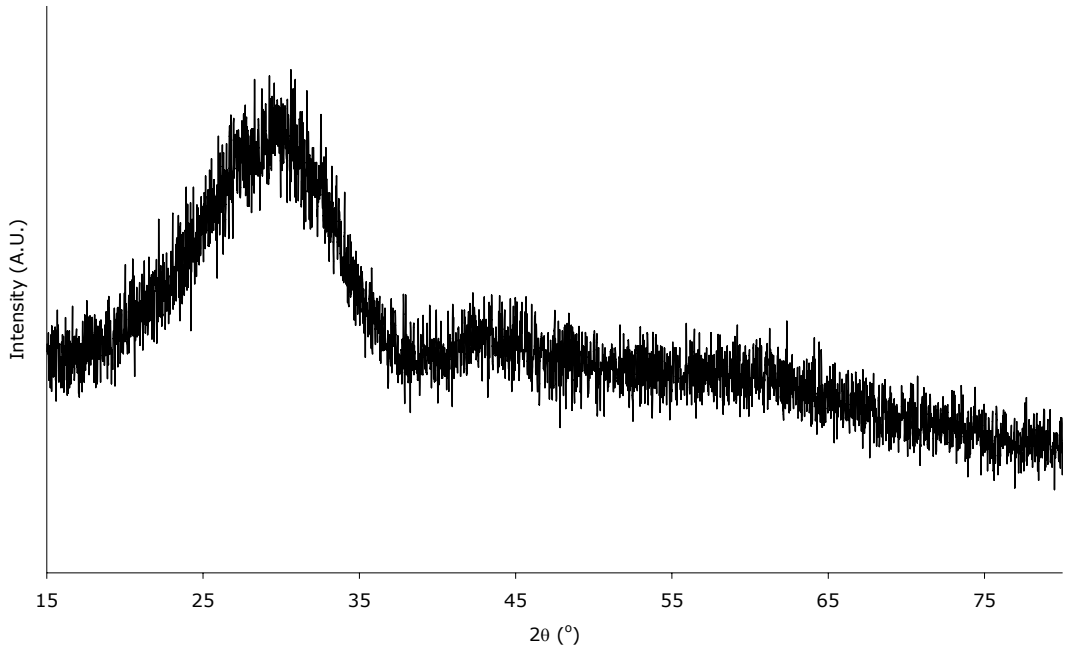

Figure 4.2 XRD diffractogram of sodium phosphate glass with 25mol.% magnesium phosphate and 25mol.% calcium phosphate.

concentration. The spectra from all glasses possessed the characteristic 'amorphous hump', figure 4.2, demonstrating their glassy nature. Partial devitrification occurred in sodium phosphate glasses containing either 50 mol.% $MgHPO_4$, 40 mol.% $CaHPO_4$ or both 40 mol.% $CaHPO_4$ and 10 mol.% $MgHPO_4$. Only the sodium phosphate 40 mol.% $CaHPO_4$ grew large enough crystals for identification by XRD analysis, figure 4.3, which identified the presence of $Ca_2(P_2O_7)$ crystals. Increasing the amount of $MgHPO_4$ or $CaHPO_4$ above 50 mol.% or 40 mol.%, in sodium phosphate glass, respectively, resulted in devitrification. For the glass series containing both $MgHPO_4$ and $CaHPO_4$, a maximum divalent salt concentration of 50 mol.% was permissible before devitrification occurs.

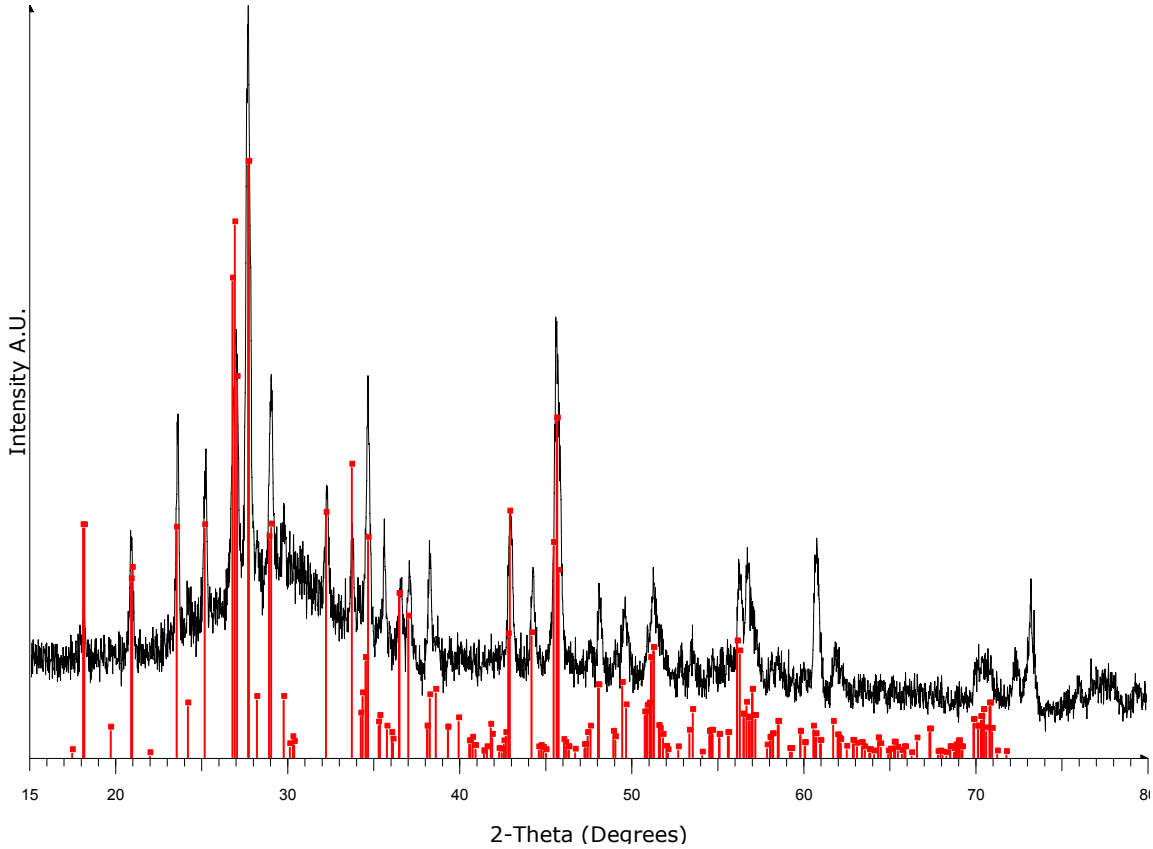

Figure 4.3 XRD diffractogram of sodium phosphate glass with 50 mol.% calcium phosphate.

4.2.2 Thermal Analysis

This section reports on how the thermal properties of phosphate glass are affected by changes in the temperature at which the glass was made and the amount of time that the melt was left at a particular temperature. The effect of magnesium and calcium on the thermal properties of sodium phosphate glass is presented, as is the effect of the crucible material.

The effect of melt time on the T_g of sodium phosphate (NaH_2PO_4) is shown in figure 4.4. Here the sodium phosphate salt was melted at various temperatures in a platinum crucible. After 1, 2, 4, 8 and 16 h the T_g was measured.

When the melt temperature was 900 °C, the T_g was found to increase from 284 °C, after a 1 h melt, to 295 °C after 16 h, figure 4.4. This trend was not linear, after 1 h the rate of increase in T_g was high, but plateaued at 295 °C after 8 h.

This experiment was repeated at 800, 1000, 1100 and 1200 °C, again with sodium phosphate in platinum crucibles, figure 4.4. At 800, 1000 and 1100 °C, the change in T_g with time followed a similar curve to the results at 900 °C. Changes between melts of differing temperatures existed within the initial T_g value after 1 h and the time taken to reach the plateau temperature. The T_g after one hour increased with the melt temperature from a value of 278 °C at 800 °C to 295 °C at 1200 °C. The time taken for the plateau temperature to be reached was dependant on the temperature of the melt, with higher melt temperatures reaching this point after shorter time periods. The plateau temperature was 295 °C in all cases except when the melt was 800 °C, here the Tg reached a plateau at 293 °C.

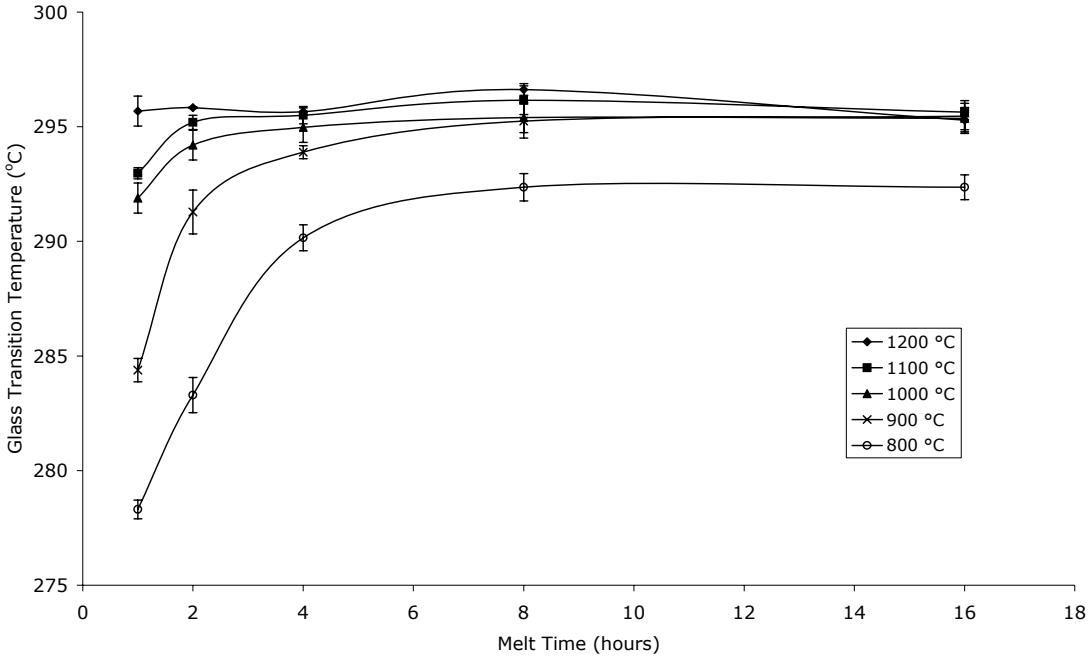

Figure 4.4 Glass transition temperature versus melt time for sodium phosphate glass prepared at differing melt temperatures. Bars are standard error of the mean, n = 2.

The composition of the glass was altered so that the phosphate glass contained 10 mol.% of either $CaHPO_4$ or $MgHPO_4$ with the balance being NaH_2PO_4, these salt mixtures were melted at 900 °C in platinum crucibles for up to 16 h, figure 4.5. The T_g for these glasses followed a similar curve to that of sodium phosphate, figure 4.4, exhibiting an increase in T_g before levelling off. Sodium phosphate glass with 10 mol.% calcium phosphate exhibited a plateau at 313 °C while the corresponding glass with magnesium phosphate demonstrated asymptotic behaviour. The initial T_g for both glasses are higher than that for pure sodium phosphate glass at 299 and 321 °C for calcium and magnesium phosphate respectively.

In separate tests, sodium phosphate salts were melted in alumina crucibles for up to 16 hours at three different temperatures (800, 900 and 1000 °C), figure 4.6. The T_g increased with melt time for all melt temperatures, with higher melt temperatures producing the greatest increases in T_g. All melts were asymptotic in nature. There was little difference between the initial T_g after 1 h, the 800 °C melt possessed a slightly lower T_g than the other melts.

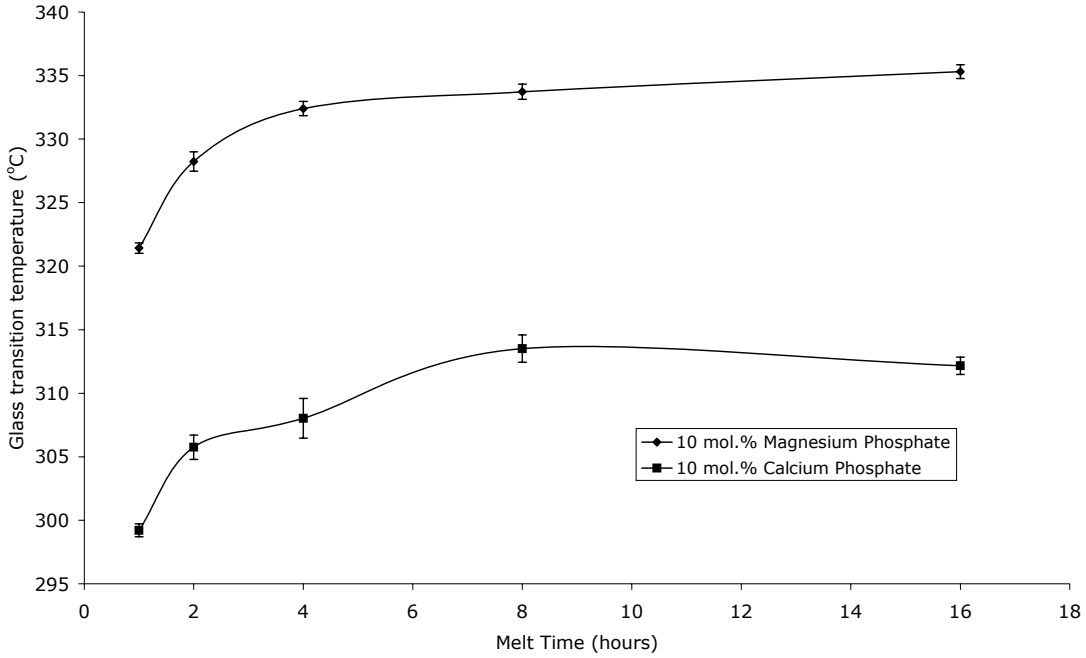

Figure 4.5 Glass transition temperature versus melt time for sodium phosphate glasses containing either 10 mol.% $CaHPO_4$ or $MgHPO_4$ prepared at 900 °C. Bars are standard error of the mean, n = 2.

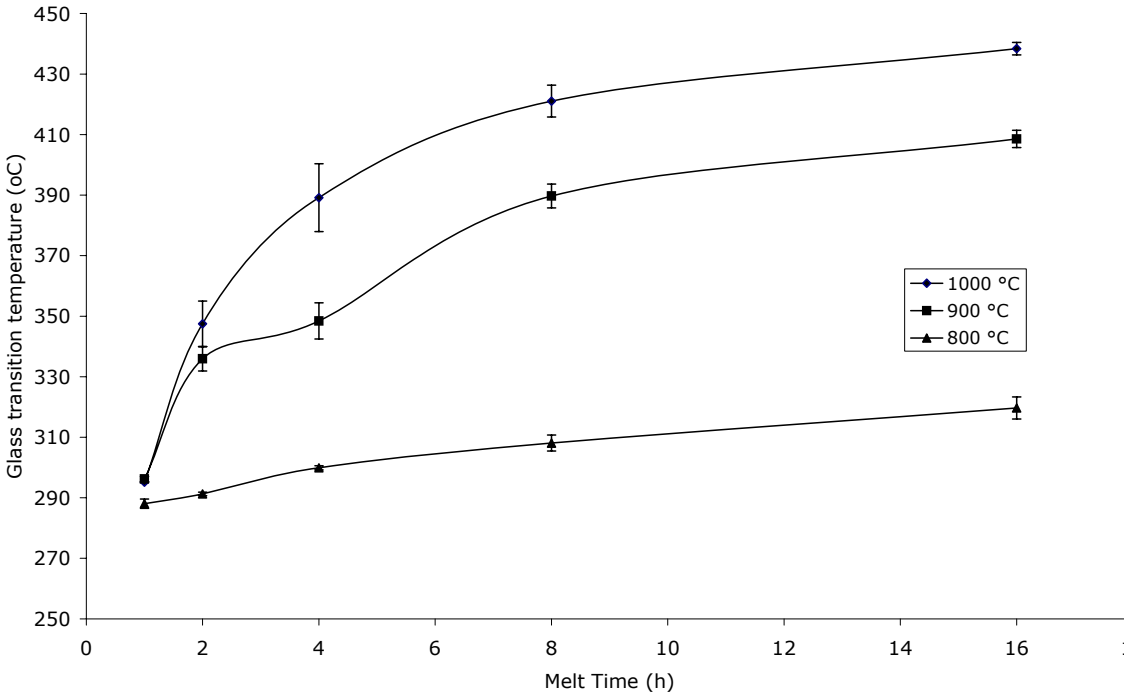

Figure 4.6 Glass transition temperature (°C) versus melt time (h) for sodium phosphate glass prepared in alumina crucibles at 800, 900 and 1000 °C. Bars represent the standard error of the mean, n = 2.

The T_g of sodium phosphate glass melted at 900 °C for 4 h is lower than expected. However, this is thought to be within experimental error.

The effect of divalent cation concentration on the T_g of phosphate glass was investigated. Increasing amounts of either $MgHPO_4$ or $CaHPO_4$ were added to

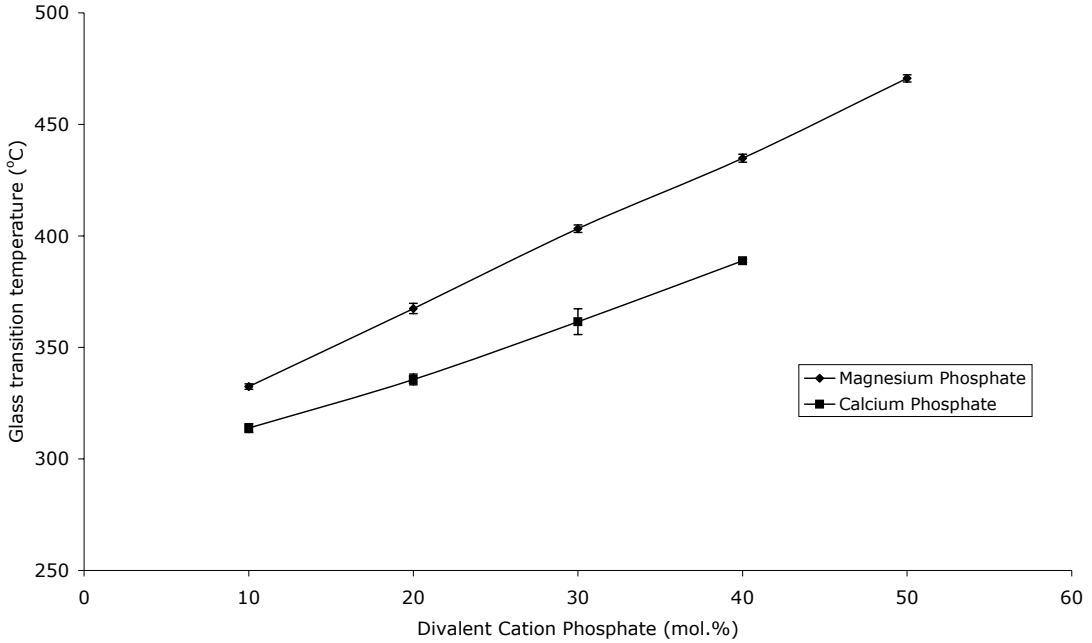

Figure 4.7 Glass transition temperature (°C) of sodium phosphate glass with increasing concentrations of either calcium phosphate or magnesium phosphate. Bars represent standard error of the mean, n = 2.

sodium phosphate in increments of 10 mol.%, figure 4.7. The addition of magnesium phosphate to sodium phosphate glass increases the T_g linearly, R^2 = 0.9996, with respect to mol% of $MgHPO_4$. The T_g of sodium phosphate glass with 10 mol.% of magnesium phosphate was 332 °C, this rose to 471 °C with the addition of 50 mol% of magnesium phosphate. Each addition of 10 mol.% magnesium phosphate caused an increase in T_g of approximately 34 °C.

The addition of calcium phosphate also increased the T_g of sodium phosphate linearly, R^2 = 0.9974, with increasing 10 mol% increments. The addition of 10 mol.% $CaHPO_4$ to sodium phosphate glass resulted in a T_g of 314 °C, which increased to 389 °C for a concentration of calcium phosphate of 40 mol.%. The rise in T_g was approximately 25 °C with each 10 mol.% increase in calcium phosphate.

The combined effect of magnesium and calcium on T_g was investigated by measuring the T_g for a range of phosphate glasses with 50 mol% $NaHPO_4$ and

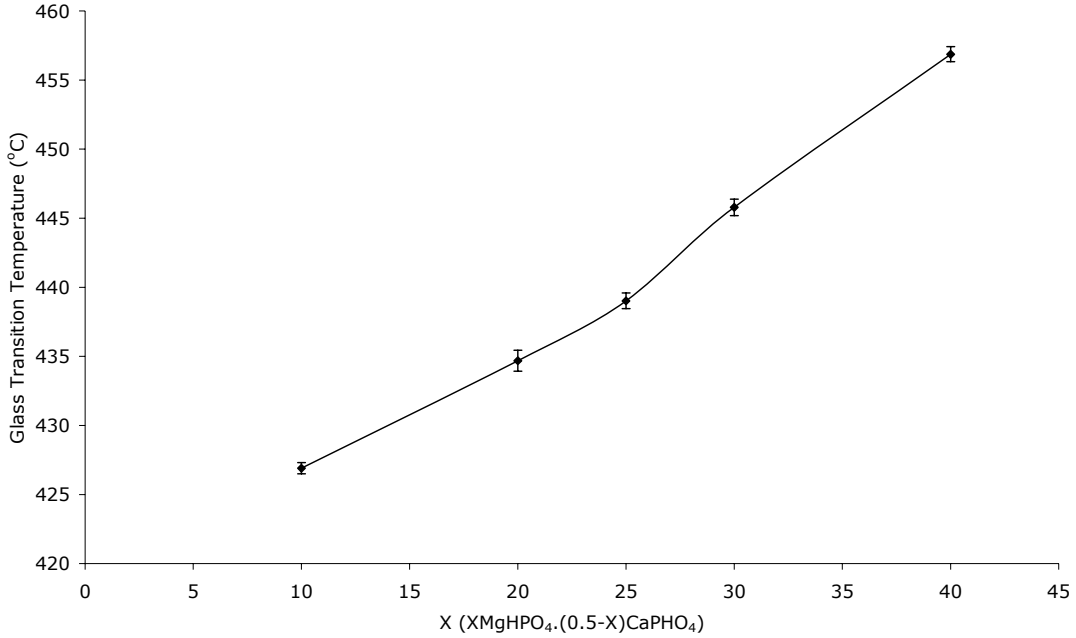

Figure 4.8 Variation in glass transition temperature for phosphate glass containing 50 mol.% NaH_2PO_4 and varying ratios of magnesium phosphate and calcium phosphate. Bars represent standard error of the mean, where n = 2.

varying amounts of $CaHPO_4$ and $MgHPO_4$, figure 4.6. The sodium phosphate glass with 10 mol.% $MgHPO_4$ and 40 mol.% $CaHPO_4$ possessed the lowest T_g of 427 °C, in this compositional range. The highest T_g value was 457 °C for the sodium phosphate glass containing 40 mol.% $MgHPO_4$ and 10 mol.% $CaHPO_4$. The relationship between the T_g and the replacement of calcium phosphate with magnesium phosphate was approximately linear. The T_g increased at a rate of approximately 10 °C for every 10 mol.% of calcium phosphate exchanged for magnesium phosphate.

4.2.3 Phosphate Glass Dissolution

This section presents the results on how the dissolution rate was affected by melt time and glass composition, specifically showing the effect of calcium and magnesium. The effect of changing the medium from triply deionised water to simulated body fluid is also reported.

Phosphate glass of the composition: 90 mol.% NaH_2PO_4/10 mol.% $MgHPO_4$ was prepared at 900 °C and melted for up to 16 hours, figure 4.9. Pure sodium phosphate glass was not used as the samples are very hygroscopic, producing a sticky mass that is impossible to weigh accurately. For all temperature regimes, the dissolution rate was high at the beginning of the experiment and decreased slowly, in a non-linear fashion, as dissolution time proceeded. For example, the dissolution rate for the glass melted for 4 hours is $11.5x10^{-3}$ g cm^{-2} h^{-1} after half an hour of dissolution, the rate drops to $9.7x10^{-3}$ g cm^{-2} h^{-1} after 4 hours then $8.7x10^{-3}$ g cm^{-2} h^{-1} after 24 hours of

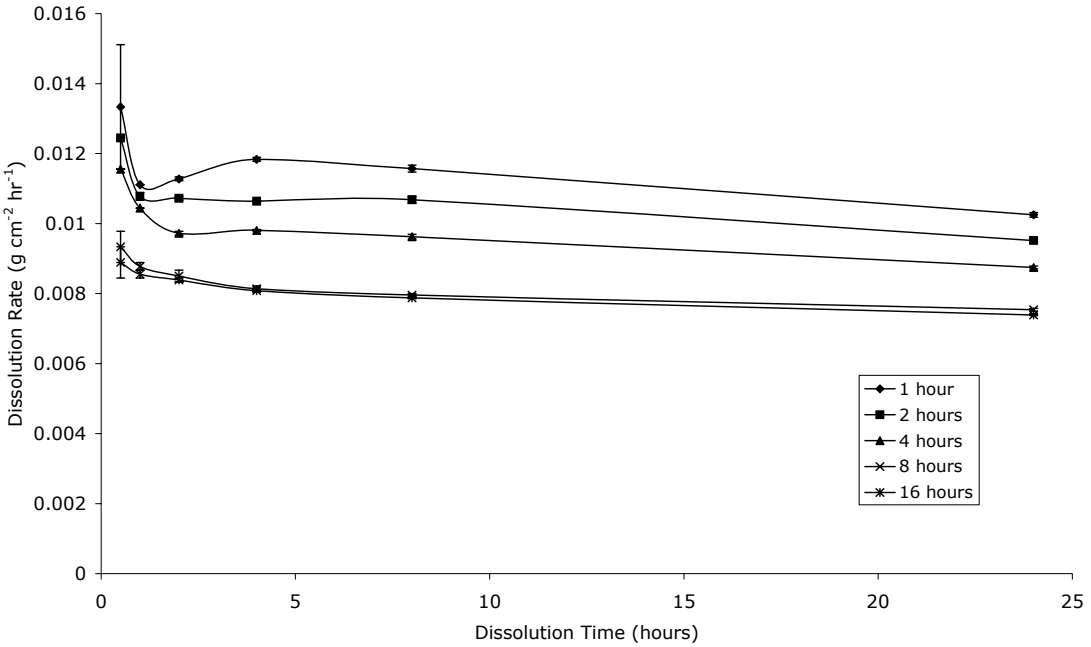

Figure 4.9 Degradation Rate (g cm^{-2} h^{-1}) against dissolution time (hours) for sodium phosphate glass, containing 10 mol.% $MgHPO_4$, prepared at 900 °C for 1, 2, 4, 8 and 16 hours and dissolved in water. Bars are standard error of the mean, n = 3.

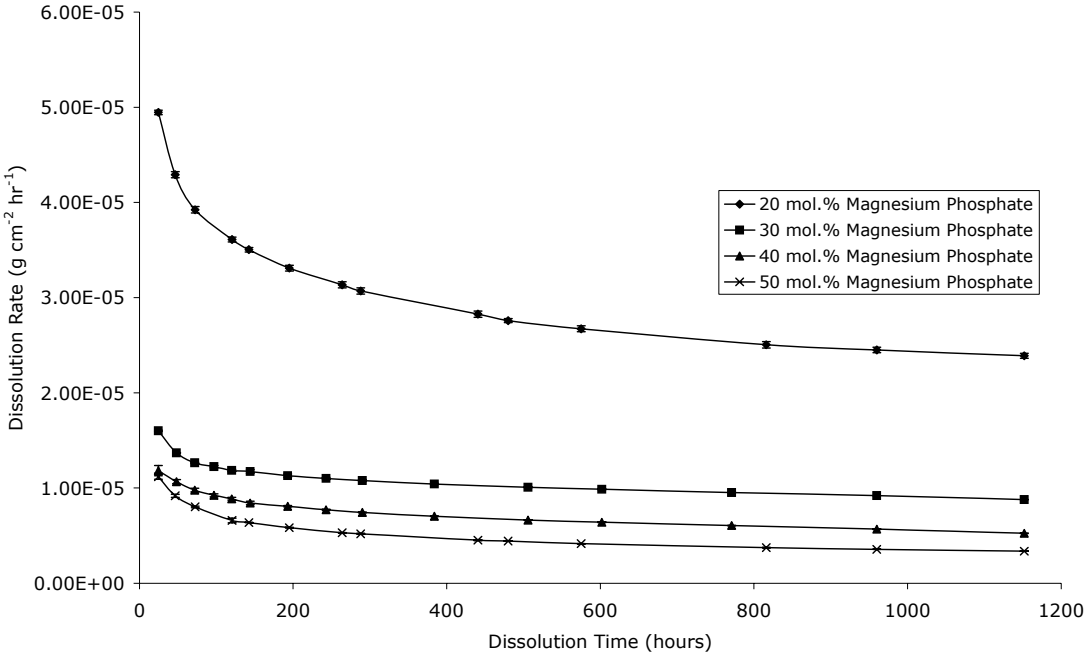

Figure 4.10 Degradation Rate (g cm^{-2} h^{-1}) versus dissolution time (hours) for sodium phosphate glass, containing concentrations of $MgHPO_4$ from 20 mol.% to 50 mol.% in water. Bars are standard error of the mean, n = 3.

dissolution. The dissolution rate decreases at all time points, with increasing melt time, the final dissolution rate is $10x10^{-3}$ g cm^{-2} h^{-1} after 24 h for glass melted for 1 h and $7x10^{-3}$ g cm^{-2} h^{-1} for glass melted for 16 h.

Sodium phosphate glass with increasing amounts of magnesium phosphate, in 10 mol% increments up to 50 mol.% $MgHPO_4$, was dissolved in water, figure 4.10. The dissolution rates for 10 mol.% $MgHPO_4$/90 mol.% NaH_2PO_4 are very high, with rates of $7x10^{-3}$ g cm^{-2} h^{-1}, hence are not shown on the graph for clarity.

With the addition of increasing amounts of $MgHPO_4$ at the expense of sodium phosphate, the dissolution rate decreases. After eight weeks, the dissolution rate is $2.4x10^{-5}$ g cm^{-2} h^{-1} for sodium phosphate glasses containing 20 mol.% $MgHPO_4$. This drops to $3.37x10^{-6}$ g cm^{-2} h^{-1} with the addition of 50 mol.% $MgHPO_4$. The most marked reduction of the dissolution rate was between the sodium phosphate glasses containing 20 and 30 mol.% $MgHPO_4$. However, the addition of $MgHPO_4$ does not cause a linear decrease in

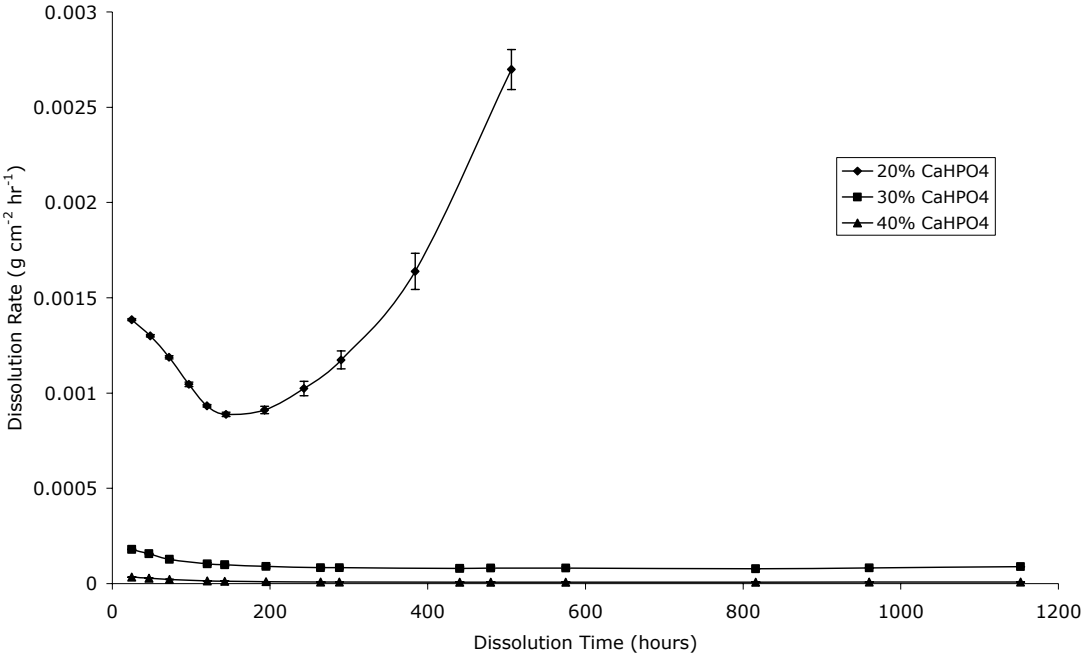

Figure 4.11 Dissolution rate (g cm^{-2} h^{-1}) against dissolution time (hours) for sodium phosphate glasses consisting of 20 – 40 mol.% $CaHPO_4$ and dissolved in water. Bars are standard error of the mean, where n = 2.

dissolution rate. The dissolution rate for any glass with the magnesium series decreased with time in an asymptotic manner. This decrease was more pronounced in those glasses which possessed a faster dissolution rate.

The effect of calcium phosphate addition, in 10 mol.% increments, to the dissolution rate of sodium phosphate glass is illustrated in figure 4.9, sodium phosphate glass with 10 mol.% calcium phosphate, which has a dissolution rate of 5.8×10^{-2} g cm^{-2} h^{-1} is omitted for clarity. The addition of $CaHPO_4$ to sodium phosphate glass has the effect of reducing the dissolution rate in a non linear manner. With the exception of 20 mol.% $CaHPO_4$, glasses from the calcium series dissolve relatively quickly at first before dissolution decreases, in the same asymptotic manner as the magnesium phosphate glasses. For 20 mol.% $CaHPO_4$, the rate of dissolution decreases until about 144 h, where the rate picks up and surpasses the initial rate.

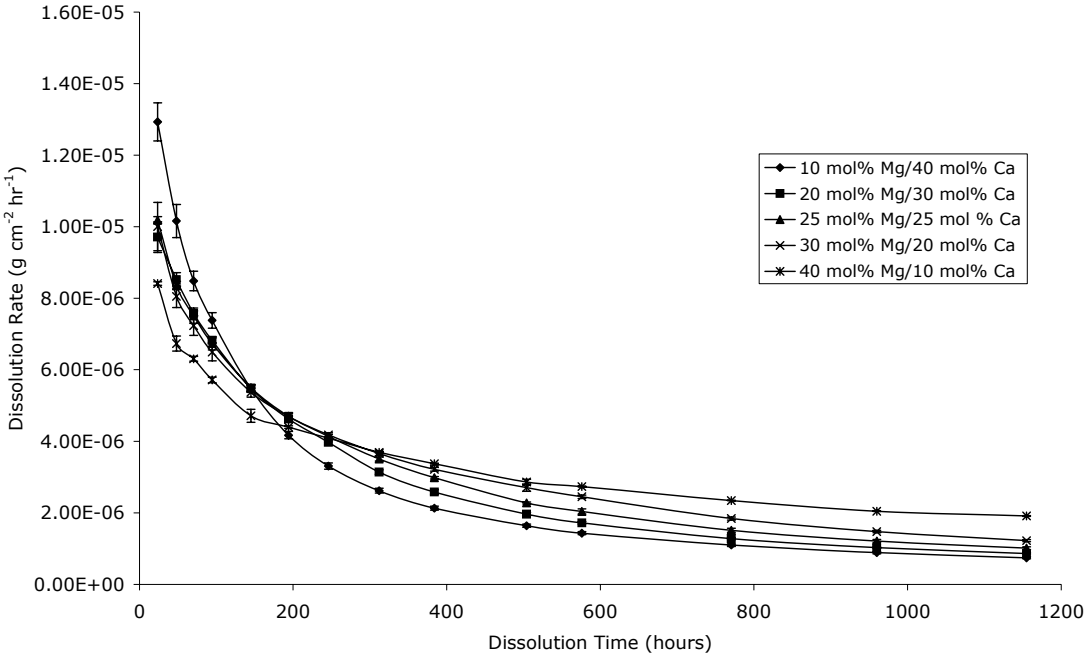

Figure 4.12 Dissolution rate (g cm^{-2} g^{-1}) versus dissolution time (hours) for phosphate glasses comprising of 50 mol.% NaH_2PO_4 and differing ratios of magnesium phosphate and calcium phosphate in water. Bars are standard error of the mean where n = 2.

For the following set of dissolution tests in water, the sodium phosphate content was kept constant at 50 mol.% and the ratio of $MgHPO_4$:$CaHPO_4$ was varied, figure 4.12.

All the glass compositions possess a relatively high dissolution rate, in the range 1.3-0.85x10^{-5} g cm^{-2} h^{-1} at the start of the experiment, which decreases in an asymptotic manner with time to a value in the 1-2x10^{-6} g cm^{-2} h^{-1} range. The glasses containing higher concentrations of $MgHPO_4$ are initially more durable than their high $CaHPO_4$ counterparts. However, as time progresses, the dissolution rates of the glasses with higher $CaHPO_4$ concentrations fell lower than those with high $MgHPO_4$, reversing the trend observed at the start of the experiment.

The results for the dissolution of sodium phosphate with increasing amounts of $MgHPO_4$, up to 50 mol.%, in SBF, figure 4.13. The dissolution rate for 20 mol.% $MgHPO_4$ decreases until at 72 hours, the rate begins to rise before again dropping linearly after approximately 500 h. The addition of 30, 40 or

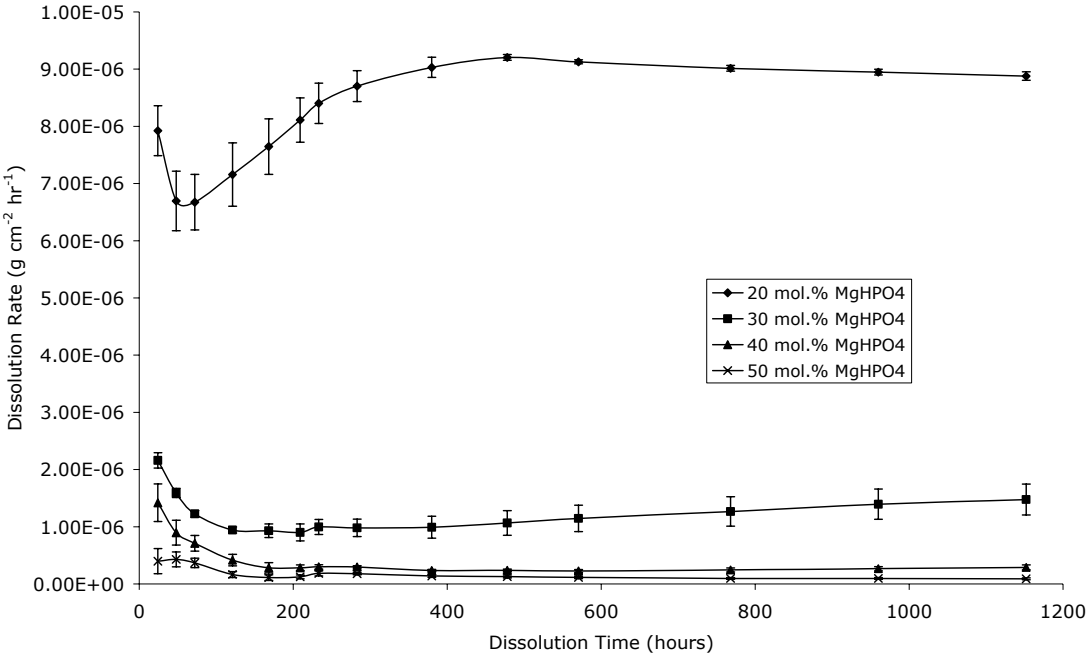

Figure 4.13 Dissolution rate against dissolution time for sodium phosphate glasses containing varying amounts of magnesium phosphate and dissolved in SBF. Bars represent the standard error of the mean where n = 3.

50 mol.% $MgHPO_4$, causes a decrease in dissolution rate with increasing magnesium phosphate content. Sodium phosphate glasses containing 30 mol.% $MgHPO_4$ or more, possess the same dissolution curve compared to the samples dissolved in water, only with a lower dissolution rate.

Sodium phosphate glass containing calcium phosphate from concentrations of 20 mol.% up to 40 mol.% was dissolved in SBF for up to eight weeks, figure 4.15. Adding calcium phosphate to sodium phosphate glass decreases the dissolution rate in a non-linear fashion.

The dissolution rate for sodium phosphate glass that contains 20 mol.% $CaHPO_4$ increases in an exponential manner with time until complete dissolution has occurred. With the addition of a further $CaHPO_4$ (30 or 40 mol.%), the dissolution rate, after 24 h, begins to drop until after 264 h it reaches a plateau at 1.70×10^{-5} and 1.45×10^{-6} g cm^{-2} h^{-1} for 30 and 40 mol.% $CaHPO_4$.

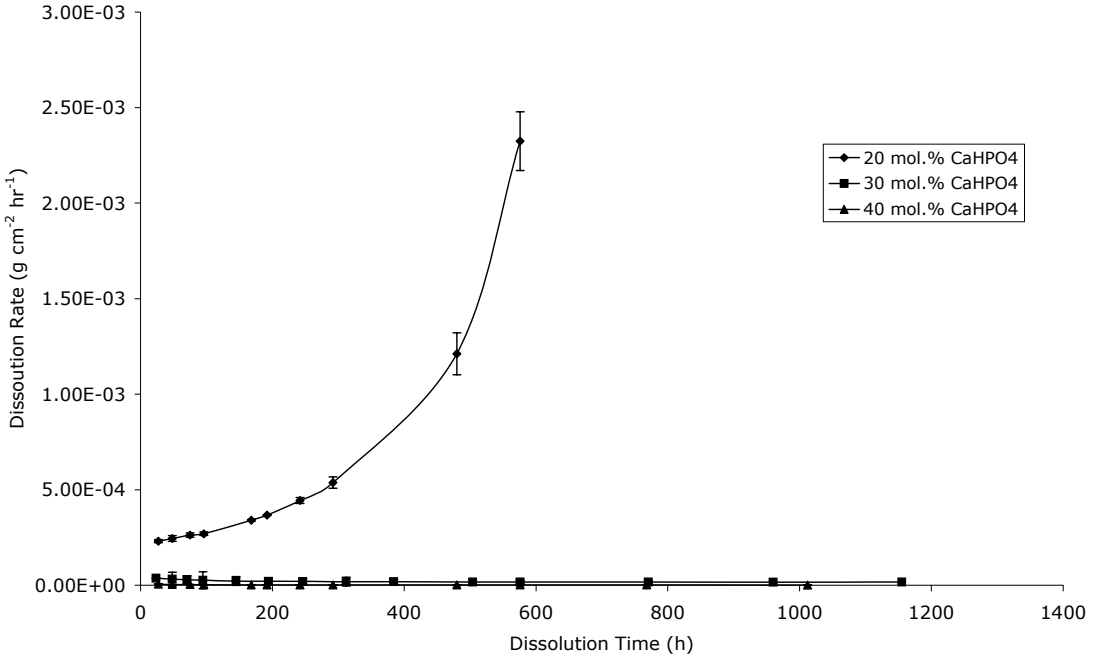

Figure 4.15 Dissolution rate (g cm^{-2} h^{-1}) against dissolution time (hours) for sodium phosphate glasses consisting of 20 to 40 mol.% $CaHPO_4$ and dissolved in SBF. Bars are standard error of the mean, where n = 2.

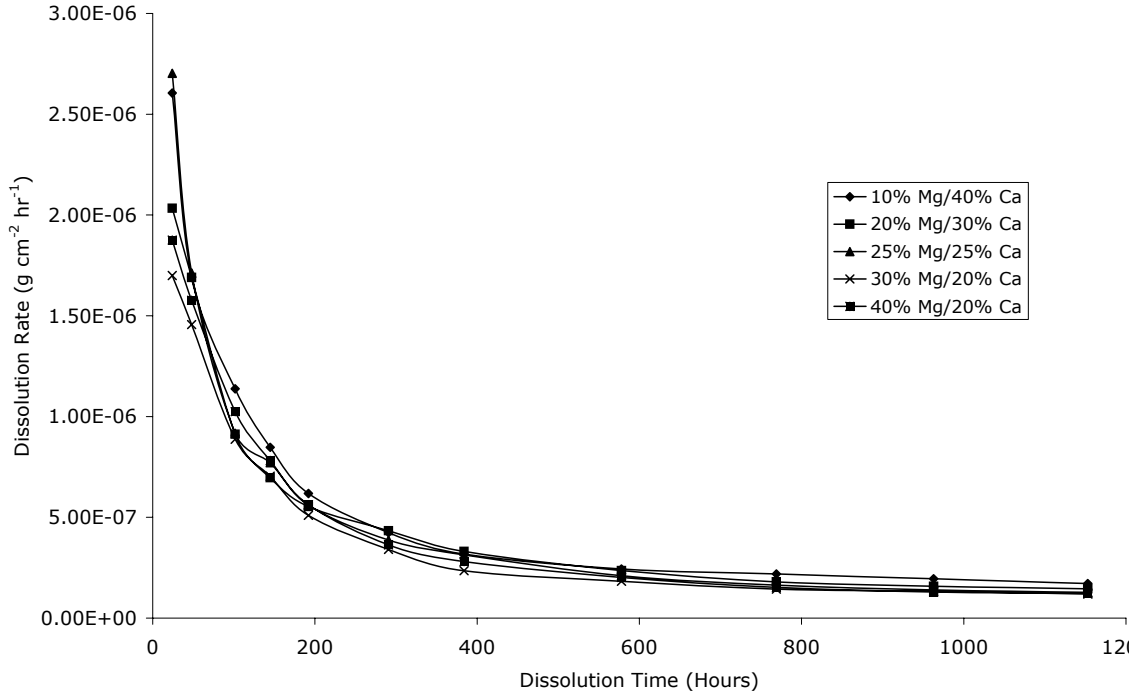

Figure 4.14 Dissolution rate (g cm^{-2} g^{-1}) versus dissolution time (hours) for phosphate glasses comprising of 50 mol.% NaH_2PO_4 and differing ratios of magnesium phosphate and calcium phosphate and dissolved in SBF. Bars are standard error of the mean where n = 2.

All of the glasses in the following range contained 50 mol.% NaH_2PO_4 with varying amounts of magnesium phosphate and calcium phosphate and were dissolved in SBF, figure 4.14. The addition of magnesium phosphate at the expense of calcium phosphate decreases the dissolution rate in SBF. The

dissolution rate for this range of glasses is in the range 2.7-1.7x10^{-6} g cm^{-2} h^{-1} after 24 hours. The rate decreased to 2.43-1.82x10^{-6} g cm^{-2} h^{-1} after 576 hours, forming a plateau. The glass which contains the highest amount of magnesium phosphate possessed the lowest dissolution rate.

4.2.4 X-Ray Photoelectron Spectroscopy

Survey scans of all the phosphate glass samples show the same peak positions for carbon, phosphorus, oxygen and sodium. Where present, calcium and magnesium were also seen in the same positions within the survey scan. The peak positions, and the shell of electron origin, are detailed in table 4-1 and illustrated in figure 4.16, which is the survey scan of 50 mol.% NaH_2PO_4, 25 mol.% $MgHPO_4$, 25 mol.% $CaHPO_4$ and gives peaks for all the elements of interest.

The high resolution scans of the elements and their deconvolution are shown in figure 4.17. The deconvolution of phosphorus, shown in figure 4.17, produced two peaks that are positioned at 134.8 eV ± 0.15 and 134.2 eV ± 0.15, with an average gap of 0.6 eV between the two. The oxygen peak was deconvoluted into three peaks, figure 4.17, which were positioned at 531.6,

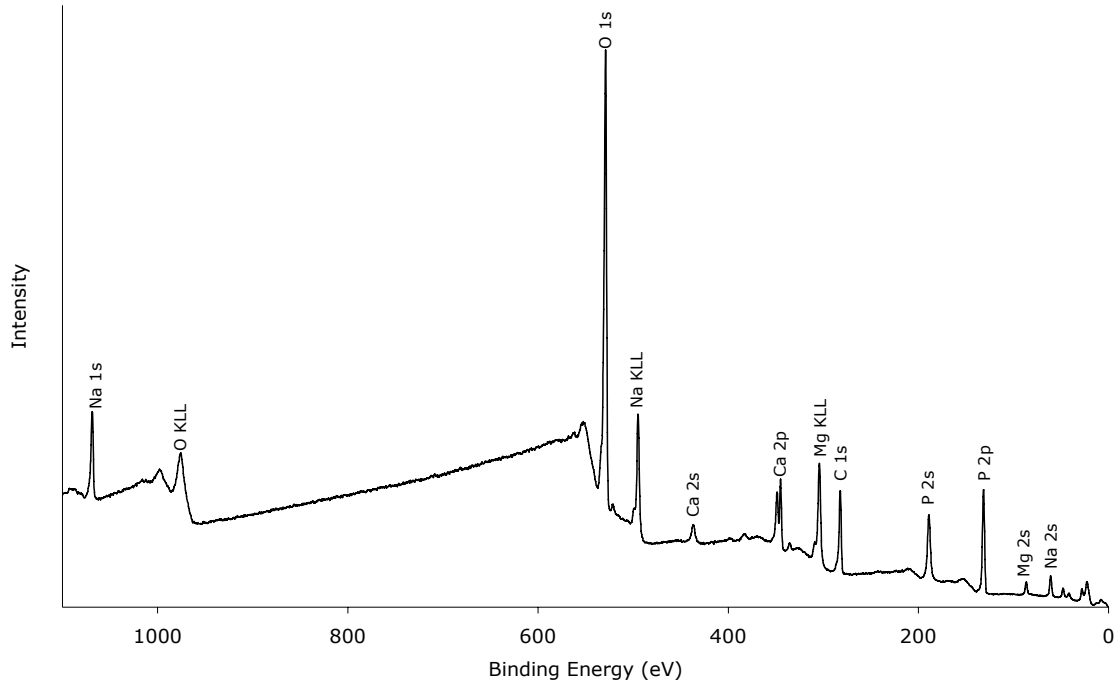

Figure 4.16 XPS spectrum showing all the peaks present in phosphate glasses containing sodium, magnesium and calcium. The carbon peak is used to correct charging effects. The four unlabelled peaks at the low binding energy end are: Mg 2p at 49 eV, Ca 3s at 41 eV, Ca 3p at 26 eV and O 2s at 23 eV

533.4 and 536.3 eV. Sodium and magnesium were positioned at 1071.75 and 50.8 eV respectively and were each fitted with a single peak. The calcium peak consisted of two separate peaks, which were both fitted with a separate, single peak that were positioned at 347.7 and 352.2 eV. Peaks from different glasses were consistently in the same position, hence separate values for each glass composition are not shown here.

The change in relative peak intensity, within the O 1s spectra, with divalent cation concentration is shown in figure 4.18. The effect of increasing the magnesium phosphate concentration, up to 50 mol.%, is shown on the left. As the concentration of $MgHPO_4$ increases, at the expense of NaH_2PO_4, the peaks at 533.4 and 536.6 eV decreases, relative to the peak at 531.6 eV, with increasing magnesium phosphate. The effect of $CaHPO_4$ addition to sodium phosphate, figure 4.18, is very similar to that of $MgHPO_4$. By increasing the concentration of calcium phosphate the peaks at 533.4 and 536.6 eV decrease with respect to the peak at 531.6 eV.

Peak Number	Element	Shell/Orbital	BE (eV)
1	O	2s	23
2	Ca	3p	26
3	Ca	3s	41
4	Mg	2p	49
5	Na	2s	64
6	Mg	2s	90
7	P	2p	130
8	C	1s	285
9	Mg	KLL	304
10	Ca	2p	346
11	Ca	2s	438
12	Na	KLL	501
13	O	1s	530
14	O	KLL	982
15	Na	1s	1072

Table 4-1 The position and identification of all possible peaks present, for phosphate glasses containing NaH_2PO_4, $MgHPO_4$ and/or $CaHPO_4$.

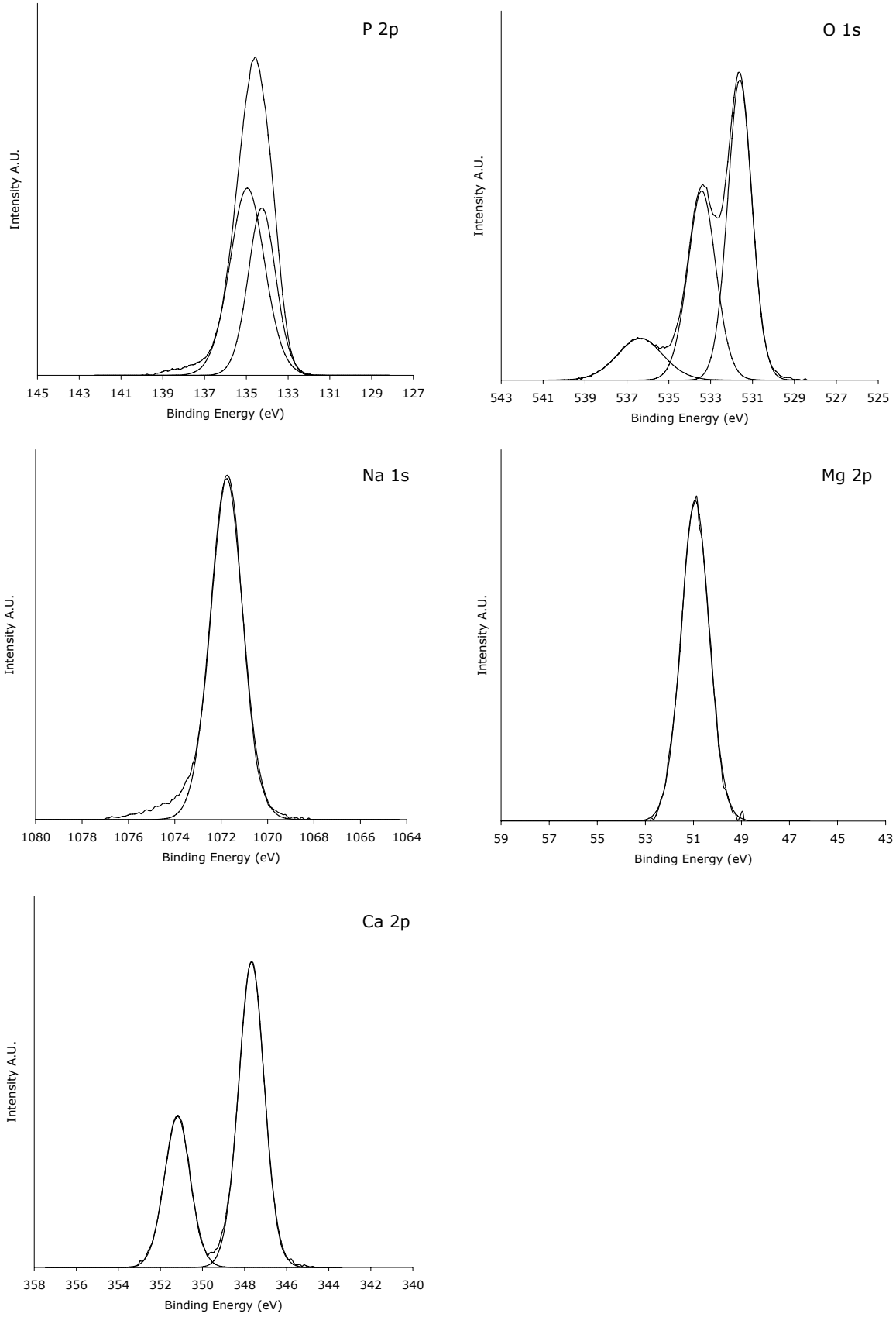

Figure 4.17 High resolution XPS scans for the elements of interest within the phosphate glasses. All peaks are from the 50 mol.% NaH_2PO_4/25 mol.% $MgHPO_4$/25 mol.% $CaHPO_4$ sample, except oxygen, which is from the 100 mol.% NaH_2PO_4 sample. All peaks are representative of the peak positions for the other glass compositions

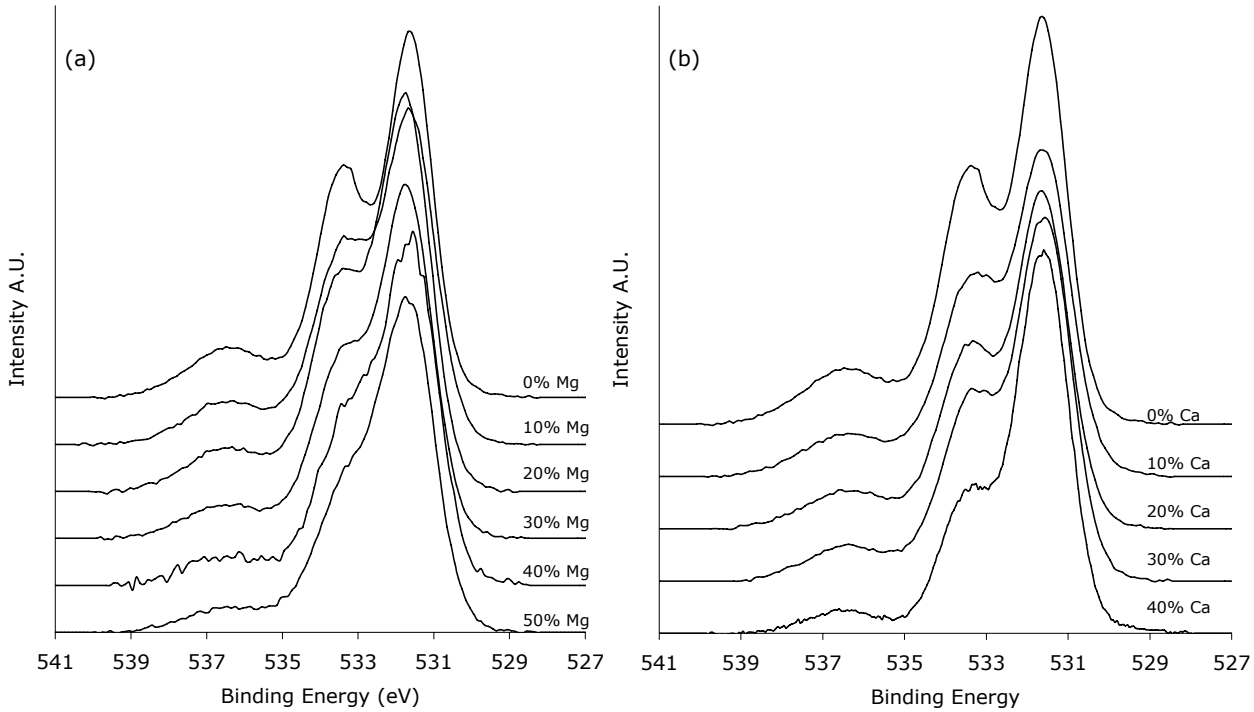

Figure 4.18 High resolution XPS scan of oxygen 1s peaks. The graph on the left shows the change in the oxygen peak with increasing magnesium, the top curve is pure sodium phosphate and each subsequent curve contains an additional 10 mol.% magnesium phosphate up to 50 mol.%. The graph on the right shows the change in the oxygen peak with increasing calcium content. Again, the top curve is pure sodium phosphate with each subsequent curve below containing an additional 10 mol.% calcium phosphate.

When the concentration of divalent cations is kept constant but magnesium phosphate is exchanged with calcium phosphate, as in the quaternary series, the relative peak intensities for oxygen 1s do not change, figure 4.19. The shoulder on the left of the main peak is more prominent on some of the curves because of slight variations in peak position rather than changes in relative intensities, table 4-2.

Glass Name	O 1s Peak Sep (eV)	BO/ NBO Ratio
10 Mg/40 Ca	1.614	0.366
20 Mg/30 Ca	1.676	0.380
25 Mg/25 Ca	1.711	0.371
30 Mg/20 Ca	1.629	0.376
40 Mg/10 Ca	1.741	0.369

Table 4-2 Relative peak separation between the O 1s BO and NBO, and the ratio between the stated peaks.

Glass composed of 80 mol.% NaH_2PO_4 and 20 mol.% $MgHPO_4$ was fractured and dissolved in triply deionised water for 0, 1, 3, 5 and 7 days before qualitative and quantitative analysis with XPS. The data indicated that the

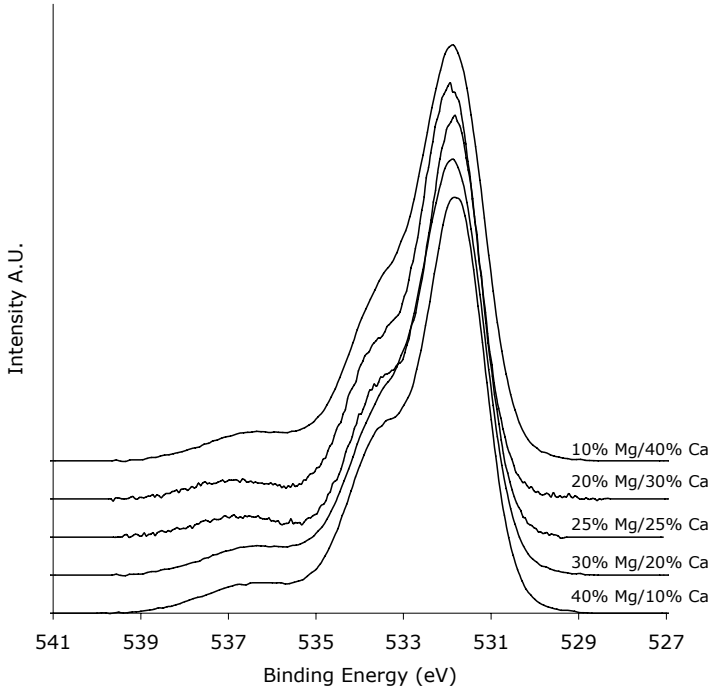

Figure 4.19 High resolution scans of the oxygen 1s peak for 50 mol.% sodium phosphate glass containing varying amounts of magnesium phosphate and calcium phosphate. The curve at the top contains the most magnesium phosphate, each subsequent curve contains higher concentrations of calcium phosphate, at the expense of magnesium phosphate.

fracture surface composition did not change after 5 days dissolution. The Na level remained at 33.45 at.% ± 0.25 %, phosphorus at 55.05 at% ± 0.25 % and magnesium at 11.70 at.% ± 0.6 %. After 7 days dissolution the Na concentration at the surface dropped to 22.59 at.% and the concentration of P and Mg rose to 63.86 and 13.55 at.% respectively. The relative intensity of the two main oxygen 1s peaks at 531.6 and 533.4 eV remain constant from 0 to 5 days, and then the peak at 533.4 eV decreases in size compared to the peak at 531.6 eV.

Analysis of the oxygen peak for the series of sodium phosphate glasses containing 10 mol.% magnesium phosphate, data not shown, that were melted at 900 °C for up to 16 h showed that the peak at 536.6 eV was largest, relative to the peak at 531.6 eV, after 1 h and then decreased at 2 h and remained at this relative size. The peak at 533.4 eV grew with melt time, in comparison with the peak at 531.6 eV, until after 4 h, it levelled out at the same proportion.

4.2.5 Infra-red Spectroscopy

Infra-red spectroscopy was performed on sodium phosphate glasses containing increasing amounts of either magnesium phosphate or calcium phosphate, figure 4.20. For the series containing magnesium, there are four peaks present. These peaks are located at approximately 1250, 1100, 900 and 750 cm^{-1}. It can be seen, that these peaks change shape and position with increasing magnesium phosphate concentration. The peak at approximately 1250 cm^{-1} slowly shifts to a lower wavenumber with increasing magnesium phosphate concentration, whilst simultaneously the peak at ~1100 cm^{-1} rapidly moves to a higher wavelength. This has the effect of closing the trough between the two peaks, producing a single broad peak. The peak at ~900 cm^{-1} becomes slightly more prevalent whilst shifting to higher wavenumbers with increasing magnesium phosphate. The peak at 750 cm^{-1} can be seen to consist of two peaks, both of which are shifting to higher wavenumbers with increasing magnesium phosphate concentration. As the magnesium phosphate concentration increases, the dominant peak at the higher wavenumber recedes, giving way to the peak at the lower wavenumber. However, this is not a complete turnabout, as at higher concentrations of magnesium phosphate there is just one broad peak, rather than a more distinct peak with a shoulder.

There are four main peaks in the IR spectra for sodium phosphate containing various amounts of calcium phosphate. These are located at wavelengths of approximately 1260, 1100, 890 and 750 cm^{-1}. The peaks at 1260 and 1100 cm^{-1} shift towards each other with increasing concentrations of calcium phosphate, while the peak at 1260 cm^{-1} simultaneously decreases in

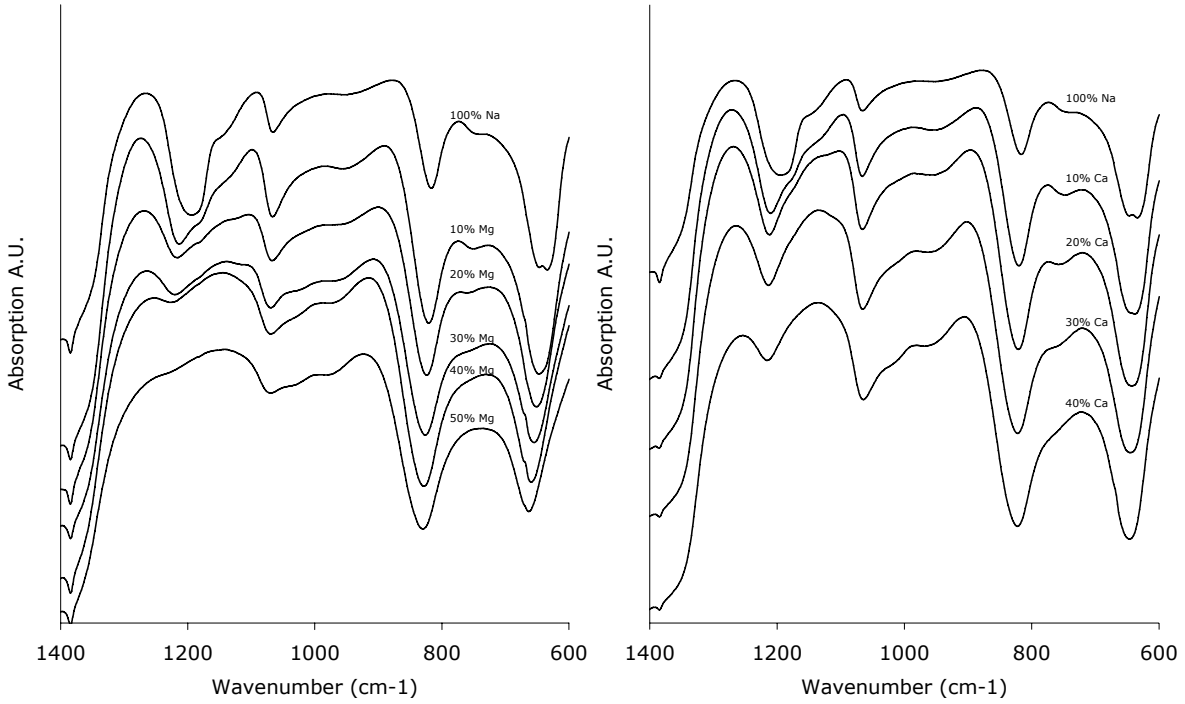

Figure 4.20 IR spectra of sodium phosphate glasses containing varying concentrations of either magnesium phosphate or calcium phosphate. The top spectrum is pure sodium phosphate, while the spectra below contain either magnesium phosphate or calcium phosphate in increasing 10 mol.% increments.

intensity and the peak at 1100 cm^{-1} becomes broader. The peak at 890 cm^{-1} moves to slightly higher wavenumbers with increasing levels of calcium phosphate. The peak at 750 cm^{-1} actually consists of two peaks, as the levels of $CaHPO_4$ increase, the peak positioned at the higher wavenumber decreases in favour of the growing peak at the lower wavenumber. This continues until at levels of 30 mol.% $CaHPO_4$, the peak previously at the higher wavenumber is just a shoulder of the lower wavenumber peak.

4.3 Discussion

4.3.1 Glass Production

It has been found that the glass forming ability of the melt is composition dependant. The naturally glass forming phosphorus pentoxide will only accept a certain concentration of cations before devitrification occurs, figure 4.1. If pure magnesium phosphate or calcium phosphate is considered as their constituent oxides, then phosphorus pentoxide accounts for 33.3 mol.%, it is the relatively low concentration of this glass former which prevents the formation of a glass melt. The addition of at least 50 mol.% sodium phosphate, which is 50 mol.% phosphorus pentoxide, increases the concentration of the glass forming constituent allowing the production of a glass.

However, it has been found that the melting point of magnesium phosphate and calcium phosphate is above 1250 °C, which is the highest temperature 95% Pt/5% Au crucibles can be heated to, while sodium phosphate melts at ~625 °C. During the melting process, the magnesium phosphate and/or calcium phosphate is taken into solution and upon cooling forms a glass. When loading the melt with high concentrations of divalent cation phosphate, ~> 60 mol. %, over saturation occurs. Cooling these melts results in heterogeneous crystal formation and growth from the remaining salt, which has not dissolved.

When divalent cation concentrations are below 60 mol.% but are 50 or 40 mol.% or higher for magnesium phosphate and calcium phosphate, respectively, only partial devitrification occurs. The melt is clear, suggesting

that all of the divalent cation salt is taken into solution but some crystallisation occurs upon casting. Crystal growth is limited to the regions of the glass samples that are exposed to the air or directly underneath these areas. These are the areas which are not in direct contact with and are near the top of the mould. Cooling rates are retarded in these areas, allowing crystal formation, which is prevalent on the surface that is in contact with the air. Changing the casting regime so that faster cooling rates are achieved, allows for the production of fully amorphous glass. However, when drawing fibres from these glasses, the required cooling rates are not achieved due to the bushing requiring a set temperature (dependant on the viscosity), which allows these glasses to crystallise before drawing occurs.

Analysis of the crystal like phase present in 50 mol.% $CaHPO_4$/50 mol.% NaH_2PO_4 using XRD, show that they consist of $Ca_2P_2O_7$ crystals. Indicating that after a set concentration, sodium phosphate cannot accept any more calcium phosphate without crystallisation. XRD of the suspected $MgHPO_4$ crystals was inconclusive due to the extremely low concentration of crystals produced. Although heating these glasses to their crystallisation temperature produced a white crystalline layer on the surface, this was not analysed as the small amount of crystals produced from overloading produced purple coloured crystals, which were obviously not the same phase.

4.3.2 XPS Analysis

X-ray photoelectron spectroscopy has been used extensively in the analysis of the structure and composition of phosphate glasses, e.g. (Gresch *et al.*, 1979; Bruckner *et al.*, 1980; Brow *et al.*, 1990a; Brow, 1996; Le Sauze *et al.*, 2000b; Salim *et al.*, 2001). The main strength in XPS lies within its ability to distinguish different elemental species.

Calcium was detected via the presence of two peaks positioned at 347.6 eV and 352.2 eV, which resulted from the ejection of electrons from the 2p orbital. Two peaks were observed here as the 2p orbital splits into $2p_{1/2}$ and $2p_{3/2}$ with a peak area ratio of 1:2 (Briggs *et al.*, 2003). As each of the two peaks are deconvoluted into single peaks, it follows that calcium is present as one species, namely as an ion with a +2 charge, corresponding well with a chemical shift of 3.5 and 4.6 eV for the $2p_{1/2}$ and $2p_{3/2}$ peaks respectively.

The peak at 1071.8 eV is deconvoluted into a single peak and is assigned to the 1s sodium orbital. The deconvolution into a single peak shows that sodium is present as only one species. There is no significant chemical shift compared to sodium metal, 1071.8 eV (Barrie *et al.*, 1975), but it is believed that sodium is ionised to Na^+, as the shift in peak position is very small, -0.2 eV (Swift, 1982). As the peak position and shape does not change with additions of magnesium or calcium, it is unlikely that these elements interact with sodium.

The presence of magnesium is confirmed by the peak at 50.8 eV, resulting from the ejection of an electron from the 2p orbital. This peak is deconvoluted into one peak, representing only a single species of magnesium in all glasses. A chemical shift in binding energy of 1.2 eV from 49.6 eV, as in metallic

magnesium, to 50.8 eV corresponds well with an oxidation state of +2 (Fuggle, 1977). The Mg 2p orbital does split into $2p_{1/2}$ and $2p_{3/2}$ but this is not observed in the high resolution scans. For elements where the 2p orbital is located at higher binding energies, the separation between the two 2p sub-orbitals is greater, e.g. Cu 2p at 932.7 and 957.3 eV and Ca as above. When the 2p orbital is located at lower binding energies, such as Mg, the 2p sub-orbitals are very close together and difficult to resolve.

The presence of magnesium, calcium and sodium in the form Mg^{2+}, Ca^{2+} and Na^{+} respectively is expected as these cations were in the phosphate salts used to produce the glass.

The peak at approximately 135 eV is due to electrons from the phosphorus 2p orbital. This corresponds to a chemical shift of 4 eV due to the phosphorus atom being part of the phosphate ion, this shift agrees well with that reported in the literature, 135.8-134.5 eV, e.g. (Gresch *et al.*, 1979; Brow *et al.*, 1994; Brow, 1996). There is some difficulty interpreting the deconvolution of the phosphorus. This is due to the small difference between the two 2p sub-orbitals as well as the possibility of the presence of more than one phosphorus species. The deconvolution of the peaks does not reveal two peaks with an area ratio of 2:1, prompting the suggestion that there is more than phosphorus species present. There are possibly four species of phosphorus relating to ultra, meta, pyro and ortho-phosphates. For the compositions studied here, ultra-phosphates and ortho-phosphates can be discarded. This leaves two possible phosphorus species, each with two sub-orbital peaks that are within close proximity of each other. This makes an accurate and reliable deconvolution of the phosphorus peak unlikely. It is better that any data to be

gained relating to the phosphate chain length can be deduced from the oxygen 1s peak.

One of the most beneficial uses of XPS, with respect to phosphate glasses, is the analysis of oxygen to determine the phosphate chain length. It was shown that the oxygen 1s peak can be deconvoluted into two separate peaks with binding energies at approximately 531 and 533 eV which are due to the non-bridging oxygen (NBO) and bridging oxygen (BO) species respectively (Gresch *et al.*, 1979), as shown in figure 4.21. Raman spectroscopy has previously been used to identify the presence of double bonded oxygen atoms and has found that they are present only in ultra-phosphate compositions (Brow *et al.*, 1994). In all other compositions, the double bond is delocalised over the remaining non-bridging oxygen atoms. Given that all the compositions here lie outside the ultra phosphate range, the number of BO and NBO for a given phosphate chain length can be predicted using the following equations:

$$BO = x - 1 \qquad \textit{Equation 4.1}$$

$$NBO = 2x + 2 \qquad \textit{Equation 4.2}$$

Where x is the phosphate chain length. These two equations can be combined to give the ratio of BO to NBO for a particular phosphate chain length:

$$y = \frac{(x-1)}{(2x+2)} \qquad \textit{Equation 4.3}$$

Where y is the ratio of BO/NBO and x is the phosphate chain length.

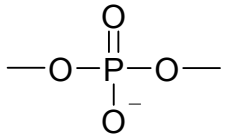

Figure 4.21 The two oxygen species present in the phosphate unit, the bridging (α) and non-bridging (β) oxygen.

This equation, equation 4.3, can be rearranged to express the phosphate chain length for a given BO and NBO ratio:

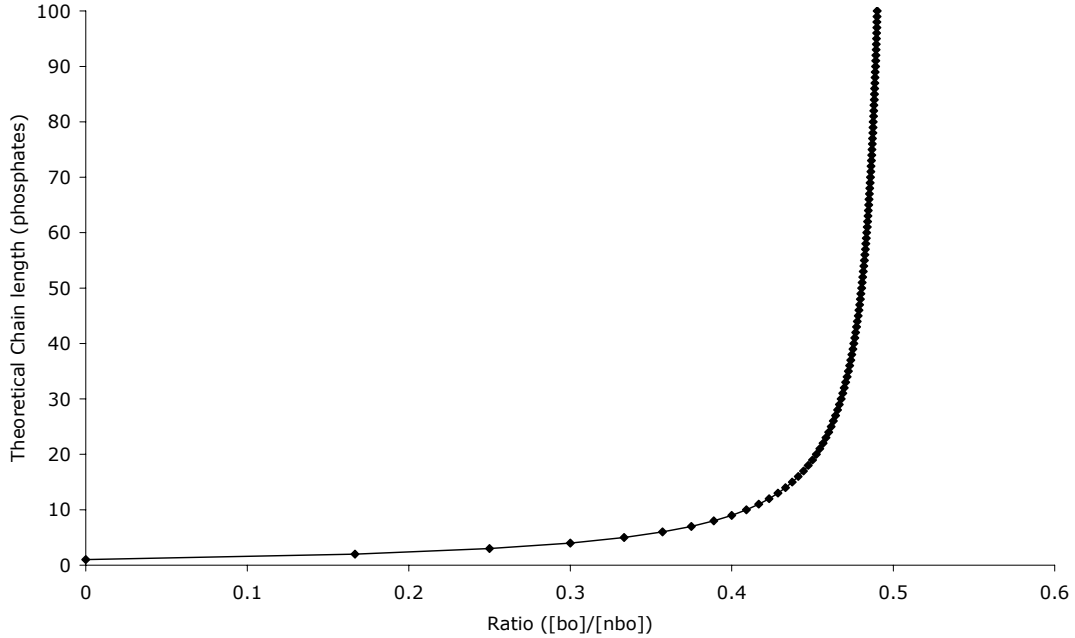

Figure 4.22 Relationship between the theoretical phosphate chain length and the ratio of bridging oxygens to non-bridging oxygens.

$$x = \frac{(2y+1)}{(1-2y)} \quad \textit{Equation 4.4}$$

Expressing these mathematical models graphically allows for the easy identification of phosphate chain length, figure 4.22.

The theoretical ratios for sodium phosphate glass containing up to 50 mol.% divalent cation salts can be calculated by assuming that each sodium phosphate molecule will give rise to a Q^2 phosphate species and each divalent cation phosphate molecule will give rise to a terminal Q^1 phosphate species. Each Q^2 species has 1 BO and 2 NBO while each Q^1 species has 0.5 BO and 3 NBO, this information can be used to deduce the total mol.% of BO and NBO, hence the [BO]/[NBO], and using equation 4.4 to calculate the theoretical chain length. Bunker *et al* proposed an equation to give the theoretical phosphate chain length from the composition of the glass with respect to phosphorus, mono-valent and divalent cation concentration:

$$n = \frac{2}{\left(\frac{M+2M'}{P} - 1\right)} \quad \textit{Equation 4.5}$$

Both equation 4.4 and equation 4.5 give identical chain lengths for the same glass compositions.

Equation 4.4 was used to calculate the phosphate chain length of all compositions of phosphate glass for a measured [BO]/[NBO] ratio, figure 4.22. The phosphate chain length is controlled by the composition of the glass (Van Wazer, 1950a; Griffith, 1995; Brow, 2000). The addition of either magnesium or calcium at the expense of sodium decreases the phosphate chain length, as expected. Whilst glasses containing constant levels of sodium and varying amounts of calcium and magnesium possess the same phosphate chain length. All glasses produced in this study possessed at least one mono valent cation for every phosphorus atom, meaning no ultra-phosphate glasses were produced. In pure sodium phosphate glass each phosphate molecule is associated with one sodium cation, producing Q^2 phosphate species, giving a meta-phosphate, possessing, in theory, infinitely long phosphate chains, figure 4.23.

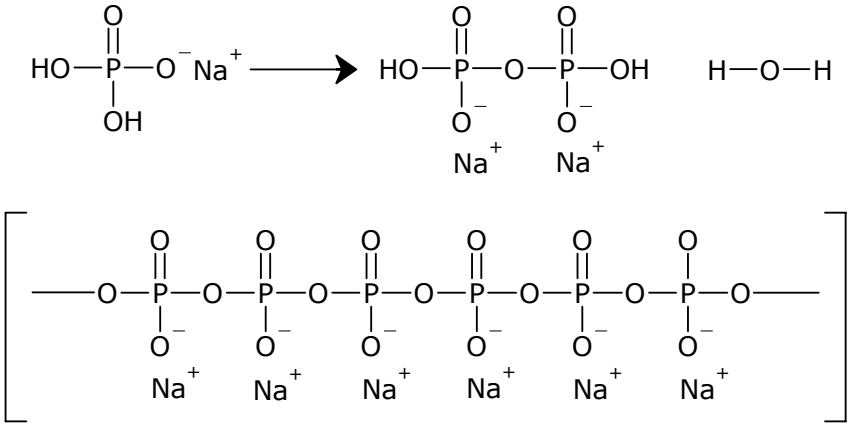

Figure 4.23 Polymerisation of pure sodium phosphate (Q2) via a condensation reaction to give a phosphate chain of, theoretically, infinitely long length.

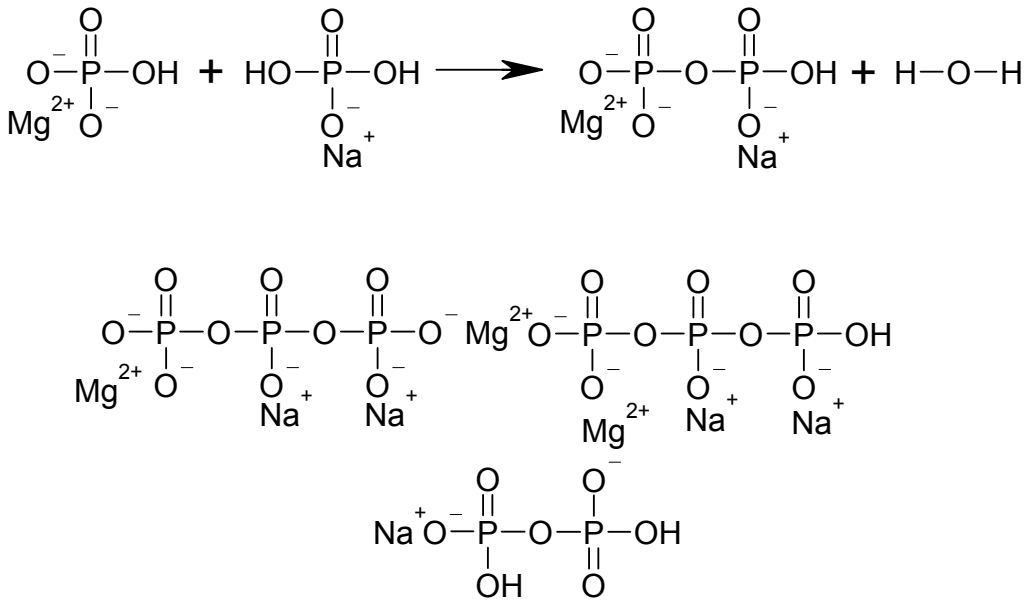

Figure 4.24 The addition of magnesium or calcium phosphate salts to the glass melt inhibits polymerisation by bonding to two oxygen atoms, reducing the number of bridging atoms per phosphate from two to one. However, network formation occurs due to the metal/phosphate cross links.

Composition	Theo [BO]/[NBO] Ratio	Measured [BO]/[NBO] Ratio	Theo Chain Length	Measured Chain Length
100% Na	0.5	0.48	∞	49
10% Mg	0.45	0.47	19.00	32.33
20% Mg	0.41	0.46	10.11	24.00
30% Mg	0.37	0.43	6.69	13.29
40% Mg	0.33	0.41	4.88	10.11
50% Mg	0.30	0.35	4.00	5.67
10% Ca	0.45	0.46	19.00	24.00
20% Ca	0.41	0.43	10.11	13.29
30% Ca	0.37	0.41	6.69	10.11
40% Ca	0.33	0.40	4.88	9.00
10% Mg/40% Ca	0.3	0.366	4.00	6.46
20% Mg/30% Ca	0.3	0.380	4.00	7.33
25% Mg/25% Ca	0.3	0.371	4.00	6.75
30% Mg/20% Ca	0.3	0.376	4.00	7.06
40% Mg/10% Ca	0.3	0.369	4.00	6.63

Table 4-3 Theoretical and measured BO/NBO ratios and phosphate chain length for all glasses studied. All compositions are mol.% phosphate salts with the balance composing of sodium phosphate salt.

The introduction of divalent cations into the glass decreases chain length by inhibiting polymerisation. Each divalent cation forms an ionic bond with two oxygen atoms, producing terminating Q^1 phosphate species that can only bond to one phosphate molecule, figure 4.24. Increasing the concentration of divalent cations further decreases the phosphate chain length, when all mono

valent cations have been substituted only terminating Q^1 species remain, giving a highly cross linked pyrophosphate molecular structure.

Error within these results increases as the BO/NBO ratios approach 0.5, as small variations in the ratio correspond to large changes in theoretical chain lengths. For example, a change in ratio from 0.15 to 0.25 corresponds to an increase in chain length from 1.85 to 3, while a change in ratio from 0.35 to 0.45 corresponds to an increase in chain length from 5.67 to 19.

The phosphate chain lengths calculated here are longer than the theoretical chain lengths, with the exception of pure sodium phosphate. This is unusual as phosphorus evaporation and water contamination, which reduces the chain length by acting as metallic ions (Griffith, 1995; Brow, 2000), normally occurs, causing a reduction in the expected chain length. Elemental analysis using CASA XPS shows that there is, on average, a 5 % reduction in sodium concentrations in all glass compositions. This may indicate that sodium is being lost during the glass melt stage via vaporisation. This problem could be reduced in future by decreasing melt time from 4 h to 1 h at 1200 °C, as DSC studies here suggest that polymerisation would be complete after 1 h. However, EDX was performed on the starting material, NaH_2PO_4, to check the composition. The expected composition is 50 mol.% Na_2O/50 mol.% P_2O_5, but the values obtained were 47.3 mol.% NaO_2/52.7 mol.% P_2O_5. The value for sodium is approximately 5 % lower than expected, showing that the changes in glass composition are due to precursor composition rather than experimental procedure. This would increase the relative amount of phosphate per metal cation charge, causing an increase in phosphate chain length. The lack of phosphorus evaporation may be due to the starting materials used in this study. Only phosphate salts were used, while, to the

knowledge of this author, either phosphorus pentoxide or ammonium phosphate is always used elsewhere to increase the phosphate concentration without introducing additional cations, e.g. (Bunker *et al.*, 1984; Brow, 1996; Franks *et al.*, 2000; Ahmed *et al.*, 2004b; Gao *et al.*, 2004a). As the phosphorus is introduced as a phosphate salt, the problem of evaporation before incorporation into a glass melt has been removed.

Unlike every other glass composition studied here, pure sodium phosphate glass does not have a higher chain length than predicted as the theoretical chain length is infinite. It has been suggested that due to contamination with water, when a phosphate glass is melted under an air atmosphere; the precise composition of the melt, and inhomogeneity of the melt, the potential chain length is severely retarded (Griffith, 1995). The same author melted sodium dihydrogen phosphate at 900 °C for 10 minutes before quenching the glass. The resulting glass possessed an average chain length of 100, where theoretically the chain length should be near 1,000,000. Repeating this experiment with a slow cool to 600 °C allowed the glass to crystallise. The glass then possessed an average chain length of 150. Crystallisation was stated to drive impurities, i.e. water, to the surface of the crystals; upon recrystallisation, more water is driven off. A maximum average chain length of only 400 was possible using this method, demonstrating that there are other factors affecting the chain length.

The phosphate chain length for sodium phosphate glasses containing varying amounts of calcium phosphate and magnesium phosphate are all very similar, ranging from 6.5 to 7.5. These are slightly higher than expected but within error if sodium evaporation is considered. This shows that the results are repeatable and that sodium evaporation is predictable.

Comparison of the phosphate chain length for a pristine 80 mol.% NaH_2PO_4/20 mol.% $MgHPO_4$ surface with surfaces that had been dissolved for 1, 3, 5 and 7 days shows that the phosphate chain length does not decrease with time, demonstrating that dissolution does not occur via chain hydrolysis as proposed by Gao *et al* but rather by the hydration of complete chains (Bunker *et al.*, 1984; Delahaye *et al.*, 1998). Bunker *et al*, used pH titration to confirm that the number average chain length of meta-phosphate calcium phosphate glass in solution was the same as that calculated for the bulk glass. Elemental analysis of the dissolving glass surface compared to a pristine surface showed that the composition remained the same, despite dissolution over a seven day period, demonstrating no selective leaching of cations.

The fracture surface analysis of oxygen from a series of glasses, containing 10 mol.% $MgHPO_4$/90 mol.%, which were melted at 900 °C for 1, 2, 4, 8 and 16 h revealed phosphate chain length elongation from 1 to 4 h before forming a plateau at 35±3 phosphate units. The chain lengths here are all higher than theoretically predicted, elemental analysis using CASA XPS shows that this is due to sodium evaporation increasing the relative phosphorus content. The increase of phosphate chain length with melt time matches the Tg and dissolution data, as they increase/decrease with increasing melt time. This indicates that changes in the phosphate chain length do affect the glass properties, albeit to a lesser degree than the cation composition.

4.3.3 IR analysis

The identification of the peaks observed in the IR wavenumber range of 1400 – 600 cm^{-1} has been well documented (Exarhos *et al.*, 1974; Arzeian *et al.*, 1991; Salim *et al.*, 1995; Karmakar *et al.*, 2001; Metwalli *et al.*, 2001; Reis *et al.*, 2001). The four peaks present are all generally believed to be due to vibrations within the phosphate tetrahedron. The peaks at approximately 1260 and 1100 cm^{-1}, and the range 1050-850 cm^{-1}, are due to non-bridging phosphorus – oxygen bonds. There is some difference in opinion as to the exact nature of these bonds. It has been suggested that the peak at the highest wavenumber is caused by the P=O double stretching bond, the peak at 1100 cm^{-1} is due to $P\text{-}O^-$, non bridging, stretching and the range is caused by $P\text{-}O^-\ M^+$ stretching bond (Arzeian *et al.*, 1991; Salim *et al.*, 1995). Cations which are present, bond to the oxygen anions, and shift the wavenumber at which the glass absorbs IR radiation by changing the length of the bond. However, Raman spectroscopy of ultra and meta sodium phosphate glasses has shown that the P=O only exists in ultra-phosphate compositions (Brow *et al.*, 1994), so the peak at 1260 cm^{-1} must be due to another molecular vibration. The other theory is that the peaks at 1260 and 1100 cm^{-1} are due to the asymmetrical and symmetrical stretching of the non bridging PO_2 unit (Exarhos *et al.*, 1974; Metwalli *et al.*, 2001). This assignment fits with the Raman results suggesting no P=O in non ultra-phosphate compositions (Brow *et al.*, 1994). These authors (Exarhos *et al.*, 1974; Metwalli *et al.*, 2001), have assigned the range at 1050-850 cm^{-1} to the asymmetrical stretch of the bridging P-O. This is in disagreement with Arzeian *et al* who suggested this

peak to $P\text{-}O^{-}\ M^{+}$, the latter fits better as the glasses possessed more than one cation, leading to more than one bond length, hence a range of wavenumbers.

The final peak at approximately 750 cm^{-1} is assigned to the P-O-P vibrations (Exarhos *et al.*, 1974; Arzeian *et al.*, 1991; Salim *et al.*, 1995; Karmakar *et al.*, 2001; Metwalli *et al.*, 2001). More specifically it was assigned to the symmetrical stretching of the P-O-P (Exarhos *et al.*, 1974; Salim *et al.*, 1995).

The peak shifts for bands at 1260, and 750 cm^{-1} are very small and can be considered to be within experimental error. The peak at approximately 750 cm^{-1}, which was assigned to P-O-P stretching, can be seen to decrease in intensity as the concentration of divalent cation is increased. This agrees with the XPS data, stating that the chain length, and hence the concentration of P-O-P bonds decreases with increasing divalent cation levels.

Subsequently the peaks at 1260 and 1100 cm^{-1}, which were assigned to the asymmetrical and symmetrical stretching of non-bridging P-O, are seen to broaden and intensify. The broadening is probably due to the addition of divalent cations giving rise to greater variation in bond length and angle. While the greater intensity is caused by an increase in terminating Q^{1} phosphate species which occurs as the chain length decreases.

The peak at approximately 900 cm^{-1} increases in intensity as the concentration of divalent cations increase. This indicates that this area of the $P\text{-}O^{-}\ M^{+}$ range is due to magnesium and calcium affecting absorbance of the $P\text{-}O^{-}\ M^{2+}$ group by altering the bond length/angle. The decrease in intensity of the area around the wavenumber of 985 cm^{-1} is synonymous with the decrease in sodium within both series of glasses. Indicating that this area of the spectra is due to absorbance by the $P\text{-}O^{-}\ Na^{+}$ group

4.3.4 Thermal Analysis

Before a detailed discussion of the glass transition temperature (T_g, a.k.a. glass transformation range) occurs, it may be useful to have a definition. The T_g is defined as the temperature at which the super-cooled liquid converts to a solid upon cooling, or, conversely, where the solid begins to behave as a visco-elastic solid upon heating (Shelby, 1997). It is above the T_g where the molecules possess enough thermal energy to assume relaxed conformations.

The change in T_g with melt time is due to changes within the molecular structure of the phosphate glass. When heated to temperatures in excess of 625 °C, sodium ortho-phosphate salt undergoes polymerisation, figure 4.25. The presence of longer chains increases the melt viscosity, thereby increasing the T_g by requiring more energy to allow the chains to acquire relaxed conformations.

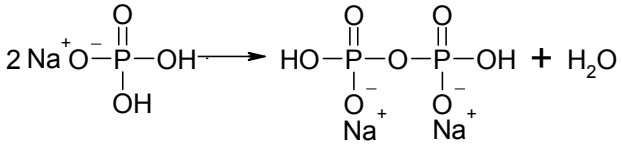

Figure 4.25 Polymerisation of sodium phosphate salt. This reaction can continue, theoretically producing chains of infinite length.

This reaction slows with time as the chance of chain ends coming into contact with ortho-phosphates or other chain ends is reduced. Until all the ortho-phosphate has reacted. When the melt is heated to 800 °C, the highest T_g attained is 293 °C. This is below the value of 295 °C obtained by heating the melt to 900 °C or above. If, in this case, the T_g is controlled by phosphate chain length, then a maximum of 295 °C would represent completion of polymerisation. Since T_g only reaches 293 °C when heated to 800 °C, then it can be assumed that full polymerisation did not occur.

This could be explained by the viscosity of the melt, with the lower viscosity of the cooler melt not allowing the phosphate groups or chain ends enough time or opportunity to come into close enough contact to polymerise. However, if this was true then the T_g should continue to rise, albeit at a retarded rate, until it eventually reaches 295 °C.

By increasing the temperature from 900 °C to 1200 °C, the melt requires decreasing periods of time to reach the maximum T_g of 295 °C. Increasing the thermal energy both produces a less viscous melt and provides more energy to drive the polymerisation reaction. Indeed, after only one hour at 1200 °C the maximum T_g is obtained, indicating that polymerisation is complete.

The addition of 10 mol.% of either magnesium phosphate or calcium phosphate produces curves of a similar shape, only at higher temperatures, figure 4.5. This demonstrates that polymerisation occurs with the addition of small amounts of magnesium phosphate or calcium phosphate to sodium phosphate glass.

Manufacture of sodium phosphate glass using alumina crucibles instead of platinum, produced higher T_g values. The increase in T_g values with time was greater compared to the corresponding values for platinum crucible made glasses, even after 4 h at 800 °C the T_g exceeds the highest T_g observed in any of the sodium phosphate glasses produced in platinum crucibles. This is thought to be caused by aluminium contamination, which occurred during the manufacturing process (Parsons *et al.*, 2004a). The phosphate glass melt is very corrosive, removing a large amount of alumina during the production process.

Sodium phosphate glass possesses a theoretically infinite phosphate chain with no branches (Griffith, 1995). With the introduction of aluminium ions, the maximum phosphate chain length will be reduced, but the trivalent aluminium ions will provide large amounts of cross-linking. The large increases in T_g shown here, compared to identical glasses made in platinum crucibles, demonstrates that the addition of aluminium ions has an overriding effect on the T_g of sodium phosphate glass. Metal ion cross-linking has been shown to have a more significant effect on the T_g than chain length (Brow, 2000), hence aluminium contamination has a significant effect.

EDX analysis has shown that aluminium is not only present in these glasses, but that the concentration increases with melt time and temperature. The curve on the aluminium concentration/melt time curve is very similar to the T_g/melt time curve, including the 'dip' at four hours for the 900 °C melt. This is evidence that the large increases in T_g are primarily due to the presence of aluminium rather than the increase in chain length, as seen for the glasses made in platinum crucibles.

Increasing levels of aluminium concentration with temperature are consistent with an ongoing erosion effect limited by viscosity (Parsons *et al.*, 2004a). Higher temperature will reduce the viscosity, increasing the rate of convection and flex-line erosion. As more aluminium is incorporated into the melt, the amount of cross-linking will increase, increasing the viscosity of the melt and hence decrease the erosion rate and incorporation of further aluminium.

Aluminium contamination from alumina crucibles was investigated in the 50 mol.% CuO/50 mol.% P_2O_5 system for temperatures up to 1200 °C and melt times of up to 20 h (Bae *et al.*, 1991). Up to 9 mol.% Al_2O_3 was

incorporated into the glass after 20 h at 1200 °C compared to 14 mol.% observed in this work for sodium phosphate glass after 16 h at 1200 °C. The differences between these results may be due to the addition of different cations affecting the melt viscosity and the different grade of crucibles.

The substitution of sodium phosphate for either calcium phosphate or magnesium phosphate increases the T_g of phosphate glass linearly, figure 4.8. This is due to the cross-linking, and hence network formation, provided by either calcium or magnesium ions present in the melt (Griffith, 1995). The greater tortuosity provided by the cross-linking requires more energy, hence heat, to allow the glass to adopt the properties of a visco-elastic solid and adopt relaxed molecular conformations. Increasing the amount of magnesium or calcium in the system provides more cross-links, creating a more complex network. Tg increases in the order Na<Ca<Mg<Al, which is supported by (Metwalli *et al.*, 2001), due to increasing cation valence and the greater

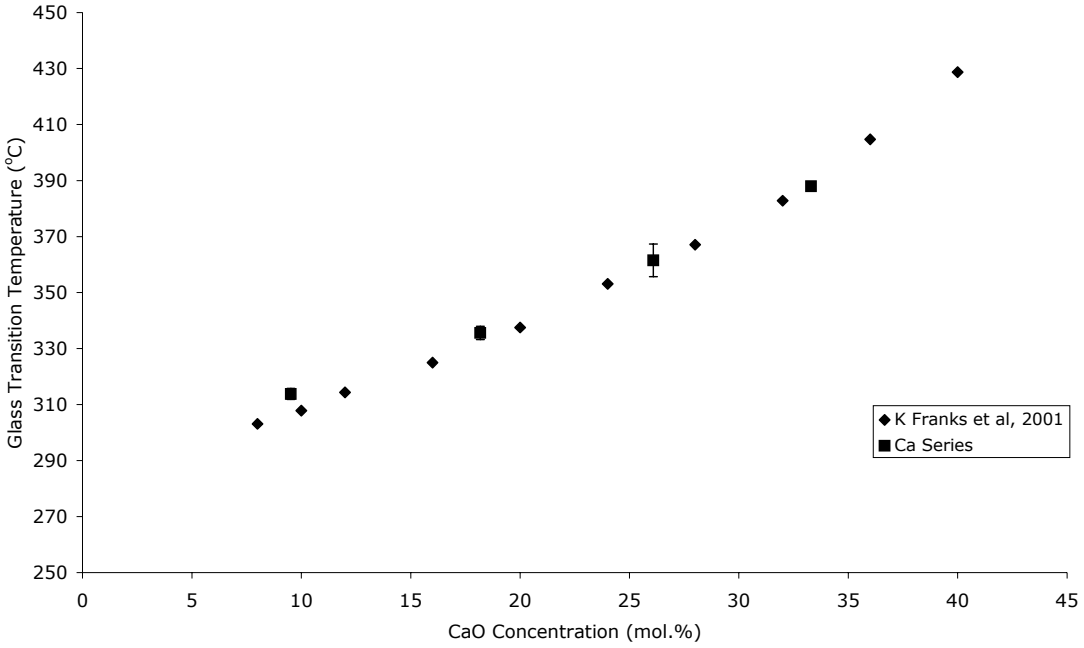

Figure 4.26 Comparison of the Tg for two series of phosphate glasses containing differing amounts of sodium and calcium. K Franks' glasses (diamonds) comprised of 45 mol.% P_2O_5, x mol.% CaO and 55-x mol.% Na_2O. The glasses in this work (squares) were made from salts hence the control of phosphorus pentoxide was not possible and the sodium/phosphorus pentoxide ratio is different for each sample.

covalent character of bonds linking the phosphate chains which is caused by the higher field strength cations (Eisenberg *et al.*, 1966; Clement *et al.*, 1999; Brow, 2000).

The greater effect of magnesium on the T_g is mirrored in the system containing 50 mol.% sodium phosphate with varying amounts of calcium phosphate and magnesium phosphate, where the substitution of calcium for magnesium causes an increase in T_g.

Phosphate glasses containing calcium and sodium were produced from their oxides and sodium phosphate salt by Ahmed *et al*. These glasses contained lower amounts of sodium and higher concentrations of calcium. However, their $P_{45}C_{30}N_{25}$ (numbers represent mol.% of oxides) glass, which is of similar composition to 40 mol.% $CaHPO_4$/60 mol.% NaH_2PO_4, has a Tg of 374.88 °C compared to 388.8 °C. The discrepancy is due to a 3.5 % higher phosphate (lower calcium oxide) concentration. Increases in T_g were stated to be due to the higher concentrations of CaO, a refractory material (Franks *et al.*, 2001).

The same group performed some earlier T_g work on glasses with the composition: 45 mol.% P_2O_5, x mol.% CaO and 55-x mol.% Na_2O (Franks *et al.*, 2001). The relationship between CaO concentration and T_g was not linear, at higher levels of CaO the Tg increased more per mol.% of CaO. Their data is very similar to the data presented here, figure 4.26, differences are explained by the slight differences in phosphorus pentoxide ratios, which were kept constant in K Franks' work but decrease with increasing calcium concentration in this study.

4.3.5 Dissolution

The decrease in dissolution rate for sodium phosphate glasses containing 10 mol.% $MgHPO_4$ with longer melt times coincides with the increase in T_g with melt time. The reducing dissolution rate is due to the increasing phosphate chain lengths, as demonstrated by XPS, requiring more time to hydrate to an extent where they can dissociate from the glass and dissolve. Dissolution rates for glasses melted for 8 and 16 h are almost identical, as are their T_g values, adding evidence to the theory that the polymerisation is complete after 8 h at 900 °C. The drop in dissolution with time is due to the increasing ionic strength of the solution (Delahaye *et al.*, 1998) and is discussed in more detail later.

Gough *et al* reported that the dissolution rate of sodium phosphate glasses decreased with increasing melt time. Decreases in dissolution rates reported were much lower than found in this work, however, the glasses prepared by

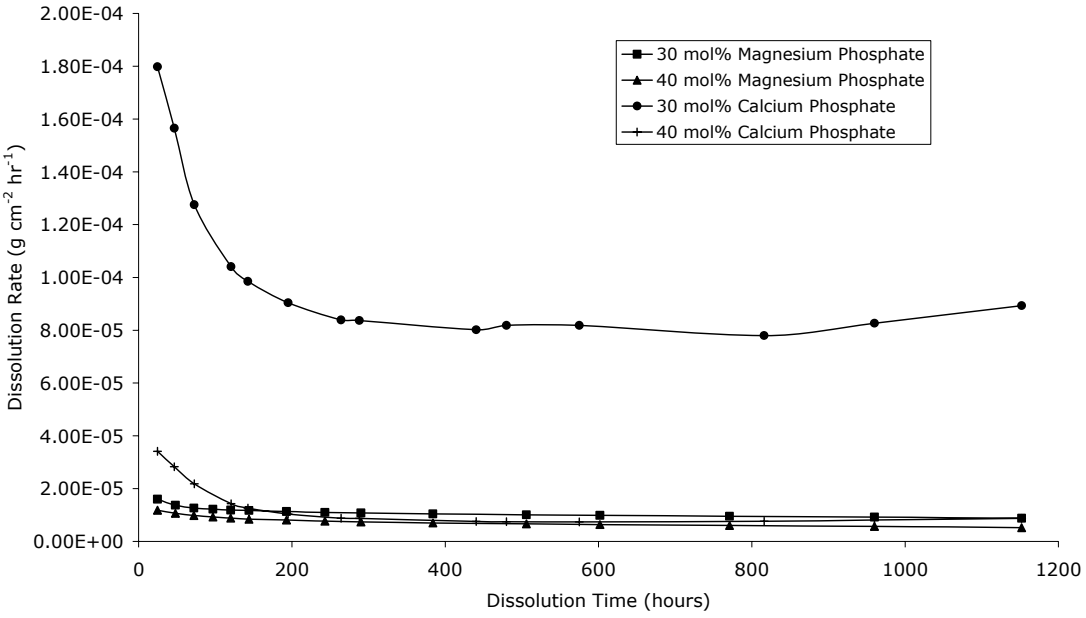

Figure 4.27 The dissolution rate against time for sodium phosphate glasses containing either 30 or 40 mol.% of either magnesium phosphate or calcium phosphate.

Gough et al were made in fused alumina crucibles and no comment was made on the effect of aluminium contamination which has been shown to be considerable in this work and by others (Parsons *et al.*, 2004a).

The addition of either magnesium phosphate or calcium phosphate to sodium phosphate has the effect of reducing the dissolution rate. Substituting the mono-valent sodium with the divalent cations introduces cross-links between phosphate chains at the expense of chain length. Increasing the divalent cation concentration provides a larger amount of cross-links, which in turn improve network formation. This supports the theory that metal oxide content has an overriding effect on the dissolution rate compared to the phosphate concentration (Uo *et al.*, 1998; Brow, 2000; Franks *et al.*, 2000; Kurkjian, 2000; Karabulut *et al.*, 2001; Marino *et al.*, 2001; Ahmed *et al.*, 2004b)

Assuming dissolution after 8 weeks is stable and linear, the dissolution rate, g cm^{-2} h^{-1}, of the ternary systems may be predicted mathematically using an exponential fit, which is based on the divalent cation phosphate salt concentration, mol.%. Using the dissolution rates for glasses with 10 mol.% divalent cation up to 40 and 50 mol.% calcium phosphate and magnesium phosphate respectively, figure 4.28, the following equations are obtained:

$$y = 1.4499e^{-3.0526x} \qquad \textit{Equation 4.6}$$

$$y = 0.0078e^{-1.788x} \qquad \textit{Equation 4.7}$$

Where y is the dissolution rate and x is the mol.% of $CaHPO_4$ and $MgHPO_4$ in equation 4.6 and equation 4.7 respectively.

These equations have R^2 values of 0.9869 and 0.7022 respectively, showing a good fit for the calcium phosphate glass. However, by omitting the dissolution rate for sodium phosphate glasses containing 10 mol.%

magnesium phosphate, an R^2 value of 0.9733 is obtained with the following equation:

$$y = 0.00004e^{-0.626x} \quad \textit{Equation 4.8}$$

Where y is the dissolution rate in g cm^{-2} h^{-1} and x is the mol.% of $MgHPO_4$.

Gough *et al* investigated the effect of calcium phosphate addition to sodium phosphate on the degradation rate. 14 mol.% $CaH_2(PO_4)_2$ was added to NaH_2PO_4 and melted at 1000 °C for up to 6 h in fused alumina crucibles. With the use of a meta-phosphate calcium phosphate precursor, it is expected that these glasses possess a higher degradation rate due to the lower relative concentration of metal oxides. This is not observed. Degradation rates are stated to decrease with melt time to a value of $1x10^{-5}$ g cm^{-2} h^{-1} after 5 h melt time, which is comparable to their sodium phosphate glass after 6 h melt time, 3.5 g cm^{-2} h^{-1}, while the 40 mol.% $CaHPO_4$ in sodium phosphate studied in this investigation has a dissolution rate of $1x10^{-5}$ g cm^{-2} h^{-1}. The unexpectedly low

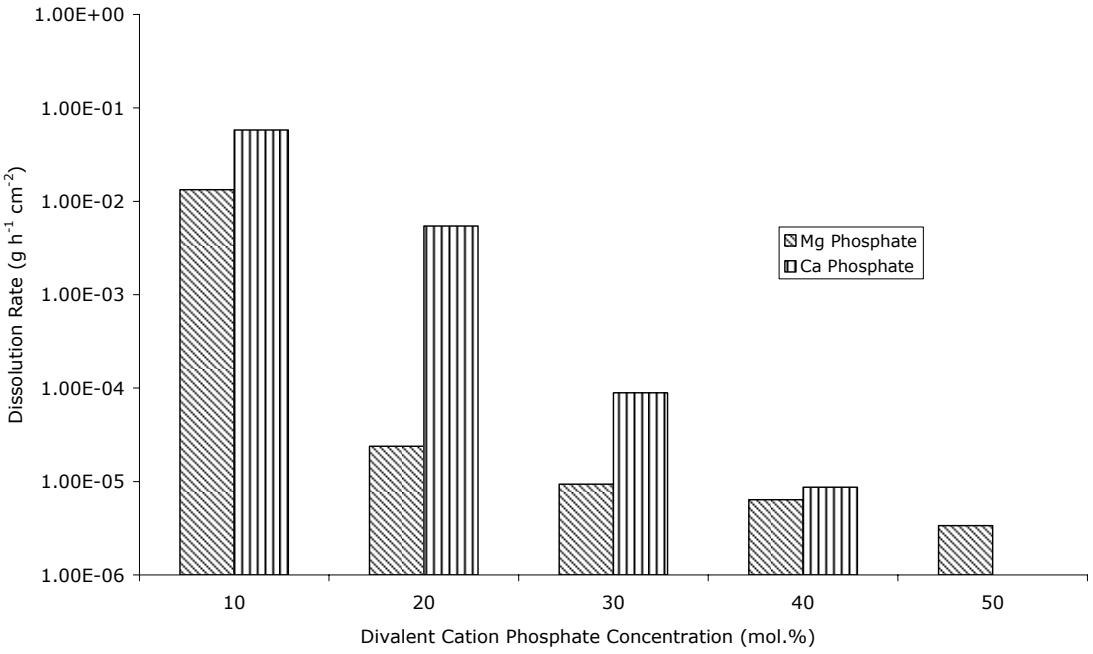

Figure 4.28 Dissolution rate (g cm^{-2} h^{-1}) of sodium phosphate glasses containing varying amounts of either magnesium phosphate or calcium phosphate after 8 weeks dissolution.

dissolution rate is due to the use of alumina crucibles in the manufacturing process and the subsequent aluminium contamination (Parsons *et al.*, 2004a).

Meta-phosphate glasses were produced from calcium diphosphate and sodium phosphate, which were dissolved in water at 40 °C (Delahaye *et al.*, 1998). It was stated that the addition of calcium at the expense of sodium reduced the dissolution rate of their glasses. Up to 30 mol.% CaO, the dissolution rate followed an exponential decay curve similar to that seen in this work except it decreased at a slower rate, figure 4.29. The reason for this is two fold, firstly, they performed the test at 40 °C, and secondly, the phosphorus pentoxide concentration was kept constant at 50 mol.% whilst in this work it decreased with increasing divalent cation content.

The solubility of glasses prepared from sodium phosphate, calcium carbonate and phosphorus pentoxide in platinum crucibles at 1000/1050 °C was investigated by Ahmed *et al*. Calcium was stated to decrease the solubility in all series analysed. Comparison with this work was limited as the CaO concentrations were generally higher than the compositions in this work. However, the 40 mol.% $CaHPO_4$/60 mol.% NaH_2PO_4 does fit nicely between their $P_{45}C_{30}N_{25}$ and $P_{45}C_{35}N_{20}$ compositions. The dissolution rate of $6.7x10^{-7}$ g cm^{-2} h^{-1} fits in between the values $1.2x10^{-6}$ and $2.0x10^{-7}$ g cm^{-2} h^{-1} showing good, while admittedly limited, correlation between the two glass compositions.

To the knowledge of the author, no data has been presented within the literature based on the phosphate glass system composing of phosphorus pentoxide, sodium and magnesium.

The quaternary system comprising of 45 mol.% phosphorus pentoxide, 23 mol.% sodium oxide and varying amounts of calcium and magnesium was

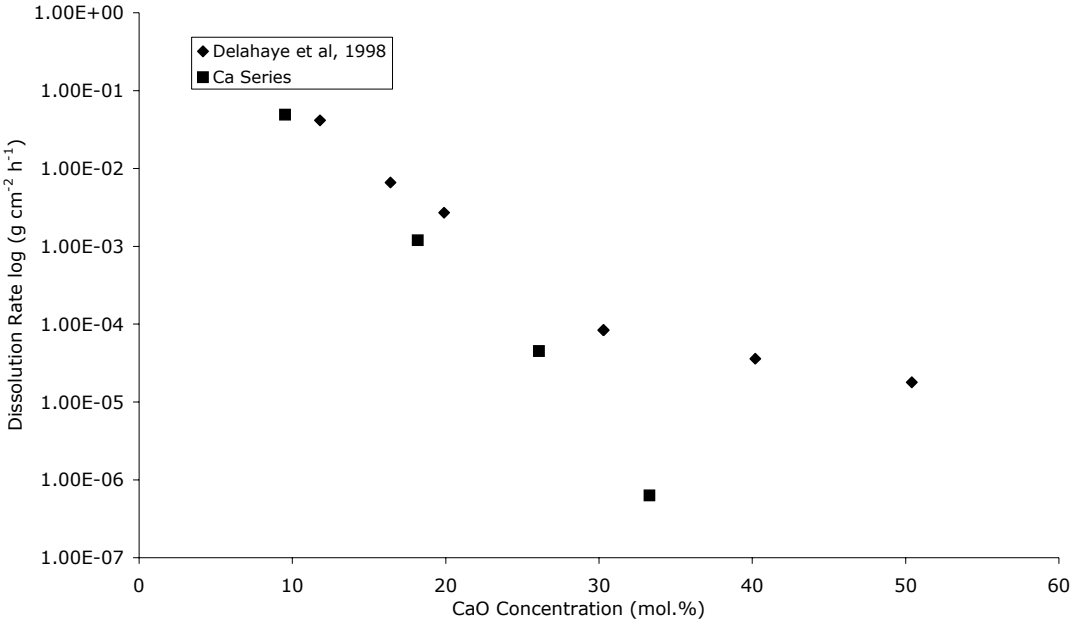

Figure 4.29 The effect of CaO concentration on the dissolution rate of sodium phosphate glasses for this work and that of Delahaye et al, 1998. Both glasses follow an exponential decrease in dissolution rate with increasing CaO concentration, but the data from Delahaye et al shows a slower decrease in dissolution rate after the addition of approximately 30 mol.% CaO.

studied by Franks *et al*. Magnesium was stated to retard dissolution more than calcium, which is reflected in this work. The divalent cation concentration was 32 mol.% while in this work it was 40 mol.% so a direct comparison of dissolution rates was not possible.

The non-linear dissolution of phosphate glasses was reported by many authors (Roshchina *et al.*, 1995; Delahaye *et al.*, 1998; Franks *et al.*, 2000; Gough *et al.*, 2002). The slowing of dissolution was reported to be due to the saturation of the dissolving media with solutes (Roshchina *et al.*, 1995). However, Bunker *et al* found that upon saturation, crystalline saturation products appeared. This did not inhibit dissolution, the glass continued to dissolve until the entire sample had been converted to crystals. Precipitate formation was observed in this study in all glasses containing calcium, but was shown to be amorphous by XRD. The use of excess media to dissolve the glasses did not affect the non-linear dissolution, as would be expected if saturation was the dominant factor (Cozien-Cazuc, 2005). Limitation of

dissolution by the transport of solutes into the bulk has been disproved as agitation of the dissolving media has been shown to have a minimal effect (Delahaye *et al.*, 1998). It has been suggested that cleavage of the bridging P-O bonds by moisture absorption prior to the dissolution test causes the initially high rate of dissolution (Gao *et al.*, 2004a). The phosphate chain length of 20 mol.% $MgHPO_4$/80 mol.% NaH_2PO_4 glasses degraded over a seven day period were found not to hydrolyse, using an XPS analysis of oxygen (Gresch *et al.*, 1979). This has also been reported in the literature, (Bunker *et al.*, 1984; Delahaye *et al.*, 1998). It is also well known that the phosphate chains are stable in water for several months (Van Wazer, 1950b; Griffith, 1995). Finally it has been hypothesised that the ionic strength of the media causes the drop in dissolution rate (Delahaye *et al.*, 1998). Delahaye *et al* tested this by replacing the dissolving media every 15 mins over a 400 min period. While the weight loss per cm^2 decreased over time for phosphate glass dissolved in stagnant media, it was linear when the media was replaced. This test was adapted for glasses dissolved in this study, figure 4.30, phosphate glass composed of 50 mol.% NaH_2PO_4, 30 mol.% $MgHPO_4$ and 20 mol.% $CaHPO_4$ was dissolved in water over an 8 week period during which the media was either changed daily or not at all. The linear nature of dissolution when the media is changed daily, along with the previous arguments, shows the dependence on the ionic strength of solution.

The initial decrease in dissolution rate is more pronounced for the glasses which contain calcium, figure 4.27. This is most likely due to the precipitate which forms during dissolution. This precipitate is amorphous and was found, by EDX analysis, to consist of equal amounts of calcium and phosphorus with a small concentration of sodium. The precipitation seems to be heterogeneous

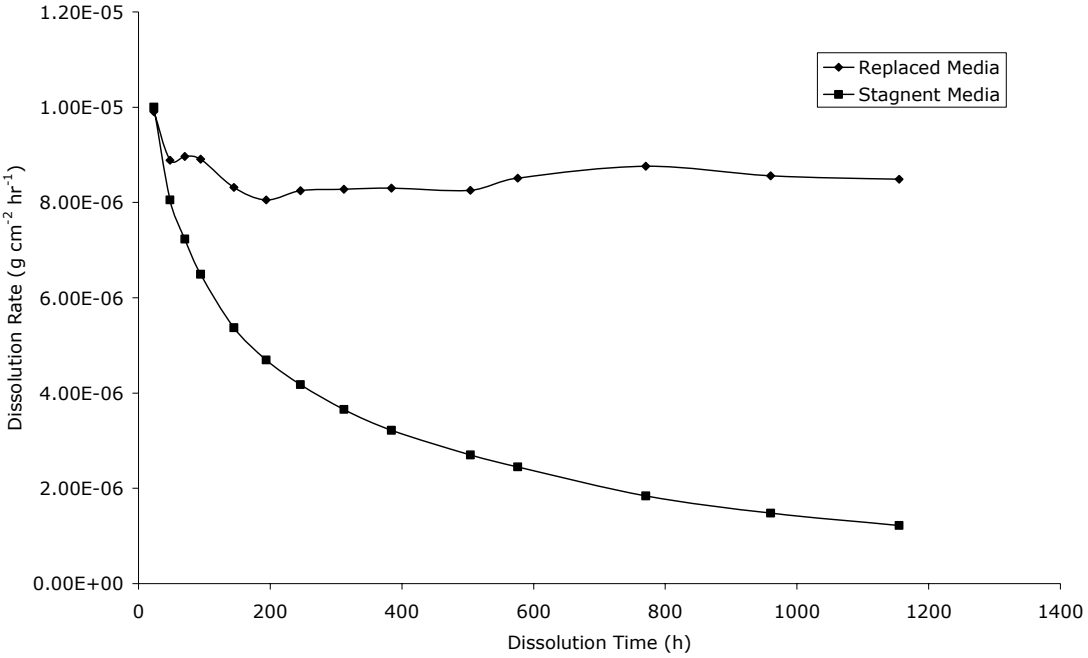

Figure 4.30 Dissolution of phosphate glass consisting of 50 mol.% NaH_2PO_4, 30 mol.% $MgHPO_4$, 20 mol.% $CaHPO_4$ in water over an eight week period. The media was either replaced with new, daily, or not at all.

as formation occurs on the sample itself or on the sides of the receptacle. It is proposed that this precipitate 'protects' the glass by inhibiting the movement of water and dissolution products. So as dissolution proceeds, the thickness of the layer increases, further retarding dissolution. Crystal precipitate formation, in this case hydroxyapatite, was observed by Bunker *et al* when dissolving phosphate glass, containing various amounts of sodium and calcium, in water at room temperature. This theory explains why the dissolution is retarded more in quaternary glasses containing higher concentrations of $CaHPO_4$, producing the lowest dissolution rates after 8 weeks despite dissolving fastest up to 200 h.

Samples were dissolved in SBF in an attempt to mimic the environment of the body. The reduction of the dissolution rate when the media is changed from water to SBF is most likely caused by the increase in ionic strength of solution caused by the additional ions in SBF (Delahaye *et al.*, 1998).

4.4 Summary

This chapter has shown that high quality fully amorphous glasses can be produced from phosphate salts containing sodium, calcium and magnesium using a simple melt and cast technique.

It has been shown that there is a maximum concentration of calcium and magnesium phosphate which can be added to the glass before devitrification occurs, and that the addition of divalent cations has a significant effect on the molecular structure of phosphate glass. Additions of divalent cation interact with the phosphate chains, inhibiting chain growth. IR and XPS was utilised to prove that the average phosphate chain length was decreasing and XPS was further used to quantify this. However, the addition of divalent cations allowed the formation of metal ion/phosphate cross links which produced a network.

It was shown that the density of this network had a profound effect on the properties of the glass. The addition of divalent cation salts increased the T_g and decreased the dissolution rate of the phosphate glass. It was argued that the cross link density, hence cation concentration, was the cause of this. The added effect of the greater covalent nature of the cross links with cations that possessed a higher charge density also contributed to the change in properties.

Overall, the work presented in this chapter has shown that the production of highly durable glasses which dissolve in water was possible and that there is potential for use of the glasses for biomedical applications if the biocompatibility is shown to be favourable.

5 Cell-Phosphate Glass Interactions

5.1 Introduction

Phosphate glass has been known and researched for many years (Zarhariasen, 1932), and has been considered for many applications including nuclear waste vitrification (Mesko *et al.*, 2000; Reis *et al.*, 2002); solid state lasers (Weber, 1990); sealant (Liang *et al.*, 2002) and optical applications. Recently, phosphate glass, especially with the addition of calcium, has come under renewed scrutiny as a potential fully degradable biomaterial, e.g. (Knowles *et al.*, 1993; Franks *et al.*, 2002; Gough *et al.*, 2003; Ahmed *et al.*, 2004c). The lack of favourable mechanical properties has been overcome by drawing the glass into fibres (Griffith, 1995), and incorporating them into a composite (Knowles *et al.*, 1993; Lowry *et al.*, 1997; Corden *et al.*, 1999). However, even with these improvements in mechanical properties, the roles for these composites have focussed on low load bearing applications.

The aim of this chapter is to investigate the biocompatibility of three series of glass compositions, compared with the recognised standard of tissue culture plastic (TCP), using human cranio-facial derived osteoblast-like cells and murine macrophages (cell line J774). All glass compositions were tested for cell metabolism, proliferation and alkaline phosphatase activity for up to 168 h before the most promising were selected for further study. Cell attachment and morphology over a 4 week period was viewed using SEM, Confocal laser scanning microscopy and fluorescence microscopy. The production of the osteoblast phenotypic markers: alkaline phosphatase, type I collagen,

osteocalcin and mineral deposition by CFCs over a 28 day period were investigated.

5.2 Results

5.2.1 Initial Screening with CFCs

5.2.1.1 Cell Metabolic Activity

The Alamar blue assay was used to determine the metabolic activity of osteoblasts grown on sodium phosphate glass containing varying amounts of magnesium phosphate for up to seven days, figure 5.1.

Metabolic activity increased over a seven day period, with an extremely significant difference between 2 and 168 h for all surfaces except 20 Mg where there was no significant change in metabolic activity. There was no significant

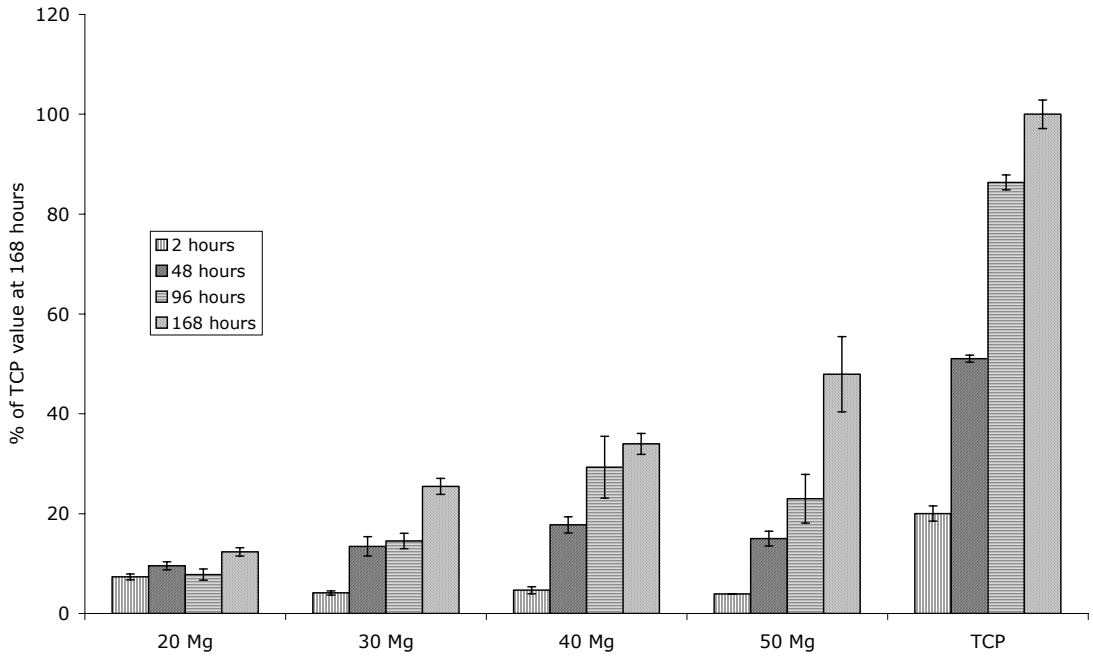

Figure 5.1 Metabolic activity of osteoblasts, as measured by the Alamar blue assay, cultured on sodium phosphate glasses containing varying concentrations of magnesium phosphate. Bar represents standard error of mean, n = 5.

difference between any two samples after 2 h. The differences between 30 Mg and 20 Mg at a given time point were not significant except for 96 h. Comparisons between 40 Mg and 50 Mg did not show any significant difference with the exception of 168 h. However, repeats of this experiment have shown almost identical results implying that the differences, though small, are significant. The difference between sample values and the positive control for a given time point were all extremely significant. Tissue culture plastic was used as a positive control, the value for metabolic activity after seven days was the greatest value and all other values are shown as a percentage of this. The differences between 0 and 2 h and the final two time points for the positive control are relatively small, 20 and 14 % respectively compared to the differences between other time points.

The Alamar blue assay shows the metabolic activity for osteoblasts cultured on sodium phosphate glass containing calcium phosphate, figure 5.2. Again TCP is used as a positive control with all values a percentage of the osteoblast

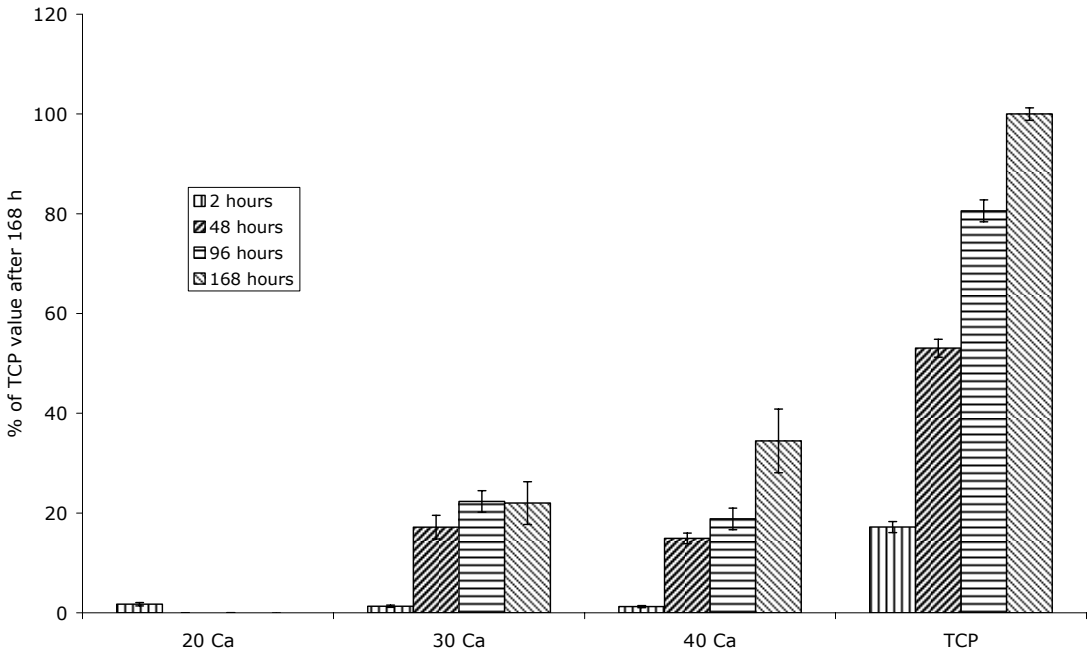

Figure 5.2 Metabolic activity of osteoblasts, as measured by the Alamar blue assay, cultured on sodium phosphate glass containing varying amounts of calcium phosphate. Bar represents the standard error of the mean, n = 5.

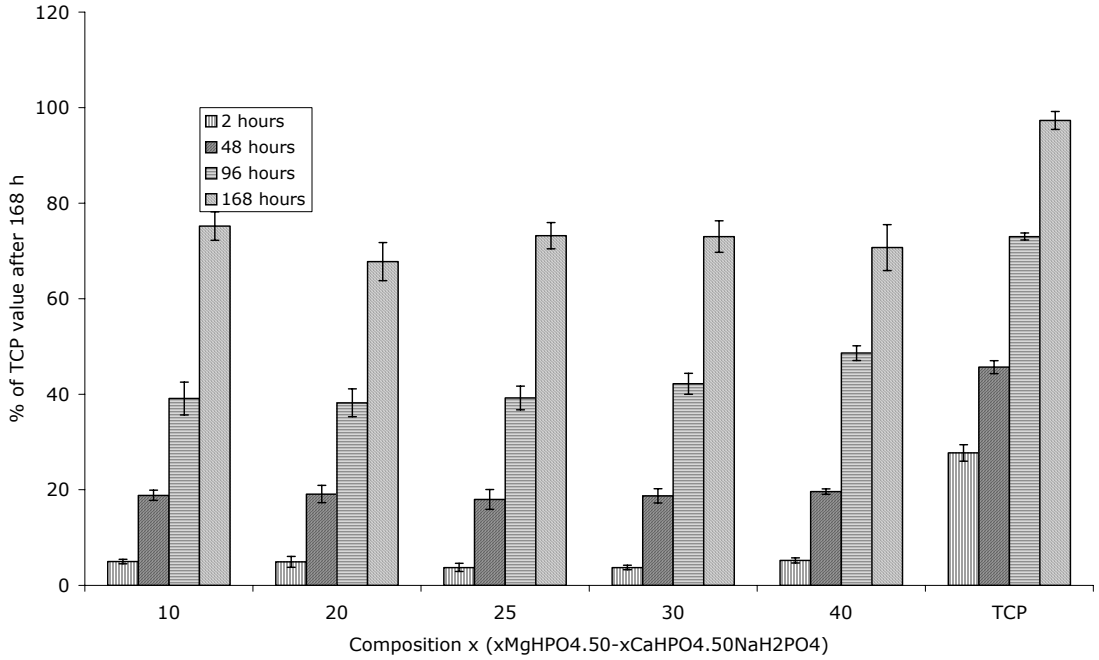

Figure 5.3 Metabolic activity of cells, as measured using the Alamar blue assay, culture on the quaternary series of phosphate glasses. Bar is standard error of the mean, n = 5.

metabolic activity on TCP after 168 hours. The differences between TCP, the positive control and all other surfaces were extremely significant at every time point.

Osteoblast metabolic activity was observed on 20 Ca after two hours but for longer time periods, there was no detectable metabolic activity. 30 Ca phosphate glass showed an increased activity after 48 hours, but after that the metabolic activity remained approximately constant with no significant difference between the final three time points. With the addition of 40 Ca, metabolic activity was seen to increase with each time point. The largest increases were at the start and end of the test with no significant difference between 48 and 96 h. There was no significant difference between sample surfaces after 2 h. No significant difference was observed between 30 Ca and 40 Ca at any time point except the final time point where a very significant difference was observed. The metabolic activity increases with time in an approximate sigmoidal pattern for the positive control, with smaller increases in metabolic activity at the beginning and end of the test.

Metabolic activity of CFC's cultured on sodium phosphate glasses containing varying amounts of calcium and magnesium phosphate was determined using the Alamar blue assay, figure 5.3.

The metabolic activity of the osteoblasts cultured on the TCP positive control increases as the test progresses. The increase is roughly linear but with a smaller increase between the final two time points. For all the samples in this series there was a similar increase in metabolic activity with time. At each time point, for all of the glass compositions, the metabolic activity of the CFCs was approximately 25 % lower compared to the positive control. The differences in metabolic activity between the glasses of the quaternary series were not significant at any time point.

5.2.1.2 Osteoblast Proliferation

This section presents the results from the DNA (Hoechst 33258) assay for up to seven days; results on selected glasses for up to twenty eight days are presented later in this chapter.

The change in cell numbers, as indicated by the DNA content of cell layers, with time for osteoblasts cultured on sodium phosphate glasses containing various amounts of magnesium phosphate was determined using a DNA assay, with TCP as a positive control, figure 5.4.

DNA concentration after two hours is approximately 0.5 μg ml^{-1} for all surfaces, where no significant difference was observed. For the 20 Mg glass surfaces, the levels of DNA increase with time up to 48 h and then the DNA concentration levels out; there is no statistical difference between the final three time points. DNA concentration increased over the seven day period to approximately double the level at 2 hours for 30 Mg and higher for 40 Mg.

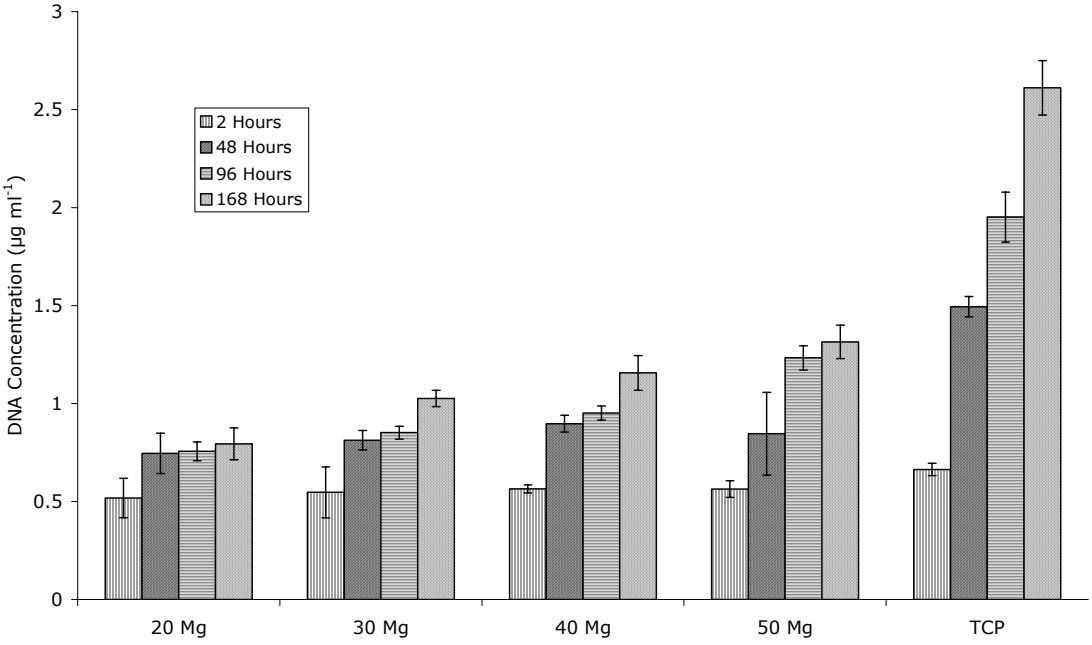

Figure 5.4 Proliferation of osteoblasts cultured on sodium phosphate glasses containing various concentrations of magnesium phosphate, as measured using the Hoechst 33258 DNA assay. Bars are standard error of the mean, n = 5.

Both compositions demonstrated no significant difference in DNA concentration between 48 and 96 h. For 50 Mg composition, the DNA concentration increased after each time point, but the rate of increase decreased with each subsequent time point, until no significant difference was observed. There was no significant difference between 40 Mg and 50 Mg at any time point, however, repeated testing showed the same results indicating that the differences are significant. TCP showed an increase in DNA concentrations after each subsequent time point.

The effect of calcium phosphate addition to sodium phosphate glass on the proliferation of osteoblasts was determined by investigating the changes in DNA concentrations, figure 5.5.

The DNA concentration was approximately 0.35 μg ml^{-1} after 2 h for all glass surfaces, between which no significant difference was observed. The levels of DNA decreased to zero for all subsequent time points when CFCs were cultured on 20 Ca glass. There was an increase in DNA between 2 h and

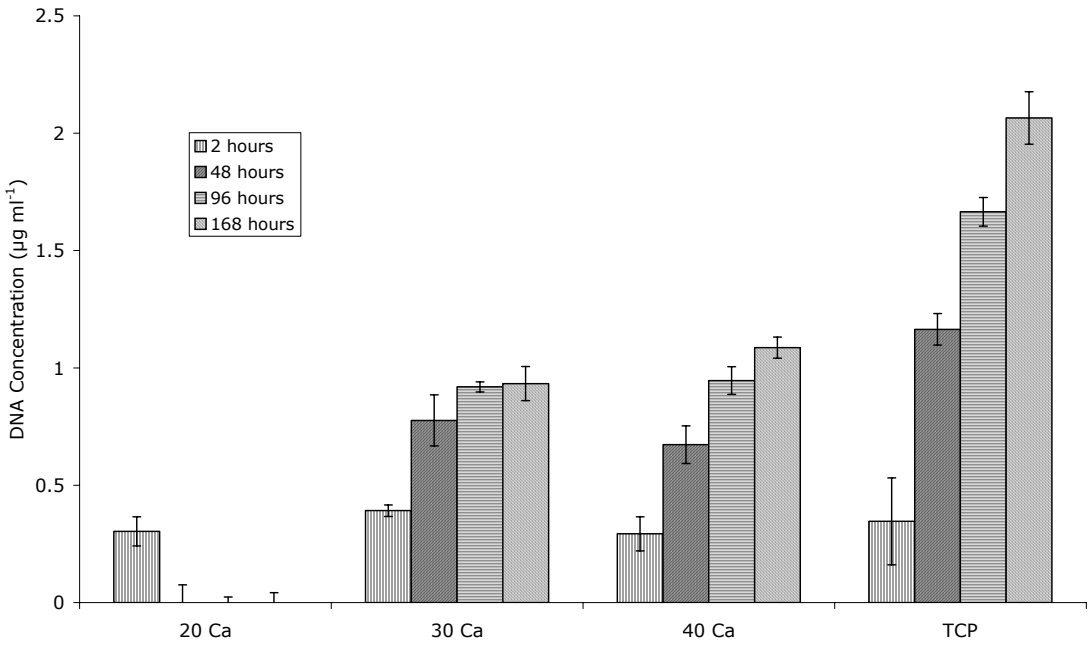

Figure 5.5 Proliferation of osteoblasts cultured on sodium phosphate glasses containing various concentrations of calcium phosphate, as measured by the Hoechst 33258 DNA assay. Bars are standard error of the mean, n = 5.

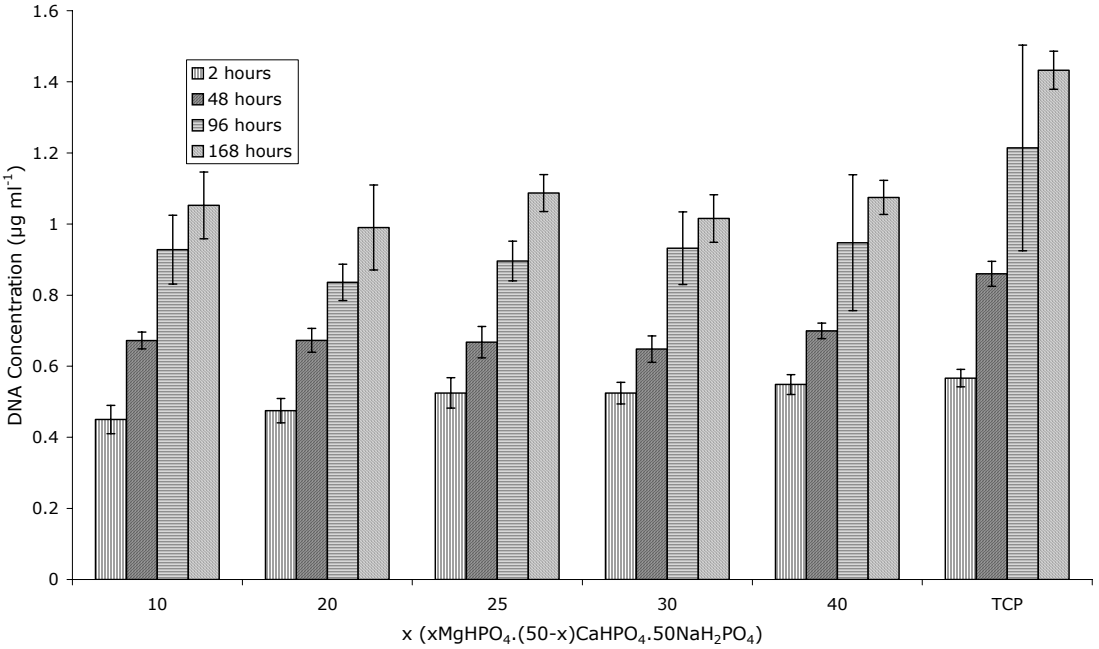

Figure 5.6 Proliferation of osteoblasts cultured phosphate glasses containing 50 mol % of sodium phosphate and varying amounts of magnesium phosphate and calcium phosphate, as measured by the Hoechst 33258 DNA assay. Bars are the standard error of the mean.

48 h, before levelling off at 0.92 µg ml^{-1} after 96 h for CFCs cultured on 30 Ca glass, there was no observed significant difference between the final three time points. There was an increase at each time point when the calcium phosphate concentration was at 40 mol.%, but each increase was subsequently smaller than the last, with a final DNA concentration of 1.09 µg ml^{-1} after 168 h. DNA levels for osteoblasts cultured on TCP proliferated rapidly over all time points, but the rate of increase slowed as the test progressed. The final DNA concentration at 168 h was 2.07 µg ml^{-1}, approximately four times the concentration after 2 h.

The proliferation of osteoblasts cultured on phosphate glass containing 50 mol.% NaH_2PO_4 and varying amounts of $CaHPO_4$ and $MgHPO_4$ was investigated using the DNA assay, figure 5.6.

DNA concentration after 2 h was approximately 0.6 µg ml^{-1} for all samples, with no significant difference between values. When cells were cultured on TCP, the DNA concentration increased at each time point by approximately

0.3 μg ml^{-1} to a final value of 1.43 μg ml^{-1}. DNA concentrations for osteoblasts cultured on the sample surfaces demonstrated no significant difference when compared to each other at the same time point.

5.2.1.3 Alkaline Phosphatase Activity

The alkaline phosphatase activity of osteoblasts that were cultured on sodium phosphate glass with varying amounts of magnesium phosphate was investigated, Figure 5.7. All data was shown as a percentage of the highest data point, which was for the TCP surface after 168 h.

For all surfaces, including the TCP positive control, there was negligible alkaline phosphatase activity after 2, 48 or 96 h. The alkaline phosphatase activity, expressed as a percentage of the maximum value, which was for TCP after 168 h, increased with magnesium phosphate concentration from 8 % for 20 mol.% $MgHPO_4$ to 33 % for 50 mol.% $MgHPO_4$. However, there was no significant difference between 20, 30 and 40 mol.% $MgHPO_4$

The alkaline phosphatase activity of osteoblasts cultured on sodium phosphate glass containing different concentrations of $CaHPO_4$ was determined, Figure 5.8. The data was plotted as a percentage of the highest

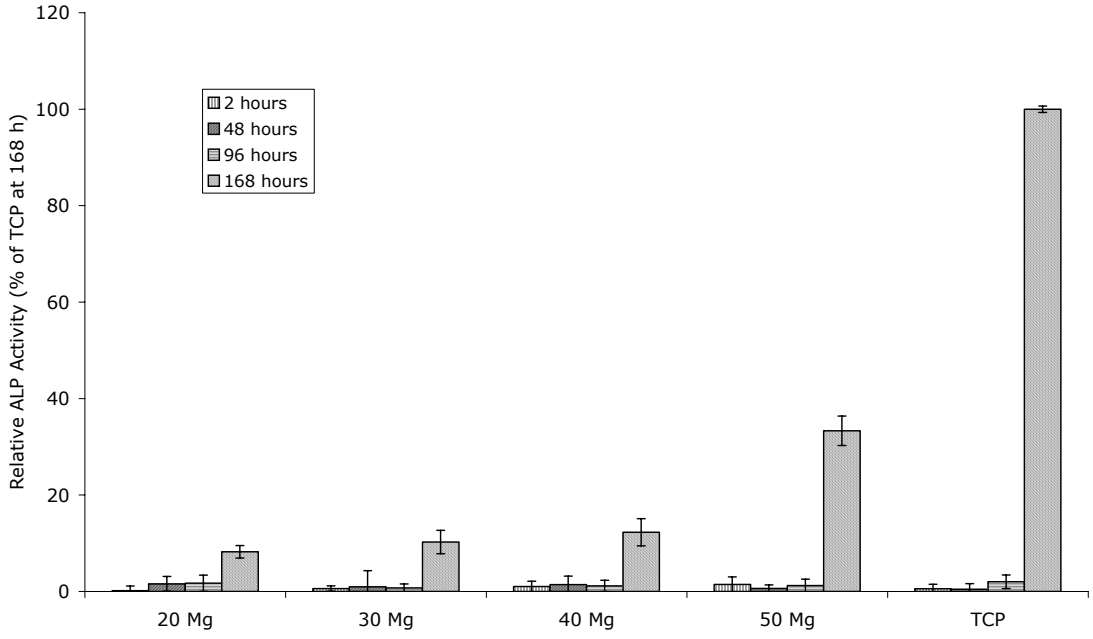

Figure 5.7 Alkaline phosphatase activity of osteoblasts cultured on sodium phosphate glass with differing amounts of magnesium phosphate. Data is plotted as a percentage of the highest value. Bar represents the standard error of the mean, n = 5.

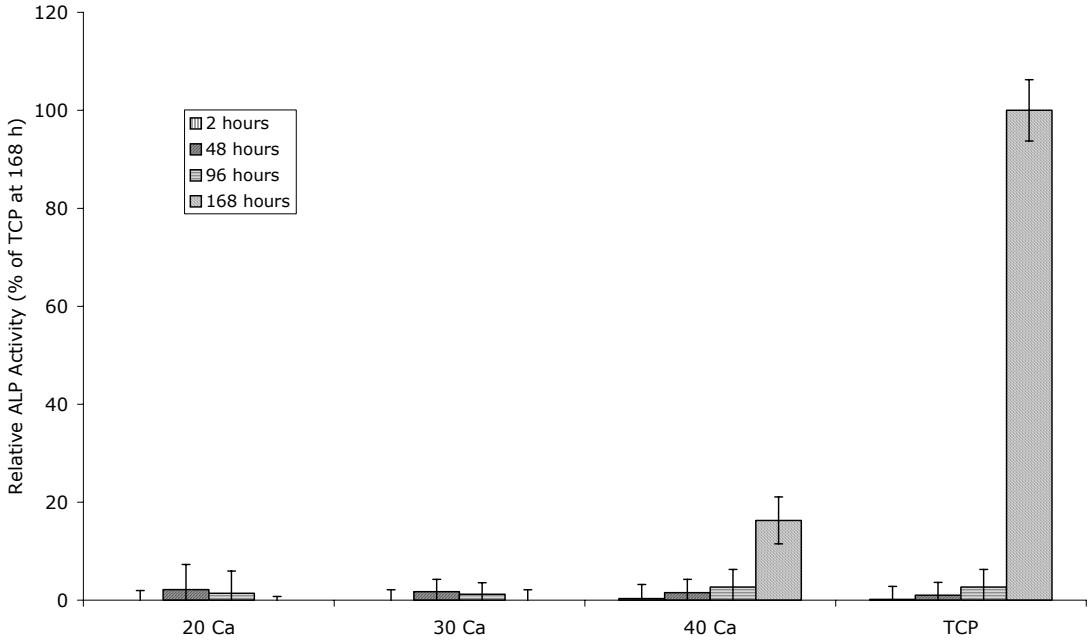

Figure 5.8 Alkaline phosphatase activity of osteoblasts cultured on sodium phosphate glass with differing amounts of calcium phosphate. Data is plotted as a percentage of the highest value. Bar represents the standard error of the mean, n = 5.

value.

Negligible alkaline phosphatase activity is detected after 2, 48 or 96 h on all of the surfaces tested. Sodium phosphate glasses containing either 20 or 30 mol.% calcium phosphate also showed no detectable alkaline phosphatase activity after 168 h. Alkaline phosphatase activity of 16 % of TCP at 168 h was detected for osteoblasts cultured on 40 Ca after 168 h, this value was significantly different to the positive control at the same time point.

The alkaline phosphatase activity of osteoblasts cultured on glasses from the quaternary series was determined, figure 5.9. The data was plotted as a percentage of the highest value, which was TCP after 168 h in culture.

For all sample surfaces, including TCP, no detectable levels of alkaline phosphatase were measured, with the following exception: after 2 h, a value of 2 % was recorded for the glass with a composition of 10 Ca/40 Mg. After 168 h, osteoblasts on all surfaces expressed alkaline phosphatase activity. As the concentration of magnesium increases at the expense of calcium, the

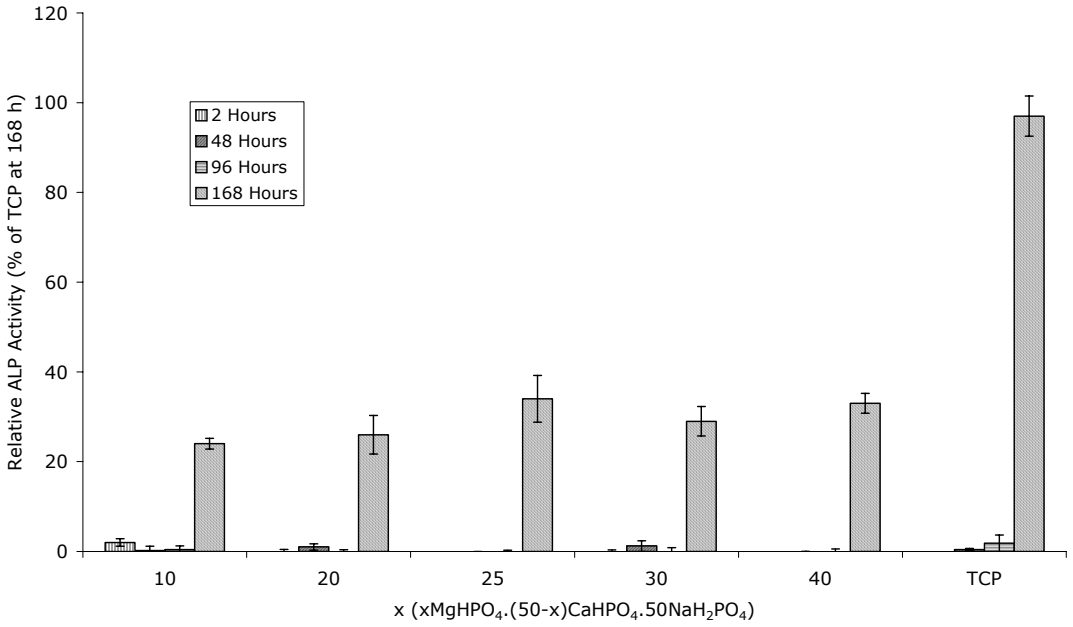

Figure 5.9 Alkaline phosphatase activity of osteoblasts cultured on 50 mol.% sodium phosphate glass varying ratios of calcium phosphate and magnesium phosphate. Data is plotted as a percentage of the highest value. Bar represents the standard error of the mean, n = 5.

alkaline phosphatase activity increases from 24 % in the most magnesium deficient to 33 % to the most magnesium rich glass. The exception to this is the glass containing 25 mol.% of both magnesium phosphate and calcium phosphate, which had an alkaline phosphatase activity of 34 %. However, the differences are not significantly different.

5.2.2 Macrophage Response

All of the following assays and imaging in this section and the next were performed on a selection of glasses that showed the greatest potential for the applications it was being considered for. The results detailing the potential of phosphate glasses to activate macrophages are presented first, followed by the culture of CFC's up to 28 days. The four glasses in question are shown in table 5-1.

	Concentration (mol.%)		
Glass Code	NaH_2PO_4	$MgHPO_4$	$CaHPO_4$
40 Ca	60	-	40
40 Mg	60	40	-
30 Mg/20 Ca	50	30	20
20 Mg/30 Ca	50	20	30

Table 5-1 Composition of the four glasses used in the long term culture and imaging involving CFCs and all culture using macrophages.

5.2.2.1 Hydrogen Peroxide Production

The results for hydrogen peroxide production by murine macrophages are presented in figure 5.10. TCP was used as a negative control to demonstrate a minimal macrophage response while copper was used as a positive control to elicit a response from macrophages; all data was presented as a percentage of the highest value, which in this case is copper after 6 h.

Hydrogen peroxide was generated by macrophages cultured on all surfaces over the six hour test period; extremely significant differences between one and six hours were present for all surfaces. The differences between sample surfaces were very small, significant differences were only observed between 40 Ca, which produced the highest level of hydrogen peroxide of any sample surface, and the other sample surfaces and TCP at 6 h. When macrophages are cultured on TCP, hydrogen peroxide production peaks at 32 % after 6 h.

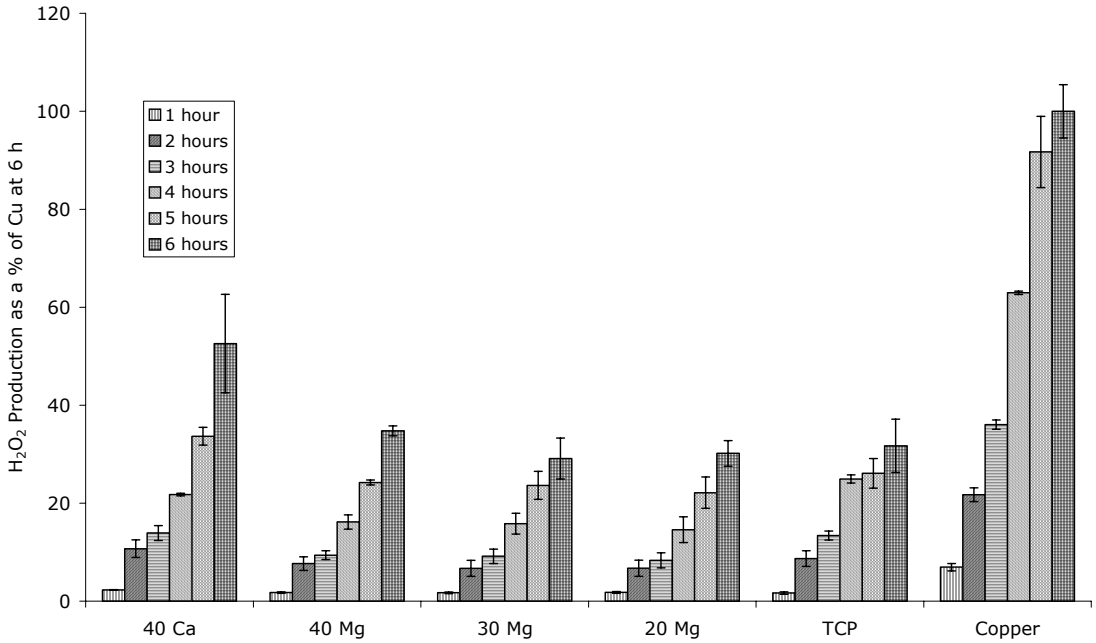

Figure 5.10 Hydrogen peroxide production of macrophages cultured on different glass surfaces (see table 5.1) and TCP and copper. Data is presented as a percentage of the highest value, in this case, copper after six hours. Bars are the standard error of the mean, where n = 3.

Hydrogen peroxide levels were extremely significantly lower for all surfaces compared to the copper positive control, while no significant difference was observed for surfaces compared to TCP, the negative control, with the exception of 40 Ca after 6 h.

5.2.2.2 Interleukin-1β Production

The effect of surface composition on IL-1β production by macrophages cultured on selected glasses, table 5-1, was investigated, figure 5.11. TCP and media supplemented with LPS were used as positive and negative controls respectively.

Macrophages cultured on TCP and given media supplemented with LPS showed no IL-1β production after 2 h, levels of IL-1β were 57 and 166 pg ml^{-1} at 48 h for media containing 10 and 100 μg ml^{-1} LPS respectively. There was limited IL-1β production on all phosphate glass surfaces, with the highest value of 2.8 pg ml^{-1} for 30% Mg after 48 h.

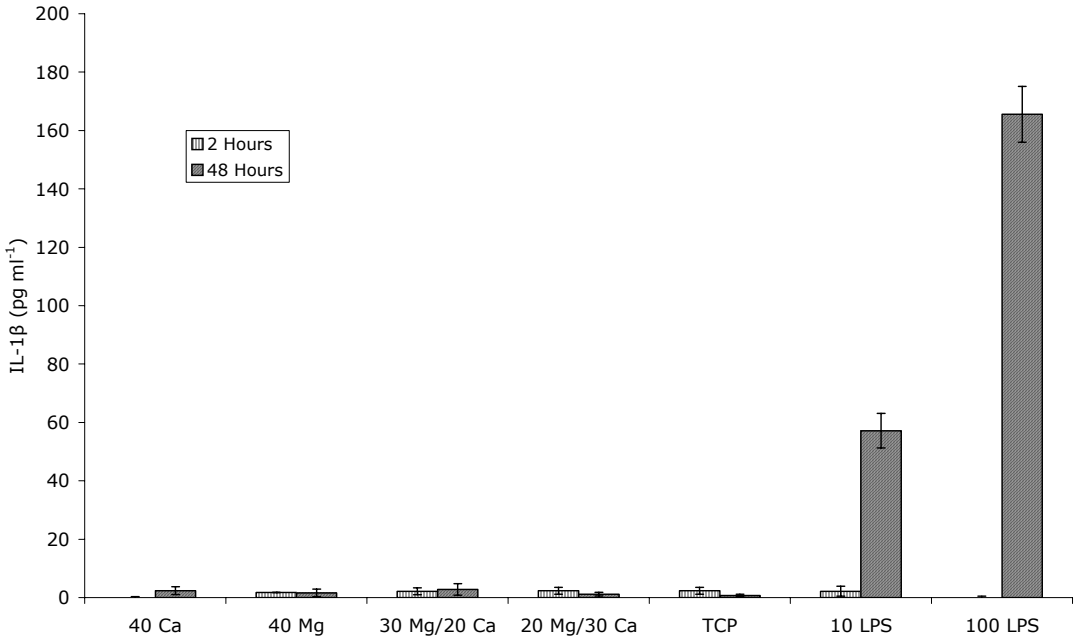

Figure 5.11 IL 1β production of macrophages cultured on different phosphate glass surfaces (see table 5.1). TCP and media supplemented with 10 x 10^{-6} and 100 x 10^{-6} g cm^{-3} were used as the positive and negative controls respectively. Bars are standard error of the mean, n = 3.

5.2.2.3 Macrophage Morphology

Macrophages cultured for 2 h on glass surfaces and TCP were few and exhibited a rounded morphology. Cells cultured on TCP in the presence of LPS for 2 h possessed a stretched morphology.

After 48 h, macrophages grown on TCP and the sample surfaces still possessed a rounded morphology but were more numerous, with cells packed close to one another so that they were impinging upon their neighbour. Cells cultured on TCP for 48 h in the presence of LPS showed a stretched, spread morphology. While cell numbers were more numerous than at 2 h, they were much less than the other samples at 48 h.

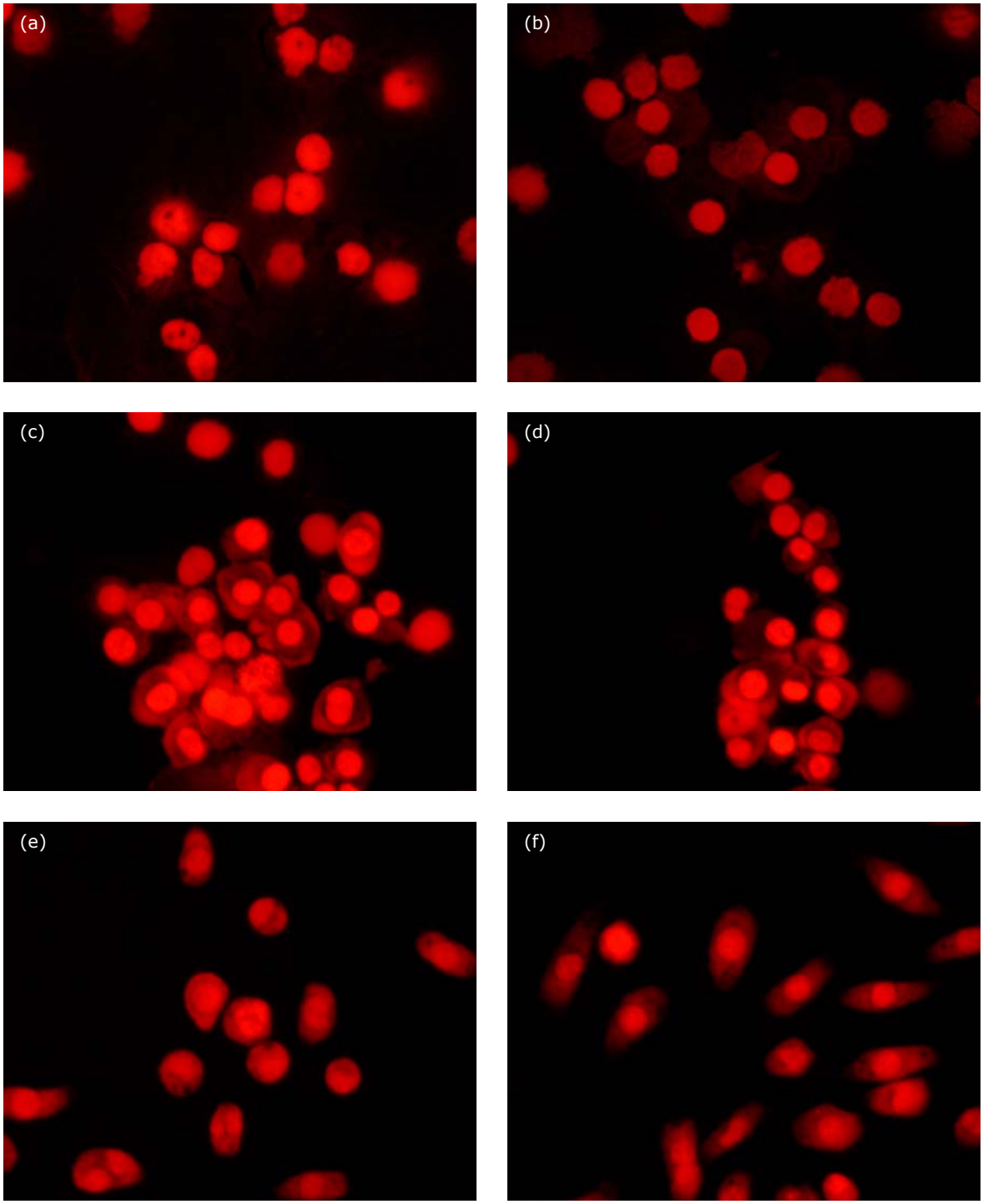

Figure 5.12 Macrophages cultured for 2 hours and viewed under a fluorescent microscope in combination with propidium iodide. Surfaces are: 40 Ca (a), 40 Mg (b), 30 Mg/20 Ca (c), 20 Mg/30 Ca (d), TCP (e) and TCP with media supplemented with 100 μg ml^{-1} LPS (f). Magnification is x100

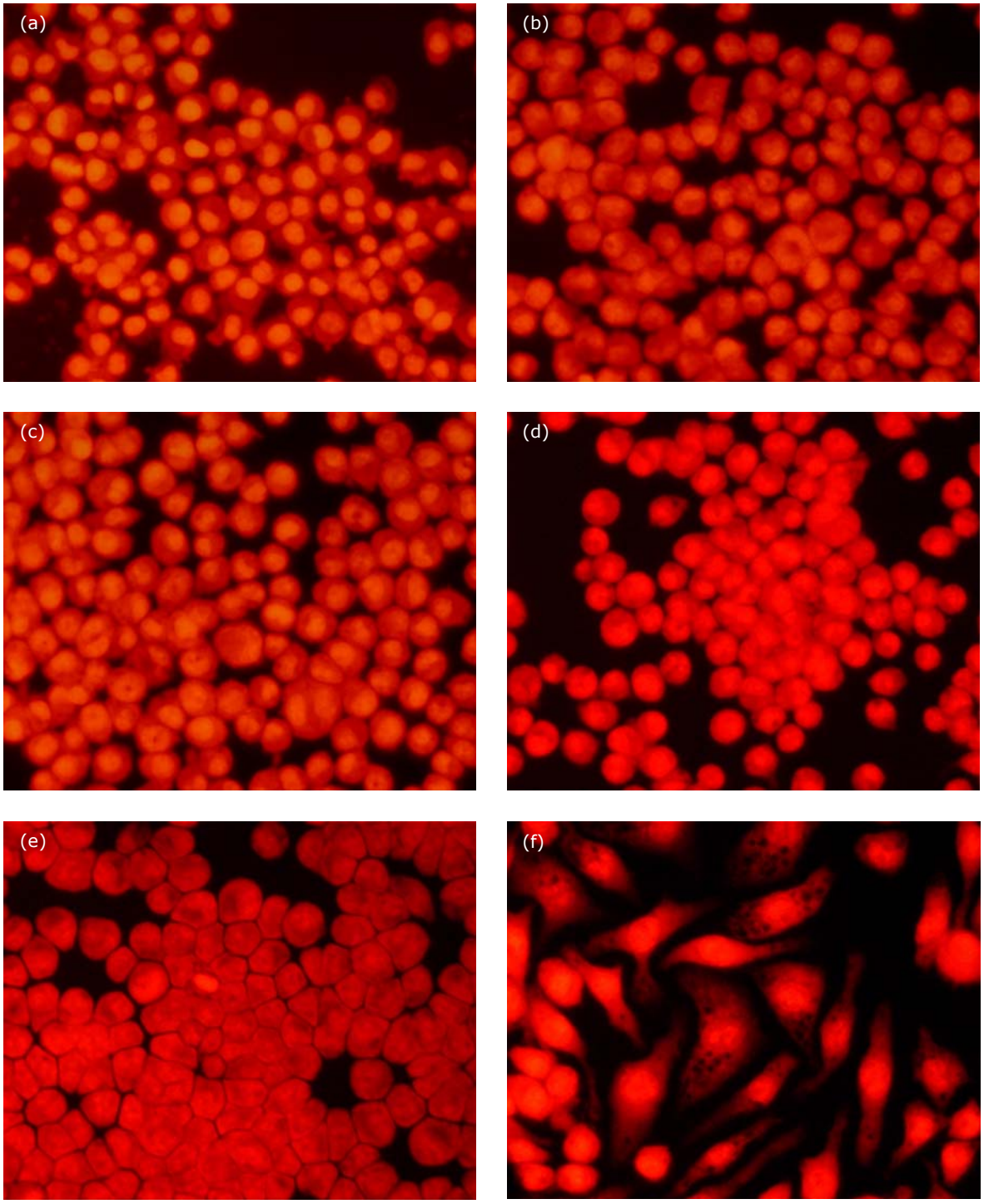

Figure 5.13 Macrophages cultured for 48 hours and viewed under a fluorescent microscope in combination with propidium iodide. Surfaces are: 40 Ca (a), 40 Mg (b), 30 Mg/20 Ca (c), 20 Mg/30 Ca (d), TCP (e) and TCP with media supplemented with 100 μg ml^{-1} LPS (f). Magnification is x100

5.2.3 CFC Culture on Selected Glasses

5.2.3.1 Cell Morphology

CFC's were cultured for two hours and viewed using the FEG ESEM, figure 5.14a-e. Cells cultured on test surfaces, are seen to be attached to the surface and are rounded as they begin to spread. Cells cultured on the positive control, TCP, can clearly be seen spreading over the surface and resembling the normal spindle-like morphology of CFC's.

CFC's were cultured on selected surfaces, table 5-1, for 48 h, figure 5.15. All surfaces show cells that are spread out, showing the typical spindle morphology, more compared to the same samples after 2 h.

The morphology of CFC's after 7, 14, 21, 28 days culture was viewed using CLSM in combination with phalloidin FITC and propidium iodide, figure 5.16. F-actin fibres were arranged in parallel and the cells possessed a long spindle like morphology. The morphology of CFCs cultured on the glass surfaces show that confluence is reached by all after 14 days culture while virtual full coverage was achieved after 7 days culture. Cell density was seen to be higher on the positive control with higher concentrations of nuclei visible. Multiply layers and nodule formation were present in all cell cultures after 28 days

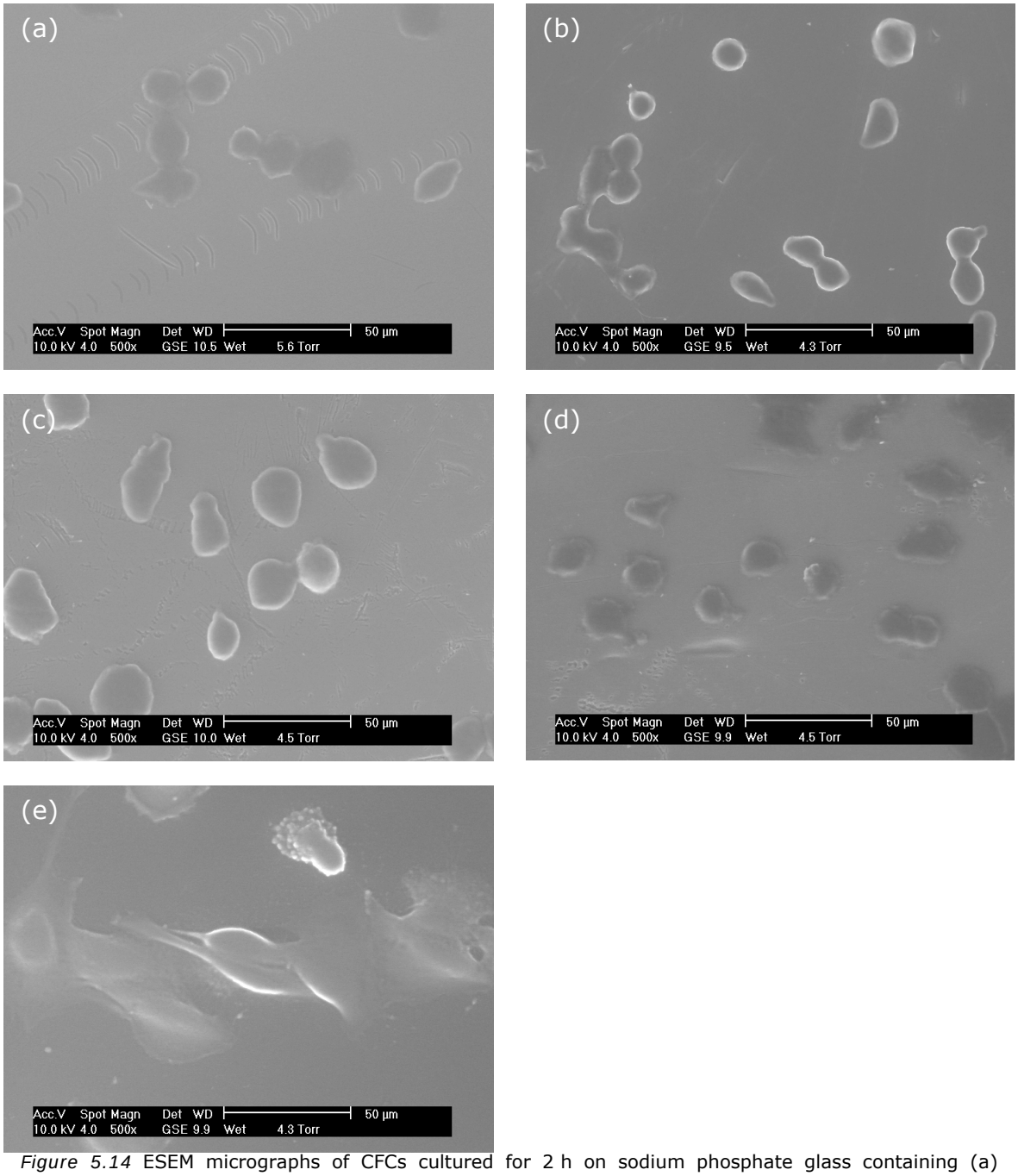

Figure 5.14 ESEM micrographs of CFCs cultured for 2 h on sodium phosphate glass containing (a) 40 mol.% $CaHPO_4$ (b) 40 mol.% $MgHPO_4$ (c) 30 mol.% $MgHPO_4$/20 mol.% $CaHPO_4$ (d) 20 mol.% $MgHPO_4$/30 mol.% $CaHPO_4$ (e) TCP.

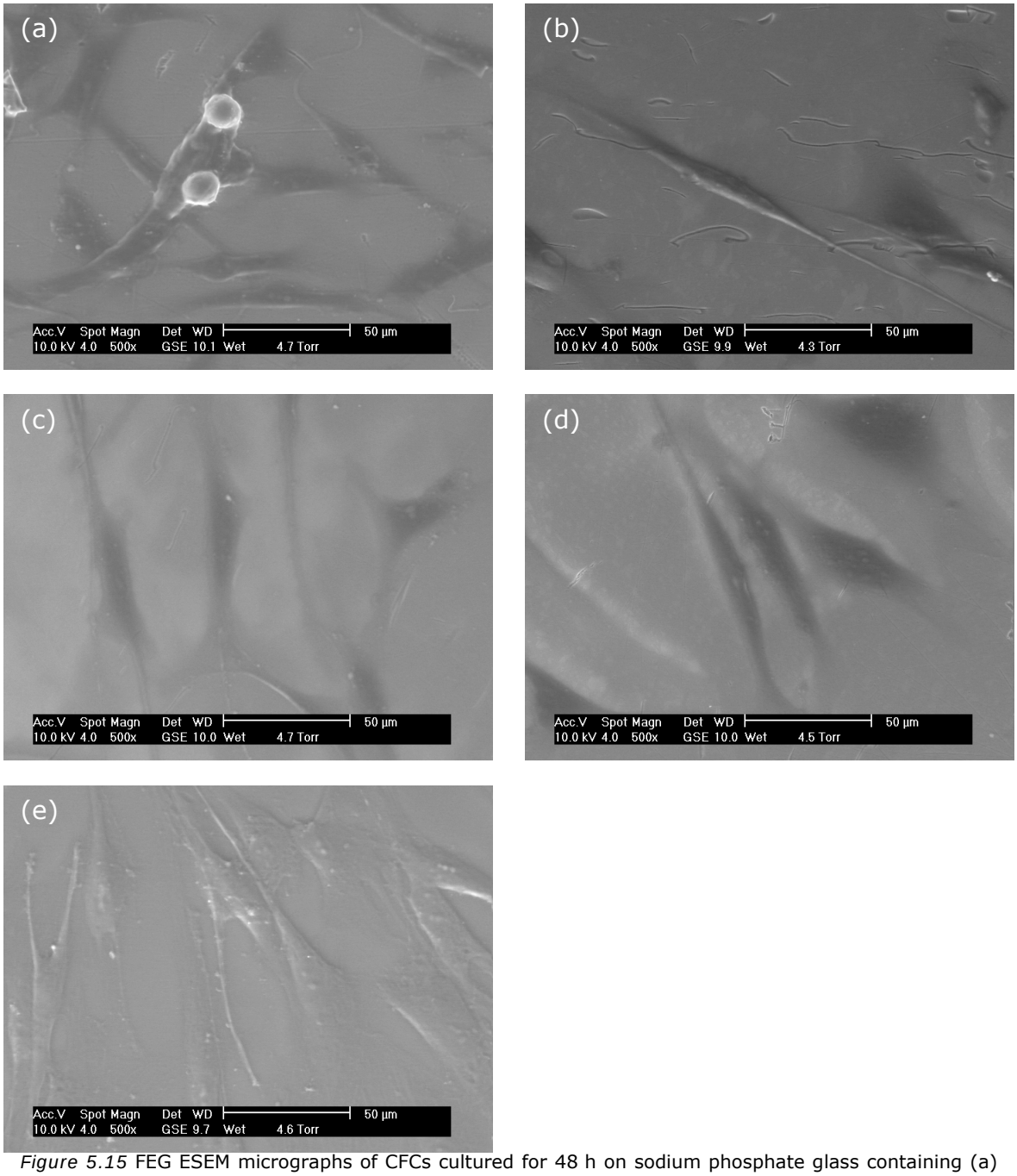

Figure 5.15 FEG ESEM micrographs of CFCs cultured for 48 h on sodium phosphate glass containing (a) 40 mol.% $CaHPO_4$ (b) 40 mol.% $MgHPO_4$ (c) 30 mol.% $MgHPO_4$/20 mol.% $CaHPO_4$ (d) 20 mol.% $MgHPO_4$/30 mol.% $CaHPO_4$ (e) TCP.

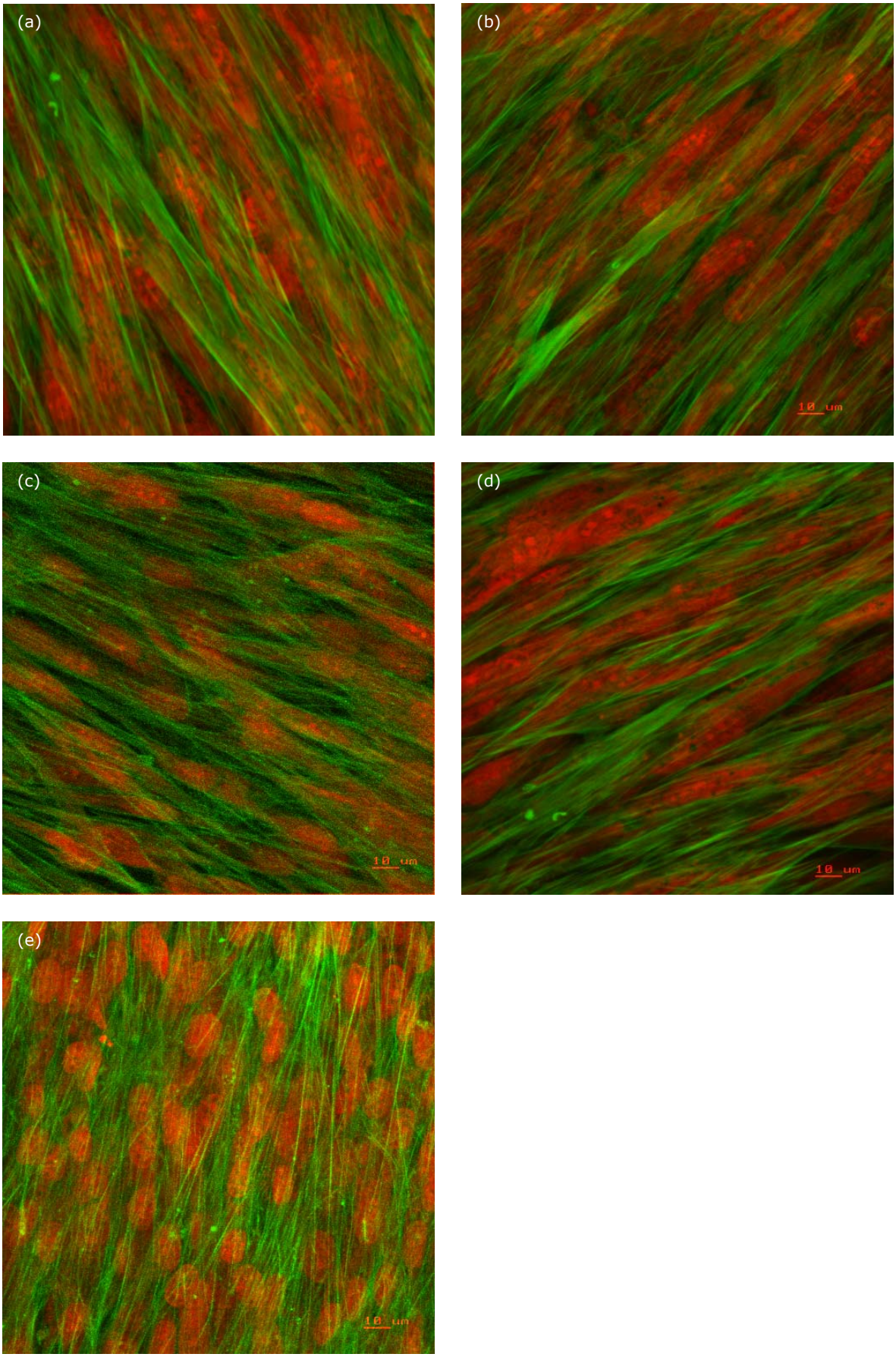

Figure 5.16 Confocal laser scanning micrographs of CFC's cultured for 28 days on sodium phosphate glass containing (a) 40 mol.% $CaHPO_4$ (b) 40 mol.% $MgHPO_4$ (c) 30 mol.% $MgHPO_4$/20 mol.% $CaHPO_4$ (d) 20 mol.% $MgHPO_4$/30 mol.% $CaHPO_4$ (e) TCP. Actin fibres are stained green and cell nuclei are stained red.

5.2.3.2 Osteoblast Proliferation

The effect of glass composition, for the selection of glasses detailed in table 5-1, on the proliferation of CFCs, is measured over a period of 28 days via the DNA content of the cell layers cultured on the surfaces, figure 5.17.

For all samples, including the TCP positive control, the DNA concentration was approximately 0.5 μg ml^{-1} after 7 days in culture. For CFCs cultured on 40 Ca, DNA levels increased at each time point, up to approximately 1 μg ml^{-1} after 28 days. When cultured on 40 Mg, DNA concentration increased at a fairly linear rate, from 0.5 to 0.75 μg ml^{-1} after 21 days. However, the next time point shows a much larger increase than before to 1.25 μg ml^{-1}. CFC proliferation on both 30 Mg/20 Ca and 20 Mg/30 Ca was very similar. Both demonstrated a small increase in DNA concentration from 7 to 14 days, approximately 0.05 μg ml^{-1}, then a much larger increase from 14 to 21 and 21 to 28 days of about 0.3 μg ml^{-1}. The TCP positive control gave a fairly linear increase to 1.15 μg ml^{-1} after 7 days.

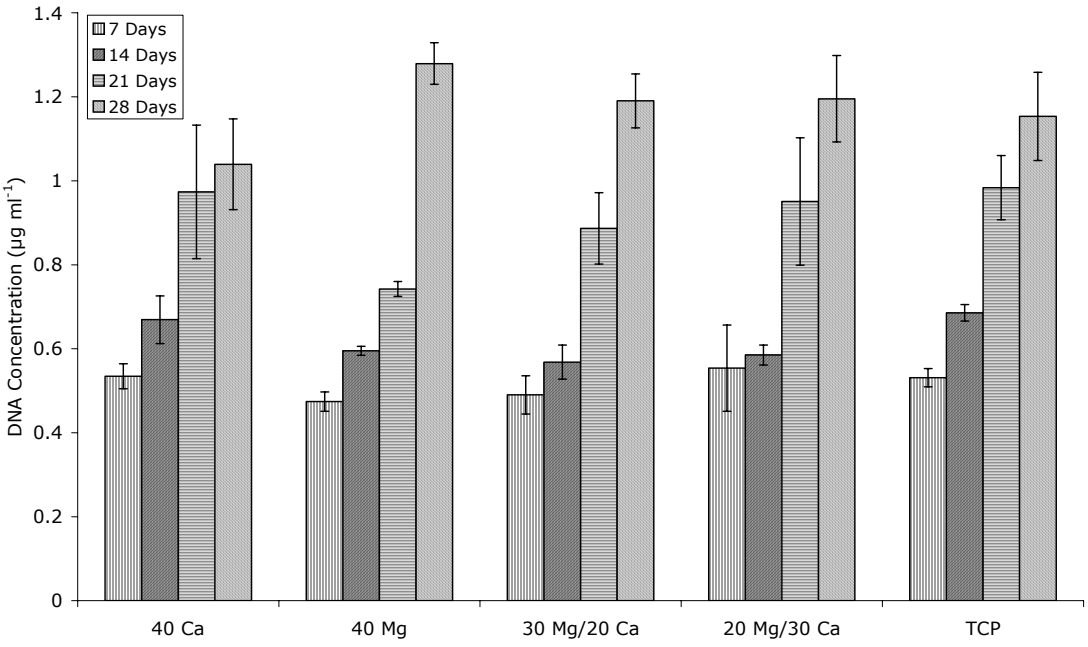

Figure 5.17 Proliferation of CFC's on selected glass surfaces (see table 5.1), as measured by the DNA (Hoechst 33258) assay. Bars are standard error of the mean, where n = 5.

5.2.3.3 Alkaline Phosphatase Activity

The alkaline phosphatase activity (AP) of CFC's cultured on a selection of glass surfaces (Table 5-1) for up to 28 days is presented, figure 5.18.

CFC's grown on 40 Ca show AP at each time point with values that increased with time. The AP was below 75 for the time points at 7 and 14 days, and then increased to 200 and 275 after 21 and 28 days respectively. The glass samples 40 Mg, 30 Mg/20 Ca and 20 Mg/30 Ca, all had a similar trend for AP. AP increased with time up to 21 days, after this the AP decreased at 28 days but to levels still above those at 14 days. Apart from the first time point, values for the positive control, TCP, were all lower than that of the test samples, excluding 40 Ca after 14 days. The AP increased from 30 at 7 days to 175 after 14 days. AP then decreased to 108 at 21 days before recovering to 130 at the final time point at 28 days.

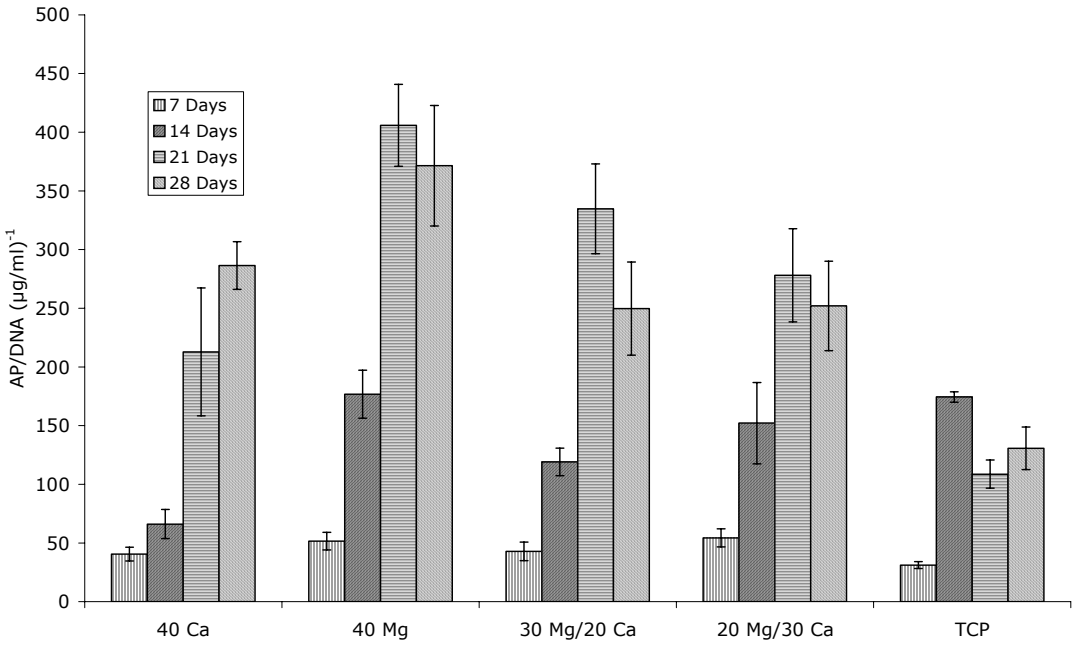

Figure 5.18 Alkaline phosphatase per µg of DNA for CFC's cultured on a selection of phosphate glasses, see table 5.1. Bars represent the standard error of the mean, where n = 5.

5.2.3.4 Collagen Production

Collagen production by CFC's cultured on a selection of phosphate glass surfaces for up to 28 days was assessed and quantified, figure 5.19.

All samples, including the TCP positive sample, showed an approximately linear increase in collagen concentration with time. Collagen deposition was highest by CFC's cultured on TCP, followed by 40 Ca. Collagen concentrations were similar for the remaining three surfaces, with 30 Mg having the most deposited upon it, followed by 20 Mg then 30 Mg

Immunohistochemical staining of CFC's cultured on selected surfaces (figure 5.20) showed the presence of ordered type I collagen on all of the surfaces tested. At the earliest time points, collagen fibres are laid in a haphazard manner. After 21 days, fibres are organised perpendicular, relative to one another and parallel to the direction of cell morphology, as indicated by the oblong morphology of the nuclei. After 28 days, multiple cell layers had formed, collagen fibres from one layer ran perpendicular to those from an adjacent layer.

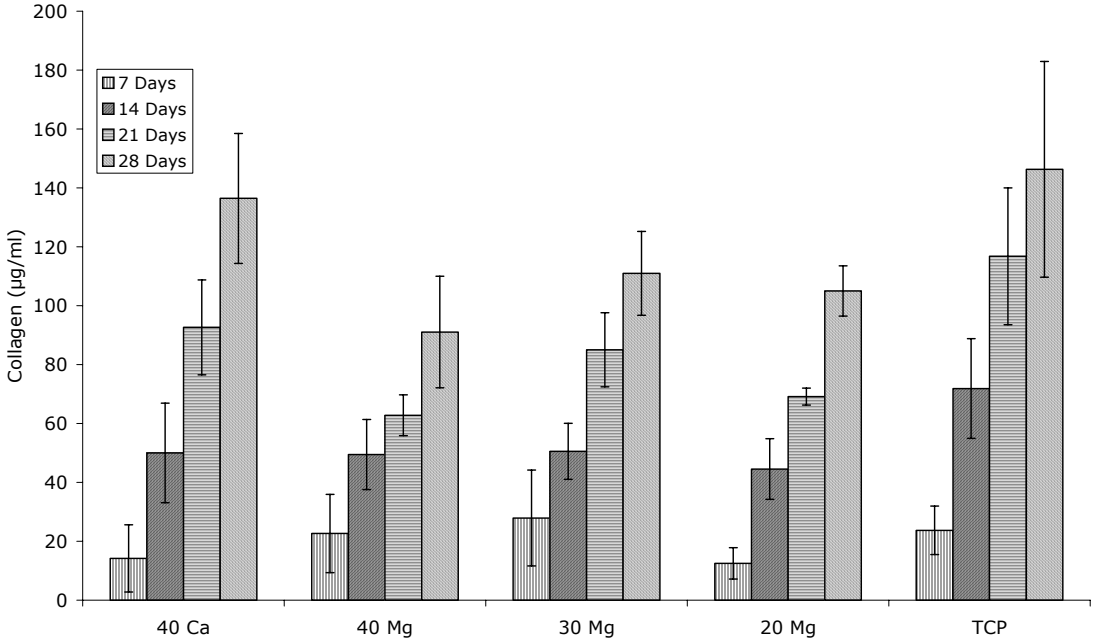

Figure 5.19 The cumulative production of collagen by CFCs cultured on a selection of phosphate glass surfaces (table 5.1) for up to 28 days. Bars represent the standard error of the mean, n = 4.

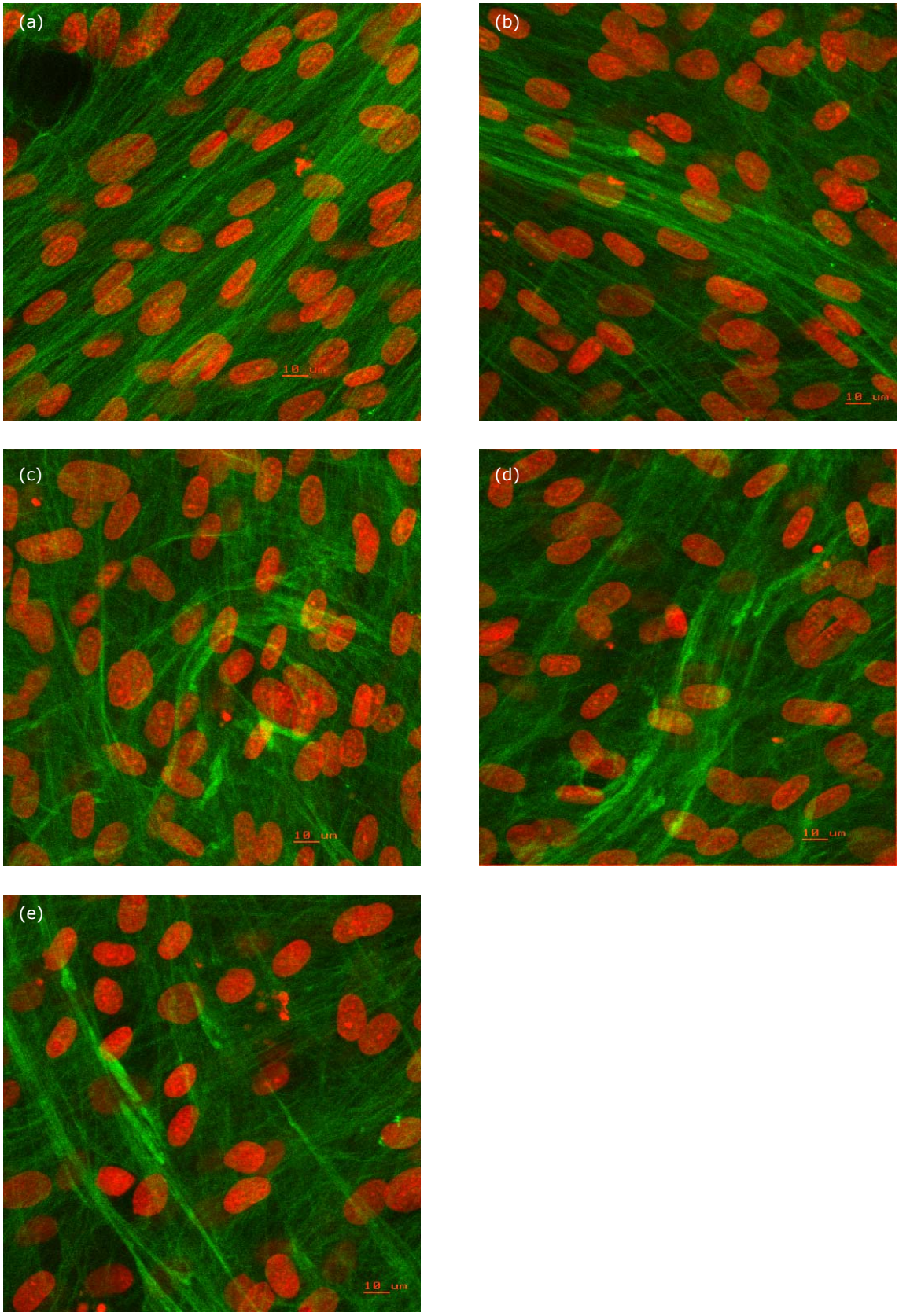

Figure 5.20 Confocal scanning laser micrographs of CFC's cultured for 28 days on (a) 40 Ca, (b) 40 Mg, (c) 30 Mg, (d) 20 Mg and (e) TCP. Green stain is type I collagen and red stain is the cell nuclei. Magnification is x 63, bar is 10 μm.

5.2.3.5 Osteocalcin Production

Osteocalcin was detected in CFC cultures on all glass surfaces from 14 days, Figure.5.21. Levels of osteocalcin increased with time for all surfaces, with 20 Mg showing the highest levels, followed by 30 Mg. Levels at all time points were lower than TCP, the positive control.

After 28 days, there was no significant difference between samples, with the exception of 40 Mg which was significantly lower than 20 Mg/30 Ca and very significantly lower than the TCP control. After 21 days, levels of osteocalcin were significantly lower than the positive control for all surfaces other than 30 Mg/20 Ca.

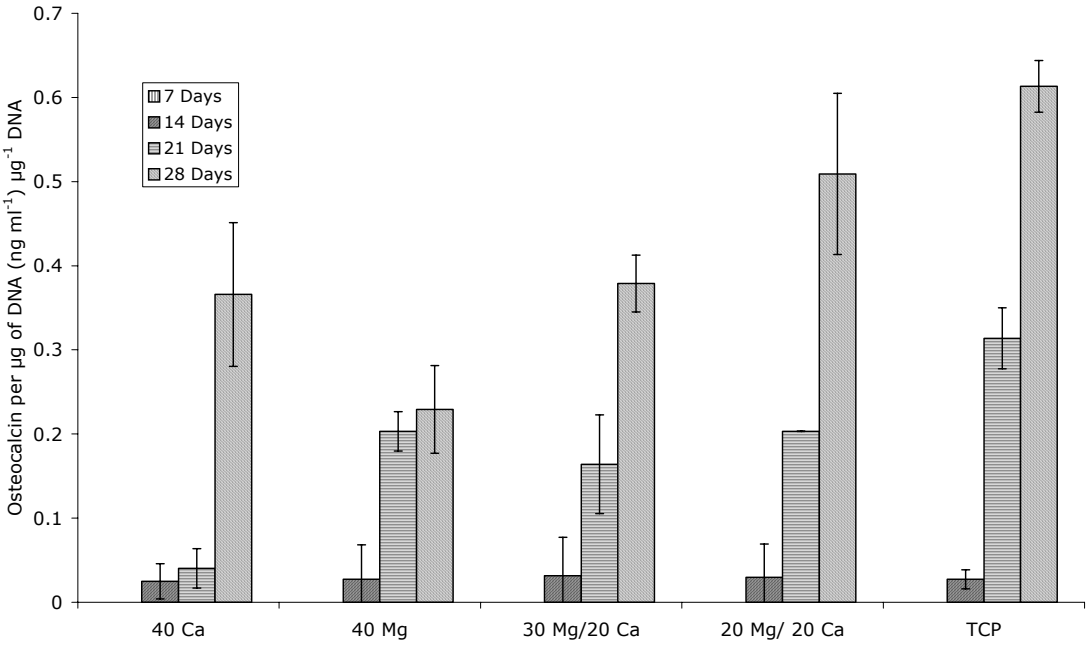

Figure.5.21 Osteocalcin production by CFC's cultured on selected surfaces, see table 5.1, for up to 28 days. Bars represent the standard error of the mean, n = 3.

5.2.3.6 Mineral Deposition

Mineral deposition by CFC's cultured on selected surfaces (table 5.1) was investigated using Alizarin Red staining, figure 5.22a-e. Mineral deposition was confirmed on all surfaces after 21 days except the 40 Ca surfaces, which reacted directly with the dye producing a totally red surface. Cells are difficult to resolve using light microscopy, to compensate this; phase contrast microscopy was used to associate the presence of cells and nodules with mineral phase. Due to the glass sample thickness, phase contrast microscopy was not able to resolve the surface of these samples.

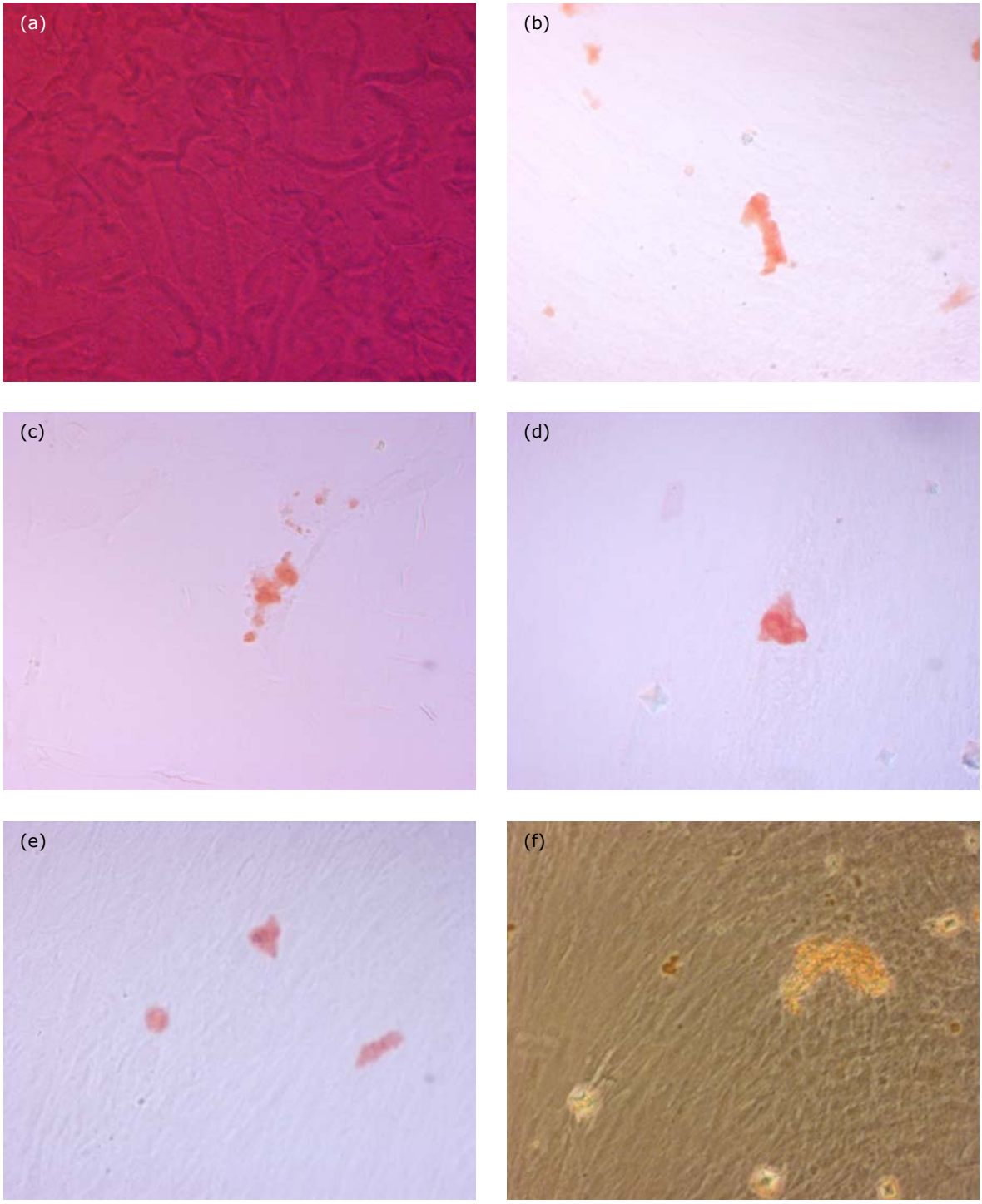

Figure 5.22 Light micrographs of Alizarin Red stained mineral produced by CFC's, which were cultured for 28 days on (a) 40 ca, (b) 40 Mg, (c) 30 Mg, (d) 20 Mg and (e) TCP, (f) is a phase contrast micrograph of Alizarin Red stained mineral produced by CFC's cultured on TCP. All mag is x100.

5.3 Discussion

5.3.1 Early Cell Attachment and Behaviour

Cell proliferation can be measured indirectly by using the Alamar blue assay to determine the metabolic activity of the CFCs, or more directly by measuring the DNA content via the Hoechst 33258 DNA assay. Both have their advantages and disadvantages. The Alamar blue assay is particularly easy to use, reducing potential experimental errors, and leaves the culture viable, allowing either the continuation of culture or further assays. However, using the Alamar blue assay to investigate proliferation forces the assumption that all cells are equally active, whether they are adhering to the surface, producing extracellular matrix or undergoing mitosis. The Hoechst 33258 assay measures DNA content of a cell culture, so proliferation results are not linked to the cell cycle. This assay is easily calibrated to give quantitative data.

The most prominent difference between the Alamar blue and Hoechst 33258 assay results are the relative values after 2 h culture. While the Hoechst 33258 assay shows similar levels for samples, compared to the positive control, the Alamar blue assay shows that the samples metabolic activity is much lower than the positive control.

The results from the Hoechst 33258 assay show that there are the same number of cells on each surface after 2 h. This means that the reduction in metabolic activity of the CFCs cultured on sample surfaces compared to TCP after 2 h is due to the cells being less metabolically active and not because there are fewer cells present. At 2 h, CFCs have yet to spread on the glass

surfaces, figure 5.14 while cells cultured on TCP are spread. This indicates that cells may be less metabolically active when they are attaching and spreading on surfaces compared to when they are spread. The relationship between cell shape and DNA synthesis was studied previously (Folkman *et al.*, 1978). Here, fibroblasts were seeded onto surfaces treated with different concentrations of poly(2-hydroxylethyl methacrylate) to surfaces with graded adhesiveness. The number of cells capable of DNA synthesis was determined via the uptake of ^{3}H-thymidine. It was shown that DNA synthesis was inversely proportional to the height of the cells, i.e. flatter, spread cells demonstrated greater proliferation.

After the initial seeding, attachment and spreading CFCs proliferate rapidly until at confluence, proliferation slows (Folkman *et al.*, 1978), and production of the extra cellular matrix dominates. The proliferation pattern follows a sigmoidal relationship with time, demonstrating the time taken for initial cell attachment before DNA replication occurs and the down regulation of proliferation upon confluence where density alters the cell shape, affecting growth (Folkman *et al.*, 1978). This model is demonstrated by both the Alamar blue and Hoechst 33258 assays.

Proliferation on the ternary glass series was retarded for each composition due to the difficulty CFCs experienced with attachment and spreading on the glass surfaces compared to the TCP control. Initial cell attachment has been shown to be harder on phosphate glass surfaces which are less durable (Parsons *et al.*, 2004b), and hence cell attachment and spreading may be compromised by surfaces which dissolve too fast. The difficulty experienced with attachment may prevent the CFCs progression to the proliferation stage of the cell cycle. Indeed, sodium phosphate glass with at least 40 mol.% of

either calcium phosphate or magnesium phosphate does not show a large increase in proliferation until after 4 days.

Glasses which possessed relatively fast dissolution rates were unable to sustain any prolonged attachment and spreading. The 20 Ca did not have any cells attached after 2 days culture. There are two possible explanations for this: either the glass dissolved faster than the cells could attach or the high level of degradation products was toxic. In a separate elution test, the toxicity of the dissolution products from the 20 Ca glass was investigated (data not shown). The cells proliferated to levels which were similar to but significantly lower than the TCP control during this test, demonstrating that the degradation products were not harmful. Elsewhere HOS and MG63 osteoblasts have been cultured on TCP using media which contained varying concentrations of dissolved calcium/sodium phosphate glasses (Salih *et al.*, 2000). It was found that presence of the dissolution products were not toxic, conversely the solutions containing higher amounts of calcium demonstrated greater proliferative capability.

Surfaces which were slightly more durable, 30 Ca and 20 Mg, allowed the attachment of CFCs over the entire 7 day test period. However, sustained proliferation did not occur. Cells may be constantly reattaching to the surface as it dissolves, hence not given the chance to spread and then proliferate.

The cell morphology of MG63 human osteosarcoma cells cultured on metaphosphate glass surfaces containing varying amounts of calcium and sodium has been studied (Bitar *et al.*, 2004). Cell morphology differed from attached, rounded cells to fully spread morphology almost matching that of the borosilicate control as the calcium concentration, and hence durability, increased from 36 to 48 mol.% CaO. Metaphosphate glasses with less than

36 mol.% CaO were reported to be too unstable to allow the attachment of osteosarcoma cells, while sustained attachment only occurred when CaO levels were 40 mol.% or greater. Direct comparisons with the glass compositions here was not possible due to the differences in phosphate concentration.

CFCs were cultured on sodium phosphate glasses containing varying amounts of iron phosphate and osteoblast attachment was investigated using microscopy (Parsons *et al.*, 2004b). It was found that cell attachment to the glass surface improved with higher iron concentration within the glass. This was thought to be due to the greater durability caused by the addition of iron and not the dissolution of iron into the culture media. Their 10, 15 and 20 % Fe glasses possessed similar dissolution rates to the 20, 30 and 40 Ca glasses investigated here, which were approximately 5.4×10^{-4}, 1.7×10^{-5} and 1.4×10^{-6} g cm^{-2} h^{-1} respectively. On the least durable 10 % Fe glass, confocal laser scanning microscopy was used to show that cells were attached to the surface after 2 h but were not present after that, which concurs with the 20 Ca Alamar blue results that cells were only present at 2 h. The 15 and 20 % Fe glass had sustained cell attachment but the confluence shown after 48 for the 20 % Fe glass was not replicated with the 15 % Fe glass, which did not support any significant proliferation despite cell attachment. This agrees with the DNA assay data here for 30 Ca, which showed that there was cell attachment but no evidence of significant proliferation. Cells were attaching to the glass surface but not spreading and without this change in cell shape DNA replication occurs at a much reduced rate (Folkman *et al.*, 1978).

Comparison of the dissolution rates from the glasses studied by Bitar *et al* (the dissolution rates for these glasses were obtained from Franks, 2000) and Parsons *et al* and the two ternary series here suggest that there is a minimum

dissolution rate required for not only cell adhesion to phosphate glass, but also for the proliferation of osteoblasts. The least durable glass that allowed sustained cell adhesion is the 30 Ca studied in this project which possessed a dissolution rate of $1.7x10^{-5}$ g cm^{-2} h^{-1}, while the least durable phosphate glass which allowed osteoblasts to proliferate were Bitar's 40 mol.% CaO glass and Parsons 20 mol.% Fe glass which possessed a dissolution rate of $3x10^{-6}$ g cm^{-2} h^{-1}. Glasses with dissolution rate below these two values do not sustain osteoblast cell adhesion or proliferation respectively.

Proliferation of CFCs cultured on the quaternary series of glasses was a closer match to that of the positive control, compared to the ternary series. Low cell metabolism after 2 h, again indicated that initial attachment was retarded while proliferation accelerated to levels within 75 % of the positive control at 168 hours, indicating cell attachment was more stable for these durable compositions compared to the ternary series. The lack of significant difference between the quaternary glasses suggests that the dissolution rate plays a more important role than the calcium and magnesium ratio.

5.3.2 Alkaline Phosphatase Activity

Alkaline phosphatase activity by osteoblasts in-vitro is temporal, with mRNA production up regulated as proliferation is retarded and down regulated as osteoblasts enter the mineralisation phase (Stein *et al.*, 1990). During this period of high alkaline phosphatase activity, the extracellular matrix undergoes a series of modifications in composition and organisation which render it suitable for mineralisation (Stein *et al.*, 1990). The up and down regulation of alkaline phosphatase, over a 28 day period was observed on all surfaces except the 40 Ca glass. There may be a lag with the cells grown in this surface and that with more time, alkaline phosphatase activity will drop. However, this cell behaviour has been reported elsewhere (Scotchford personal communication). Human osteoblasts that were cultured on hydroxyapatite for up to 35 days, showed increasing alkaline phosphatase activity that plateaued over this period. All glasses containing magnesium that were cultured for 28 days demonstrated greater alkaline phosphatase activity per DNA at every time point compared to the positive control, TCP, which is in agreement with others (Lee *et al.*, 2004).

Alkaline phosphatase activity appears to be inversely proportional to the glass durability of the three compositions. Studies of *E. coli* alkaline phosphatase, a closely related but non-glycosylated enzyme, have shown the enzyme to be a dimeric metalloprotein with 4 Zn^{2+} and 2 Mg^{2+} present as functional ions within the active site (Wuthier *et al.*, 1984). It is also reported that magnesium acts as an activator for alkaline phosphatase, although not an absolute requirement for the enzyme reaction to occur (Doty *et al.*, 1976). This suggests that magnesium ion release rather than durability may be the

cause for the differences in alkaline phosphatase activity. In this assay, the culture medium was changed two days before the cell layer was harvested, the amount of magnesium in the solution (ignoring any already present) is 4.5, 1.4 and 1.1 µg for the 40 Mg, 30 Mg/20 Ca and 20 Mg/30 Ca glasses respectively. The higher amount of magnesium release appears to be related to the higher alkaline phosphatase activity seen by CFCs cultured on these glasses. Indeed, Mg has been shown to increase the activity of plasma alkaline phosphatase (Heaton, 1965). The increase in alkaline phosphatase activity/DNA after 28 days for cells cultured on TCP was unexpected and not significant but has been reported elsewhere (Gough *et al.*, 2003).

The alkaline phosphatase activity of CFCs cultured on calcium phosphate glass over 28 days was reported elsewhere (Gough *et al.*, 2003). The characteristic up and down regulation of alkaline phosphatase activity was not observed as significant difference from the TCP at any time point or between time points was reported.

During the short term culture (up to 7 days) of CFCs on all glass composition surfaces, alkaline phosphatase activity was detected an all surfaces which were able to support cell attachment, except the 30 Ca glass. As no DNA was detected on the 20 Ca glass, it follows that no osteoblast markers were detected. Although cells are detected via the Hoechst 33258 assay, on the 30 Ca surface, no alkaline phosphatase activity was observed. This may be due to the instability of the glass surface, as although the osteoblasts can attach and proliferate to a certain extent, confluence is not reached and without cell-cell contact, proliferation continues unabated and the temporal transition to extra cellular matrix maturation and mineralisation does not occur (Stein *et al.*, 1990). However, it is known that if the interaction

between integrins and the ECM is disrupted then osteoblast differentiation does not occur (Franceschi, 1999). The dissolving surface may compromise serum protein absorption to the glass and hence reduce the number of possible interactions between osteoblasts and the ECM.

The increase in alkaline phosphatase activity with magnesium concentration for cultures performed over seven days may be due to two possibilities, either an increase in Mg concentration within the media as the glass dissolves, or greater durability provided by the inclusion of increasing amounts of magnesium cations in solution. Calculations show that magnesium cation release from the glasses is inversely proportional the original magnesium concentration within the glasses. Release rate of magnesium from the glasses per day range from 39 µg for 20 Mg to 0.85 µg for 50 Mg. If this increase in alkaline phosphatase activity is due to magnesium release, then it would be expected that despite the much lower dissolution rate, the higher magnesium content compensates for this. However, this is not the case, as the glasses possessing the highest levels of Mg have the slowest release rate for this element. The differences in glass durability may then be the cause of the differences in alkaline phosphatase activity. A more durable surface allows for greater attachment and proliferation, which leads to more alkaline phosphatase production at an earlier time point. However, the Hoechst 33258 assay results show that CFCs do not proliferate on the 20 Mg and the presence of any alkaline phosphatase activity is unexpected. It is possible that some CFCs did attach to the surface well enough to proliferate and that there may be islands of cells where the density was high enough for them progress to the next stage of the cell cycle.

Alkaline phosphatase activity of primary rat osteoblasts cultured on PLA, PGA or copolymers of the two was reported to be significantly less than the TCP control over a 14 days period, with the exception of 75:25 PLA/PGA which demonstrated comparable alkaline phosphatase activity to the positive control (Ishaug *et al.*, 1994). This is in contrast with results reported elsewhere (Matsuzaka *et al.*, 1999). In this study primary rat osteoblasts were cultured on PLA with various depth grooves for up to 16 days and the alkaline phosphatase activity measured. It was reported that the alkaline phosphatase activity of osteoblasts on smooth PLA was approximately twice that of the polystyrene control.

The activity of alkaline phosphatase from MG63 osteosarcoma cells cultured on electropolished titanium over a 14 day period was reported to be the same as the 'plastic' positive control (Martin *et al.*, 1995). This is in agreement with work performed elsewhere (Schmidt *et al.*, 2001), here primary femoral head derived osteoblasts were grown on polished titanium. It was reported that there was no significant difference compared to the TCP control over a 19 day period

Alkaline phosphatase activity of osteoblasts cultured on phosphate glass was approximately three times that of the positive control. This is higher than the alkaline phosphatase activity reported for materials which are currently used in maxillofacial surgery, namely titanium, PLA and PLA/PGA copolymers. Suggesting phosphate glass may be a superior material as far as osteoblast differentiation is concerned.

5.3.3 Long Term CFC Culture

Proliferation of CFCs on glass surfaces up to 28 days is much closer to the positive control compared to earlier time points. Once a confluent layer is formed on the surface, proliferation is less dependant on the glass surface as further cell growth was seen to occur on top of the present cell layer, forming up to 3 layers after 28 days.

Magnesium, (Michishita *et al.*, 1992; Lee *et al.*, 1995), and calcium (Ajroud *et al.*, 2004) are known to form part of the structural integrity of integrins and are important in metal ion dependant adhesion sites (MIDAS) which binds protein ligands. The presence of elevated levels of these cations in the media and surfaces may be responsible for proliferation over a 28 day period which is not significantly different from the positive control.

The ion implantation of calcium (Nayab *et al.*, 2005) and magnesium (Howlett *et al.*, 1994) into the surfaces of titanium and alumina respectively, has been reported to improve the adhesion and spreading of cells compared to unmodified surfaces. Also, magnesium cations and phosphate ions (20 mM and 10 mM respectively), which are in the media have been reported to increase the proliferation of fibroblasts and epidermal cells (Tennenbaum *et al.*, 1990).

Osteoblasts were able to form a type I collagen rich matrix containing calcium deposits on all glass surfaces tested. This is essential if the material is to be considered for orthopaedic use, as the glass must be able to support bone formation. It is evident that type I collagen is produced by the osteoblast in an haphazard manner, resembling that of woven bone, during the short term and an ordered manner, after 21 days culture, suggesting that

remodelling of the matrix is taking place. This agrees with another study (Gough *et al.*, 2003), where cranio-facial osteoblasts were cultured on 'sodium phosphate' and 'calcium phosphate' glasses (exact compositions not given). An ordered collagen fibre rich matrix was reported after 14 days. The lack of significant difference between the amount of collagen produced by osteoblasts cultures on the phosphate glass surfaces or the positive control, indicate that the composition and stability do not affect the rate at which collagen is produced.

Collagen production by primary rat osteoblasts cultured on PLA, PGA and their copolymers over a 14 day period was investigated (Ishaug *et al.*, 1994). It was reported that collagen synthesis on the polymers did not increase over time and was not significantly different from the TCP control. Titanium surfaces were reported to reduce the production of collagen by MG63 osteosarcoma cells compared to 'plastic' controls (Martin *et al.*, 1995). Collagen production on phosphate glass seems to be the same or greater than the currently used materials in maxillofacial surgery.

Osteocalcin is a major non-collagenous matrix protein in bone found in close association with hydroxyapaptite, which is a highly specific osteoblastic marker (Hauschka *et al.*, 1989a). It is produced by osteoblasts grown on all selected glasses and the positive control, indicating that osteoblasts were fully differentiated and had reached the last stage in matrix maturation. Osteocalcin levels on 40 Mg significantly lower than the other phosphate glass surfaces and TCP, indicating that these cells were less differentiated. The exact causes for the changes in osteocalcin levels are unknown but TGF-β has previously been implicated, in an autocrine manner, in its regulation (Bonewald *et al.*, 1992; Lincks *et al.*, 1998).

Osteocalcin production by primary human osteoblasts on titanium was reported to be higher than TCP over a 19 day period (Schmidt *et al.*, 2001). However, the greatest osteocalcin expression was after 7 days, the pattern of expression was unusual, with an up and down regulation of the protein similar to that expected for alkaline phosphatase. This is in agreement with work reported elsewhere (Lincks *et al.*, 1998), here MG63 osteosarcoma cells were cultured on polished and course ground commercially pure titanium. Osteocalcin levels were calculated 24 h after cells had reached confluence. There was no significant difference between smooth titanium and TCP but osteocalcin expression was approximately double that of TCP for the course ground titanium. Primary human osteoblasts cultured on PLA and PLGA (50:50) were reported to express significantly less osteocalcin after 72 h compared to TCP (El-Amin *et al.*, 2002). PLA produced only a third of the osteocalcin expressed by osteoblasts grown on TCP. This is in disagreement with results published elsewhere (Di Toro *et al.*, 2004), here primary human osteoblasts were grown on PLGA (50:50 and 75:50) and osteocalcin levels were measured after 14 days. No significant difference was observed between TCP and the test surfaces.

Calcium deposition upon the 40 Ca glass is unconfirmed as the material itself tested positive for the alizarin red stain. However, small deposits of calcium were observed on all other glasses. Difficulty arose when attempting to discover where the calcium was deposited as it is very difficult to resolve cells using the light microscope. Phase contrast microscopy was employed to clearly identify cells, and calcium deposits were seen to occur within cell nodules, in agreement with others (Bellows *et al.*, 1986). Calcium deposition on calcium phosphate glass was reported elsewhere in the literature (Gough *et*

al., 2003). Here calcium deposits were less well defined than shown by Gough *et al*, 2003, with lower specific densities of calcium deposition covering larger areas.

The developmental/differentiation sequence of osteoblasts is known to consist of three distinct temporal periods; proliferation, matrix development (or maturation) and mineralisation (Shalhoub *et al.*, 1989; Stein *et al.*, 1990; Stein *et al.*, 1996). Here, progression from one period to the next is linked to the down regulation of genes from the preceding phase, for review see Stein *et al.*, 1996. The first phase, proliferation, is dominated by the expression of genes associated with cell proliferation; namely H4, C-*fos* and C-*myc* (Shalhoub *et al.*, 1989), and also type I collagen (Stein *et al.*, 1989b). The matrix maturation phase is subsequently dominated by alkaline phosphatase activity (Alborzi *et al.*, 1996) while mineralisation involves calcium deposition and the up regulation of osteocalcin, figure 5.23.

All glasses studied over the 28 day period demonstrated the same temporal pattern with respect to the production of proteins quantified. Differences only occurred between the levels of protein production at each time point. As such, only the data from the 30 Mg/20 Ca sample is shown and compared to the literature.

Plotting the alkaline phosphatase and osteocalcin data normalised to DNA concentration and collagen, as a percentage of the maximum value in each series (all values are for CFCs cultured on 30 Mg/20 Ca) against culture time, figure 5.24, allows for a comparison with figure 5.23. However, the data from Stein *et al.*, 1990 is from the quantification of mRNA while the data presented here is the quantification of the products themselves or their activity, and as such, some discrepancies will be present. The greatest differences present will

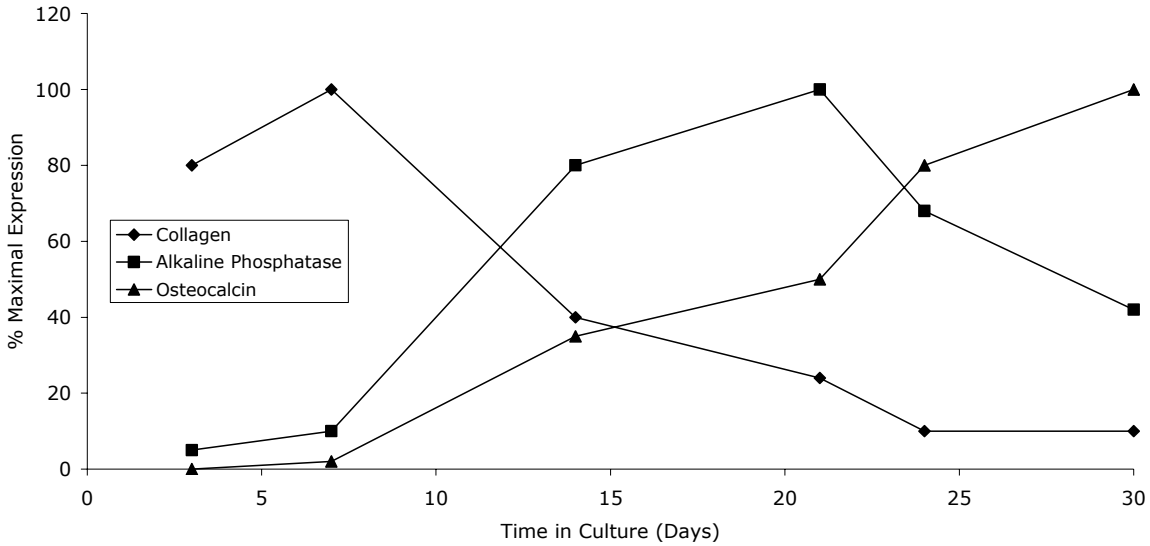

Figure 5.23 Temporal expression of osteoblast phenotype related genes during the development of the osteoblast phenotype *in vitro*. From rat primary osteoblasts. Figure adapted from Stein et al, 1990; Stein et al, 1996.

be between the structural proteins and their mRNA. Eukaryotic cells use translational control extensively to control protein synthesis, levels of mRNA are quickly decreased after demand for the protein which is encoded has stopped (Mathews *et al.*, 2000).

The most striking difference lies with type I collagen, mRNA concentration decreases from 7 days (Stein *et al.*, 1989b), while levels of actual collagen increase from day 7 and remain above 90 % for the duration of the test. This agrees with Aronow *et al*, who reported that the levels of collagen produced by osteoblasts increased over a 35 day period. The close transcription level control of mRNA (Mathews *et al.*, 2000) may be the cause of the discrepancy as mRNA levels do not directly lead to corresponding levels of protein. Unlike enzymes, collagen is a stable, insoluble protein which increases in concentration cumulatively with time although it is degraded by collagenase, a matrix metalloprotein during remodelling of woven bone (Partridge *et al.*, 1996). So despite the reduction in the encoding mRNA and enzymes which

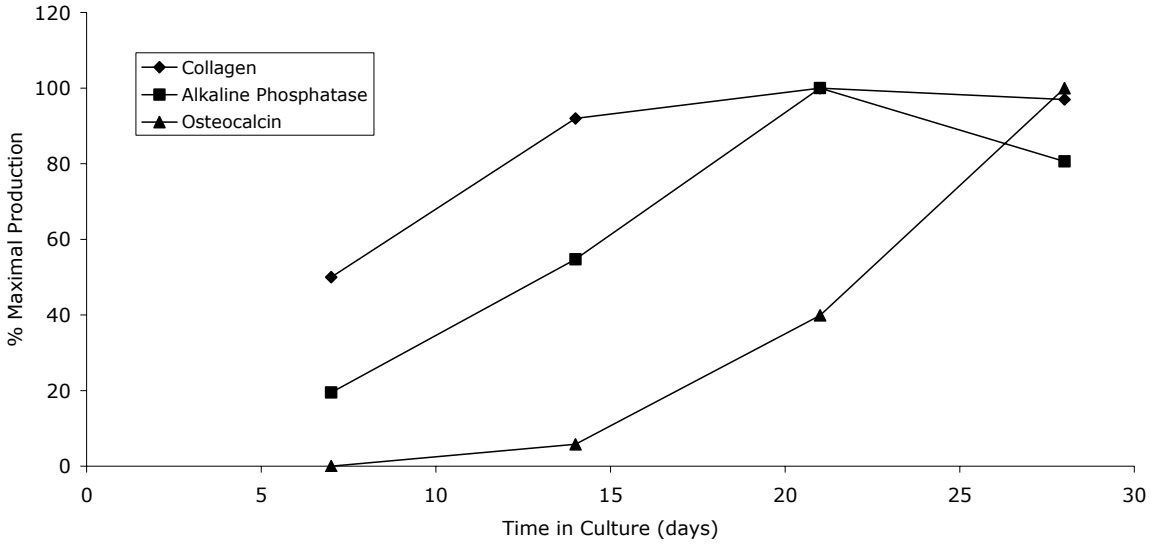

Figure 5.24 Temporal production of osteoblast phenotype related proteins from primary human cranial facial derived osteoblast like cells cultured on 30 Mg/20 Ca phosphate glass. All data is normalised to the DNA concentration.

lead to its production, levels will remain high compared to cell numbers as proliferation is retarded when osteoblasts enter the matrix maturation phase.

Alkaline phosphatase activity and its encoding mRNA show the typical rise and fall of concentrations as the matrix maturation phase begins and ends. Levels of alkaline phosphatase derived here lag those stated by others (Stein *et al.*, 1990; Stein *et al.*, 1996). However, phenotypic expression by osteoblasts derived from the cranium has been shown to lag behind osteoblasts derived from the femoral head (McDougall, 2001).

There is a slight lag between the emergence of osteocalcin mRNA (Stein *et al.*, 1990), and the appearance of the protein itself, as quantified in this work, but both increase exponentially with time. Osteocalcin is known to be involved in the regulation of osteoclasts, hence this may indicate a greater presence with the deposition of the mineral phase of bone (Hauschka *et al.*, 1989a; Hauschka *et al.*, 1989b).

Overall, osteoblasts cultured on selected phosphate glasses have been shown to express proteins from each of the three temporal differential phases,

demonstrating that these surfaces do not unduly affect the normal osteoblast cell cycle. Comparison of these results with those in the literature for materials currently used in maxillofacial surgery (titanium. PLA and PLGA) show that phosphate glasses are, at worst, comparable with respect to collagen and osteocalcin function, leading to the belief that phosphate glasses may perform with the same level of 'osteoblastic biocompatibility' as currently used materials.

5.3.4 Macrophage Activation

Macrophages were cultured on the glass surfaces to assess whether the samples elicited any activation. Activation of macrophages refers to a state of enhanced cellular metabolism, mobility, lysosomal enzyme activity and cytocidal capacity (Adams *et al.*, 1984), and is often accompanied by the elaboration of important products from the mononuclear phagocyte family, including the IL-1 cytokine family (Ross *et al.*, 2002). IL-1 is secreted in response to stimuli such as infections and microbial endotoxins (hence is produced in response to treatment by lipopolysaccharide). The principal effects of IL-1 are primarily lymphocyte activation, macrophage stimulation, increased lymphocyte and endothelial adhesion and pyrexia; all of which are achieved by the production of further types of cytokines. Another important effect in the context of this work is the stimulation of bone resorption by IL-1 (Gowen *et al.*, 1986; Sato *et al.*, 1986; Dewhirst *et al.*, 1987). Activation of macrophages can be caused by receptor-ligand interactions (including receptors for Fc regions of immunoglobulin and complement components, see (Adams *et al.*, 1984) for a review), which results in a 'respiratory burst' which involves the metabolism of large quantities of glucose and increased levels of cytotoxic agents including hydrogen peroxide and hydroxyl radicals via superoxide production by the membrane bound oxidase complex (Babior, 1984). Thus activation of macrophages may be quantified by analysis of hydrogen peroxide and IL-1β.

Over a time period of two days, macrophages did not show any significant activation, as assessed by IL-1β production, hydrogen peroxide production and cell morphology.

A spread morphology is thought to be a marker of *in vitro* activation (Miller *et al.*, 1998), however, cells cultured on phosphate glass remained rounded and proliferated, showing no morphological signs of activation after 2, or 48 h. Macrophages activated with lipopolysaccharide possessed a spread morphology and a lower cell number than macrophages cultured on the TCP or phosphate glass surfaces.

Hydrogen peroxide is produced by metabolising macrophages, hence is expected to be produced from macrophages on all surfaces (Babior, 1984). However, levels of production were lower than that of copper, the positive control which induces the respiratory burst, and not significantly different to the negative control, TCP, with the exception of 40 Ca after 5 hours which was higher than the other phosphate glass surfaces studied. This suggests that the phosphate glass compositions tested caused no undue increases in macrophage metabolism. An increase in hydrogen peroxide production was observed by Parsons *et al* for sodium phosphate glass containing iron, where the least durable composition expressed significantly more hydrogen peroxide than the negative control but also significantly less than the copper positive control.

No IL-1β was detected from macrophages cultured on phosphate glass or TCP, the negative control, indicating no microbial infection type immune response (Burke *et al.*, 2002). However, IL-1β production by macrophages cultured in the presence of lipopolysaccharide was approximately 3 times higher when the concentration of lipopolysaccahride was increased 10 fold from 10 μg ml^{-1} to 100 μg ml^{-1}. The lower than expected increase in IL-1β concentration may be due to the maximum production rate of this cytokine being achieved.

Gough et al, 2002, cultured macrophages (and osteoblasts) on sodium phosphate glass and found a significant difference in hydrogen peroxide production compared to the negative control but no elevated levels IL-1β. This is despite the fact that sodium phosphate glasses have been shown in work performed by the author to dissolve extremely quickly. The glasses produced by Gough et al, 2002, were produced in alumina crucibles and it is proposed that aluminium contamination (Parsons *et al.*, 2004a), gave the glasses improved durability (Brow, 1993), while possibly serving as a source of the elevated hydrogen peroxide levels.

5.4 Summary

The work presented in this chapter has shown that the most durable phosphate glasses investigated were of a high enough quality to support osteoblast attachment, proliferation and differentiation.

Sodium phosphate glasses containing as least 20 mol.% $MgHPO_4$ or 30 mol.% $CaHPO_4$ were demonstrated to support osteoblast attachment, proliferation and entry into the matrix maturation phase of the osteoblast cycle (via the production of alkaline phosphatase after seven days). However, the greatest amount of proliferation, which occurred over seven days, was with the most durable compositions. This implied that initial attachment and proliferation had greater dependence on the stability of the surface rather than any positive benefit which might occur from ion release.

Over longer periods of time the stability of the surface played an increasingly minor role, as the calcium and magnesium affected, not only, the way osteoblasts differentiate, but also the activity of active products such as alkaline phosphatase. There was no single glass composition which exhibited better potential biocompatibility than any other, allowing for physical properties to be the deciding factor when it comes to deciding which glass should be further investigated for use as a possible biomaterial.

Comparison with work performed on other materials currently used in maxillofacial surgery suggested that phosphate glasses would perform as well or better with respect to the effect on the expression of osteoblastic markers, namely collagen, alkaline phosphatase and osteocalcin.

An immunological reaction was not observed. Macrophages on the sample surfaces produced the same levels of hydrogen peroxide when cultured on the

negative control and significantly less than the positive control. No IL-1β was detected from macrophages cultured on the sample surfaces.

Overall, selected phosphate glasses have been shown to possess suitable *in vitro* biocompatibility, allowing osteoblasts to deposit mineral whilst not invoking an immune response.

6 Conclusions

This study has shown that it is possible to produce high quality glasses from relatively safe phosphate salt precursors, as compared to oxide starting materials. Comparison of the T_g and dissolution rate between the glasses made here and those presented in the literature, which were made from phosphorus pentoxide and metal oxides have shown that there is little difference between glasses of similar composition. The properties of phosphate glasses are independent of the starting materials. However, phosphate salts are less flexible than their oxide counterparts as the phosphate to cation ratio is fixed.

The choice of crucible material was crucial in the production of high quality phosphate glasses. The use of alumina crucibles led to contamination of the glasses with aluminium. The erosion of alumina into the melt led to differences in composition within the melt, upon cooling this caused internal stress inside the glass causing it to shatter. Also the aluminium affects the T_g of the glass, increasing it by large values so that the internal stresses had not dissipated upon cooling and annealing.

The T_g and dissolution rate were similarly affected by the method of glass preparation and the composition of the glass. The length of time the melt is held at a particular temperature increases the T_g by up to 10 °C to 295 °C and decreases the dissolution rate up to a plateau value, 0.008 g cm^{-2} h^{-1}. Increasing the temperature shortens the time required to reach the plateau value. Analysis by XPS revealed that the phosphates were forming chains and that the length of the length of these chains was responsible for the observed changes in glass properties.

Introducing divalent cations to the glass caused a greater increase in both the T_g and the durability of the glass compared to the melt regime alone. The T_g of sodium phosphate glass was increased linearly with the addition of $MgHPO_4$ and $CaHPO_4$, while dissolution was reduced exponentially with the addition of these salts. XPS was used to show that the average chain length was decreasing, implying that this was not the cause of the change in properties. The changes in property values were due to cation/non-bridging oxygen cross-links forming a new network. Increasing the concentration of cations caused a greater number of cross-links and hence further increased the T_g and durability of the glass.

The dissolution rate of the glass was initially relatively fast but then slowed until it reached a plateau value. There were many theories in the literature which attempted to explain this, including hydrolysis of the phosphate chains by moisture in the air prior to testing. However, analysis of the dissolution surface with time revealed that the phosphate chain length was not shortened as the glass dissolved, leading to the conclusion that the dissolution mechanism is hydration rather than hydrolysis. The initial leaching of sodium was thought to be the cause but XPS analysis showed that the composition of the glass surface remained constant throughout dissolution. Experiments performed in the literature accompanied by the tests performed here suggest that the initial drop in dissolution rate is due to the increasing ionic strength of solution.

Initial cell culture testing performed over a seven day period showed that proliferation occurred on a range of glasses. Alkaline phosphatase, a marker of osteoblast differentiation was expressed after seven days by osteoblasts cultured on all surfaces which allowed cells to adhere. The most durable

glasses, which contained higher concentrations of divalent cations, showed the greatest osteoblast proliferation and alkaline phosphatase activity. This was thought to be due to the greater stability of the surface allowing greater cell adherence and spreading, which is required before the cell can produce and mature the extracellular matrix. Comparison of the glass durability with cell adhesion and proliferation led to approximate minimum dissolution rates that were required for cell adhesion ($1.7x10^{-5}$ g cm^{-2} h^{-1}) and proliferation ($3x10^{-6}$ g cm^{-2} h^{-1}).

Longer culture performed on selected glasses showed that proliferation and osteoblast differentiation was not unduly effected. Collagen production was observed after seven days in an unorganised manner and in an organised manner after 21 days. Levels of collagen increased over the 28 day period for all surfaces. Alkaline phosphatase activity increased over 21 days and then decreased on all surfaces except 40 Ca which did not exhibit a decrease. Glasses containing the highest levels of magnesium showed the highest levels of alkaline phosphatase activity despite being the least durable, as magnesium ions are known to be part of the active site in alkaline phosphatase. Osteocalcin, an extremely selective marker for osteoblast differentiation, was produced by cells cultured on all selected surfaces after 21 days. Overall, phosphate glasses did not unduly affect the osteoblast cell cycle.

Immunological testing of phosphate glass surfaces showed that no activation of the immune system occurred within the scope of the tests performed here.

Overall, it was shown that the most durable glasses possess the greatest potential for use as a possible use as a biomaterial, as they are sufficiently

stable not to impair proliferation while not greatly altering the behaviour of osteoblasts cultured on them, as well as not activating macrophages.

7 Future Work

The work presented in this thesis is part of a larger programme looking at the possibility of using a totally degradable composite to replace titanium and PLA/PGA as the materials of choice for maxillo-facial bone repair and replacement. All of this needs more research, including in-vivo experimentation, to produce a viable product. However, the future work suggested here is of direct consequence of this study only.

This thesis has shown how phosphate salts can be used as a successful replacement for phosphorus pentoxide and metal oxide. It follows that other cations could be incorporated into the glass. Higher valence ions such as transition metals could be used in an attempt to improve the durability of the glass, allowing the calcium and magnesium concentrations to be tailored to meet the requirements for improved biocompatibility. Zinc is known to improve the durability without large increases in T_g, this could be used to reduce the final cost of the fibres produced by lowering the drawing temperature.

Analysis of highly durable phosphate glasses is fraught with error as the weight loss over relatively large periods of time is very small, as well as being time consuming. Ways of increasing the dissolution rate, so that larger weight losses with less error can be recorded, such as higher temperatures and more extreme pH, especially acidic conditions, are possible. However, it needs to be known if the mechanism of dissolution is the same for these new conditions and if the actual dissolution rate when dissolved in an ideal media is the same as these accelerating conditions

As was seen, cation release affected the differentiation of osteoblasts and the activity of their products. The use of glasses with a higher dissolution rate may improve the biocompatibility and mineral deposition in ways not observed with the durable glasses tested.

It is well known that the topography of material surfaces affects the behaviour of osteoblasts. Drawing the glasses into fibres will cause a distinct change in the topography that an osteoblast will come into contact with. It is not known how the attachment, proliferation and differentiation of osteoblasts are affected.

Finally, all new biomaterials must undergo in-vivo testing to deduce whether or not the material is suitable for biomaterials applications. As in-vitro testing can not replicate the complex environment of the human body.

References

Abe, Y. (1983). Topics in Phosphorus Chemistry. M. Grayson and E. J. Griffith. New York, Wiley. **11:** 19.

Adams, D. O. and T. A. Hamilton (1984). "The Cell Biology of Macrophage Activation." Annual Review of Immunolgy **2**: 283-318.

Ahmed, I., C. A. Collins, M. P. Lewis, I. Olsen and J. C. Knowles (2004a). "Processing, Characterisation and Biocompatibility of Iron- Phosphate Glass Fibres for Tissue Engineering." Biomaterials **25**(16): 3223-3232.

Ahmed, I., M. Lewis, I. Olsen and J. C. Knowles (2004b). "Phosphate Glasses for Tissue Engineering: Part 1. Processing and Characterisation of a Ternary-Based P_2O_5-CaO-Na_2O Glass System." Biomaterials **25**(3): 491-499.

Ahmed, I., M. Lewis, I. Olsen and J. C. Knowles (2004c). "Phosphate Glasses for Tissue Engineering: Part 2. Processing and Characterisation of a Ternary-Based P_2O_5-CaO-Na_2O Glass Fibre System." Biomaterials **25**(3): 501-507.

Ahn, D. K., C. D. Sims, M. A. Randolph, D. Oconnor, P. E. M. Butler, M. T. J. Amarante and M. J. Yaremchuk (1997). "Craniofacial skeletal fixation using biodegradable plates and cyanoacrylate glue." Plastic and Reconstructive Surgery **99**(6): 1508-1515.

Ajroud, K., T. Sugimori, W. H. Goldmann, D. M. Fathallah, J.-P. Xiong and M. A. Arnaout (2004). "Binding Affinity of Metal Ions to the CD11b A-domain Is Regulated by Integrin Activation and Ligands." Journal of Biological Chemistry **279**(24): 25483-25488.

alamarBlue. (2003). Serotec Product Datasheet, http://www.serotec.com/pdf/alamarblue.pdf.

Alborzi, A., K. Mac, C. A. Glackin, S. S. Murray and J. H. Zernik (1996). "Endochondral and Intramembrous Fetal Bone Development: Osteoblastic Cell Proliferation, and Expression of Alkaline Phosphatase, m-twist, and Histone H4." Journal of Craniofacial Genetics and Development Biology **16**: 94-106.

Allen, W. M., B. F. Sansom, C. F. Drake and D. C. Davies (1978). "New Method for Prevention of Trace-Element Deficiencies." Veterinary Science Communications **2**(1): 73-75.

Allen, W. M., B. F. Sansom, P. T. Gleed, C. B. Mallinson and C. F. Drake (1984). "Boluses of Controlled Release Glass for Supplementing Ruminants with Copper." Veterinary Record **115**(3): 55-57.

Allen, W. M., B. F. Sansom, C. B. Mallinson, R. J. Stebbings and C. F. Drake (1985). "Boluses of Controlled Release Glass for Supplementing Ruminants with Cobalt." Veterinary Record **116**(7): 175-177.

Anderson, J. M. (2004). Inflammation, Wound Healing and the Foreign Body Response. Biomaterials Science: An Introduction to Materials in Medicine. B. D. Ratner, A. S. Hoffman, F. J. Schoen and J. E. Lemons. London, Elsevier Academic Press.

Anselme, K. (2000). "Osteoblast adhesion on biomaterials." Biomaterials **21**(7): 667-681.

Aronow, M. A., L. C. Gerstenfeld, T. A. Owen, M. S. Tassinari, G. S. Stein and J. B. Lian (1990). "Factors that Promote Progressive Development of the Osteoblast Phenotype in Cultured Fetal Rat Calvaria Cells." Journal of Cellular Physiology **143**: 213-221.

Arzeian, J. M. and C. A. Hogarth (1991). "Some Structural, Electrical and Optical-Properties of Copper Phosphate-Glasses Containing the Rare-Earth Europium." Journal of Materials Science **26**(19): 5353-5366.

Aubin, J. E. (2000). Osteogenic Cell Differentiation. Bone Engineering. J. E. Davies. Toronto, Canada, Rainbow Graphic Design Inc.

Babior, B. M. (1984). "The Respiratory Burst of Phagocytes." Journal of Clinical Investigation **73**: 599-601.

Bae, B. S. and M. C. Weinberg (1991). "Oxidation-Reduction Equilibrium in Copper Phosphate-Glass Melted in Air." Journal of the American Ceramic Society **74**(12): 3039-3045.

Barrie, A. and F. J. Street (1975). "Auger and X-Ray Photoelectron Spectroscopic Study of Sodium Metal and Sodium Oxide." Journal of Electron Spectroscopy and Related Phenomena **7**(1): 1-31.

Bellows, C. G., J. E. Aubin, J. N. M. Heersche and M. E. Antosz (1986). "Mineralized Bone Nodules Formed *In Vitro* from Enzymatically Released Rat Calvaria Cell-Populations." Calcified Tissue International **38**(3): 143-154.

Bernas, T. and J. Dobrucki (2002). "Mitochindrial and Nonmitochondrial Reduction of MTT: Interaction of MTT with TMRE, JC-1 and NAO Mitochindrial Flourescent Probes." Cytometry **47**: 236-242.

Bitar, M., V. Salih, V. Mudera, J. C. Knowles and M. P. Lewis (2004). "Soluble Phosphate Glasses: *In Vitro* Studies Using Human Cells of Hard and Soft Tissue Origin." Biomaterials **25**(12): 2283-2292.

Bloom, D. and R. Fawcett (2002). Concise Histology. London, Hodder Arnold.

Bonewald, L. F., M. B. Kester, Z. Schwartz, L. D. Swain, A. G. Khare, T. L. Johnson, R. J. Leach and B. D. Boyan (1992). "Effects of Combining Transforming Growth Factor β and 1,25-dihydroxyvitamin D_3 on Differentiation of a Human Osteosarcome (MG63)." Journal of Biological Chemistry **267**: 8943-8949.

Boyan, B. D., T. W. Hummert, D. D. Dean and Z. Schwartz (1996). "Role of material surfaces in regulating bone and cartilage cell response." Biomaterials **17**(2): 137-146.

Briggs, D. and J. T. Grant (2003). Surface Analysis by Auger and X-ray Photoelectron Spectroscopy. Charlton, Manchester, IM Publications. SurfaceSpectra Limited.

Brow, R. K. (1993). "Nature of Alumina in Phosphate-Glass .1. Properties of Sodium Aluminophosphate Glass." Journal of the American Ceramic Society **76**(4): 913-918.

Brow, R. K. (1996). "An XPS Study of Oxygen Bonding in Zinc Phosphate and Zinc Borophosphate Glasses." Journal of Non-Crystalline Solids **194**: 267-273.

Brow, R. K. (2000). "Review: The Structure of Simple Phosphate Glasses." Journal of Non-Crystalline Solids **263-264**: 1-28.

Brow, R. K., R. J. Kirkpatrick and G. L. Turner (1990a). "Local Structure of xAl_2O_3.(1-x)$NaPO_3$ Glasses: An NMR and XPS Study." Journal of the American Ceramic Society **73**(8): 2293-2300.

Brow, R. K., R. J. Kirkpatrick and G. L. Turner (1990b). "The Short Range Structure of Sodium Phosphate Glasses I. MAS NMR studies." Journal of Non-Crystalline Solids **116**(1): 39-45.

Brow, R. K., C. C. Phifer, G. L. Turner and R. J. Kirkpatrick (1991). "Cation Effects on P-31 MAS NMR Chemical-Shifts of Metaphosphate Glasses." Journal of the American Ceramic Society **74**(6): 1287-1290.

Brow, R. K., M. R. Reidmeyer and D. E. Day (1988). "Oxygen Bonding in Nitrided Sodium-Metaphosphate and Lithium-Metaphosphate Glasses." Journal of Non-Crystalline Solids **99**(1): 178-189.

Brow, R. K., D. R. Tallant, J. J. Hudgens, S. W. Martin and A. D. Irwin (1994). "The Short-Range Structure of Sodium Ultraphosphate Glasses." Journal of Non-Crystalline Solids **177**: 221-228.

Bruckner, R., H.-U. Chun, H. Goretzki and M. Sammet (1980). "XPS Measurements and Structural Aspects of Silicate and Phosphate Glasses." Journal of Non-Crystalline Solids **42**: 49-60.

Bunker, B. C., G. W. Arnold and J. A. Wilder (1984). "Phosphate-Glass Dissolution in Aqueous-Solutions." Journal of Non-Crystalline Solids **64**(3): 291-316.

Bunker, B. C., D. R. Tallant, C. A. Balfe, R. J. Kirkpatrick, G. L. Turner and M. R. Reidmeyer (1987). "Structure of Phosphorus Oxynitride Glasses." Journal of the American Ceramic Society **70**(9): 675-681.

Burke, B. and C. E. Lewis (2002). The Macrophage. Oxford, Oxford University Press.

Butler, W. T. (1989). "The Nature and Significance of Osteopontin." Connective Tissue Research **23**(2-3): 123-136.

Butler, W. T., A. L. Ridall and M. D. McKee (1996). Osteopontin. Principles of Bone Biology. J. P. Bilezikian, L. G. Raisz and G. A. Rodan. London, Academic Press.

Byrne, J. E., J. H. Lovasko and D. M. Laskin (1973). "Corrosion of Metal Fracture Fixation Appliances." Journal of Oral Surgery **31**(8): 639-645.

Calderwood, D. A., D. S. Tuckwell, J. Eble, K. Kuhn and M. J. Humphries (1997). "The Integrin alpha 1 A-domain Is a Ligand Binding Site for Collagens and Laminin." Journal of Biological Chemistry **272**(19): 12311-12317.

Clement, J., J. M. Manero, J. A. Planell, G. Avila and S. Martinez (1999). "Analysis of the Structural Changes of a Phosphate Glass During its Dissolution in Simulated Body Fluid." Journal of Materials Science-Materials in Medicine **10**(12): 729-732.

Clokie, C. M. L., R. Coulson, S. A. F. Peel and G. K. L. Sandor (2000). Approaches to Bone Regeneration in Oral and Maxillofacial Surgery. Bone Engineering. J. E. Davies. Hong Kong, Rainbow Graphic and Printing Ltd.

Cooke, F. W., J. E. Lemons and B. D. Ratner (1996). Properties of Materials. Biomaterials Science: An Introduction to Materials in Medicine. B. D. Ratner, A. S. Hoffman, F. J. Schoen and J. E. Lemons. London, Academic Press**:** 11-36.

Corden, T. J., I. A. Jones, C. D. Rudd, P. Christian and S. Downes (1999). "Initial Development into a Novel Technique for Manufacturing a Long Fibre Thermoplastic Bioabsorbable Composite: *In-Situ* Polymerisation of Poly-Epsilon-Caprolactone." Composites Part a-Applied Science and Manufacturing **30**(6): 737-746.

Cozien-Cazuc, S. (2005). Personal Communication.

Cruickshank, D. (1961). "Role of 3d-Orbitals in Π-Bonds Between. A. Silicon, Phosphorus, Sulphur, or Chlorine and .B. Oxygen or Nitrogen." Journal of the Chemical Society(DEC): 5486-&.

Daniels, A. U., M. K. O. Chang, K. P. Andriano and J. Heller (1990). "Mechanical-Properties of Biodegradable Polymers and Composites Proposed for Internal-Fixation of Bone." Journal of Applied Biomaterials **1**(1): 57-78.

De Diego, M. A., N. J. Coleman and L. L. Hench (2000). "Tensile Properties of Bioactive Fibers for Tissue Engineering Applications." Journal of Biomedical Materials Research **53**(3): 199-203.

Delahaye, F., L. Montagne, G. Palavit, J. Claude Touray and P. Baillif (1998). "Acid Dissolution of Sodium-Calcium Metaphosphate Glasses." Journal of Non-Crystalline Solids **242**(1): 25-32.

Dewhirst, F. E., J. M. Ago, W. J. Peros and P. Stashenko (1987). "Synergism between Parathyroid Hormone and Interleukin 1 in Stimulating Bone Resorption in Organ Culture." Journal of Bone Mineral Research **2**: 127-134.

Di Toro, R., V. Betti and S. Spampinato (2004). "Biocompatibility and integrin-mediated adhesion of human osteoblasts to poly(DL-lactide-co-glycolide) copolymers." European Journal of Pharmaceutical Sciences **21**(2-3): 161-169.

Doty, S. B. and B. H. Schofield (1976). "Enzyme Histochemistry of Bone and Cartilage Cells." Progress in Histochemistry and Cytochemistry **8**: 1-38.

Ducy, P. and G. Karsenty (1996). Skeletal Gla Proteins: Gene Structure, Regulation of Expression, and Function. Principles of Bone Biology. J. P. Bilezikian, L. G. Raisz and G. A. Rodan. London, Academic Press Ltd**:** 183-195.

Ebendorff-Heidepriem, H. and D. Ehrt (2000). "Formation and UV absorption of cerium, europium and terbium ions in different valencies in glasses." Optical Materials **15**(1): 7-25.

Ebendorff-Heidepriem, H. and D. Ehrt (2002a). "Effect of Europium Ions on X-ray-Induced Defect Formation in Phosphate Containing Glasses." Optical Materials **19**(3): 351-363.

Ebendorff-Heidepriem, H., C. Riziotis and E. R. Taylor (2002b). "Novel Photosensitive Glasses." Glass Science and Technology **75**: 54-59.

Eisenberg, A., H. Farb and L. G. Cool (1966). "Glass Transitions in Ionic Polymers." Journal of Polymer Science Part A-2-Polymer Physics **4**(6PA2): 855-868.

El-Amin, S. F., M. Attawia, H. H. Lu, A. K. Shah, R. Chang, N. J. Hickok, R. S. Tuan and C. T. Laurencin (2002). "Integrin expression by human osteoblasts

cultured on degradable polymeric materials applicable for tissue engineered bone." Journal of Orthopaedic Research **20**(1): 20-28.

El-Amin, S. F., H. H. Lu, Y. Khan, J. Burems, J. Mitchell, R. S. Tuan and C. T. Laurencin (2003). "Extracellular matrix production by human osteoblasts cultured on biodegradable polymers applicable for tissue engineering." Biomaterials **24**(7): 1213-1221.

Ellenbogen, R. and L. Rubin (1975). "Injectable Fluid Silicone Therapy - Human Morbidity and Mortality." Jama-Journal of the American Medical Association **234**(3): 308-309.

Eppley, B. L., A. M. Sadove and R. Z. German (1990). "Evaluation of Htr Polymer as a Craniomaxillofacial Graft Material." Plastic and Reconstructive Surgery **86**(6): 1085-1092.

Exarhos, G. J., P. J. Miller and W. M. Risen (1974). "Interionic Vibrations and Glass Transitions in Ionic Oxide Metaphosphate Glasses." Journal of Chemical Physics **60**(11): 4145-4155.

Fiala, T. G. S., K. T. Paige, T. L. Davis, T. A. Campbell, B. R. Rosen and M. J. Yaremchuk (1994). "Comparison of Artifact from Craniomaxillofacial Internal-Fixation Devices - Magnetic-Resonance-Imaging." Plastic and Reconstructive Surgery **93**(4): 725-731.

Fields, R. D. and M. V. Lancaster (1993). "Dual-attribute Continuous Monitoring of Cell Proliferation/Cytotoxicity." Am. Biotechnol. Lab. **11**: 48-50.

Fisher, L. W., G. R. Hawkins, N. Tuross and J. D. Termine (1987). "Purification and Partial Characterization of Small Proteoglycan-I and Proteoglycan-Ii, Bone Sialoprotein-I and Sialoprotein-Ii, and Osteonectin from the Mineral Compartment of Developing Human-Bone." Journal of Biological Chemistry **262**(20): 9702-9708.

Fisher, L. W., J. D. Termine and M. F. Young (1989). "Deduced Protein-Sequence of Bone Small Proteoglycan-I (Biglycan) Shows Homology with Proteoglycan-Ii (Decorin) and Several Nonconnective Tissue Proteins in a Variety of Species." Journal of Biological Chemistry **264**(8): 4571-4576.

Fisher, S. E. (2001). Personnel Communication.

Folkman, J. and A. Moscona (1978). "Role of Cell-Shape in Growth-Control." Nature **273**(5661): 345-349.

Franceschi, R. T. (1999). "The developmental control of osteoblast-specific gene expression: Role of specific transcription factors and the extracellular matrix environment." Critical Reviews in Oral Biology & Medicine **10**(1): 40-57.

Franks, K. (2000). The Structure and Properties of Soluble Phosphate Based Glasses. Faculty of Dentistry. London, University of London.

Franks, K., I. Abrahams, G. Georgiou and J. C. Knowles (2001). "Investigation of Thermal Parameters and Crytallisation in a Ternary CaO-Na_2O-P_2O_5-Based Glass System." Biomaterials **22**(5): 497-501.

Franks, K., I. Abrahams and J. C. Knowles (2000). "Development of Soluble Glasses for Biomedical use Part I: *In vitro* Solubility Measurement." Journal of Materials Science-Materials in Medicine **11**(10): 609-614.

Franks, K., V. Salih, J. C. Knowles and I. Olsen (2002). "The Effect of MgO on the Solubility Behavior and Cell Proliferation in a Quaternary Soluble Phosphate Based Glass System." Journal of Materials Science-Materials in Medicine **13**(6): 549-556.

Fuggle, J. C. (1977). "XPS, UPS and XAES Studies of Oxygen-Adsorption on Polycrystalline Mgat-100 and -300k." Surface Science **69**(2): 581-608.

Gabriel, S. E., W. M. Ofallon and L. T. Kurland (1994). "Breast Implants and Connective-Tissue Diseases - Reply." New England Journal of Medicine **331**(18): 1233-1234.

Galeener, F. L. and J. C. Mikkelsen (1979). "The RAMEN Spectra and Structure of Pure Vitreous P_2O_5." Solid State Communications **30**: 505-510.

Galeener, F. L., J. C. Mikkelsen, R. H. Geils and W. J. Mosby (1978). "The Relative Raman Cross Sections of Vitreous SiO_2, GeO_2, B_2O_3, and P_2O_5." Applied Physics Letters **32**(1): 34-36.

Gao, H., T. Tan and D. Wang (2004a). "Dissolution Mechanism and Release Kinetics of Phosphate Controlled Release Glasses in Aqueous Medium." Journal of Controlled Release **96**: 29-36.

Gao, H., T. Tan and D. Wang (2004b). "Effect of Composition on the Release Kinetics of Phosphate Controlled Release Glasses in Aqueous Medium." Journal of Controlled Release **96**: 21-28.

Gillespie, W. J., C. M. A. Frampton, R. J. Henderson and P. M. Ryan (1988). "The Incidence of Cancer Following Total Hip-Replacement." Journal of Bone and Joint Surgery-British Volume **70**(4): 539-542.

Gonzalez, R. J. and J. B. Tarloff (2001). "Evaluation of Hepatic Subcellular Fractions for Alamar Blue and MTT Reductase Activity." Toxicology in Vitro **15**(3): 257-259.

Gough, J. E., P. Christian, C. A. Scotchford and I. A. Jones (2003). "Long-Term Craniofacial Osteoblast Culture on a Sodium Phosphate and a Calcium/Sodium Phosphate Glass." Journal of Biomedical Materials Research Part A **66A**(2): 233-240.

Gough, J. E., P. Christian, C. A. Scotchford, C. D. Rudd and I. A. Jones (2002). "Synthesis, Degradation, and *In Vitro* Cell Responses of Sodium Phosphate Glasses for Craniofacial Bone Repair." Journal of Biomedical Materials Research **59**(3): 481-489.

Gowen, M. and G. R. Mundy (1986). "Actions of Recombinant Interleukin 1, Interleukin 2 and Interferon-Gamma on Bone Resorption In-Vitro." Journal of Immunology **136**: 2478-2482.

Graham (1833). "Research on the Arsenates and Phosphates and Modification of Phosphoric Acid." Philosophical Transactions of the Royal Society **123**: 263-284.

Gresch, R. and W. Muller-Warmuth (1979). "X-Ray Photoelectron Spectroscopy of Sodium Phosphate Glasses." Journal of Non-Crystalline Solids **34**: 127-136.

Griffith, E. J. (1995). Phosphate Fibers. New York, Plenum Publishing Corporation.

Gronthos, S., K. Stewart, S. E. Graves, S. Hay and P. J. Simmons (1997). "Integrin expression and function on human osteoblast-like cells." Journal of Bone and Mineral Research **12**(8): 1189-1197.

Grzesik, W. J. and P. G. Robey (1994). "Bone-Matrix Rgd Glycoproteins - Immunolocalization and Interaction with Human Primary Osteoblastic Bone-Cells in-Vitro." Journal of Bone and Mineral Research **9**(4): 487-496.

Hagg, G. (1935). "The Vitreous State." Journal of Chemical Physics **3**(1): 42-49.

Hamid, R., Y. Rotshteyn, L. Rabadi, R. Parikh and P. Bullock (2004). "Comparison of Alamar Blue and MTT Assays for High Through-put Screening." Toxicology in Vitro **18**(5): 703-710.

Hauschka, P. V., J. B. Lian, D. E. C. Cole and C. M. Gundberg (1989a). "Osteocalcin and Matrix Gla Protein - Vitamin K-Dependent Proteins in Bone." Physiological Reviews **69**(3): 990-1047.

Hauschka, P. V., J. B. Lian and P. M. Gallop (1975). "Direct Identification of Calcium-Binding Amino-Acid, Gamma-Carboxyglutamate, in Mineralized Tissue." Proceedings of the National Academy of Sciences of the United States of America **72**(10): 3925-3929.

Hauschka, P. V. and F. H. Wians (1989b). "Osteocalcin-Hydroxyapatite Interaction in the Extracellular Organic Matrix of Bone." Anatomical Record **224**(2): 180-188.

Heaton, F. W. (1965). "Effect of Magnesium Deficiency on Plasma Alkaline Phosphatase Activity." Nature **207**(5003): 1292-&.

Hench, L. L. (1996). Ceramics, Glasses and Glass-Ceramics. Biomaterials Science: An Introduction To Materials in Medicine. B. D. Ratner, A. S. Hoffman, F. J. Schoen and J. E. Lemons. London, Academic Press.

Henthorn, P. S. (1996). Alkaline Phosphatase. Principles of Bone Biology. J. P. Bilezikian, L. G. Raisz and G. A. Rodan. London, Academic Press.

Hiki, Y., H. Takahashi and Y. Kogure (1999). "Relaxation of Thermal Properties Observed in Glasses." Physica B-Condensed Matter **263**: 353-356.

Hoppe, U., G. Walter, R. Kranold and D. Stachel (2000). "Structural Specifics of Phosphate Glasses Probed by Diffraction Methods: a Review." Journal of Non-Crystalline Solids **263**(1-4): 29-47.

Hoppe, U., G. Walter, D. Stachel and A. C. Hannon (1995). "Short-Range Order Details of Metaphosphate Glasses Studied by Pulsed-Neutron Scattering." Zeitschrift Fur Naturforschung Section a-a Journal of Physical Sciences **50**(7): 684-692.

Howlett, C. R., H. Zreiqat, R. Odell, J. Noorman, P. Evans, B. A. Dalton, C. McFarland and J. G. Steele (1994). "The Effect of Magnesium-Ion Implantation into Alumina Upon the Adhesion of Human Bone-Derived Cells." Journal of Materials Science-Materials in Medicine **5**(9-10): 715-722.

Huang, W. H., D. E. Day, C. S. Ray, C. W. Kim and A. Mogus-Milankovic (2004a). "Vitrification of High Chrome Oxide Nuclear Waste in Iron Phosphate Glasses." Journal of Nuclear Materials **327**(1): 46-57.

Huang, W. H., D. E. Day, C. S. Ray, C. W. Kim and S. T. D. Reis (2004b). "Properties and Solubility of Chrome in Iron Alumina Phosphate Glasses Containing High Level Nuclear Waste." Glass Science and Technology **77**(5): 203-210.

Huang, W. H., N. Zhou, D. E. Day and C. S. Ray (2005). "Effect of Cr_2O_3 on the HLW Iron Phosphate Glass Wasteforms." Journal of Inorganic Materials **20**(4): 842-850.

Hudgens, J. J., R. K. Brow, D. R. Tallant and S. W. Martin (1998). "Raman Spectroscopy Study of the Structure of Lithium and Sodium Ultraphosphate Glasses." Journal of Non-Crystalline Solids **223**(1-2): 21-31.

Hudgens, J. J. and S. W. Martin (1993). "Glass Transition and Infrared Spectra of Low Alkali, Anhydrous Lithium Phosphate Glasses." Journal of the American Ceramic Society **76**(7): 1691-1696.

Ishaug, S. L., M. J. Yaszemski, R. Bizios and A. G. Mikos (1994). "Osteoblast Function on Synthetic Biodegradable Polymers." Journal of Biomedical Materials Research **28**(12): 1445-1453.

Karabulut, M., E. Melnik, R. Stefan, G. K. Marasinghe, C. S. Ray, C. R. Kurkjian and D. E. Day (2001). "Mechanical and Structural Properties of Phosphate Glasses." Journal of Non-Crystalline Solids **288**(1-3): 8-17.

Karmakar, B., P. Kundu and R. N. Dwivedi (2001). "IR Spectra and their Application for Evaluating Physical Properties of Fluorophosphate Glasses." Journal of Non-Crystalline Solids **289**(1-3): 155-162.

Kasperk, C., J. Wergedal, D. Strong, J. Farley, K. Wangerin, H. Gropp, R. Ziegler and D. J. Baylink (1995). "Human Bone Cell Phenotypes Differ Depending on Their Skeletal Site of Origin." Journal of Clinical Endocrinology and Metabolism **80**(8): 2511-2517.

Kepes, E. R., L. Becsey and Underwoo.Ps (1972). "Intraoperative Death Associated with Acrylic Bone Cement - Report of 2 Cases." Journal of the American Medical Association **222**(5): 576-&.

Kim, C. W. and D. E. Day (2004). "Iron Phosphate Glasses for Vitrifying DOE High Priority Nuclear Wastes." Abstracts of Papers of the American Chemical Society **227**: U1044-U1045.

Kirkpatrick, R. J. and R. K. Brow (1995). "Nuclear-Magnetic-Resonance Investigation of the Structures of Phosphate and Phosphate-Containing Glasses - a Review." Solid State Nuclear Magnetic Resonance **5**(1): 9-21.

Knowles, J. C. and G. W. Hastings (1993). "*In vitro* and *In vivo* Investigation of a Range of Phosphate Glass- Reinforced Polyhydroxybutyrate-Based Degradable Composites." Journal of Materials Science-Materials in Medicine **4**(2): 102-106.

Kreidl, N. J. (1983). Glass Forming Systems. Glass Science and Technology. N. J. Kreidl and D. R. Uhlmann. New York, Academic Press. **1:** 192.

Kurkjian, C. R. (2000). "Mechanical Properties of Phosphate Glasses." Journal of Non-Crystalline Solids **263-264**: 207-212.

Lancaster, M. V. and R. D. Fields (1996). Antibiotic and Cytotoxic Drug Susceptability Assays using Resazurin and Poising Agents. U.S., Patent No. 5,501,959.

Le Sauze, A. and R. Marchand (2000a). "Chemically Durable Nitrided Phosphate Glasses Resulting from Nitrogen/Oxygen Substitution within PO_4 Tetrahedra." Journal of Non-Crystalline Solids **263**(1-4): 285-292.

Le Sauze, A., L. Montagne, G. Palavit, F. Fayon and R. Marchand (2000b). "X-ray Photoelectron Spectroscopy and Nuclear Magnetic Resonance Structural Study of Phosphorus Oxynitride Glasses, 'LiNaPON'." Journal of Non-Crystalline Solids **263**(1-4): 139-145.

Le Sauze, A., L. Montagne, G. Palavit and R. Marchand (2001). "Nitridation of Alkali Metaphosphate Glasses: a Comparative Structural Analysis of the Na-P-O-N and Li-Na-P-O-N Systems." Journal of Non-Crystalline Solids **293**: 81-86.

Lee, J. O., P. Rieu, M. Amin Aranout and R. Liddington (1995). "Crystal Structure ofthe A Domain from the α Subunit of Integrin CR3 (CD11b/CD18)." Cell **80**: 631-638.

Lee, Y. K., J. Song, H. J. Moon, S. B. Lee, K. M. Kim, K. N. Kim, S. H. Choi and R. Z. LeGeros (2004). In vitro and in vivo evaluation of non-crystalline calcium phosphate glass as a bone substitute. Bioceramics, Vol 16. Zurich-Uetikon, TRANS TECH PUBLICATIONS LTD. **254-2:** 185-188.

Liang, W., J. J. Cheng, H. P. Wang and H. Luo (2002). "Water Resistance of a New Nonlead Phosphate Sealing Glass." Physics and Chemistry of Glasses **43**(3): 158-160.

Lincks, J., B. D. Boyan, C. R. Blanchard, C. H. Lohmann, Y. Liu, D. L. Cochran, D. D. Dean and Z. Schwartz (1998). "Response of MG63 Osteoblast like Cells to Titanium and Titanium Alloy is Dependant on Surface Roughness and Composition." Biomaterials **19**(23): 2219-2232.

Lippmaa, E., M. Magi, A. Samoson, G. Engelhardt and A. R. Grimmer (1980). "Structural Studies of Silicates by Solid-State High-Resolution Si-29 Nmr." Journal of the American Chemical Society **102**(15): 4889-4893.

Lowry, K. J., K. R. Hamson, L. Bear, Y. B. Peng, R. Calaluce, M. L. Evans, J. O. Anglen and W. C. Allen (1997). "Polycaprolactone/Glass Bioabsorbable Implant in a Rabbit Humerus Fracture Model." Journal of Biomedical Materials Research **36**(4): 536-541.

Marchand, R. (1983). "Nitrogen-Containing Phosphate-Glasses." Journal of Non-Crystalline Solids **56**(1-3): 173-178.

Marchand, R., D. Agliz, L. Boukbir and A. Quemerais (1988). "Characterization of Nitrogen Containing Phosphate-Glasses by X- Ray Photoelectron-Spectroscopy." Journal of Non-Crystalline Solids **103**(1): 35-44.

Marino, A. E., S. R. Arrasmith, L. L. Gregg, S. D. Jacobs, G. Chen and Y. Duc (2001). "Durable Phosphate Glasses with Lower Transition Temperatures." Journal of Non-Crystalline Solids **289**(1-3): 37-41.

Mark, M. P., C. W. Prince, T. Oosawa, S. Gay, A. Bronckers and W. T. Butler (1987). "Immunohistochemical Demonstration of a 44-Kd Phosphoprotein in Developing Rat Bones." Journal of Histochemistry & Cytochemistry **35**(7): 707-715.

Marks, S. C. and S. N. Popoff (1988). "Bone Cell Biology: The Regulation of Development, Structure, and Function in the Skelaton." The American Journal of Anatomy **183**: 1-44.

Martin, J. Y., Z. Schwartz, T. W. Hummert, D. M. Schraub, J. Simpson, J. Lankford, D. D. Dean, D. L. Cochran and B. D. Boyan (1995). "Effect of Titanium Surface-Roughness on Proliferation, Differentiation, and Protein-Synthesis of Human Osteoblast-Like Cells (Mg63)." Journal of Biomedical Materials Research **29**(3): 389-401.

Martin, S. W. (1991). "Review of the Structures of Phosphate Glasses." European Journal of Solid State Inorganic Chemistry **28**: 163-205.

Mathews, C. K., K. E. van Holde and K. G. Ahern (2000). Biochemistry. San Francisco, Benjamin Cummings.

Matic, A. and L. Borjesson (1998). "Structure and Dynamics of Phosphate Glasses." Philosophical Magazine B **77**(2): 357-362.

Matsuzaka, K., X. F. Walboomers, J. E. de Ruijter and J. A. Jansen (1999). "The effect of poly-L-lactic acid with parallel surface micro groove on osteoblast-like cells in vitro." Biomaterials **20**(14): 1293-1301.

Matthews, C. K., K. E. van Holde and K. G. Ahern (2000). Biochemistry. San Francisco, Benjamin Cummins.

McDougall, K. E. (2001). Evaluation of Biocompatibilty using Human Craniofacial Bone Cells. Nottingham, University of Nottingham**:** 197.

Mesko, M. G., D. E. Day and B. C. Bunker (2000). "Immobilization of CsCl and SrF2 in iron phosphate glass." Waste Management **20**(4): 271-278.

Metwalli, E. and R. K. Brow (2001). "Modifier Effects on the Properties and Structures of Aluminophosphate Glasses." Journal of Non-Crystalline Solids **289**(1-3): 113-122.

Michishita, M., V. Videm and M. Amin Aranout (1992). "A Novel Divalent Cation Binding Site in the A Domain of the β2 Integrin CR3 (CD11b/CD18) is Essential for Lingand Binding." Cell **72**: 857-867.

Miller, K. M., R. A. Huskey and J. M. Anderson (1998). "Characterisation of Biomedical Polymer-Adherent Macrophages: Interleukin 1 Generation and Scanning Electron Microscopy Studies." Biomaterials **10**: 187-196.

Milne, I. S. (1973). "Hazards of Acrylic Bone Cement - Report of 2-Cases." Anaesthesia **28**(5): 538-543.

Mitchell, K. A. (1969). "Use of Outer D Orbitals in Bonding." Chemical Reviews **69**(2): 157-&.

Mogus-Milankovic, A., A. Gajovic, A. Santic and D. E. Day (2001). "Structure of Sodium Phosphate Glasses containing Al_2O_3 and/or Fe_2O_3. Part I." Journal of Non-Crystalline Solids **289**(1-3): 204-213.

Montagne, L., R. Delaval and G. Palavit (1998). "Effect of ZnO on the properties of (100-x)(NaPO3)-xZnO glasses." Journal of Non-Crystalline Solids **223**(1-2): 43-47.

Montagne, L., G. Palavit, A. Shaim, M. Et-Tabirou, P. Hartmann and C. Jager (2001). "Structure and Ionic Conductivity of Sodium Titanophosphate Glasses." Journal of Non-Crystalline Solids **293**: 719-725.

Monteny, E., J. Oleffe and M. Donkerwolke (1978). "Methylmethacrylate Hypersensitivity in a Patient with Cemented Endoprosthesis - Case-Report." Acta Orthopaedica Scandinavica **49**(6): 554-556.

Mosmann, T. (1983). "Rapid Colorimetric Assay for the Cellular Growth and Survival: Application to Proliferation and Cytotoxic Assays." Journal of Immunological Methods **65**: 55-63.

Navarro, J. M. F. (1998). "Oxynitride Glasses." Glastechnische Berichte-Glass Science and Technology **71**(9): 263-276.

Nayab, S. N., F. H. Jones and I. Olsen (2005). "Effects of calcium ion implantation on human bone cell interaction with titanium." Biomaterials **26**(23): 4717-4727.

Nelson, B. N. and G. J. Exarhos (1979). "Vibrational Spectroscopy of Cation-Site Interactions in Phosphate Glasses." Journal of Chemical Physics **71**(7): 2739-2747.

Northup, S. J. (2004). *In Vitro* Assessment of Tissue Compatibilty. Biomaterials Science. B. D. Ratner, A. S. Hoffman, F. J. Schoen and J. E. Lemons. London, Elsevier Academic Press.

O'Brien, J., I. Wilson, T. Orton and F. Pognan (2000). "Investigation of the Alamar Blue (resazurin) Fluorescent Dye for the Assessment of Mammalian Cell Cytotoxicity." European Journal for Biochemistry **267**(17): 5421-5426.

Oldberg, A., A. Franzen and D. Heinegard (1987). "Cloning and Sequence Analysis of Rat Bone Sialoprotein (Osteopontin) cDNA Reveals An Arg-Gly-Asp Cell Binding Sequence." Proceedings of the National Academy of Sciences of the United States of America **83**: 8819-8823.

Owen, T. A., M. Aronow, V. Shalhoub, L. M. Barone, L. Wilming, M. S. Tassinari, M. B. Kennedy, S. Pockwinse, J. B. Lian and G. S. Stein (1990). "Progressive Development of the Rat Osteoblast Phenotype In Vitro: Reciprocal Relationships in Expression of Genes Associated with Osteoblast Proliferation and Differentiation During Formation of the Bone Extracelluar Matrix." Journal of Cellular Physiology **143**: 420-430.

Parfitt, A. M. (1994). "Osteonal and Hemi-Osteonal Remodeling: the Spatial and Temporal Framework for Signal Traffic in Adult Bone." Journal of Cell Biochemistry **55**: 273-286.

Parfitt, A. M. (1995). "Problems in the Application of In Vitro Systems to the Study of Human Bone Remodeling." Calcified Tissue International **56(6)**: S5-S7.

Parsons, A. J., L. D. Burling, C. D. Rudd, C. A. Scotchford and G. S. Walker (2004a). "The Effect of Production Regime and Crucible Materials on the Thermal Properties of Sodium Phosphate Glasses Produced from Salts." Journal of Biomedical Materials Research Part B-Applied Biomaterials **71B**(1): 22-29.

Parsons, A. J., M. Evans, C. D. Rudd and C. A. Scotchford (2004b). "Synthesis and Degradation of Sodium Iron Phosphate Glasses and their *In Vitro* Cell Response." Journal of Biomedical Materials Research Part A **71A**(2): 283-291.

Partridge, N. C. and S. K. Winchester (1996). Osteoblast Protinases. Principles of Bone Biology. J. P. Bilezikian, L. G. Raisz and G. A. Rodan. London, Academic Press.

Peebles, D. J., S. D. K. Stride, B. R. J. Simpson and R. H. Ellis (1972). "Cardiovascular Effects of Methylmethacrylate Cement." British Medical Journal **1**(5796): 349-&.

pharyngula (2003). A comparison of human bone, fossilized dinosaur bone, and Ed Conrad's putative Carboniferous bone, http://pharyngula.org/index/weblog/2003/11/.

Philipps, J. F., T. Topfer, H. Ebendorff-Heidepriem, D. Ehrt and R. Sauerbrey (2001). "Spectroscopic and Lasing Properties of Er^{3+}: Yb^{3+}-Doped Fluoride Phosphate Glasses." Applied Physics B-Lasers and Optics **72**(4): 399-405.

Philipps, J. F., T. Topfer, H. Ebendorff-Heidepriem, D. Ehrt and R. Sauerbrey (2002). "Energy Transfer and Upconversion in Erbium-Ytterbium-Doped Fluoride Phosphate Glasses." Applied Physics B-Lasers and Optics **74**(3): 233-236.

Pietrzak, W. S. and B. L. Eppley (2000). "Resorbable Polymer Fixation for Craniomaxillofacial Surgery: Development and Engineering Paradigms." Journal of Craniomaxillofacial Surgery **11**(6): 575-585.

Poser, J. W., F. S. Esch, N. C. Ling and P. A. Price (1980). "Isolation and Sequence of the Vitamin-K-Dependent Protein from Human-Bone - Undercarboxylation of the 1st Glutamic-Acid Residue." Journal of Biological Chemistry **255**(18): 8685-8691.

Price, P. A. (1985). "Vitamin K-Dependant Formation Of Bone Gla Protein (Osteocalcin) and its Function." Vitamins and Hormones **42**: 65-108.

Price, P. A., A. S. Otsuka, J. W. Poser, J. Kristaponis and N. Raman (1976). "Characterization of a Gamma-Carboxyglutamic Acid-Containing Protein from Bone." Proceedings of the National Academy of Sciences of the United States of America **73**(5): 1447-1451.

Puleo, D. A. and R. Bizios (1991). "Rgds Tetrapeptide Binds to Osteoblasts and Inhibits Fibronectin-Mediated Adhesion." Bone **12**(4): 271-276.

Rammelt, S., M. Neumann, U. Hanisch, A. Reinstorf, W. Pompe, H. Zwipp and A. Biewener (2005). "Osteocalcin Enhances Bone Remodeling Around Hydroxyapatite/Collagen Composites." Journal of Biomedical Materials Research Part A **73A**(3): 284-294.

Ramoshebi, L. N., T. N. Matsaba, J. Teare, L. Renton, J. Patton and U. Ripamonti (2002). "Tissue Engineering: TGF-beta Superfamily Members and Delivery Systems in Bone Regeneration." Expert Reviews in Molecular Biology.

Ratner, B. D. (2004). Biological Testing of Biomaterials. Biomaterials Science: An Introduction to Materials in Medicine. B. D. Ratner, A. S. Hoffman, F. J. Schoen and J. E. Lemons. London, Elsevier Academic Press.

Reidmeyer, M. R., M. Rajaram and D. E. Day (1986). "Preparation of Phosphorus Oxynitride Glasses." Journal of Non-Crystalline Solids **85**(1-2): 186-203.

Reis, S. T., D. L. A. Faria, J. R. Martinelli, W. M. Pontuschka, D. E. Day and C. S. M. Partiti (2002). "Structural Features of Lead Iron Phosphate Glasses." Journal of Non-Crystalline Solids **304**: 188-194.

Reis, S. T., M. Karabulut and D. E. Day (2001). "Chemical Durability and Structure of Zinc-Iron Phosphate Glasses." Journal of Non-Crystalline Solids **292**(1-3): 150-157.

Rezania, A., C. H. Thomas, A. B. Branger, C. M. Waters and K. E. Healy (1997). "The detachment strength and morphology of bone cells contacting materials modified with a peptide sequence found within bone sialoprotein." Journal of Biomedical Materials Research **37**(1): 9-19.

Richards, J. (2004). Personal Communication.

Rinehart, J. D., T. D. Taylor, Y. Tian and R. A. Latour (1999). "Real-Time Dissolution Measurement of Sized and Unsized Calcium Phosphate Glass Fibers." Journal of Biomedical Materials Research **48**(6): 833-840.

Robey, P. G. (1996). Bone Matrix Proteoglycans and Glycoproteins. Principles of Bone Biology. J. P. Bilezikian, L. G. Raisz and G. A. Rodan. London, Academic Press.

Robey, P. G. and A. L. Boskey (1995). The Biochemistry of Bone. Osteoporosis. R. Marcus, D. Feldman, J. P. Bilezikian and J. Kelsey. New York, Academic Press.

Roshchina, Y. V., T. S. Tsekhomskaya, G. P. Roskova and I. S. Ivanovskaya (1995). "Rate of Chemical Decomposition of Sodium Zinc Phosphate-Glass with Hydrochloric-Acid - Effect of the Ratio of the Solution Volume to the Glass-Surface Area." Glass Physics and Chemistry **21**(5): 371-376.

Ross, F. P., J. Chappel, J. I. Alvarez, D. Sander, W. T. Butler, M. C. Farachcarson, K. A. Mintz, P. G. Robey, S. L. Teitelbaum and D. A. Cheresh (1993). "Interactions between the Bone-Matrix Proteins Osteopontin and Bone Sialoprotein and the Osteoclast Integrin Alpha-V-Beta-3 Potentiate Bone-Resorption." Journal of Biological Chemistry **268**(13): 9901-9907.

Ross, J. A. and M. J. Auger (2002). The Biology of the Macrophage. The Macrophage. B. Burke and C. E. Lewis. Oxford, Oxford University Press.

Rossert, J. and B. de Crombrugghe (1996). Type I Collagen: Structure, Synthesis, and Regulation. Principals of Bone Biology. J. P. Bilezikian, L. G. Raisz and G. A. Rodan. London, Academic Press.

Rouse, G. B., P. J. Miller and W. M. Risen (1978). "Mixed Alkali Glass Spectra and Structure." Journal of Non-Crystalline Solids **28**: 193-207.

Rubin, J. P. and M. J. Yaremchuk (1997). "Complications and Toxicities of Implantable Biomaterials used in Facial Reconstructive and Aesthetic Surgery: A Comprehensive Review of the Literature." Plastic and Reconstructive Surgery **100**(5): 1336-1353.

Sales, B. C., J. U. Otaigbe, G. H. Beall, L. A. Boatner and J. O. Ramey (1998). "Structure of Zinc Polyphosphate Glasses." Journal of Non-Crystalline Solids **226**(3): 287-293.

Salih, V., K. Franks, M. James, G. W. Hastings, J. C. Knowles and I. Olsen (2000). "Development of Soluble Glasses for Biomedical Use Part II: The

Biological Response of Human Osteoblast Cell Lines to Phosphate-Based Soluble Glasses." Journal of Materials Science-Materials in Medicine **11**(10): 615-620.

Salim, M. A., G. D. Khattak, P. S. Fodor and L. E. Wenger (2001). "X-ray Photoelectron Spectroscopy (XPS) and Magnetization Studies of Iron-Vanadium Phosphate Glasses." Journal of Non-Crystalline Solids **289**(1-3): 185-195.

Salim, M. A., G. D. Khattak and M. Sakhawat Hussain (1995). "X-ray Photoelectron Spectroscopy, Fourier Transform Infrared Spectroscopy and Electical Conductivity Studies of Copper Phosphate Glasses." Journal of Non-Crystalline Solids **185**: 101-108.

Sanchezguerrero, J., G. A. Colditz, E. W. Karlson, D. J. Hunter, F. E. Speizer and M. H. Liang (1995). "Silicone Breast Implants and the Risk of Connective-Tissue Diseases and Symptoms." New England Journal of Medicine **332**(25): 1666-1670.

Sato, K., Y. Fujii, K. Kasono, W. Saji, T. Tsushima and K. Shizume (1986). "Stimulation of Prostagladin E2 and Bone Resorption by Recombinant Human Interleukin 1 Alpha in Fetal Mouse Bones." Biochemical and Biophysical Research Communications **138**: 618-624.

Saxe, A. W., J. L. Doppman and M. F. Brennan (1982). "Use of Titanium Surgical Clips to Avoid Artifacts Seen on Computed-Tomography." Archives of Surgery **117**(7): 978-979.

Schmidt, C., A. A. Ignatius and L. E. Claes (2001). "Proliferation and Differentiation Parameters of Human Osteoblasts on Titanium and Steel Surfaces." Journal of Biomedical Materials Research **54**(2): 209-215.

Schoen, F. J. (2004). Host Reactions to Biomaterials and Their Evaluation. Biomaterials Science: An Introduction to Materials in Medicine. B. D. Ratner, A. S. Hoffman, F. J. Schoen and J. E. Lemons. London, Elsevier Academic Press.

Scotchford, C. A. (2005). Personal Communication.

Seeley, R. R. (2000). Anatomy & Physiology. Boston, Mass., McGraw-Hill.

Shalhoub, V., L. C. Gerstenfeld, D. Collart, J. B. Lian and G. S. Stein (1989). "Down-Regulation of Cell-Growth and Cell-Cycle Regulated Genes During Chick Osteoblast Differentiation with the Reciprocal Expression of Histone Gene Variants." Biochemistry **28**(13): 5318-5322.

Shelby, J. E. (1997). Introduction To Glass Science and Technology. Cambridge, The Royal Society of Chemistry.

Shih, P. Y., S. W. Yung and T. S. Chin (1998). "Thermal and Corrosion Behavior of P_2O_5-Na_2O-CuO Glasses." Journal of Non-Crystalline Solids **224**(2): 143-152.

Siebers, M. C., P. J. ter Brugge, X. F. Walboomers and J. A. Jansen (2005). "Integrins as linker proteins between osteoblasts and bone replacing materials. A critical review." Biomaterials **26**(2): 137-146.

Sircol (1992). "Sircol Soluble Collagen Assay Handbook." http://www.biocolor.co.uk/manuals/Sircolmanual.pdf.

Somerman, M. J., C. W. Prince, J. J. Sauk, R. A. Foster and W. T. Butler (1987). "Mechanism of Fibroblast Attachment to Bone Extracellular-Matrix - Role of a 44-Kilodalton Bone Phosphoprotein." Journal of Bone and Mineral Research **2**(3): 259-265.

Sowadski, J. M., B. A. Foster and H. W. Wyckoff (1981). "Structure of Alkaline-Phosphatase with Zinc-Magnesium Cobalt or Cadmium in the Functional Metal Sites." Journal of Molecular Biology **150**(2): 245-272.

Stein, G., J. Lian, J. Stein, R. Briggs, V. Shalhoub, K. Wright, U. Pauli and A. Vanwijnen (1989a). "Altered Binding of Human Histone Gene-Transcription Factors During the Shutdown of Proliferation and Onset of Differentiation in Hl-60 Cells." Proceedings of the National Academy of Sciences of the United States of America **86**(6): 1865-1869.

Stein, G. S., J. B. Lian, L. G. Gerstenfeld, V. Shalhoub, M. Aronow, T. Owen and E. Markose (1989b). "The Onset and Progression of Osteoblast Differentiation Is Functionally Related to Cellular Proliferation." Connective Tissue Research **20**(1-4): 3-13.

Stein, G. S., J. B. Lian and T. A. Owen (1990). "Relationship of Cell-Growth to the Regulation of Tissue- Specific Gene-Expression During Osteoblast Differentiation." Faseb Journal **4**(13): 3111-3123.

Stein, G. S., J. B. Lian, J. L. Stein, A. J. van Wijnen, B. Frenkel and M. Montecino (1996). Mechanisms Regulating Osteoblast Proliferation and Differentiation. Principles of Bone Biology. J. P. Bilezikian, L. G. Raisz and G. A. Rodan. London, Academic Press**:** 69-86.

Stevens, A. and J. Lowe (1997). Human Histology. London, Mosby.

Sun, K. H. (1947). "Fundamental Condition of Glass Formation." Journal of the American Ceramic Society **30**(9): 277-281.

Suzuya, K., D. L. Price, C.-K. Loong and S. W. Martin (1998). "Structure of Vitreous P_2O_5 and Alkali Phosphate Glasses." Journal of Non-Crystalline Solids **232-234**: 650-657.

Swift, P. (1982). "Adventitious Carbon - the Panacea for Energy Referencing." Surface and Interface Analysis **4**(2): 47-51.

Tennenbaum, T., S. H. Yuspa and J. Kapitulnik (1990). "Magnesium and Phosphate Enrichment of Culture Medium Stimulates the Proliferation of Epidermal Cells from Newborn and Adult Mice." Journal of Cellular Physiology **143**: 431-438.

Termine, J. D., H. K. Kleinman, S. W. Whitson, K. M. Conn, M. L. McGarvey and G. R. Martin (1981). "Osteonectin, a Bone-Specific Protein Linking Mineral to Collagen." Cell **26**(1): 99-105.

Thomas, C. H., C. D. McFarland, M. L. Jenkins, A. Rezania, J. G. Steele and K. E. Healy (1997). "The role of vitronectin in the attachment and spatial distribution of bone-derived cells on materials with patterned surface chemistry." Journal of Biomedical Materials Research **37**(1): 81-93.

Thomas, K. A., S. D. Cook, A. F. Harding and R. J. Haddad (1988). "Tissue Reaction to Implant Corrosion in 38 Internal-Fixation Devices." Orthopedics **11**(3): 441-451.

Uchino, T. and Y. Ogata (1995a). "*Ab Initio* Molecular Orbital Calculations on the Electronic Structure of Phosphate Glasses. Binary Alkali Metaphosphate Glasses." Journal of Non-Crystalline Solids **191**(1-2): 56-70.

Uchino, T. and Y. Ogata (1995b). "*Ab Initio* Molecular Orbital Calculations on the Electronic Structure of Phosphate Glasses. Sodium Phosphate Glasses." Journal of Non-Crystalline Solids **181**(1-2): 175-188.

Uo, M., M. Mizuno, Y. Kuboki, A. Makishima and F. Watari (1998). "Properties and Cytotoxicity of Water Soluble Na_2O-CaO-P_2O_5 Glasses." Biomaterials **19**(24): 2277-2284.

Van Wazer, J. R. (1950a). "Structure and Properties of the Condensed Phosphates. II. A Theory of the Molecular Structure of Sodium Phosphate Glasses." Journal of the American Ceramic Society **72**(2): 644-647.

Van Wazer, J. R. (1950b). "Structure and Properties of the Condensed Phosphates. III. Solubility Fractionation and Other Solubility Studies." Journal of the American Ceramic Society **72**(2): 647-655.

Van Wazer, J. R. (1958). Phosphorus and its Compounds. London, Interscience Publishers Ltd.

Van Wazer, J. R. and K. A. Holst (1950). "Structure and Properties of the Condensed Phosphates. I. Some General Considerations about Phosphoric Acids." Journal of the American Ceramic Society **72**(2): 639-644.

Walter, G., J. Vogel, U. Hoppe and P. Hartmann (2001). "The Structure of CaO-Na_2O-MgO-P_2O_5 Invert Glass." Journal of Non-Crystalline Solids **296**(3): 212-223.

Wang, M., L. L. Hench and W. Bonfield (1998). "Bioglass (R) High Density Polyethylene Composite for Soft Tissue Applications: Preparation and Evaluation." Journal of Biomedical Materials Research **42**(4): 577-586.

Wasi, S., K. Otsuka, K. L. Yao, P. S. Tung, J. E. Aubin, J. Sodek and J. D. Termine (1984). "An Osteonectinlike Protein in Porcine Periodontal-Ligament and Its Synthesis by Periodontal-Ligament Fibroblasts." Canadian Journal of Biochemistry and Cell Biology **62**(6): 470-478.

Weber, M. J. (1990). "Science and Technology of Laser Glass." Journal of Non-Crystalline Solids **123**(1-3): 208-222.

Wei, T. Y., Y. Hu and L. G. Hwa (2001). "Structure and Elastic Properties of Low-Temperature Sealing Phosphate Glasses." Journal of Non-Crystalline Solids **288**(1-3): 140-147.

Westman, A. E. R. and P. A. Gartaganis (1957). "Constitution of Sodium, Potassium, and Lithium Phosphate Glasses." Journal of the American Ceramic Society **40**(9): 293-299.

Williams, D. F. (1987). Definitions in Biomaterials. European Society for Biomaterials, Chester UK, Elsevier.

Woodruff, M. A. (2005). The use of Proteomics to Study Cell/Surface Interactions. Mechanical, Materials, Manufacturing Engineering. Nottingham, University of Nottingham.

Wuthier, R. E. and T. C. Register (1984). Role of Alkaline Phosphatase, a Polyfunctional Enzyme, in Mineralising Tissues. The Chemistry and Biology of Mineralised Tissues. W. T. Butler. Birmingham, Ebsco Media**:** 113-124.

Xiong, J. P., T. Stehle, B. Diefenbach, R. Zhang, R. Dunker, D. L. Scott, A. Joachimiak, S. L. Goodman and M. Amin Aranout (2001). "Crystal Structure of the Extracellular Segment of Integrin αVβ3." Science **294**: 339-345.

Young, M. F., A. A. Day, P. Dominquez, C. I. McQuillan, L. W. Fisher and J. D. Termine (1990a). "Structure and Expression of Osteonectin Messenger-Rna in Human Tissue." Connective Tissue Research **24**(1): 17-28.

Young, M. F., A. A. Day, P. G. Robey and J. D. Termine (1990b). "Interaction of Osteonectin and Type-I Collagen in Bone-Cells." Annals of the New York Academy of Sciences **580**: 526-528.

Zarhariasen, W. H. (1932). "The Atomic Arrangment in Glass." Journal of the American Chemical Society **54**(10): 3841-3851.

Zhmyreva, I. A., V. P. Kolobkov, S. G. Lunter, I. N. Morozova, Y. K. Federov and A. N. Chikovskii (1988). Fiz. Khim. Stekla (Eng. Trans.) **13**(6): 464.

Zhou, W. C., H. S. Zhao and D. M. Zhu (2000). "Preparation and Properties of Lead Halide Phosphate Glasses." Journal of Non-Crystalline Solids **263**(1-4): 277-284.